

**FEDERAL UNIVERSITY OF SÃO CARLOS**  
**CENTER OF EXACT SCIENCES AND TECHNOLOGY**  
**GRADUATE PROGRAM IN MATERIALS SCIENCE AND ENGINEERING**

SYNTHESIS AND GRAPHITIZATION OF PHENOLIC RESINS FOR CARBON-  
CONTAINING REFRACTORY APPLICATIONS

Talabi Segun Isaac

São Carlos-SP  
2020



**FEDERAL UNIVERSITY OF SÃO CARLOS**  
**CENTER OF EXACT SCIENCES AND TECHNOLOGY**  
**GRADUATE PROGRAM IN MATERIALS SCIENCE AND ENGINEERING**

SYNTHESIS AND GRAPHITIZATION OF PHENOLIC RESINS FOR CARBON-  
CONTAINING REFRACTORY APPLICATIONS

Talabi Segun Isaac

Dissertation presented to the  
Graduate Program in Materials Science and  
Engineering as partial requirement for  
obtaining the title of PhD in MATERIALS  
SCIENCE AND ENGINEERING.

Supervisor: Alessandra de Almeida Lucas, PhD  
Assistant Supervisor: Ana Paula da Luz, PhD  
Funding Agency: TWAS-CNPq – 190109/2015-7

São Carlos-SP  
2020





## DEDICATION

This thesis is dedicated to God Almighty, the invisible, everlasting and unchangeable.

## RESUME

Master in Metallurgical and Materials Engineering from UNILAG (2011),  
Undergraduation in Metallurgical and Materials Engineering from FUTA  
(2008)



---

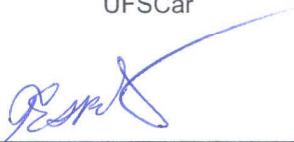
**Folha de Aprovação**

---

Assinaturas dos membros da comissão examinadora que avaliou e aprovou a Defesa de Tese de Doutorado do candidato Segun Isaac Talabi, realizada em 03/02/2020:

  
\_\_\_\_\_  
Profa. Dra. Alessandra de Almeida Lucas  
UFSCar

  
\_\_\_\_\_  
Prof. Dr. Carlos Henrique Scuracchio  
UFSCar

  
\_\_\_\_\_  
Profa. Dra. Rosario Elida Suman Bretas  
UFSCar

  
\_\_\_\_\_  
Profa. Dra. Elisabete Frollini  
USP

  
\_\_\_\_\_  
Profa. Dra. Camila Alves de Rezende  
UNICAMP



## ACKNOWLEDGEMENTS

My profound gratitude goes to God Almighty, the author of life who sustained me throughout this PhD programme.

I appreciate the effort and guidance of my supervisor, Prof. Lucas Alessandra de Almeida who supported me and saw to the timely completion of my experimental work, articles publication and the thesis writing. I could not have overcome the numerous demands of doctoral training without her continuous belief in my ability. My thanks go to my co-supervisor, Prof. Luz Ana Paula for her support and counsel throughout the programme. Her contribution to the experiments design, training and review of every write-up cannot be over-emphasized, coupled with her encouraging words. I will also like to appreciate Prof. Pandolfelli Victor Carlos, who initial conceived the topic idea but graciously asked Prof. Lucas to continue the supervision when the subject appears to be tending more towards polymer aspect during the early stages of the research work. Nevertheless, he continued to provide his support, guidance and counsel, especially in the aspect of publishing the research findings.

Beside every successful man, there is a woman goes the popular adage. I am highly grateful to my wife (Mrs. Talabi Ibukunoluwa Tola) who made unquantifiable sacrifices throughout my PhD programme. She is a pillar that encourages, inspires and bears with me at all times. To our loving babies, Deborah and Samuel (who happen to be Brazilian!), daddy loves you.

I thanked my family members, parents (Mr and Mrs Talabi), sister (Dr Olusegun C. F.) and her husband, in-laws and friends for their prayers, support and counsel. In addition, I appreciate all my Brazilian friends, especially, Guilherme at Alcoa lab, my project mates, and the members of Methodista Igreja, Sao Carlos. I appreciate the love of Prof. Basmaji Pierre (he was like a father to our family) and Mr Vincent. It is a pleasure knowing all these great people!

Finally, I am grateful to TWAS-CNPq (The World Academy of Sciences-National Council for Scientific and Technological Development) for providing the fellowship that was used for this PhD programme and University of Ilorin, Ilorin Nigeria for granting me a study leave. The contributions of FIRE-Omega project, INCT/MIDAs, FIBRIA and RHI-MAGNESITA are all acknowledged. This study

was financed in part by the Coordenação de Aperfeiçoamento de Pessoal de Nível Superior - Brasil (CAPES) - Finance Code 001.

## RESUMO

Os refratários contendo carbono (CCRs) apresentam propriedades químicas e termomecânicas especiais que dependem diretamente da presença da fase carbonácea contida na microestrutura, a qual preferencialmente deve ter estrutura semelhante à grafite. No entanto, resinas fenólicas que são comumente usadas como ligante nesses refratários dão origem a geração de carbono amorfo, o que pode limitar seu desempenho. Conseqüentemente, esta pesquisa concentrou-se na síntese e grafitação dessas resinas sob temperaturas e condições adequadas para aplicação em refratários. No estudo, alguns conjuntos de experimentos foram conduzidos para investigar o papel do óxido de boro, ácido bórico e ferroceno como agente de grafitação para resinas fenólicas sob várias condições de processamento. Resinas convencionais (produtos sintetizados comerciais e laboratoriais) e resinas fenólicas modificadas com lignina foram avaliadas. As amostras de carbono resultantes foram caracterizadas utilizando Difratômetro de Raios-X (XRD) para determinar a quantidade de carbono grafítico gerado após a carbonização da resina. O Microscópio Eletrônico de Transmissão e o Microscópio Eletrônico de Varredura também foram utilizados para corroborar as informações baseadas na técnica de XRD. Os resultados mostram que estes aditivos podem induzir a geração de carbono grafítico durante pirólise, dependendo da química da resina e dos parâmetros de processamento como a técnica de mistura e o processo de aquecimento. O mecanismo responsável pela cristalização de carbono foi atribuído à formação da ligação B–O–C para a resina modificada com compostos de boro e à presença de  $Fe_3C$  na resina contendo ferroceno. A ligação B–O–C tem menor energia de ligação (comparado com C–C) que permite a rotação/reorganização necessária durante a carbonização, enquanto  $Fe_3C$  atua como locais ativos para geração de grafite. As análises termogravimétricas das amostras de carbono indicaram que vários fatores como força de ligação, composição e arranjo de átomos controlam sua resistência à oxidação. Além disso, os concretos de CCR preparados mostram melhor resistência à oxidação devido a grafitação *in-situ* do componente ligante.

**Palavras-chave:** síntese; grafitação; refratários; resinas fenólicas.





## ABSTRACT

### SYNTHESIS AND GRAPHITIZATION OF PHENOLIC RESINS FOR CARBON-CONTAINING REFRACTORY APPLICATIONS

Carbon-containing refractories' (CCRs) present special chemical and thermomechanical properties, which depend on the presence of carbonaceous phase with a structure similar to those of graphite. However, phenolic resins that are commonly used as binder for such refractories produce amorphous carbon, which can limit their performance. Consequently, this research focused on the synthesis and graphitization of these resins under temperatures and conditions suitable for refractory production. In the study, some series of experiments were conducted to investigate the role of boron oxide, boric acid and ferrocene as graphitizing agent for phenolic resins under various processing conditions such as mixing technique and heating procedure. Both conventional (commercial and laboratory synthesized products) and lignin modified phenolic resins were considered. The resulting carbon samples were characterized using X-ray Diffractometer (XRD) to determine the amount of generated graphitic carbon after carbonization. Transmission Electron Microscope (TEM) and Scanning Electron Microscope (SEM) were also used to corroborate the information obtained from the XRD analysis. The results showed that these additives can induce crystalline carbons generation during pyrolysis depending on the resin chemistry and processing parameters. The mechanism leading to carbon crystallization was attributed to the formation of B–O–C bonds for the boron compounds modified resins. The B–O–C bonds has a lower binding energy (compared to C–C), which permits the rotation/reorganization that is necessary for graphitic carbons production. Similarly,  $\text{Fe}_3\text{C}$  acted as active sites for crystalline carbon generation during pyrolysis of the resins-ferrocene formulations. Thermogravimetric analysis (TGA) of the carbon samples show that several factors such as bond strength, composition and atoms arrangement control their oxidation resistance. Moreover, the prepared CCR castables show improved oxidation resistance based on in-situ graphitization of the binder component.

**Keywords:** synthesis; graphitization; refractories; phenolic resins.



## PUBLICATIONS

1. Talabi, S. I., Luz, A. P., Lucas A. A., Pandolfelli V. C. Catalytic graphitization of novolac resin for refractory applications. *Ceramics International*, 2018. **44**(4): p. 3816-3824.
2. Talabi S. I., Luz A. P., Pandolfelli V. C., Lucas A. A. (2018). Structural evolution during the catalytic graphitization of a thermosetting refractory binder and oxidation resistance of the derived carbons. *Materials Chemistry and Physics*, 2018. **212**: p. 113-121.
3. Talabi, S. I., Luz, A. P., Pandolfelli, V. C., Bernardes, J. S., Lucas, A. A. (2019). Synthesis and graphitization of resole resins by ferrocene. *Progress in Natural Science: Materials International.*, 2019. **29**(1): p. 71-80.
4. Talabi, S. I., Luz, A. P., Pandolfelli, V. C., Lima, V. H., Botaro V., Lucas A. A. Graphitization of lignin-phenol-formaldehyde resins by boron oxide, boric acid and ferrocene. *Materials Research*. **Accepted subject to revision**.
5. Talabi, S. I., Luz, A. P., Pandolfelli, V. C., Lucas, A. A. (2019). Catalytic graphitization of lignin-phenol-formaldehyde resin for refractory applications. Poster presentation at Innovations in Design, Fabrication and Application of Polymeric Materials, June 8<sup>th</sup>-9<sup>th</sup>, Mount Holyoke College, South Hadley, Massachusetts, USA.



## TABLE OF CONTENTS

	Pag.
APPROVAL SHEET .....	i
ACKNOWLEDGEMENTS .....	iii
RESUMO .....	v
ABSTRACT .....	vii
PUBLICATIONS .....	ix
TABLE OF CONTENTS .....	xi
INDEX OF TABLES .....	xv
INDEX OF FIGURES .....	xix
SYMBOLS AND ABBREVIATIONS .....	xxv
1 INTRODUCTION .....	1
1.1 Statement of the Problem .....	3
1.2 Significance of the Study .....	4
1.3 Objectives .....	5
1.3.1 Specific Objectives .....	5
2 LITERATURE REVIEW .....	7
2.1 Refractory materials .....	7
2.2 Carbon-containing Refractory Materials.....	10
2.2.1 Roles and challenges of carbon in carbon-containing refractories .....	11
2.2.2 Binders for carbon-containing refractories .....	15
2.3 Phenolic resin pyrolysis: carbonization mechanism, degradation pathway and characteristic of the derived carbons.....	25
2.4 Graphitization of thermosetting resin and its benefits to CCRs .....	34
2.5 Graphitization of phenolic resin by boron-containing compounds .....	43
2.6 Graphitization of novolac resin by ferrocene and its reaction pathway...	53
2.7 Characterization Techniques for evaluating graphitization degree in carbons.....	54
2.7.1 X-ray diffraction technique .....	55
2.7.2 Raman Spectroscopy .....	56
2.7.3 Some other relevant techniques .....	60
3 MATERIALS AND METHODOLOGY.....	63

3.1	Graphitization of commercial novolac type phenolic resin .....	63
3.2	Conventional resole and lignin-modified phenolic resins synthesis and graphitization.....	67
3.2.1	Conventional resole resins synthesis and graphitization .....	70
3.2.2	Lignin-modified phenolic resins synthesis and graphitization .....	71
3.3	Production of resin bonded Al <sub>2</sub> O <sub>3</sub> -MgO refractory castables .....	73
3.4	Characterization techniques employed during the study .....	74
3.4.1	Characterization techniques associated with lignin and the resins .....	74
3.4.1.1	Viscosity measurement .....	74
3.4.1.2	Fourier Transform Infrared Measurement of the resins and lignin material.....	75
3.4.1.3	Molecular weights measurement of the lignin samples.....	75
3.4.2	Characterization techniques associated with the study of carbons derived from the resins and graphitization mechanism.....	75
3.4.2.1	X-ray Diffraction (XRD) analysis.....	76
3.4.2.2	Raman Spectroscopy analysis .....	78
3.4.2.3	Thermogravimetric analysis .....	78
3.4.2.4	Microstructural analysis.....	79
3.4.2.5	Graphitization mechanism study by X-ray Photoelectron Spectrometer (XPS).....	80
3.4.2.6	Graphitization mechanism determination by Fourier Transform Infrared Spectroscopy measurements .....	80
3.4.3	Characterization of the CCR (Al <sub>2</sub> O <sub>3</sub> -MgO-C) castables .....	81
3.4.3.1	Apparent porosity (AP) and Bulk density Measurements.....	81
3.4.3.2	Cold Crushing Strength (CCS) Measurement .....	82
3.4.3.3	Oxidation Resistance Measurements.....	82
4	RESULTS AND DISCUSSION.....	85
4.1	Part 1: Catalytic graphitization of commercial novolac resin by boric acid, boron oxide and ferrocene.....	85
4.1.1	Structure of carbons derived from novolac resin formulations containing boric acid and boron oxide .....	86

4.1.2 Influence of processing parameters on the catalytic graphitization of novolac resin containing boron source compounds.....	94
4.1.3 Raman spectra of some selected carbon samples from novolac resin containing boric acid and boron oxide.....	104
4.1.4 Chemical evolution during pyrolysis of novolac resins containing boric acid or boron oxide.....	106
4.1.5 Oxidation resistance of carbons derived from novolac resin containing boron compounds additives after carbonization using A3-procedure .....	121
4.1.6 Catalytic graphitization of novolac resin by ferrocene .....	125
Based on the results attained at this stage of the experimental the following principal conclusions can be made: .....	128
4.2 Part 2: Synthesis and graphitization of resole resin by ferrocene and boron compounds additives .....	130
4.2.1 Viscosity of the plain and modified resoles .....	131
4.2.2 FTIR-ATR analysis of commercial and laboratory synthesized resole resins.....	132
4.2.3 Graphitization of commercial and laboratory synthesized resoles containing ferrocene .....	133
4.2.4 Microstructural analysis .....	138
4.2.5 Chemical changes during the pyrolysis of resole containing ferrocene..	141
4.2.6 Oxidation resistance of carbons derived from modified and unmodified phenol-formaldehyde resin.....	143
4.2.7 Role of boron oxide and boric acid on the atomic arrangement and oxidation resistance of carbon derived from resole resin.....	149
4.2.8 Combined role of ferrocene and boron compounds on the atomic arrangement and oxidation resistance of carbon derived from resole resin....	152
4.3 Part 3: Synthesis and graphitization of lignin-phenol-formaldehyde resins by ferrocene and boron compounds additives.....	156
4.3.1 FTIR-ATR analysis of the as-received and heat-treated lignin .....	156
4.3.2 Glass transition temperature measurement .....	159
4.3.3 Molecular weight measurements .....	159
4.3.4 FTIR-ATR analysis of the lignin-phenol-formaldehyde resins .....	160

4.3.5	Structural organization of carbons derived from pristine lignin-phenol-formaldehyde .....	163
4.3.6	Structural organization of carbons derived from lignin-phenol-formaldehyde formulations containing boron compound additives.....	164
4.3.7	Structural organization of carbons derived from lignin-phenol-formaldehyde formulations containing ferrocene .....	168
4.3.8	Oxidation resistance of the carbon samples prepared from the resin formulations containing boric acid, boron oxide and ferrocene .....	172
4.4	Part 4: Physical and mechanical properties of resin-bonded castables developed based on in-situ graphitization of the binder component .....	175
4.4.1	Castables physical description during the preparation stages .....	176
4.4.2	Apparent porosity and bulk density results.....	176
4.4.3	Cold crushing strength .....	178
4.4.4	Oxidation resistance measurement.....	179
5	CONCLUSIONS .....	183
6	SUGGESTION FOR FUTURE STUDIES.....	187
7	REFERENCES .....	189



## INDEX OF TABLES

	Pag.
Table 2.1: Classification of refractory material based on chemical composition.	8
Table 2.2: Classification of refractories according to refractoriness.....	9
Table 2.3: Comparison of the main features of phenolic resins. ....	17
Table 2.4: Dissociation energy of relevant bonds in phenolic resin network. ....	27
Table 2.5: Peak identification of pyrolysis products of Novolac resin.....	32
Table 2.6: Compared properties of MgO-C bricks prepared using ordinary phenolic resin and the catalyzed resin after coking at 900 °C .....	39
Table 2.7: Selected results on the effects of boron incorporation in phenolic resin. ....	51
Table 2.8: Binding energy of bonds formed during the pyrolysis of boron compounds-modified phenolic resin.....	52
Table 2.9: IR bands and functional groups of cured phenolic resins.....	61
Table 3.1: General information about raw materials and samples description...	65
Table 3.2: Details of the heating steps and mixing techniques carried out to induce graphitization. ....	66
Table 3.3: General information about the materials used during the second experimental stage.....	67
Table 3.4: Description of investigated compositions and samples designations. ....	69
Table 3.5: Information about raw materials used for the preparation of the resin-bonded castables.....	73
Table 4.1: Crystal parameters of pyrolytic carbon samples fired at 1000 °C for 5h under reducing atmosphere (for the composition without HMTA, the results represent the average and standard deviation of 6 measurements in 3 different batches).....	92
Table 4.2: Comparison of the average graphitization level (GL <sub>a</sub> ) for samples prepared with mechanical mixing or with mechanical + ultrasonic mixing. All materials were fired up to 1000 °C for 5h and under reducing atmosphere. ....	97

Table 4.3: Comparison of the average graphitization level ( $GL_a$ ) for samples prepared with mechanical mixing and with or without applying vacuum degassing during the processing steps. All materials were fired up to 1000 °C for 5h and under reducing atmosphere.....	99
Table 4.4: Comparison of graphitization level for the prepared samples produced using different heating rates. ....	101
Table 4.5: Comparison of graphitization level for samples produced using the different heating sequence. ....	103
Table 4.6: Raman and XRD parameters.....	105
Table 4.7: IR bands detected in the plain and cured novolac resin.....	108
Table 4.8: FTIR spectra of novolac resin containing boron source additives heat treated up to 230 °C, 500 °C, and 1000 °C.....	113
Table 4.9: Effect of graphitization, increased addition of HMTA and preparation procedure on the carbons' oxidation resistance.....	124
Table 4.10: Raman and XRD parameters.....	128
Table 4.11: Peaks absorbance intensity of ortho and para linkages .....	133
Table 4.12: Structural parameters of carbon samples derived after pyrolysis of commercial and LSRs at 1000 °C for 5h.....	137
Table 4.13: Effect of graphitization and composition on oxidation stability of resole resin carbons.....	145
Table 4.14: Carbon loss at different temperature range.....	148
Table 4.15: Effect of graphitization and composition on oxidation stability of resole resin carbons.....	151
Table 4.16: Oxidation resistance of carbons obtained from the formulations containing either the individual or combined additives. ....	154
Table 4.17: The average molecular weight and polydispersity index ( $M_w/M_n$ ) values of the as-received and thermally treated kraft lignin. ....	159
Table 4.18: Proportion of ortho and para-substituted linkages.....	162
Table 4.19: Interlayer spacing and crystallite height values of carbon derived from plain LPF resins after thermal treatment at 1000 °C for 5h under reducing environment. ....	164

Table 4.20: Interlayer spacing and crystallite height values of carbon derived from plain LPF resins containing boron compounds after firing at 1000 °C or 1500 °C/5h.....	166
Table 4.21: Interlayer spacing and crystallite height values of carbon derived from LPF resins containing ferrocene.....	171
Table 4.22: Oxidation resistance of carbons derived the lignin-phenol-formaldehyde resins.....	174
Table 4.23: Description of samples designation .....	175
Table 4.24: Apparent porosity of green and fired resin-bonded castables prepared with the plain and modified resole resin. AP = apparent porosity and BD = bulk density.....	177



## INDEX OF FIGURES

	Pag.
Figure 2.1: The crystal structure of graphite. ....	12
Figure 2.2: Reactions leading to novolac resin production. ....	18
Figure 2.3: Reactions leading to resole resin production. ....	19
Figure 2.4: Step-growth polymerization during resole production (stage A prepolymers).....	19
Figure 2.5: Overall reaction sequence for preparing phenolic resin, F:P = formaldehyde to phenol molar ratio. ....	20
Figure 2.6: Three units in lignin chemical structures: (1) 4-hydroxyphenyl (2) guaiacyl (3) syringyl. ....	22
Figure 2.7: Addition reaction of lignin with formaldehyde at the C-5 position of the benzene ring in the guaiacyl unit. ....	23
Figure 2.8: Schematic structure of fully carbonized phenolic resin. ....	28
Figure 2.9: XRD profiles of the carbonized resin as a function of firing temperature. ....	29
Figure 2.10: Initial degradation processes of phenolic resins ....	30
Figure 2.11: Char-forming reactions in phenolic resin systems. ....	31
Figure 2.12: Gas chromatogram of pyrolysis products of cured novolac resin..	31
Figure 2.13: Franklin model for: (a) non-graphitizing, (b) partially and (c) graphitizing carbons. ....	35
Figure 2.14: Structural changes of 004 diffraction profile of coke with HTT under atmospheric pressure and 0.5 GPa.....	36
Figure 2.15: X-ray diffraction profiles of the resin carbon, heat-treated at 2500 °C. (a) catalyzed; (b) uncatalyzed; and Si, an internal standard.....	37
Figure 2.16: XRD profiles of carbon obtained from (a) ordinary phenolic resin (b) catalyzed phenolic resin after pyrolysis at 900 °C, 1200 °C and 1500 °C.....	40
Figure 2.17: Microstructure of carbons prepared by pyrolysis of (a) sucrose in nitrogen at 1000 °C, (b) anthracene at 1000 °C. ....	40
Figure 2.18: Preparation and structure of cured phenolic resin modified with phenylboronic acid. ....	45
Figure 2.19: Curing reaction of phenolic resin- hyperbranched polyborate.....	45

Figure 2.20: Possible structure of cured phenolic resin modified with boric acid .....	46
Figure 2.21: Pyrolysis process of boric acid-modified novolac resin. ....	48
Figure 2.22: Graphitization of novolac resin containing ferrocene. ....	53
Figure 2.23: Example of the generated curve and data by OriginPro software. ....	56
Figure 2.24: Scheme of Raman spectroscopy. ....	57
Figure 2.25: General description of carbon Raman spectra. ....	58
Figure 3.1: Description of the experiments involving novolac resin. ....	64
Figure 3.2: Experimental set-up for the production of resole and lignin-modified phenolic resin. ....	68
Figure 3.3: Description of the experiments involving resole resins. ....	71
Figure 3.4: Description of the experiments involving lignin-modified resins. ....	72
Figure 3.5: Example of the simulation report generated by OriginPro software. ....	77
Figure 3.6: TG profile pointing out parameters used to determine the actual carbon loss of the prepared samples. ....	79
Figure 4.1: X-ray diffraction pattern of novolac resin + 10 wt% HMTA (reference composition) after firing at 1000 °C for 5h using A3-procedure. ....	87
Figure 4.2: XRD profiles showing the effect of boron-based additives on graphitization of a commercial novolac resin (with and without 10 wt% HMTA) after firing at 1000 °C for 5h under reducing atmosphere. ....	88
Figure 4.3: XRD profiles of the evaluated compositions showing the effect of HMTA additions on catalytic graphitization of novolac resin: (a) with boron oxide (b) boric acid as the graphitizing agents after firing at 1000 °C for 5h under reducing atmosphere. ....	94
Figure 4.4: XRD profiles of the prepared samples showing the effect of additional ultrasonic mixing on catalytic graphitization of novolac resin after firing at 1000 °C for 5h under reducing atmosphere. ....	96
Figure 4.5: XRD profiles of the prepared samples showing the effect of vacuum degassing on catalytic graphitization of novolac resin after firing at 1000 °C for 5h under reducing atmosphere. ....	98

Figure 4.6: Effect of heating rates on graphitization of carbonized novolac resin containing: (b-e) boron oxide or (g-j) boric acid as graphitizing agent and (a, f) reference composition.....	100
Figure 4.7: XRD profiles of the evaluated compositions showing the effect of different heat treatment sequence on graphitization of catalyzed novolac resin after firing at 1000 °C for 5h under reducing atmosphere..	102
Figure 4.8: Raman spectra of selected carbon based on differences in heating sequence: carbons from novolac resin containing (a) 10 wt% boric acid (b) 6 wt% boron oxide.....	105
Figure 4.9: FTIR spectra of the graphitizing agents: (a) boric acid (b) boron oxide. ....	107
Figure 4.10: (a) FTIR spectra of plain and cured novolac resin at 230 °C, (b) X-ray diffraction pattern of carbon derived from the plain novolac resin at 1000 °C/5h.....	109
Figure 4.11: (a) Novolac resin + 10 wt% HMTA (reference composition) heat-treated up to 230 °C, (b) X-ray diffraction pattern of reference composition after firing up to 1000 °C and a hold time of 5h. ....	110
Figure 4.12: (a) FTIR spectra of novolac resin composition containing 10 wt% boric acid, heated up to 230 °C/1h, 500 °C/1h and 1000 °C/5h, (b) Structural representation of cured boric acid-modified novolac resin, (c) XRD diffraction pattern of carbon derived from novolac resin containing 10 wt% boric acid....	111
Figure 4.13: XPS spectra of cured and heat-treated novolac resin containing 10 wt% boric acid.....	115
Figure 4.14: B1s high-resolution spectra of cured and heat-treated novolac resin containing 10 wt% boric acid.....	116
Figure 4.15: C1s high-resolution spectra of cured and heat-treated novolac resin containing 10 wt% boric acid.....	117
Figure 4.16: (a) FTIR spectra of novolac resin composition containing 6 wt% boron oxide heat treated up to 230 °C/1h, 500 °C/1h and 1000 °C/5h (b) Structural representation of cured boron oxide-modified novolac resin, (c) XRD diffraction pattern of carbon derived from novolac resin containing 6 wt% boron oxide. .	118

Figure 4.17: XPS spectra of cured and heat-treated novolac resin containing 6 wt% boron oxide.....	119
Figure 4.18: B1s high-resolution spectra of cured and heat-treated novolac resin containing 6 wt% boron oxide: (a) 300 °C, (b) 500 °C, (c)1000 °C/1h, (d) 1000 °C/5h.....	120
Figure 4.19: C1s high-resolution spectra of cured and heat-treated novolac resin containing 6 wt% boron oxide: (a) 300 °C, (b) 500 °C, (c)1000 °C/1h, (d) 1000 °C/5h.....	121
Figure 4.20: (a) Descriptive TG curves (b) Descriptive DSC curves of carbons derived boron catalyzed novolac resin. ....	123
Figure 4.21: XRD profiles showing the effect of different heat treatment sequence on graphitization of catalyzed novolac resin by ferrocene.....	127
Figure 4.22: Raman spectra of selected carbons derived from novolac resin containing 3 wt% ferrocene and 10 wt% HMTA based on two different heating sequence. ....	128
Figure 4.23: Viscosity of commercial and LSR resin with and without ferrocene, boron oxide and boric acid additions at 30 °C. ....	131
Figure 4.24: FTIR-ATR spectra of commercial and the laboratory synthesized resole resins.....	133
Figure 4.25: X-ray Diffraction pattern of uncatalyzed resole resin after carbonization at 1000 °C. ....	134
Figure 4.26: XRD profiles showing the effect of ferrocene additions on the graphitization of carbonized resole resins after 1000 °C.....	136
Figure 4.27: Microstructural and chemical information of carbons derived from Rs and 1.5Rs-5Fc formulations after thermal treatment at 1000 °C for 5 hours under reducing atmosphere: HRTEM images of (a) Rs-A3 and (b) 1.5Rs-5Fc-A3. SAED images of (c) Rs-A3 and (d) 1.5Rs-5Fc-A3. TEM images of (e) Rs-A3 and (f) 1.5Rs-5Fc-A3. Chemical composition of (g) Rs-A3, and (h) Rs-A3 1.5Rs-5Fc-A3. ....	140
Figure 4.28: The XPS Cls spectra of 1.5Rs-5Fc formulation as a function of heat treatment temperatures. ....	142



Figure 4.29: The XPS Fe2p spectra of 1.5Rs-5Fc formulation as a function of heat treatment temperatures.....	143
Figure 4.30: TG curves of carbons derived from (a) plain commercial resin (b) plain and modified 1.5Rs resin (c) plain and modified 2Rs during oxidation resistance measurement.....	144
Figure 4.31: (a) XRD profiles showing the effect of boron compound additives on the graphitization of resole resin carbons, (b) structural description: (1) novolac resin (2) resole resin. ....	150
Figure 4.32: TG curves of carbons derived from (a) plain and boron compounds-modified 1.5Rs resin (b) plain and boron compounds-modified 2Rs during oxidation resistance measurement.....	151
Figure 4.33: Chemical composition of carbons derived from boron compounds-modified resole resin based on EDS analysis (a) 1.5Rs + 10 wt% boron acid formulation (b)1.5Rs + 6 wt% boron oxide formulation. ....	152
Figure 4.34: Diffractogram of carbons derived from resole resins containing boron compounds and ferrocene after pyrolysis at 1000 °C for 5 hours.. ....	153
Figure 4.35: TG curves of carbons derived from resole containing ferrocene, boron oxide, boric acid or the combination of these additives. ....	154
Figure 4.36: As-received and heat-treated kraft lignin samples spectra. ....	158
Figure 4.37: As-received and thermally treated kraft lignin overlaid molecular weight distributions from GPC measurements. ....	160
Figure 4.38: FTIR spectra of lignin-phenol-formaldehyde resins, equivalent unmodified resin and commercial resole product.. ....	161
Figure 4.39: Diffractograms of lignin-phenol-formaldehyde resins carbons after pyrolysis at 1000 °C/5h.. ....	163
Figure 4.40: XRD profiles of carbons derived from lignin-phenol-formaldehyde resins containing boron compounds after pyrolysis at: (a-b) 1000 °C and (c-e) 1500 °C for 5hours.....	166
Figure 4.41: (a) TEM, (b) HRTEM and (c) SAED images of 20LPF-10H carbon sample prepared using sequential heat treatment process up to 1500 °C.....	168

Figure 4.42: XRD profiles of carbons derived from lignin-phenol-formaldehyde resins containing ferrocene after pyrolysis at (a-c) 1000 °C, (d-g) 1500 °C for 5 hours.....	170
Figure 4.43: (a) TEM, (b) HRTEM and (c) SAED images of 20LPF-5Fc carbon sample prepared using sequential heat treatment process up to 1500 °C for 5 hours.....	172
Figure 4.44: TG curves of carbon samples derived from plain LPF resin and the ones containing boron oxide, boric acid and ferrocene (a) 10LPF, (b) 20LPF and (c) 30LPF, synthesized with 10 wt%, 20 wt% and 30 wt% kraft lignin, respectively. ....	173
Figure 4.45: Al <sub>2</sub> O <sub>3</sub> -MgO resin-bonded castables (a) after casting, (b) after curing at temperature up to 110 °C for 24 hours, (c) sample cut from the dried castable and (d) sample fired at temperature up to 1500 °C for 5 hours. ....	176
Figure 4.46: Cold crushing strength of green and fired resin bonded Al <sub>2</sub> O <sub>3</sub> -MgO castables.....	178
Figure 4.47: Oxidation resistance of the resin-bonded castables at temperatures up to 1000 °C. a = oxidation index measurement, b = weight loss measurement. ....	179

## SYMBOLS AND ABBREVIATIONS

- A2** – heating procedure = 100 °C/4h + 500 °C/1h + 1000 °C/5h at 2 °C/min
- A3** – heating procedure = 100 °C/4h + 500 °C/1h + 1000 °C/5h at 3 °C/min
- A4** – heating procedure = 100 °C/4h + 500 °C/1h + 1000 °C/5h at 4 °C/min
- A5** – heating procedure = 100 °C/4h + 500 °C/1h + 1000 °C/5h at 5 °C/min
- BE** – binding energy
- BPR** – boron-containing phenolic resin
- B3** – heating procedure = 80 °C/4h + 100 °C/1h + 150 °C/30mins + 500 °C/1h + 1000 °C/5h at 3 °C/min
- BD** – bulk density
- CCS** – cold crushing strength
- CCRs** – carbon-containing refractories
- C3** – heating procedure = 100 °C/2h + 220 °C/1h + 500 °C/2h + 1000 °C/5h at 3 °C/min
- DSC** – Differential Scanning Calorimetry
- EAF** – electric arc furnace
- EDS** – Energy Dispersive X-Ray Spectroscopy
- F** – formaldehyde
- FTIR** – Fourier Transform Infra-red spectroscopy
- GL** – graphitization level
- GL<sub>a</sub>** – average graphitization level
- HRTEM** – high-resolution transmission electron microscope
- HMTA** – hexamethylenetetramine
- HTT** – heat treatment temperature
- IR** – Infrared
- LPF** – lignin-phenol-formaldehyde
- M** – mechanical mixing
- MO<sub>i</sub>** – mass at onset of carbon oxidation
- M-U** – mechanical mixing + ultrasonic mixing
- M-V** – mechanical mixing + vacuum degassing
- NG** – non-graphitic
- NS** – not significant

**Nv** – novolac resin

**Nv-6B** – Nv + 6 wt% B<sub>2</sub>O<sub>3</sub>

**Nv-10H** – Nv + 10 wt% H<sub>3</sub>BO<sub>3</sub>

**Nv-HMTA** – Nv + 10 wt% HMTA

**Nv-HMTA-6B** – Nv + 10 wt% HMTA + 6 wt% B<sub>2</sub>O<sub>3</sub>

**Nv-1HMTA-6B** – Nv + 1 wt% HMTA + 6 wt% B<sub>2</sub>O<sub>3</sub>

**Nv-5HMTA-6B** – Nv + 5 wt% HMTA + 6 wt% B<sub>2</sub>O<sub>3</sub>

**Nv-HMTA-10H** – Nv + 10 wt% HMTA + 10 wt% H<sub>3</sub>BO<sub>3</sub>

**Nv-1HMTA-10H** – Nv + 1 wt% HMTA + 10 wt% H<sub>3</sub>BO<sub>3</sub>

**Nv-5HMTA-10H** – Nv + 5 wt% HMTA + 10 wt% H<sub>3</sub>BO<sub>3</sub>

**Nv-11HMTA-10H** – Nv + 11 wt% HMTA + 10 wt% H<sub>3</sub>BO<sub>3</sub>

**Nv-12HMTA-10H** – Nv + 12 wt% HMTA + 10 wt% H<sub>3</sub>BO<sub>3</sub>

**Nv-13HMTA-10H** – Nv + 13 wt% HMTA + 10 wt% H<sub>3</sub>BO<sub>3</sub>

**OSHA** – Occupational Safety and Health Administration

**P** – phenol

**RM<sub>f</sub>** – final residual mass

**Rs** – resole resin

**RS** – Raman spectroscopy

**SEM** – scanning electron microscope

**TEM** – transmission electron microscope

**TG** – thermogravimetric

**TGA** – thermogravimetric analysis

**T<sub>g</sub>** – glass transition temperature

**T<sub>i</sub>** – onset of carbon oxidation

**U** – ultrasonic mixing

**V** – vacuum degassing

**XRD** – X-ray diffraction

**XPS** – X-ray photoelectron spectroscopy

**AP** – apparent porosity

**1.5Rs** – LSR with Formaldehyde: Phenol equal to 1.5

**1.5Rs-3Fc** – 1.5Rs +3 wt% ferrocene

**1.5Rs-4Fc** – 1.5Rs +4 wt% ferrocene

**1.5Rs-5Fc** — 1.5Rs +5 wt% ferrocene

**2Rs** — LSR with Formaldehyde: Phenol equal to 2.0

**2Rs-3Fc** — 2Rs +3 wt% ferrocene

**2Rs-4Fc** — 2Rs +4 wt% ferrocene

**2Rs-5Fc** — 2Rs +5 wt% ferrocene

**3Fc** — 3 wt% Ferrocene

**6B** — 6 wt% Boron oxide ( $B_2O_3$ )

**10H** — 10 wt% Boric acid ( $H_3BO_3$ )

**10LPF** — lignin-phenol-formaldehyde resin synthesized with 10 wt% lignin as a substitute for phenol

**10LPF-3Fc** — lignin-phenol-formaldehyde resin synthesized with 10 wt% lignin as a substitute for phenol + 3 wt% ferrocene

**10LPF-4Fc** — lignin-phenol-formaldehyde resin synthesized with 10 wt% lignin as a substitute for phenol + 4 wt% ferrocene

**10LPF-5Fc** — lignin-phenol-formaldehyde resin synthesized with 10 wt% lignin as a substitute for phenol + 5 wt% ferrocene

**10LPF-6B** — lignin-phenol-formaldehyde resin synthesized with 10 wt% lignin as a substitute for phenol + 6 wt% boron oxide

**10LPF-10H** — lignin-phenol-formaldehyde resin synthesized with 10 wt% lignin as a substitute for phenol + 10 wt% boric acid

**20LPF** — lignin-phenol-formaldehyde resin synthesized with 20 wt% lignin as a substitute for phenol

**20LPF-6B** — lignin-phenol-formaldehyde resin synthesized with 20 wt% lignin as a substitute for phenol + 6 wt% boron oxide

**20LPF-10H** — lignin-phenol-formaldehyde resin synthesized with 20 wt% lignin as a substitute for phenol + 10 wt% boric acid

**20LPF-3Fc** — lignin-phenol-formaldehyde resin synthesized with 20 wt% lignin as a substitute for phenol + 3 wt% ferrocene

**20LPF-4Fc** — lignin-phenol-formaldehyde resin synthesized with 20 wt% lignin as a substitute for phenol + 4 wt% ferrocene

**20LPF-5Fc** — lignin-phenol-formaldehyde resin synthesized with 20 wt% lignin as a substitute for phenol + 5 wt% ferrocene

**30LPF-3Fc** — lignin-phenol-formaldehyde resin synthesized with 30 wt% lignin as a substitute for phenol + 3 wt% ferrocene

**30LPF-4Fc** — lignin-phenol-formaldehyde resin synthesized with 30 wt% lignin as a substitute for phenol + 4 wt% ferrocene

**30LPF-5Fc** — lignin-phenol-formaldehyde resin synthesized with 30 wt% lignin as a substitute for phenol + 5 wt% ferrocene

**30LPF** — lignin-phenol-formaldehyde resin synthesized with 30 wt% lignin as a substitute for phenol

**30LPF-6B** — lignin-phenol-formaldehyde resin synthesized with 30 wt% lignin as a substitute for phenol + 6 wt% boron oxide

**30LPF-10H** — lignin-phenol-formaldehyde resin synthesized with 30 wt% lignin as a substitute for phenol + 10 wt% boric acid

## 1 INTRODUCTION

Refractories are materials that can withstand high temperatures, rapid temperature fluctuations and usually possess good resistance to corrosion and erosion by molten metal, glass, slag or hot gases. The principal user of refractories, which account for about 70 % of their total production, is the iron and steel industries [1]. They are applied in lining furnace environments to reduce heat losses and save energy. The importance of these materials cannot be over-emphasized as many of the technological inventions and developments would not have been possible without them.

The recent technology used in steel production demands eco-friendly refractories with improved performance and life cycles. The addition of carbon to these materials has led to an improvement in the chemical and thermomechanical properties of such bricks and castables. These types of products are referred to as carbon-containing refractories (CCRs) and are mainly applied in converters, electric arc furnace, and steel treatment ladles [2]. CCRs' properties are highly dependent on the presence of carbonaceous phases with features close to graphite. Nevertheless, their development is still associated with challenges like performance inconsistency due to inhomogeneous microstructure, poor oxidation resistance and limited compressibility of graphite in the mixture to obtain a dense structure [3].

Graphite is responsible for the excellent thermal shock resistance, good conductivity, lower thermal expansion, and high toughness exhibited by CCRs [4]. Similarly, graphite non-wetting property, which is associated with its crystal orderliness and anisotropic behaviour resulted in compositions with excellent resistance to slag attack.

The materials used to link the coarse and fine refractory particles together is another carbon source in CCRs. Traditionally, coal tar or pitch was used as binder for refractory oxides such as MgO, Al<sub>2</sub>O<sub>3</sub>, which are susceptible to hydration reactions due to their excellent binding action. However, because of environmental/health challenges associated with their use (release of toxic substances), they are being replaced with synthetic thermosetting resins. Phenolic resins (novolac and resole) offer the advantage of minimal emissions of

polycyclic aromatic hydrocarbons and other toxic substances during their pyrolysis thereby providing better environmental and health benefits [5, 6]. In addition, they enhance green mechanical strength, thermal shock resistance and reduce the porosity level of CCRs [7, 8]. However, the unaided pyrolysis of these resins is exclusively a solid-state process without the formation of liquid or semi-liquid components, and usually yield glassy or non-graphitic carbons. Such organic precursors have been considered as non-graphitizable materials because they do not pass through mesophase stage during thermal treatment and produce what is regarded as “hard carbons” at temperatures up to 3000 °C [9]. Moreover, this isotropic carbon is believed to possess inferior oxidation resistance, offers no way to compensate for excess stresses (except by limited microcracks formation) and are therefore highly sensitive to thermomechanical stresses and impact loads [10]. Hence, their usefulness in the development of refractory products for high-temperature applications is still limited [11]. Consequently, there is increasing interest at investigating ways to induce graphitization of thermosetting resin (binder) carbons using processing parameters that can be adopted to produce CCRs. The product from their carbonization can be an additional source of crystalline carbon, which could improve the thermomechanical properties of such refractories. The advantages that can arise from the binder’s crystallization was reported by Grosse et al. [12] and Jansen et al. [3] and highlighted in chapter two.

Several methods based on the application of compressive force, magnetic field, radiation, etc., have been employed to induce the conversion of disordered-hard-carbons into crystalline ones [13-16]. However, the most successful technique that can be adopted for CCRs development may involve the use of graphitizing additives through a process referred to as catalytic graphitization [17]. This approach can lead to the transformation of glassy carbons from phenolic resin to graphitic ones during their carbonization in the presence of some elements or compounds, at a lower temperature and shorter heat treatment time (HTT). Nickel, boron, organometallics (e.g., metallocenes, benzoates, octoates and naphthenates, ferrocene), metal oxides, boron compounds (hyperbranched polyborate, phenylboronic acid, boric acid, hyperbranched polyborate) were



found to be suitable graphitizing agents for disordered carbons [18-22]. These materials can accelerate graphite/graphitic carbons generation at elevated temperatures. The additives are usually incorporated into the thermosetting resins before carbonization. Notwithstanding, the primary objective of several published studies on the subject is the development of carbon-based composites with improved thermal resistance [20-22]. Consequently, less attention has been focused on the applicability of such methods in the production of carbon-containing refractories.

Another essential aspect is the reduction of production cost and environmental friendliness of the resin components. Generally, the development of low cost and eco-friendly phenolic resin through the incorporation of abundantly available lignin agro-based material is beginning to gain attention. Although several studies have been carried out on replacing phenol for lignin in phenolic resin [23-25], the emphasis has not been on their application as a binder for CCRs.

In this study, the influence of several processing parameters and catalytic additives on the generation of graphitic carbons from commercial and laboratory synthesized phenolic resins, as well as the lignin-modified ones, was investigated. Moreover, the effect of in-situ graphitization of CCR binder component was evaluated using  $\text{Al}_2\text{O}_3\text{-MgO}$  castable. The physicomechanical properties and oxidation resistance of the developed refractory with crystalline carbons from the binder component were evaluated.

## **1.1 Statement of the Problem**

1. The emerging trend and innovations in steelmaking technology coupled with demand for refractories with reduced production cost, improved thermomechanical properties, extended lifespan and environmental friendliness have resulted in high interest for the development of novel carbon-based binders.

2. The challenge of poor oxidation resistance and limited service life associated with carbon-containing refractories are aggravated by the isotropic nature of carbons derived from their thermosetting binders.
3. The production cost and environmental friendliness of thermosetting resins is another problem that can be mitigated.
4. The absence of processing specifications and understanding the science of catalytic graphitization is another problem leading to systematic drawbacks in the realization of efficient crystallization of such thermosetting resin.
5. Despite the attempt to induce graphitic carbon generation during carbonization of phenolic resins, it is also important to know if the crystallization will take place in a heterogeneous manner in which the crystalline phase would be isolated in a non-graphitic one (which may affect the overall performance of the refractories).

Consequently, a research study that seeks to provide answers to the problems outlined above has a prospect that is appealing and attractive to produce novel CCRs' with improved thermomechanical properties and extended service life.

## **1.2 Significance of the Study**

The present study will expand understanding and knowledge base of catalytic graphitization of thermosetting resin (phenolic) and provides insight on ways to promote innovation in the development of carbon-containing refractories. The drawbacks associated with CCRs could be mitigated by providing an additional source of crystalline carbons that can lead to improved thermomechanical properties.

### 1.3 Objectives

This research was designed to help in the development of carbon-containing refractories with improved thermomechanical properties by carrying out effective graphitization of their thermosetting resins binder under temperatures and conditions suitable for their production. The catalytic graphitization of commercial phenolic resins and laboratory synthesized ones, which will include environmentally friendly lignin-phenol-formaldehyde resoles, will be studied. Several processing parameters such as vacuum degassing, mixing techniques, heating rates, temperature and graphitizing agents will be selected for investigation.

#### 1.3.1 Specific Objectives

The aim of this research will be achieved through the following specific objectives:

1. To evaluate the effect of graphitizing agents ( $B_2O_3$ ,  $H_3BO_3$ , ferrocene powder) and some processing parameters (i.e., temperature, dwell time, heating rate, cross-linking additives and mixing technique) on the graphitization of commercial and laboratory synthesized phenolic resins for application as a binder in carbon-containing refractories.
2. To synthesize environmentally friendly thermosetting resins based on the replacement of phenol with lignin and promote their graphitization through the addition of graphitizing agents.
3. To carry out chemical, microstructural and thermal characterization of the resulting carbons to establish a relationship between their structures, properties and processing conditions.
4. To ascertain reproducibility and homogeneity level of pyrolytic carbons derived from the carbonization of these catalyzed resins.
5. To conduct physical and thermo-mechanical characterization of carbon-containing refractory castables, developed based on in-situ catalytic graphitization of their binder.



## 2 LITERATURE REVIEW

This section discussed essential aspects of the research work such as refractories, carbon-containing refractories (CCRs), suitable binder materials (pitch, phenolic resin, and lignin-modified phenolic resin), carbonization and catalytic graphitization of carbon derived from non-graphitizable organic precursors, and some relevant techniques employed during the study.

### 2.1 Refractory materials

Refractories are heat-resistant materials with chemical and physical properties that make them applicable for structures, or as components of systems, which are exposed to elevated temperatures. They perform some essential functions that include:

- i. act as a thermal barrier between a hot medium and the wall of the containing vessel;
- ii. prevent wall erosion by the circulating hot medium;
- iii. stand as a chemical protective barrier against corrosion;
- iv. act as thermal insulation to ensure heat retention.

Refractories have found extensive applications in the manufacture of metals, glass, cement, ceramic and petroleum products, and in nuclear industries. However, the iron and steel making industries are the largest consumers of refractories [26]. For such applications, they are usually inorganic, non-metallic, porous and heterogeneous materials composed of thermally stable mineral aggregates, a binder phase and additives. High alumina refractories faced with SiC are used as the linings of the upper stack of a blast furnace to resist abrasion and thermal shock. Flint clay, bauxite bricks are used to line ladles, which are for transport purposes, while unfired resin-bonded alumina-graphite,  $\text{Al}_2\text{O}_3\text{-MgO-C}$  and  $\text{MgO-Al}_2\text{O}_3\text{-C}$ , can be used for treatment ladle. Magnesite-graphite is the typical refractory for lining converters, furnaces and steel ladle.

Refractories are classified based on chemical composition, manufacture methods, physical form or according to their applications. Regarding chemical composition, these materials are classified as acidic, basic and neutral refractories as shown in Table 2.1. The first and second classifications are used in areas where the slag is acidic and basic, respectively. Acid refractories are stable to acids but attacked by alkalis while the basic ones are stable to alkaline materials but react with acids. Neutral refractories are used in areas where slag is either acidic or basic and are chemically stable to both acids and bases.

Table 2.1: Classification of refractory material based on chemical composition.

Term	Reaction	Refractory Material
Acidic	Oxide + H <sub>2</sub> O → acid	Silica, Al <sub>2</sub> O <sub>3</sub> -SiO <sub>2</sub> -products, zircon silicate
Basic	Oxide + H <sub>2</sub> O → base (hydroxide)	Products with magnesia, magnesite and dolomite base
Neutral	Neutral to acids and bases	Alumina, zirconia, chromite, picrohromite, spinel, forsterite

According to their physical form, refractories are grouped into shaped and unshaped. Shaped refractories that have fixed size and configuration are further divided into standard and special shapes. Standard shapes have dimensions, which are conformed to by most refractory manufacturers and are generally applicable to kilns or furnaces of the same types. The ones with unique appearance are made for specific kilns or furnaces. Unshaped or monolithic refractories are without a definite form and their structure is defined upon application. The typical examples are plastic masses, ramming masses, castables, gunning masses, fettling mix and mortars.

Based on refractoriness, refractories are classified as shown in Table 2.2.

Table 2.2: Classification of refractories according to refractoriness.

<b>Types of Refractories</b>	<b>Refractoriness (°C)</b>	<b>Example</b>
Low heat duties refractories	1520-1630	Silica bricks
Intermediate heat duties refractories	1630-1670	Fireclay bricks
High heat duties refractories	1670-1730	Chromite bricks
Superheat duties refractories	>1730	Magnesite bricks

To a lesser extent, refractories are also classified according to their manufacturing techniques as [4]:

- i. Fused cast
- ii. Hand moulded
- iii. Formed (Normal, fired or chemically bonded)
- iv. Unformed (Monolithic- Plastic, ramming and gunning mass, castables).
- v. Dry press process.

Refractories manufacturing is based on knowing what combination of chemical compounds and materials will produce the required refractoriness, thermal stability, corrosion-resistant, thermal expansion and other essential properties.

The bricks production process can be grouped into four, namely: raw material processing, forming, firing, and final processing. The raw materials preparation steps include crushing, grinding and size classification. This may be followed by calcining and drying when necessary. During the forming stage, the refractory oxide(s), binder and other additives are mixed together and cast into the desired shapes in a prepared mould. The firing stage involves heating the materials to high temperatures in a kiln (continuous or periodic) to form the ceramic bond and achieve the required properties. The final processing involved milling, grinding, and sandblasting of the finished product.

However, the manufacturing process for monolithic refractories is different because they do not need to be pre-shaped and pre-fired. Many of the castables are prepared by mixing aggregate of various particle size and matrix components

together. Homogeneity is of great importance to achieve optimum performance. The materials overall size distribution and uniformity will determine the quality of the composition. Four stages are involved in their manufacturing, which are crushing, grinding, classification by size and mixing.

## **2.2 Carbon-containing Refractory Materials**

Continuous demand for refractories that can withstand high working temperatures, possess long refractory life, withstand tough working conditions and perform optimally in service has led to the development of carbon-containing refractories. These enhancements are mainly due to carbon's high thermal resistant, good thermal shock characteristic and excellent corrosion resistant. Carbon comprising refractories do not have well-ordered crystalline structure as this depends on the initial raw materials and the temperature attained during manufacturing [4].

These types of refractories are formulated based on their expected service conditions, furnace type, and the slag composition that they will be in contact with during usage. They are mainly based on either individual or combinations of up to six oxides, namely:  $\text{SiO}_2$ ,  $\text{Al}_2\text{O}_3$ ,  $\text{MgO}$ ,  $\text{CaO}$ ,  $\text{Cr}_2\text{O}_3$ ,  $\text{ZrO}_2$  and carbon [4]. However, magnesium oxide ( $\text{MgO}$ ) and alumina ( $\text{Al}_2\text{O}_3$ ) are the primary coarse components commonly used for the preparation of CCRs. The formulations comprised of a suitable range of all the various materials to balance thermal shock resistance and slag infiltration [4]. The bricks behaviour depends on the aggregates' physical and chemical characteristic.

$\text{MgO}$  (seawater, fused and sintered magnesia) is used because of its high strength and good resistance to chemical attack. The high-temperature firing of magnesium hydroxide extracted from seawater will produce seawater magnesia, whereas fused magnesia is obtained when this oxide is fused in an electric furnace and sintered magnesia is produced from natural magnesite [4, 27]

Generally, the refractories compositions consist of 80-93 wt%  $\text{MgO}$ , 7-20 wt% graphite and 2-3 wt% of antioxidants [27, 28].  $\text{MgO}$ -C bricks are produced under high pressure involving uniaxial pressing and are usually of the unburned



type. Green MgO–C bricks have low porosity (2–5 vol. %). The porosity of the brick is determined by the behaviour of the raw materials, the type and technique with which the binder is added to the mix, and the efficiency of the press used [27]. These refractories have found wide applications in areas such as basic oxygen furnaces, electric arc furnaces (EAF), and steel ladles. They are used in EAF because the high graphite content maximizes thermal conductivity and in steel ladles because of their resistance to slag attacks.

### **2.2.1 Roles and challenges of carbon in carbon-containing refractories**

Carbon can act as an additive or participate in the formation of the refractory structure and provide some specific properties. As an additive, the preformed and fired refractory brick is impregnated in the carbon-based binder (pitch) under vacuum and subsequently heated to fill the pore with carbon. For it to participate in the refractory structure formation, the oxide components are mixed with graphite and binder, shaped and subsequently fired [29]. Consequently, both ordered and disordered carbons are usually present in CCRs through the addition of graphite (the primary source of carbon for CCRs), carbon black and carbons derived from the binder phase.

Natural graphite flake because of its excellent crystalline structure (Figure 2.1), anisotropic characteristic and wetting ability is still the best carbon source for CCRs. These characteristics provide them with the ability to withstand high temperature, possess good slag corrosion resistant and thermal properties. Moreover, graphite releases lesser amount of volatiles products, does not form unwanted phases and accelerate the refractory materials heating [the thermal conductivity of graphite (96.3 W/mK at 1000 °C) is higher than the usual refractory oxides (10.1 W/mK at 1000 °C for MgO, 9.5 W/mK at 1000 °C for Al<sub>2</sub>O<sub>3</sub>)] during sintering.

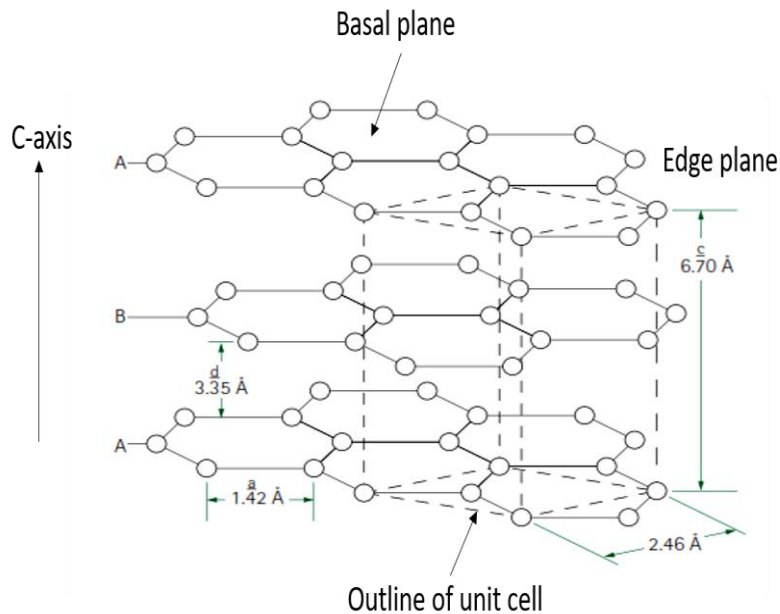


Figure 2.1: The crystal structure of graphite.

Graphite significant role in CCRs can be summarized thus:

- a. It fills the brick structure and covers the spaces in the refractory grains.
- b. Due to its wettability characteristic, graphite prevents slag penetration into CCRs [30, 31]. However, it must be noted that the chemical composition of the slag affects graphite's non-wetting characteristics [32].
- c. Enhanced the bricks thermal shock resistance because of its high thermal conductivity and low thermal expansion characteristics.
- d. It has excellent mechanical properties at low and elevated temperatures.

Despite the many advantages offered by graphite incorporation in CCRs, its inclusion can also lead to many possible drawbacks [33, 34], as outlined below:

- i. Increased oxidation of carbon during the steelmaking process (lancing) can lead to carbon pick up, which can result in a porous structure with poor mechanical strength, decrease corrosion resistance and eventually increase slag penetration. Moreover, this challenge can also occur during ladle preheating (in ambient atmosphere) resulting in refractory de-bonding and increased porosity.

- ii. The reaction between the oxide and graphite. For example, at 1400 °C, a dense layer of MgO is formed at the slag-castable interface in a MgO-C refractory system as shown in equation 2.1 and 2.2. Despite the benefit associated with the reaction, it also results in graphite consumption, which decreases the refractory corrosion resistance and can lead to higher porosity.



Nevertheless, this challenge does not apply to alumina-carbon system. Based on  $\text{Al}_2\text{O}_3$ -C binary phase diagram [35, 36], alumina carbothermic reduction has been reported to occur at high temperatures around 1900 °C to 2200 °C under atmospheric condition. The reaction can occur according to equation 2.3 and include the formation of other volatiles such as  $\text{Al}_2\text{O}_{(g)}$  and  $\text{CO}_{(g)}$ . Consequently, the reaction between alumina and graphite can be ignored since the temperature at which it occurs is higher than what is typically used during a steel-making process (1600 °C).



- iii. Due to high refractory conductivity, there can be increase in energy loss and ladle metal shell temperature, which can result in its deformation and eventual damage.
- iv. Greenhouse effect due to carbon loss is also under consideration since CCRs are prepared with up to 20 wt.% carbon.
- v. The reaction between carbon and easily reducible oxides such as FeO can cause corrosion of CCRs. However, MgO has little wettability for molten steel and possess a higher resistance to chemical attack by ferrous alloys. Consequently, the combinations of MgO with graphite possess a combined advantage to minimize both slag and metal attack.
- vi. More so, graphite's lamellar morphology and the large density difference with refractory oxides limits their dispersion, facilitate segregation, impair

densification during processing, which can lower the bricks overall mechanical strength (high porosity) and increase their susceptibility to high-temperature oxidation [37, 38].

Out of all the highlighted challenges, the importance of improving the carbon oxidation resistance in CCRs cannot be over-emphasized. The rate of carbon oxidation at temperatures below 1400 °C is very high [39], and graphite oxidation mechanism can be summarized into three; solid-gas reactions, solid-liquid reactions and solid-solid reactions [40]. The kinetics of such transformations increases exponentially with temperature. The low-temperature process is believed to be dependent on the rate at which oxygen interactions occur on the carbon active surface area, whereas at higher temperatures, oxidation is driven by a diffusion-controlled regime [41]. According to Ghosh et al. [42], the oxidation rate of MgO-C in air can be divided into three:

- i. From 800-1400 °C: The oxidation rate increased with temperature. At this stage, oxidation is believed to be controlled by a porous decarburized layer (pore diffusion mechanism) [43].
- ii. From 1400-1600 °C: The oxidation rate is more or less constant.
- iii. Above 1600 °C: The oxidation rate reduces due to subsequent deposition of MgO. At these temperatures, Mg vapour will be formed due to the reduction of MgO by carbon, which will consequently be oxidized to MgO near the surface where oxygen partial pressure was high.

Consequently, attention has been given to the development of CCRs with reduced carbon content. One of the approaches involves the use of carbon nanoparticles and nanometer-sized particulate additives. The choice of nanoparticles offers the advantage of increased surface area, resulting in a wide distribution of carbon particles (even at low percentages) within the entire matrix of the castables or bricks [33, 44, 45]. The nanometer-sized additives fill up the interior pores and gaps between the various refractory materials particles, improves their resistance to thermal shock, oxidation, and corrosion [42]. However, the challenge remains the ability to lower the graphite content without sacrificing the beneficial thermo-chemical properties.

Another approach involved the use of antioxidant additives. The antioxidants that are often used in CCRs include Al, Si and B<sub>4</sub>C. These additives can react with oxygen to form protective oxides and prevent carbon oxidation or act by reducing CO to C [46]. Furthermore, depending on the type of antioxidant used, their presence can lead to the formation of carbides and nitrides' whiskers with different shapes, dimensions and distributions. These intermetallic compounds have been reported to produce a positive impact on the mechanical properties of such refractories [46, 47].

Carbon black is another carbon source. It is produced through the incomplete combustion or thermal decomposition of hydrocarbons (such as coal tar, ethylene cracking tar) under controlled conditions. It is virtually a pure elemental carbon in the form of colloidal particles with a physical appearance like a black, finely divided pellet or powder. It is mainly in spherical form but with different ash content, depending on the manufacturing process. Unlike graphite, carbon black is not crystalline. According to Fan et al. [48], for a low-temperature application ( $\leq 1000$  °C), no significant difference in mechanical properties was observed in a CCR system (Al<sub>2</sub>O<sub>3</sub>-C) when graphite flake or carbon black was used after coking at that temperature. However, for high-temperature applications, the thermomechanical performance of graphite flake containing Al<sub>2</sub>O<sub>3</sub>-C was found to be better than those of the carbon black containing refractory.

In addition to their binding role, the binder component of carbon-containing refractories is another carbon source after sintering. Coal-tar pitch, furan resin, and phenolic resin are typical binders used for CCRs production due to their excellent compatibility, dispersibility, press-mouldability and high residual carbon after firing.

### **2.2.2 Binders for carbon-containing refractories**

Pitch and phenolic resins are the primary binders used for the production of carbon-containing refractories. The advantages and challenges associated with their usage are discussed briefly in this section.

**i. Pitch**

Pitch is a carbonaceous binder that undergoes pyrolytic decomposition to form a carbon bond for various high-temperature-resistant products. It is produced by distillation of high-temperature coke-oven tars or petroleum. Its ability to form carbon bond has long been employed in the production of specialized refractory materials [49]. At the initial stage of heating pitch binder, decomposition occurs with significant physical changes such as dehydration, formation of a transitional moulding phase, micro-cracking and structure modifications. The final structure consists of stable residual carbon in a disordered amorphous phase. Pitch graphitization in refractory compositions might result in a liquid phase formation within their microstructure at high temperatures [50]. The process helps to generate crystalline carbon, which provides better oxidation resistance and minimize the bricks dissolution by slag. Although the working temperatures during application of coal-tar bonded refractories do not allow for complete graphitization, the obtained carbons show properties close to that of graphite. More so, pitch-bonded refractories show excellent resistance to thermal shock and conductivity (compared to the thermosetting resins bonded ones). The tar also possesses the advantage of providing fluidity in the refractory composition during the mixing process and it is cheaper. Despite these advantages, there have been some demands to replace pitch/tar in CCRs because of environmental issue (release of toxic substances such as carcinogenic aromatics, notably benzo[a]pyrene) associated with its production and use. In addition, pitch does not offer the benefit of cold-mixing technology in refractory production.

**ii. Phenolic Resin**

Phenolic resins are a better environment-friendly alternative to benzo[a]pyrene rich coal tar pitch. Hence, they are the most commonly used organic binder in the production of CCR bricks [50]. These polymers are classified into two broad groups, namely, novolacs and resoles, according to the molar ratio of the reactant compounds used for their synthesis (i.e., formaldehyde to phenol ratio). Both types are used as a binder for CCRs production. Their production mechanism usually involved a condensation polymerization reaction, leading to

the release of water. Some of the differences that exist between these two groups are summarized in Table 2.3.

Table 2.3: Comparison of the main features of phenolic resins [5].

<b>Kind of resin</b>	<b>Catalyst</b>	<b>Molar F/P</b>	<b>Physical state</b>	<b>Stability of products</b>	<b>Functional groups</b>
Resole	Base or Metal salt	$\geq 1$	Liquid, solid, solution	Limited	Methylol, Phenolic
Novolac	Acid or metallic salt	$<1$	High viscous material	Stable	Phenolic

Novolacs are phenolic resins with formaldehyde to phenol molar ratio of less than one. The resins are produced by an acid-catalyzed reaction of excess phenol with formaldehyde. The polymerization is brought to completion using catalysts such as hydrochloric acid, oxalic acid and sulfonic acids. The phenol units are mainly linked by methylene and/or ether groups at either the ortho or para positions of the phenolic aromatic rings. It usually proceeds as described in Figure 2.2. During the synthesis of novolacs, protonated formaldehyde reacts forming an electrophile, which reacts with nucleophilic phenol ring to produce methylol ketone that gives rise to para and ortho methylol phenols. Methylol phenol precursors can then react with phenol, formaldehyde or with themselves via a water producing condensation reactions [51].

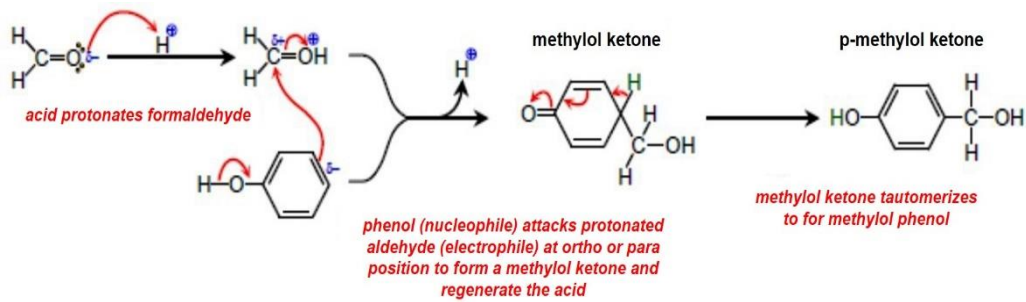


Figure 2.2: Reactions leading to novolac resin production [51].

Novolac resin cross-polymerization occurs at temperatures from 150 °C in the presence of a cross-linking agent (typically hexamethylenetetramine), which decompose to produce formaldehyde and ammonia [52]. The phenol units in different novolac chains are connected by the methylene bridges. According to Gardziella et al. [5], the curing reactions occur in two stages. In the first step, intermediates such as benzoxazines ( $C_8H_7NO$ ) and benzylamines ( $C_6H_5CH_2NH_2$ ) are formed. The second stage involves decomposition, oxidation, and/or further reactions of the initial intermediates into methylene that connects phenolic rings and other minor functional groups such as amines, amides/imides, imines, methyl phenol, benzaldehyde.

Resoles are base-catalyzed phenol-formaldehyde resins prepared from formaldehyde (F) and phenol (P) based on F:P greater than one. For this preparation, resole, phenol, formaldehyde and catalyst are mixed in the desired amount (depending on the desired resole type) and heated inside a vessel. The initial stage of the reaction, which occurred at around 70 °C, forms a thick reddish-brown tacky material that is rich in hydroxymethyl and benzylic ether groups. For this reaction, the base ( $^-OH$ ) catalyst deprotonates phenol to form phenoxide that reacts with formaldehyde and produce methylol phenoxides as described in Figure 2.3 [51].



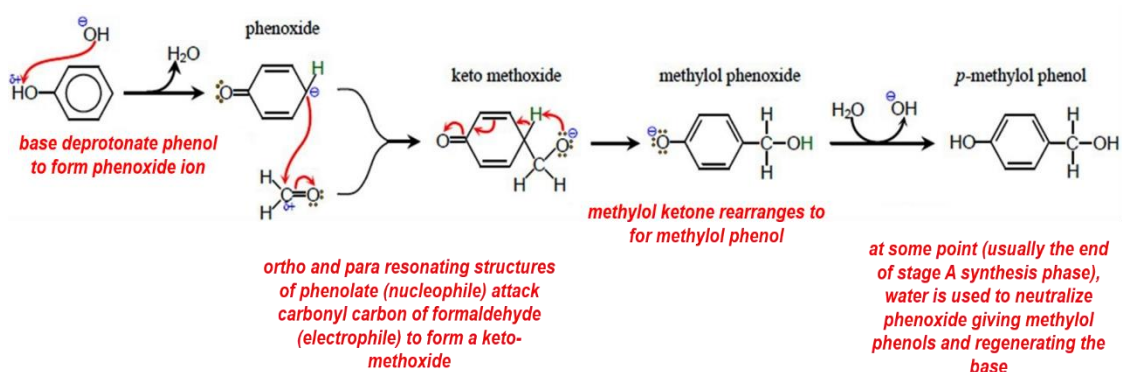


Figure 2.3: Reactions leading to resole resin production [51].

The initial stage of resole production (stage A) involving the formation of methylene-linked and methoxy-linked phenols dimers and trimers such as dihydroxy mono and disubstituted phenyl methanes, and ethers as shown in Figure 2.4. These undergo step-growth polymerization to form substituted poly phenol methylene-linked oligomers (A-staged pre-polymers). Unlike novolac, it can be hardened by heat without the addition of cross-linking agents.

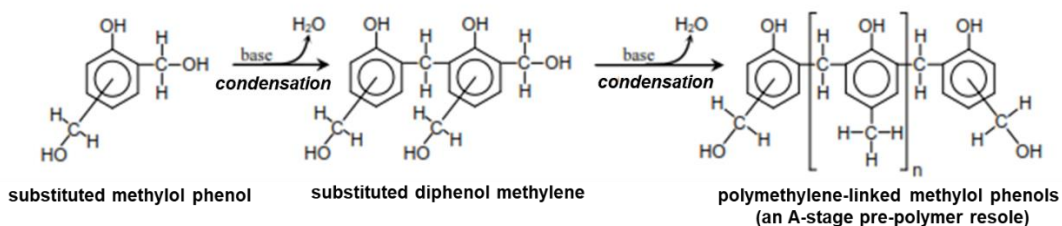


Figure 2.4: Step-growth polymerization during resole production (stage A prepolymers) [51].

The overall reaction sequence for preparing phenolic resins can be represented as shown in Figure 2.5. The final cured resin matrix usually contained methylene and ether links.

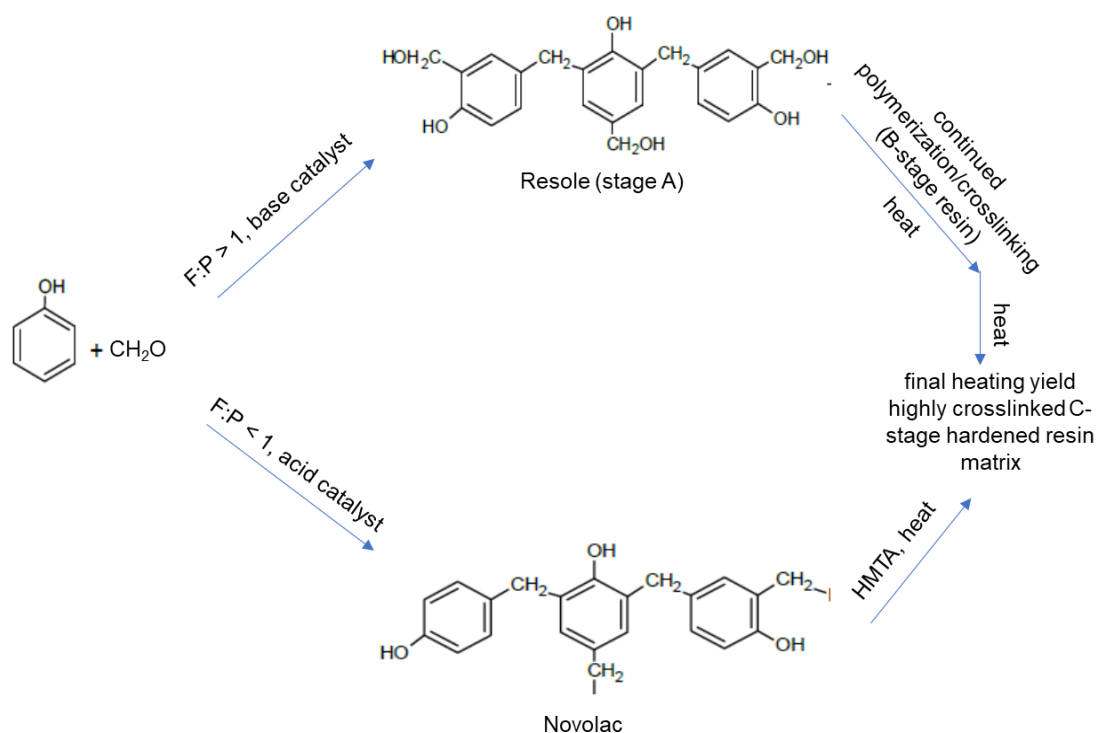


Figure 2.5: Overall reaction sequence for preparing phenolic resin, F:P = formaldehyde to phenol molar ratio.

The use of thermosetting resins as a binder in CCRs offers the following advantages, which can be limited by their chemistry:

- i. Cold mixing technology and reduced energy consumption during refractory processing compared to pitch [8].
- ii. A high ratio of fixed carbon can be generated after their pyrolysis [54].
- iii. Their products do not pass through a liquid phase as pitch-bonded refractories [1].
- iv. Low emission of hazardous materials compared to tar.
- v. They offer excellent adhesion to oxygen/oxide-free filler and provide better flow parameters [8].
- vi. The resin bonded refractory products possess high green mechanical strength with superior heat resistant because of the 3-dimensional structure of the polymer formed during curing [1, 54].
- vii. The isotropic glassy carbons from these resins can compensate for the high thermal expansion coefficient of MgO [55].

- viii. More so, Wu et al. [56, 57] and Khanna et al. [58], suggested that carbon derived from thermosetting resins may have better resistance to dissolution in iron alloys.

Despite these benefits, carbons derived from these resins possess inferior oxidation-resistance compared to graphite because of their isotropic nature. They are classified as “hard carbons” and are therefore non-graphitizable at temperatures as high as 3000 °C [9]. In addition, they possess limited ability to compensate for excess stress (except by microcracks formation), which can affect the CCRs thermomechanical properties [10, 50].

The total amount of generated carbon can be described as a balanced function of the original carbon content in the resin and the quantity of volatile components that escape during pyrolysis. The amounts of evolved carbon oxides also described the sensitivity of the resin in an oxidizing environment. The volatiles produced during carbonization depend on crosslink density and configuration of the molecules before and after curing as well as the presence of heteroatoms in their chemical structure [1, 5]. Consequently, both the resin chemistry and external variables such as temperature will affect the overall carbon yield.

The resin viscosity is another critical feature in refractory preparation as it affects mixing time, resin capacity to wet the components, ability to compact and final fluid composition. The environment/temperature influences this property. At summer, when viscosity can be low, the refractory brick green mechanical strength can reduce. However, in winter, viscosity increases leading to dispersion problem [59]. For example, novolac resin viscosity should be around 8000 cps to ensure proper mixing of the raw materials during the refractories production.

### **iii. Lignin-modified phenolic resin**

The use of green materials provides an alternative way to solve environmental problems associated with bio-based processes. Their by-products can be obtained in abundance, at low cost and are from renewable biomass. All

these advantages provide an opportunity for the development of low cost and environment-friendly materials for various engineering applications.

Furthermore, fluctuation in oil price and concerns associated with exposure to phenol during production have led researchers to investigate the used of bio-based materials from renewable resources as phenol substitute in phenolic resins production [23, 60]. Occupational Safety and Health Administration (OSHA) has set the daily permissible exposure limit (8 hours/day and 40 hours/week) to phenol as 19 mg/m<sup>3</sup>. Lignin, a by-product of many agro-based processes such as pulp, paper and bioethanol industries can serve as an alternative replacement to phenol in the synthesis of phenolic resin [5]. It is a sustainable material with an annual production estimated in the range of 5–36 x 10<sup>8</sup> tons [61]. It is also an amorphous biopolymer with a complex chemical structure comprising a repeating unit of 1-(*p*-hydroxyphenyl) propane-3-ol that have methoxyl group in the *ortho* position of the phenolic ring. Lignin consists of three primary building blocks or units, which are guaiacyl (G), syringyl (S) and *p*-hydroxypropane (*p*-H) as described in Figure 2.6. Consequently, it can be classified as a polyphenolic compound. It can exhibit various structures, depending on the vegetal species it is derived from.

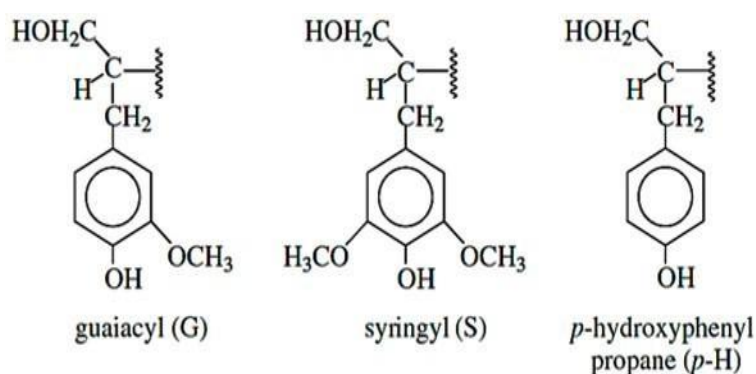


Figure 2.6: Three units in lignin chemical structures: (1) 4-hydroxyphenyl (2) guaiacyl (3) syringyl [62].

Lignin possesses the ability to react with formaldehyde at the C-5 ortho position of the aromatic ring of the guaiacyl unit (Figure 2.7) and at the C-β location in the phenylpropane unit [25]. Lignin reactivity depends on the functional

groups such as methoxyl groups, phenolic and aliphatic hydroxyl groups and aldehyde groups in its structure. These functional groups occupy the interunit linkages, thereby limiting its ability to react [63].

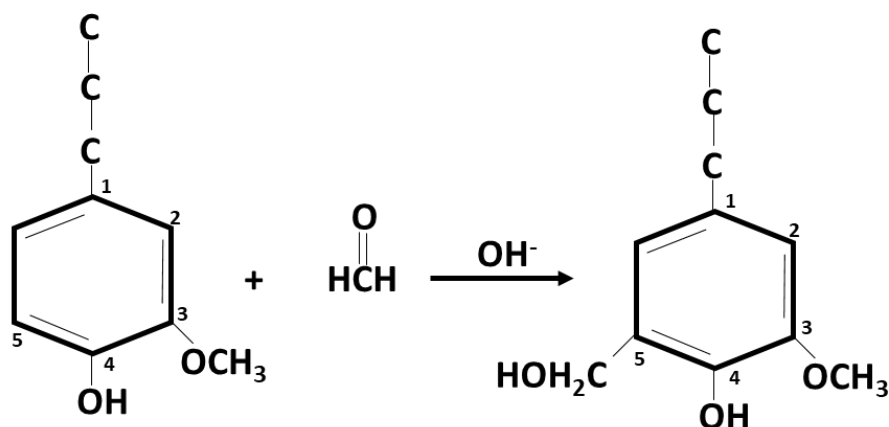


Figure 2.7: Addition reaction of lignin with formaldehyde at the C-5 position of the benzene ring in the guaiacyl unit [64].

Although it can be obtained from different pulping processes, only liginosulfonates are available in large commercial quantities making them attractive for the synthesis of lignin-phenol-formaldehyde resin (LPF). Ammonium liginosulfonates has been reported as the most suitable candidate from the family of liginosulfonates to produce phenolic resins because of their solubility in an organic solvent [23, 65]. Nevertheless, this type has higher molecular weight and lower reactivity compared to organosolv lignin and kraft lignin [66-71]. Consequently, kraft and organosolv lignin could be a more appropriate alternative to synthesize LPF resins. Nevertheless, the feedstock from which the lignin is derived plays a more significant role in determining their suitability for phenolic resins production. Generally, softwoods lignin contains a higher amount of G-component unlike the hardwood ones, which comprise G and S-components. Hydrolysis lignin [72-74], soda lignin [75] and biorefinery residue [76, 77] have also been used to produce lignin-modified phenolic resins.

The synthesis of lignin-modified phenolic resins has been the subject of several research studies [24, 25, 75]. The different types of lignin that are used

for this purpose are usually rich in hydroxyl group in the aromatic ring, less in methoxyl group and low molecular weight [78].

Due to its low reactivity toward formaldehyde efforts have been geared toward addressing this aspect through techniques such as methylation, phenolation and demethylation [23, 60, 79]. The first two methods introduce reactive functional groups to lignin molecules while the third modifies lignin to form catechol moieties in lignin macromolecule [60]. Methylation reaction is usually carried out in an alkaline medium with formaldehyde [80]. During this process, hydroxymethyl group is added to the lignin structure. Phenolation process by mixing lignin, phenol, NaOH and water and heating the mixture to temperatures between 80 °C and 100 °C [81]. This technique introduced more phenolic groups, cause ether cleavage and decrease the lignin molecular weight. Regarding demethylation, one or two methoxyl groups are removed from the ortho positions in lignin structure and converted to a more reactive hydroxyl group [60].

Other techniques such as reduction, selective oxidation of  $\beta$ -O-4 linkages using nitrobenzene [82, 83], sulfonation [84] and hydrolysis have also been studied to improve lignin reactivity or produce phenolic compounds from lignin.

The disadvantages of these methods are the additional time, energy and chemical cost involved. Consequently, at the moment, these processes may not be economically attractive for industrial applications [60].

Based on the literature considered in this review, cured lignin-modified phenolic resins show improved thermomechanical characteristics compared to the conventional resins [24, 25, 76, 78, 85, 86].

Although several investigations have been carried out on the production of LPF resin, such studies have not involved graphitization of the resulting carbons. Moreover, the applicability of the lignin-modified resins for the development of CCRs has not been extensively investigated. However, the study by Wang et al. [87] shows that LPF can enhance the thermomechanical properties of CCRs such as  $Al_2O_3$ -C. The lignin substitution degree for phenol was 30 wt% in the modified resin with formaldehyde:phenol molar ratio equal to

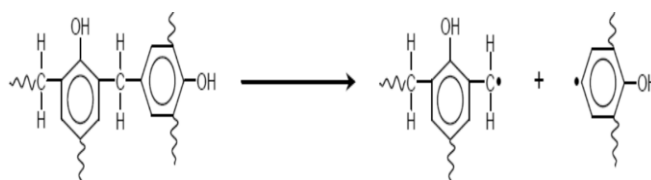
1.5. The reaction was catalyzed with NaOH and silicon particles were incorporated into the synthesized resin.

### 2.3 Phenolic resin pyrolysis: carbonization mechanism, degradation pathway and characteristic of the derived carbons

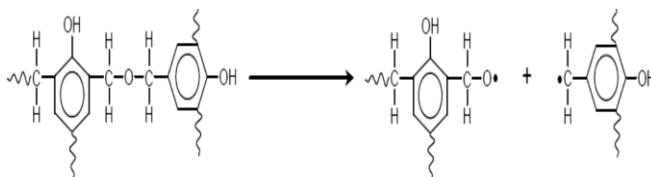
The production of glassy, non-graphitic carbon from phenolic resins is exclusively a solid-state process without the formation of liquid or semi-liquid components. Hence, they are classified as non-graphitizable organic precursors since graphene planes alignment is prevented during pyrolysis at temperatures up to 3000 °C [9]. The carbon-carbon chains remain intact, coalescing with their neighbours while heteroatoms are driven off [16]. The final material is substantially isotropic in nature. The term non-graphitic (and not amorphous) has also been suggested to be more appropriate since such carbon still presents some limited (nanometre scale) atomic organization.

The thermal degradation of free radical polymeric material is not always a straightforward concept because of the numbers of possible conditions and parameters that can have significant effect on the reaction rates and activation energies [51]. Lee [51] classified bonds cleavage during the pyrolysis of phenolic resin into seven categories:

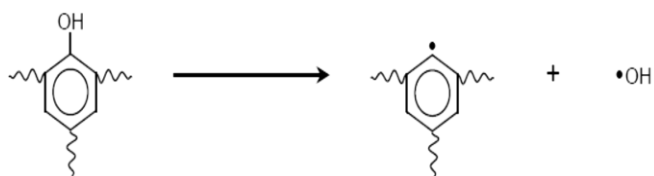
i. Cleavage of methylene link to form benzyl and phenyl radicals.



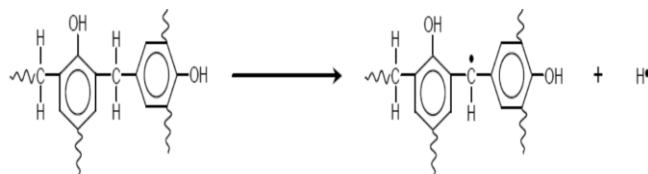
ii. Cleavage of methoxy link to form a benzoxy and benzyl radicals.



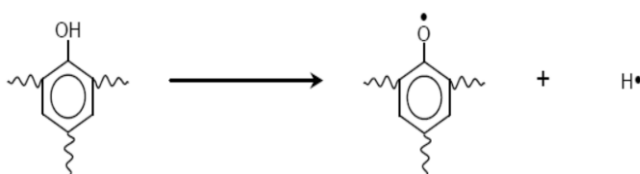
iii. Cleavage of hydroxyl link to form a phenyl and hydroxy radicals.



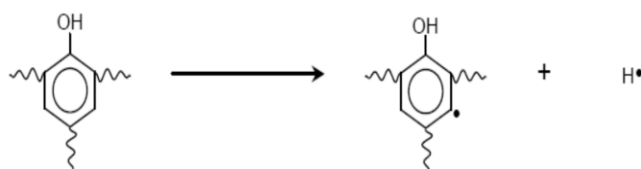
iv. Cleavage of methylene hydrogen to form diphenyl methyl radical.



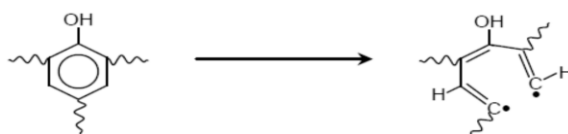
v. Cleavage of hydroxyl hydrogen to form phenoxy radical.



vi. Cleavage of primary phenyl hydrogen to form phenyl radical.



vii. Cleavage of the aromatic ring to produce a linear diradical (a ring-opening process).



According to Lee [51], the thermal degradation process is expected to proceed in an order described above since some radicals are more stable than others. The author suggested that methylene cleavage is the initial point during thermal degradation of phenolic resin. However, the bond rupture may not necessarily follow a simplified route. For example, if the phenyl ring remains intact, the associated phenyl-hydrogen bond also stays until later in the process. Nevertheless, the transformation order depends on the binding energies of the various bonds. The bond dissociation energies in a phenolic network are presented in Table 2.4.



Table 2.4: Dissociation energy of relevant bonds in phenolic resin network [51].

Bond description	Formula	kJ/mol
Benzyl-benzoxy (ether) link	$C_6H_5CH_2-OCH_2C_6H_5$	280
Hydrogen-phenoxy link	$H-OC_6H_5$	331
Phenyl-methylene link	$C_6H_5-CH_2C_6H_5$	333
Hydrogen- methylene link	$C_6H_5H - CHC_6H_5$	334
Hydrogen-benzene link	$H-C_6H_5$	463
Hydroxy-phenyl link	$OH-C_6H_5$	470
Carbon=carbon benzene link	$\sim CH_2=CH_2\sim$	503

According to Chang et al. [88], complete destruction via this route should produce a mixture of aliphatics. However, methane was the only aliphatic detected at temperatures up to 1400 °C, indicating that phenyl rings are not generally disintegrated during pyrolysis. Therefore, the mechanism leading to carbon formation did not involve phenyl ring fusion [51]. Moreover, the decomposition process does not usually result in a complete breakdown of the methylene structure. The final carbon structure is usually visualized as comprising of randomly spaced 6-member  $sp^2$  carbon that is strongly bonded within a network of  $sp^3$  crosslink (Figure 2.8). This linkage prevents mesophase formation and the necessary rotation required for graphite generation during carbonization. Hence, the original cross-linkages are substantially retained and it bears a resemblance to the organic precursor [51].

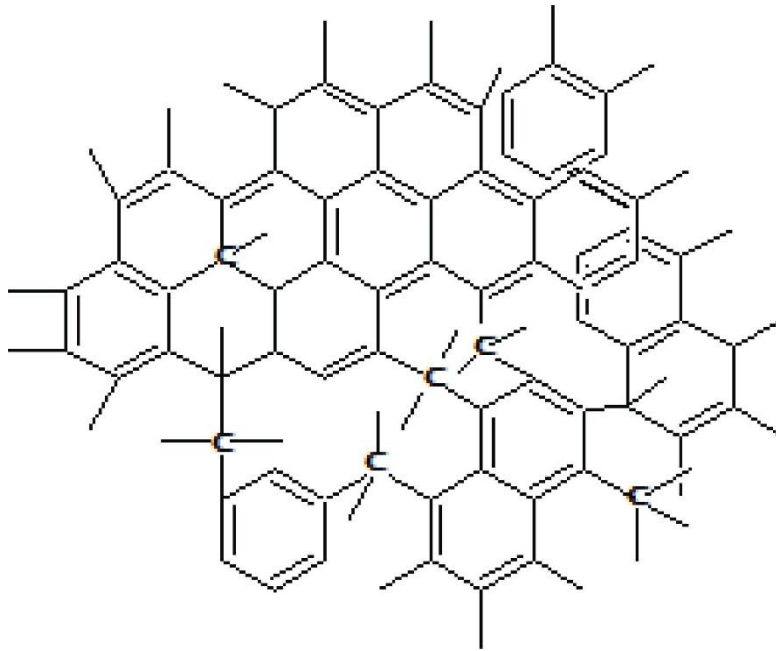


Figure 2.8: Schematic structure of fully carbonized phenolic resin [51, 89].

The microstructural changes and density variation that occurs during the carbonization of phenolic resin was monitored by Ko et al. [90]. The diffraction profiles of the resin after heat treatment at different temperatures, ranging from 100 °C to 2400 °C was presented in Figure 2.9. The chemical evolution was characterized by the appearance of a broad peak at 19° up to 600 °C after which it completely disappeared. At 500 °C, a new peak appeared at ~23° and shifted to ~25° when the temperature reached 600 °C. More so, another peak emerged at 43° corresponding to (010) reflections plane. This peak was ascribed to glassy carbon formation. Due to lengthening and broadening of the carbon basal planes, the intensity of these peaks increased slightly with increasing temperatures.

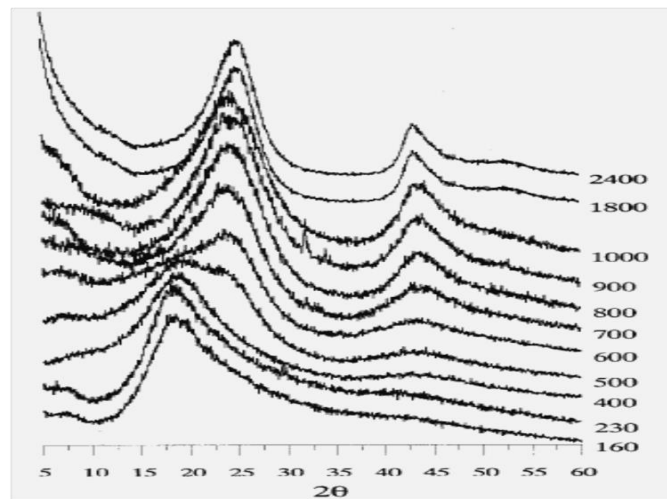


Figure 2.9: XRD profiles of the carbonized resin as a function of firing temperature [90].

Conley and Quinn [91], proposed a model for the degradation and char-forming reactions during phenolic resin pyrolysis in a book titled “Flame-Retardant Polymeric Materials” as shown in Figure 2.10 and 2.11. Figure 2.10 summarized the initial degradation that occurs when the resin was heated in the air between 120 °C and 250 °C. The ether bond plays a significant role in the oxidative degradation of phenolic resins.

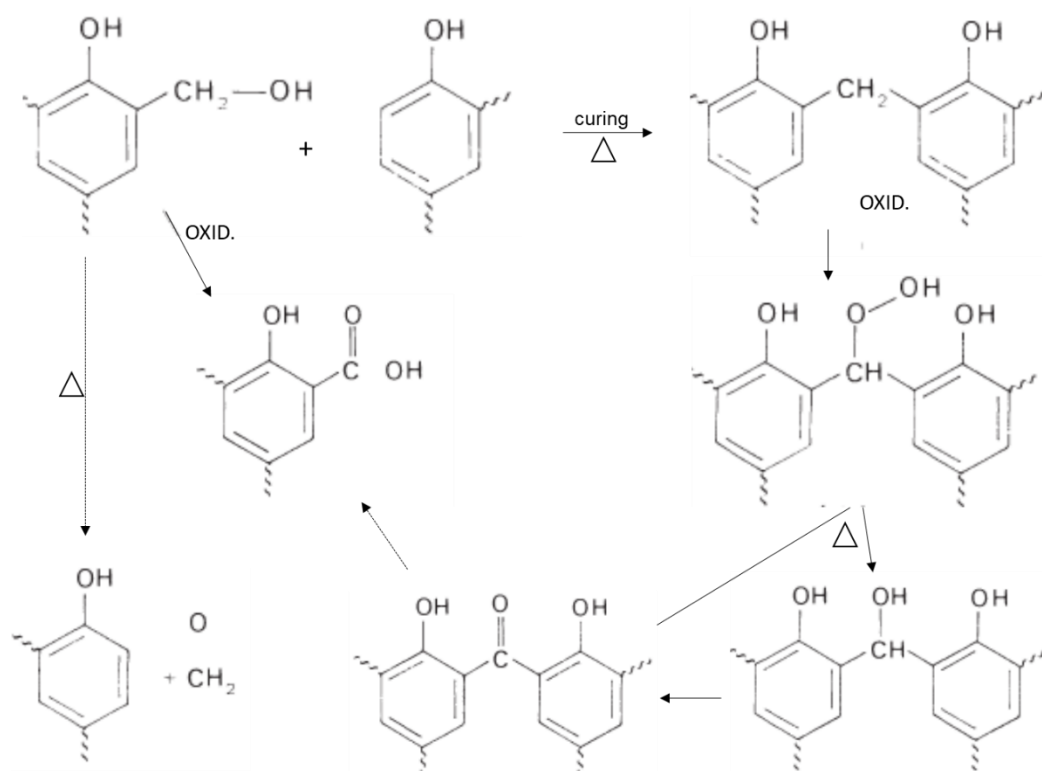


Figure 2.10: Initial degradation processes of phenolic resins [91].

During degradation at temperatures above 250 °C, char formation and carbon monoxide evolution co-occur. In addition, water, paraformaldehyde, methane and various aromatics products were also formed. Both thermal bond rupture and oxidation process compete during phenolic resin decomposition. However, oxidation was designated as the primary mode at temperatures up to 750 °C. According to the authors, the process occurring at elevated temperatures depends on the thermal and oxidative stability of dihydroxydiphenylmethane unit.

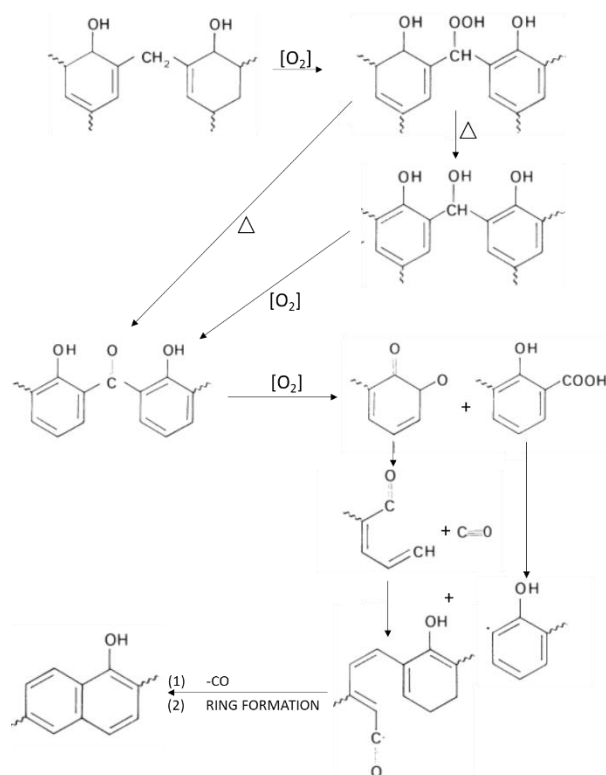


Figure 2.11: Char-forming reactions in phenolic resin systems [91].

The pyrolysis products of novolac resin at 750 °C was studied by Dungan *et al.* [92], via Pyrolysis-Gas Chromatography-Mass Spectrometry [93]. The results are presented in Figure 2.12.

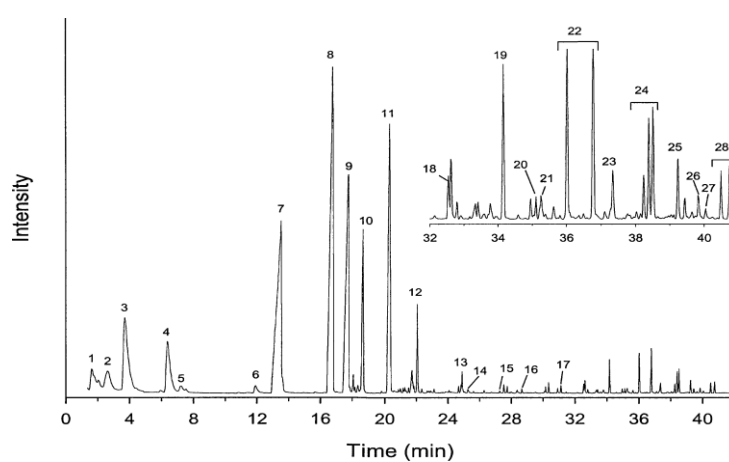


Figure 2.12: Gas chromatogram of pyrolysis products of cured novolac resin [93]. For more details about the identified peaks pointed out in the graphs, see Table 2.5.

Table 2.5: Peak identification of pyrolysis products of Novolac resin [93].

No.	Compound Name	Molecular Weight
1	Ethylamine	45
2	Benzene	78
3	Toluene	92
4	<i>o</i> -Xylene	106
5	<i>p</i> -Xylene	106
6	1,3,5-Trimethylbenzene	120
7	Phenol	94
8	2-Methylphenol	108
9	3-Methylphenol	108
10	2,3-Dimethylphenol	122
11	3,5-Dimethylphenol	122
12	2,4,6-Trimethylphenol	136
13	4-Cyano-3,5-dimethylphenol	147
14	2-Methylnaphthalene	142
15	2-Ethenylnaphthalene	154
16	2-Methyl-1,1'-biphenyl	168
17	2,2'-Dimethylbiphenyl	182
18	Fluorene	166
19	9H-Xanthene	181
20	2-Methyldodecane	184
21	3-Methyl-9H-fluorene	180
22	(2-Methylphenyl)-phenyl methanone	196
23	9-Methylene-9H-fluorene	178
24	2,4-Dimethylbenzophenone	210
25	2,5-Dimethylbenzophenone	210
26	2-Methylphenanthrene	192
27	1-Methylanthracene	192
28	2,4,6-Trimethylbenzophenone	224

In the early degradation stages, oxidation/combustion process and inert pyrolysis coexisted. This observation was attributed to the presence of hydroxyl groups, reaction water, absorbed moisture, air pockets and other oxygen sources in the phenolic structure. During inert pyrolytic decomposition, oxygen radicals are generated, which induced oxidation reactions with the polymer sites. Glassy chars obtained from novolac resin typically include porosity developed during the pyrolysis process. Moreover, the carbon yield increased with the degree of pyrolysis. The amounts of volatiles produced below 500 °C were observed to be insignificant compared to those released at 750 °C and 980 °C. Toluene (3) and *o*-Xylene (4) formation depends on oxygen available in the source structure [92].

Generally, the thermal degradation of phenolic resin involves inert pyrolysis and partial oxidation/combustion reactions. However, the latter process is more pronounced in novolac resins since they contain more oxygen (ether) and less methylene cross-links than resole. This observation suggests that resoles are the better carbonizing resin.

The process leading to gas evolution and water generation during thermal decomposition of phenolic resin was grouped into five sections by Lee [51]. These reactions determine the weight loss percentage that occurs during phenolic resin decomposition.

1. Pyrolytic erosion of polymer end groups that produce CH<sub>4</sub>, CO and aromatic derivatives.
2. Aliphatic and aromatic hydrogen dehydrogenation to form molecular hydrogen.
3. Pyrolytic decomposition via ring cleavage leading to the release of CH<sub>4</sub> and CO.
4. Oxidative degradation via ring destruction generating CO<sub>2</sub> and H<sub>2</sub>O.
5. Residual phenol hydroxy groups' abstraction and destruction to produce reactive oxygen.

## 2.4 Graphitization of thermosetting resin and its benefits to CCRs

Graphitization is a thermally activated kinetic process involving the structural rearrangement of disordered carbons into graphitic ones. The evolutionary operation occurs by the gradual elimination of intralayer defects and stacking faults. It is also a high-temperature procedure, which involves controlled heating of organic precursors to produce crystalline carbons. The 3D progressive reordering of carbon layers from organic precursor during heat treatment usually occurs in an inert or non-oxidizing environment.

During graphitization, the carbon interlayer spacing ( $d_{002}$ ) usually decreases from the characteristic values of a non-graphitic structure to 0.335 nm belonging to graphite. Hence, graphitization degree is a measure of  $d_{002}$  transition. The process depends on factors such as mesophase formation, cross-linking, heating procedure, ambient atmosphere, catalysis and the presence of heteroatoms [55, 94-100].

Organic carbon precursors are classified as:

- i. Graphitizable: Naturally non-crystalline but capable of conversion to graphitic carbons at elevated temperature in an inert atmosphere. Graphitizing organic carbons usually pass through a molten or fluid stage during pyrolysis. This stage is crucial as it allows the planar aromatic molecules to align with each other and form a pre-graphite lattice. The subsequent high-temperature heat treatment completes the solid-state transformation into the final crystal lattice of graphite. Pitch is an example of such organic material.
- ii. Partially graphitizable: Intermediate between graphitizable and non-graphitizable. Inducing graphitization of non-graphitizable precursors typically made them partially graphitizable in many instances, producing both graphitic and non-graphitic carbons (turbostratic carbon).
- iii. Non-Graphitizable: These do not convert to graphitic carbons at elevated temperatures. Such a category does not pass through a mesophase stage during heat treatment and produce what is generally referred to as “hard carbons”. These carbons will not undergo a reconstructive transformation under ordinary carbonization conditions. Most thermosetting resins and



thermoplastic such as polyacrylonitrile, fall under this classification as they yield isotropic carbons with no evidence of graphite-like structure during pyrolysis.

This classification is captured in a model proposed by Franklin et al. [55] as shown in Figure 2.13.

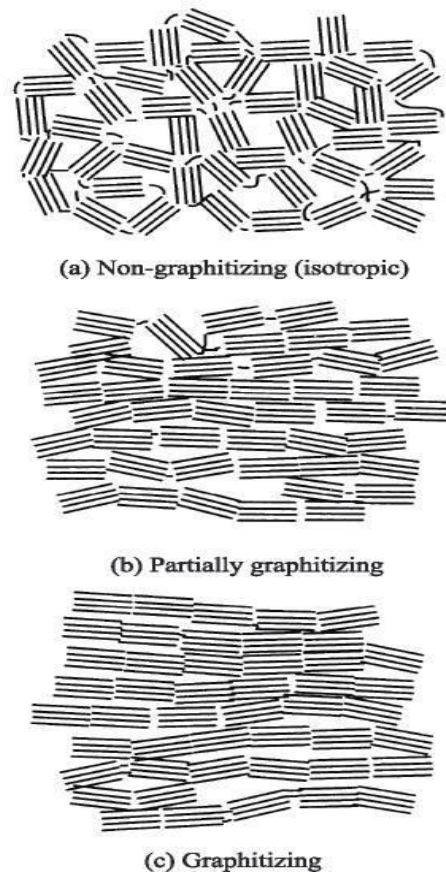


Figure 2.13: Franklin model for: (a) non-graphitizing, (b) partially and (c) graphitizing carbons [55].

CCRs properties are closely related to the carbonaceous phase with a structure close to that of graphite [101]. Hence, the lack of graphitization of carbon derived from phenolic resin aggravates the challenges associated with poor oxidation resistance, thermomechanical performance and service life of these refractories. Consequently, there is a significant interest to find alternative routes to induce effective graphitization of such polymeric components at temperatures and conditions similar to the ones used in the manufacturing of carbon-containing refractories. Several techniques such as the application of compressive forces,

radiation, magnetic fields, and others [13, 102, 103] are available to induce crystallization of non-graphitic carbons.

The incorporation of pressure during the resin pyrolysis facilitates increased graphitization (Figure 2.14). This type of process leading to graphitic carbon generation is commonly referred to as stress-graphitization [16]. The reaction driving force may be associated with the organic precursor volume reduction. The crystallization process appears to occur in the vicinity of stress accumulation [104]. Another route involved inducing molecular alignment in a polymer precursor by introducing electrohydrodynamic forces during the synthesis stage and exerting electro-mechanical stress during the cross-linking phase. Based on this method, a non-graphitizable polymer precursor can be graphitized. This aspect was reported by Ghazinejad et al. [105], in their work on graphitizing non-graphitizable carbons by stress-induced routes.

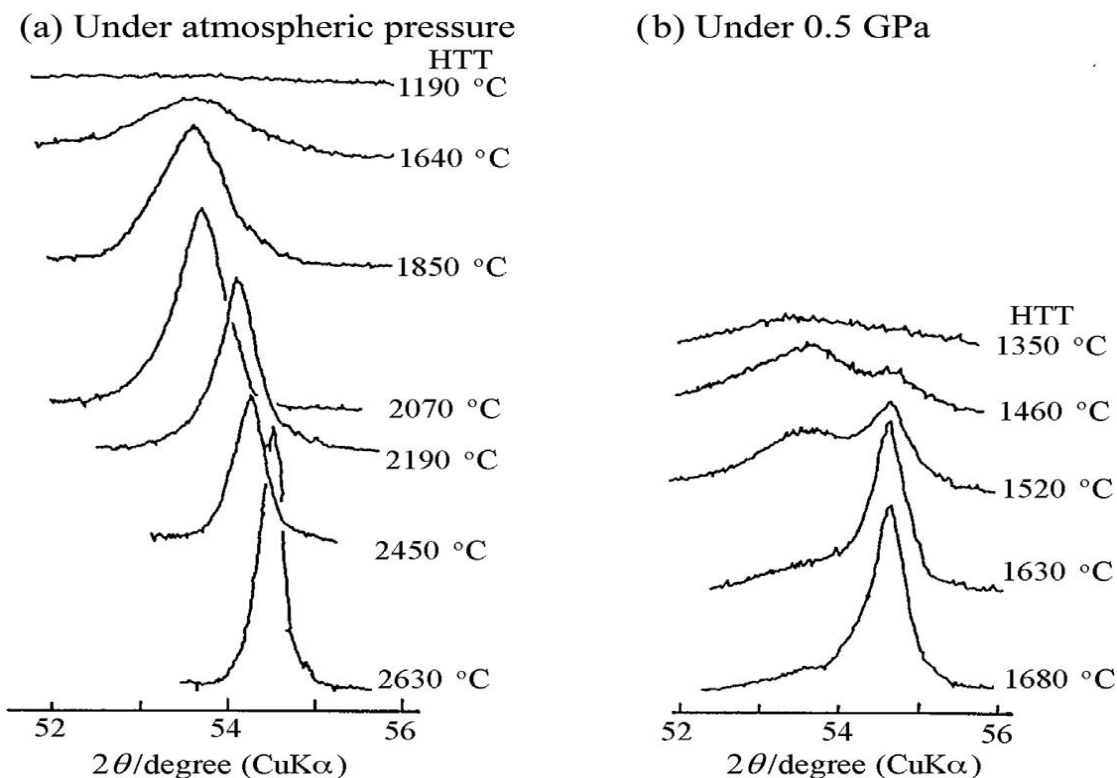


Figure 2.14: Structural changes of 004 diffraction profile of coke with HTT under atmospheric pressure and 0.5 GPa [106].

At other times, graphitization may be due to the presence of certain additives through a process generally referred to as catalytic graphitization. This route appears to be the most viable method for use in the refractory-making field. The additions of these foreign species (which can be elements or compounds) to the thermosetting resins can lead to graphitic carbon generation at elevated temperatures and accelerate its crystallization. The graphitization process occurs at a lower temperature and shorter heat treatment time compared to when the catalytic substances are absent. The disruption and structuring of the non-graphitizing carbons usually result in the formation of three types of component, namely: graphitic carbons, turbostratic carbons (random rotation of the layers, giving no stacking sequence and large interlayer spacing), uncatalyzed component (A-component) as described in Figure 2.15 [18]. The term turbostratic was first used to describe disordered carbons during a study involving the pyrolysis of carbon black. This type of structure is usually found in graphite layers that are roughly arranged, parallel and equidistant but randomly stacked [107]. Nowadays, carbons with features that lie between amorphous carbon and graphite are referred to as turbostratic carbons. This type of material has graphene layers of relatively small extent.

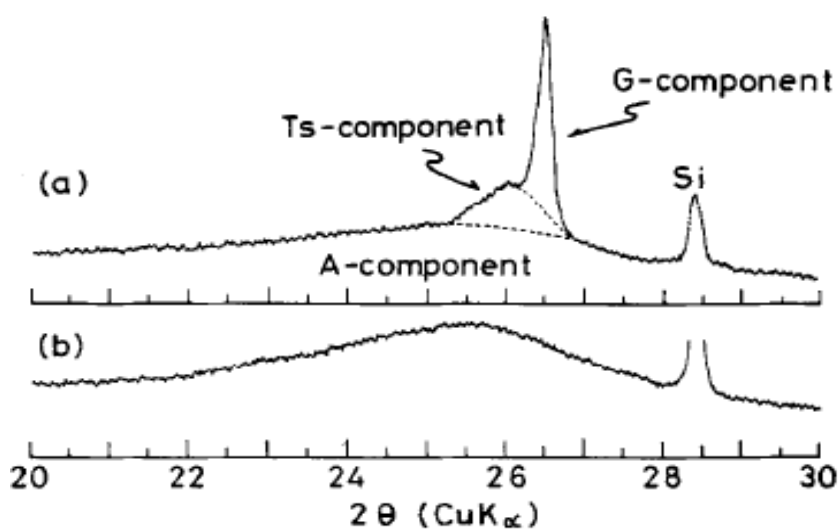
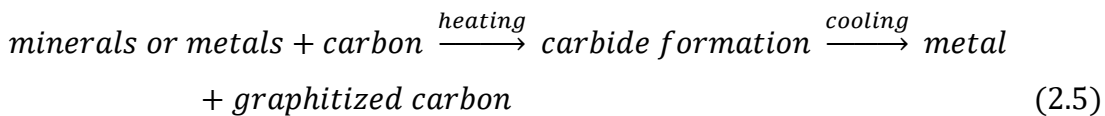
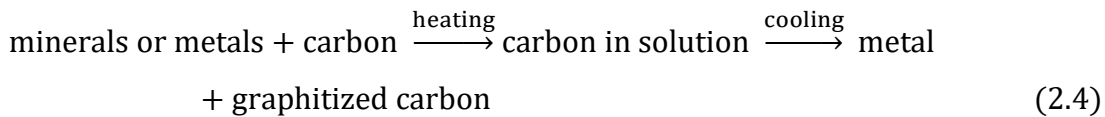


Figure 2.15: X-ray diffraction profiles of the resin carbon, heat-treated at 2500 °C. (a) catalyzed; (b) uncatalyzed; and Si, an internal standard [18]. Ts = turbostratic carbon and G = graphitic carbon.

Two mechanisms involving dissolution/precipitation of carbon atoms (equation 2.4), and formation/decomposition of metal carbide (equation 2.5) have been proposed to explain catalytic graphitization of organic precursors [106].



The effect of such additives depends on experimental conditions such as the carbon precursor type, the catalyst type (e.g., metallic elements, oxide, carbonate), particle size, and their degree of dispersion as well as heat treatment temperatures and the adopted heating rate/sequence [19, 94, 108-110]. Various compounds such as organometallics (metallocenes, benzoates, octoates and naphthenates), metal salt soluble in thermosetting resins and chemically precipitated or micronized metal oxides have shown good graphitizing behaviour for carbons crystallization [12].

As earlier mentioned, achieving graphitization of the binder component (resin) of CCRs is a novel concept. An accomplishment like this can lead to an improvement in the thermomechanical properties and service of such refractories. For example, in an experiment conducted by Sheikholeslami et al. [111], carbon black nanoparticles were used to induce graphitization of resole-type phenolic resin. The resin composition was subsequently used to develop a MgO-C refractory. Firstly, increased carbon yield, better brick compaction and low apparent porosity were achieved due to the presence of carbon black. Furthermore, the refractory prepared with the modified resin showed improved mechanical properties after curing and coking. Specifically, the sintered MgO-C brick (1300 °C) showed about 25 % and 75 % increase (compared to the conventional one) in modulus of rupture and cold crushing strength, respectively. Rotary slag corrosion test was also carried out at 1600 °C based on ASTM C874. The slag penetration amount of the traditional formulation containing 10 wt% and 12 wt% graphite was calculated as 8.86 % and 7.01 %, respectively. However, the newly developed refractory prepared with 10 wt% of graphite has a value of

5.12 % (which is about 40 % decrease) of slag penetration. Similarly, Jansen et al. [3], catalytically activated the graphitization of phenolic resin during MgO-C sintering. The developed CCR also possessed improved thermomechanical properties and superior thermal shock resistance compared to when the ordinary resin was used as the binder. The properties of both refractories are presented in Table 2.6.

Table 2.6: Compared properties of MgO-C bricks prepared using ordinary phenolic resin and the catalyzed resin after coking at 900 °C [3]

<b>Property</b>	<b>Ordinary Phenolic resin</b>	<b>Catalytically activated resin</b>
Bulk Density (g/cm <sup>3</sup> )	3.03	3.02
Young Modulus (GPa)	10.44	11.12
Open porosity (%)	10.39	10.16
Cold compression strength (MPa)	25.20	29.90
Modulus of rupture (MPa)	2.81	3.83
Hot Modulus of rupture (MPa)		
1000 °C	4.41	6.23
1200 °C	3.90	6.02
1500 °C	2.71	3.81
Work of Fracture (Nmm)		
1000 °C	69.06	90.19
1200 °C	61.34	149.52
1500 °C	50.94	159.46

The XRD patterns of the plain and catalyzed phenolic resin after pyrolysis at temperatures up to 1500 °C are shown in Figure 2.16. The peak at ~26° indicates good crystallization of the pyrolytic carbons. Moreover, the carbons derived from the unmodified resin show a broad peak in the same region confirming its glassy nature. The authors attributed the resin graphitization to a

reduction in the activation energy required for the creation of crystal graphitic lattice.

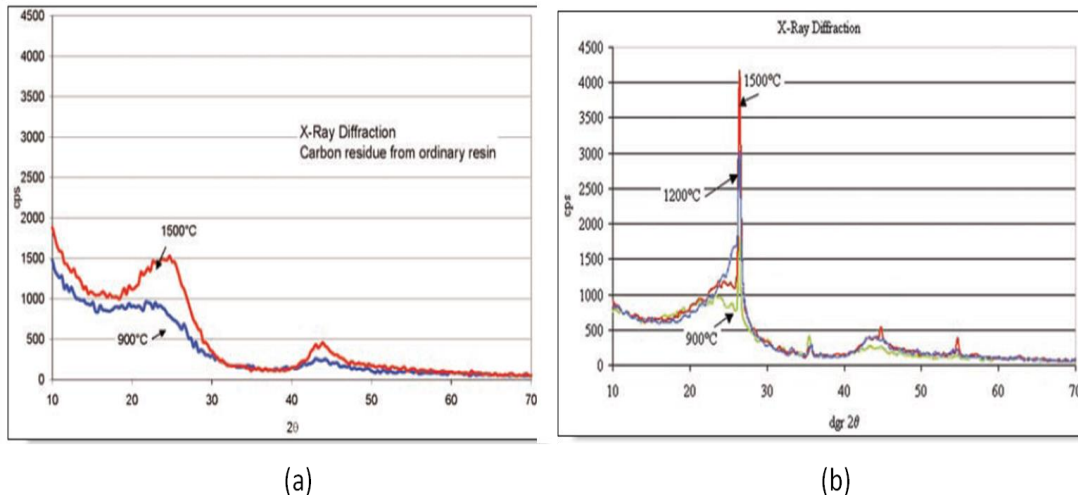


Figure 2.16: XRD profiles of carbon obtained from (a) ordinary phenolic resin (b) catalyzed phenolic resin after pyrolysis at 900 °C, 1200 °C and 1500 °C [3].

An illustration is provided on the difference in the orderliness degree of two types of carbons based on TEM images shown in Figure 2.17. Figure 2.17a represents that of non-graphitizing carbon with a disordered structure and usually exhibits isotropic behaviour. Figure 2.17b shows that of graphitizing carbon with some level of atomic orderliness and anisotropic characteristic. They were derived from sucrose and anthracene, respectively.

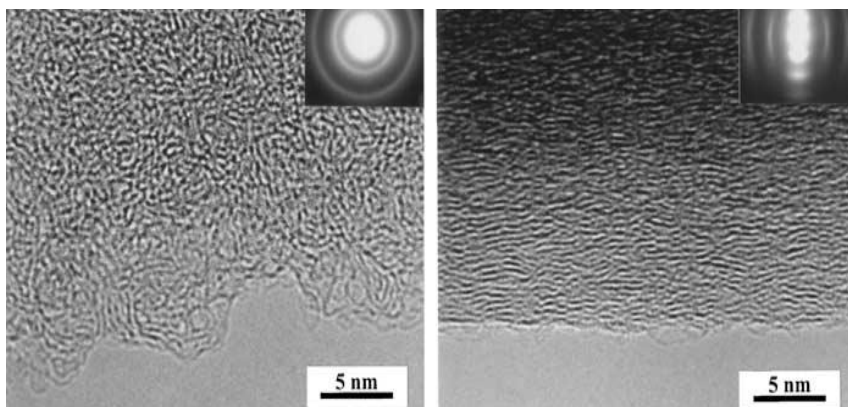


Figure 2.17: Microstructure of carbons prepared by pyrolysis of (a) sucrose in nitrogen at 1000 °C, (b) anthracene at 1000 °C [112].

The advantages derived from crystalline carbon generation from the thermosetting resin component of CCRs can be summed up as follows:

- i. **Development of highly anisotropic carbons:** The physical and chemical properties of graphite depend on its anisotropic characteristic. However, glassy carbons derived from unaided pyrolysis of thermosetting resins show isotropic behaviour with inferior relevant properties compared to the crystalline ones. Consequently, their graphitization will induce a structural orderliness and anisotropic characteristic that can lead to advantages such as improved thermal conductivity, excellent resistance to slag penetration, better resistance to mechanical stress, etc., provided by the presence of graphite/graphite-like carbon in CCRs.
- ii. **Improved oxidation resistance:** The oxidation resistance of carbons derived from the thermosetting resins is inferior to graphite. Its graphitization can lead to a reduction in the amount of edge site atoms (the edge atoms are more reactive than those of basal plane) [113-115] and consequently improves the resistance to carbon loss in an oxidizing environment. This invariably should lead to an increased CCRs lifespan.

#### 2.4.1 Factors affecting catalytic graphitization

Some factors influencing graphitization of polymeric materials are highlighted and discussed below:

1. **Mesophase Formation:** Organic precursor graphitization depends significantly on whether it passes through mesophase during pyrolysis. All graphitizable carbons pass through this state during the inert heating before developing a substantial hexagonal  $sp^2$  carbon character, except when being subjected to an oxidative stabilization process. Polymeric carbons that pass through a fusion stage during pyrolysis generally exhibit higher graphitization degree compared to those that do not show this characteristic [94]. The subsequent stage completes the solid-state transformation to the final graphite' crystal lattice. Mesophase is usually observed in the temperature range of 400 °C–520 °C. During that state,

the spheres appear and increased in size with increased temperature or soaking time and eventually coalesce to form a mosaic structure [95]. After sphere coalesces, the mesophase solidified into semi-coke that is readily graphitizable [96]. The degree of mobility exhibited by mesophase networks facilitates the formation of graphitic layer planes. The liquid stage is therefore crucial as it allows the planar aromatic molecules to align with each other and form a pre-graphite lattice. The presence of an excess amount of sulphur in the organic precursor may inhibit spheres formation at the mesophase stage [116].

2. **Cross-linking:** A certain level of cross-linking must occur in the decomposing polymer for carbon formation. However, a high cross-linking degree can inhibit fusion and dispersion or diffusion of catalytic additive during catalytic graphitization thereby reducing the possible graphitization degree [94]. To realize ordered atomic arrangement, the carbon binding energy must be much weaker to allow the nuclei formed during the initial stages of carbonization remain relatively mobile [55, 97, 98]. Other factors such as hydrogen bonding, ether links formation that affect cross-linking and fusion will consequently affect graphitic carbon generation during pyrolysis.
3. **Heating procedure:** Pyrolysis can be described as a chemical reaction involving decomposition and formation of new products. The process proceeds over a wide temperature range in which initially formed products undergo further transformation and decomposition reactions that may or may not be detrimental to the graphitization degree. The reaction speed also determines the temperature gradient between the heating apparatus and the substrate. Consequently, heating rate and the pyrolysis duration influence the crystallization process. However, for analytical purpose, fast pyrolysis, which limits several side reactions is usually preferred. Nevertheless, the later stage of the heat treatment should provide sufficient time to allow for necessary atoms' rearrangement.
4. **Ambient Atmosphere:** The environments in which graphitization process takes place may affect the amount of generated graphite. In a vacuum



(unlike another inert atmosphere types), the possibility of secondary reaction or further decomposition of pyrolytic products is prevented. For example, Okazaki et al. [99] found that carbon powder graphitization proceeds more readily in a nitrogen environment compared to argon.

5. **Catalysis:** The addition of inorganic and organometallic materials has been found to influence the graphitization level of organic materials. With the addition of such graphitizing agents, carbonized polymeric materials can undergo crystallization at relatively much lower temperatures.
6. **Heteroatoms:** The graphitizability of organic materials can be reduced or suppressed due to the presence of heteroatoms such as nitrogen and sulphur, which promote increased cross-linking reaction [100].

## 2.5 Graphitization of phenolic resin by boron-containing compounds

Boron has been known to induced graphitization of phenolic resins carbons in a manner that is directly proportional to the additives quantity and heating temperature [20]. Its incorporation has been reported to accelerate homogeneous and continuous graphitization of the entire carbons without the formation of separate, distinct carbon components at elevated temperatures  $\geq 1800$  °C [20]. Boron possesses the ability to enter carbon's lamellar structure interstitial or by substitution method [20]. Compounds containing this element are also applied in CCRs as antioxidant agents to increase their service life [117].

To increase char yield, improve thermal stability and induce graphitization, various boron-containing compounds (phenylboronic acid [118], boric acid [101, 119, 120], hyperbranched polyborate [121], boric acid terminated hyperbranched polyborate [122], bis(benzo-1,3,2-dioxaborolanyl) oxide [123], bis(4,4,5,5-tetramethyl-1,3,2-dioxa-borolanyl) oxide [123], boron carbide [124], etc.,) have been added to phenolic resins. The amount of generated graphitic carbon/graphitization degree after the pyrolysis of boron compounds-modified phenolic resins depends on the type of boron source additives and adopted processing parameters.

Several methods have been used to synthesize boron-containing phenolic resin (BPR). Generally, the process involved either the direct addition of such compounds to phenolic resin by mechanical/magnetic mixing or through synthesis from phenol, formaldehyde and the boron-source additives. The compositions may be prepared with and without the addition of curing agents depending on the expected application area. Some examples of these preparation procedures are presented below.

Wang et al. [101], prepared BPR from phenol, formaldehyde and boric acid. The phenol and formaldehyde were mixed with the aid of a magnetic stirrer inside a four-necked round bottom flask in the presence of barium hydroxide. The mixture was stirred under reflux for 1.5 hours and the water produced was removed. Boric acid was added after the mixture was cooled down to 60 °C. Thereafter, the temperature was gradually raised to 95 °C and maintained for 1.5 hours while the generated water was removed under pressure. A similar procedure was followed by Wang et al. [125], which involve the use of phenylboronic acid. However, in this instance, the mixture was maintained at 95 °C for 1 hour.

Liu et al. [122], blend hyperbranched polyborate with resole-type phenolic resin in acetone under magnetic stirring for 12 hours. The formulation was then concentrated at 60 °C for 4 hours under vacuum. Similarly, Hamid et al. [119], mechanically stirred a mixture of 2 g boric acid and 18 g of novolac resin for 45 minutes at 120-135 °C to obtain a yellow coloured BPR polymer.

Abdalla et al. [126], synthesized BPR from triphenyl borate and paraformaldehyde or boric acid and resoles using two different reaction routes: (i) a solvent-less reaction process was used to develop BPR from paraformaldehyde and triphenyl borate. Paraformaldehyde was added to the initially melted ester at 60-70 °C and the temperature of the mixture raised to 90 °C, 120 °C or 130 °C; (ii) the boric acid was added directly to resole, which was initially prepared from aqueous formaldehyde and phenol and then stirred in a round bottom flask. In this case, the reaction temperature was maintained between 102 °C and 110 °C for 40 min.

Direct addition of these additives is usually associated with challenges such as inhomogeneous dispersion and processing difficulties [53]. The modification process and pyrolysis can occur as depicted in Figures 2.18 and 2.19.

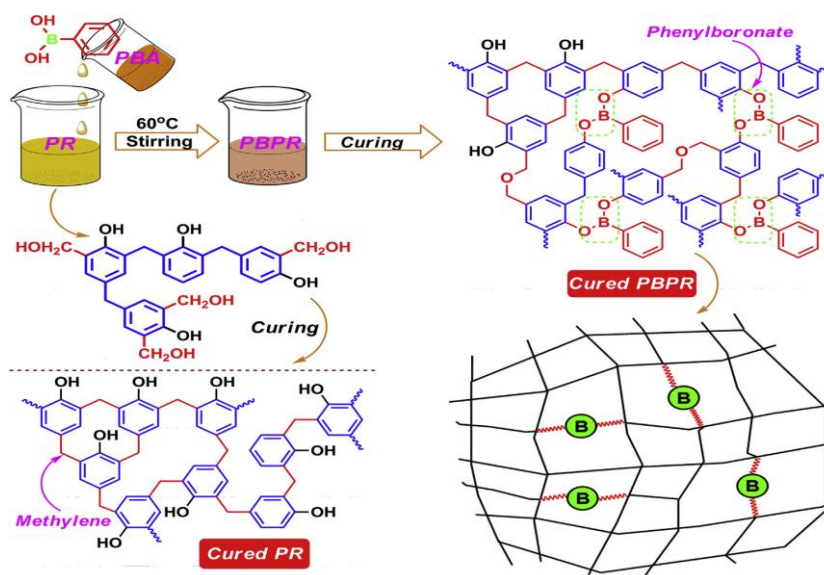


Figure 2.18: Preparation and structure of cured phenolic resin modified with phenylboronic acid [118].

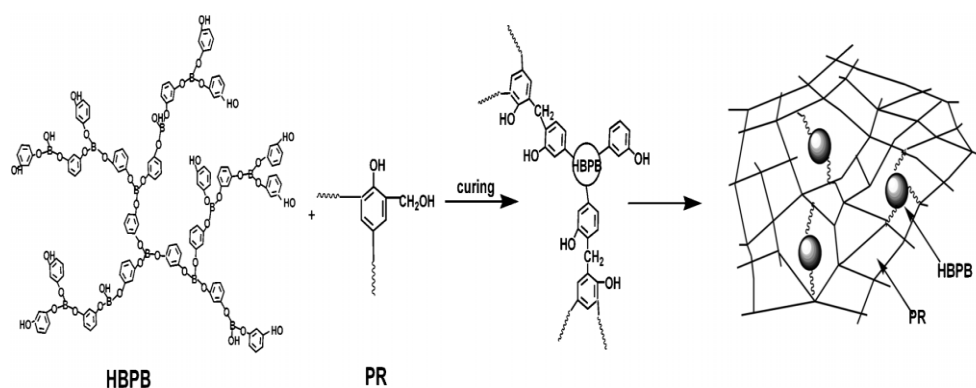


Figure 2.19: Curing reaction of phenolic resin-hyperbranched polyborate [121].

A stepwise-like curing system, which promotes complete polymerization and maximum cross-linking of the modified phenolic was employed in most instances. This procedure was used so as to develop thermally stable carbon-based composites or modified phenolic resin with improved mechanical properties. In some instances, the heating sequence was based on information

derived from the Differential Scanning Calorimetry (DSC) measurement. For example, with the use of phenylboronic acid, the mixture was heat-treated at 110 °C for 2 hours, followed by 160 °C for 4 hours and finally at 200 °C for 4 hours [118]. In another study involving the use of boric acid terminated hyperbranched polyborate, a different kind of curing sequence based on DSC analysis was employed [122].

Wang et al. [101] described the possible structure of cured modified resin containing boric acid as shown in Figure 2.20. The authors observed that a cross-linking between phenolic hydroxyl and B–OH groups led to the formation of phenyl borates in addition to methylene, ether linkages and carbonyl groups. The lower reactivity of B–OH with phenolic hydroxyl groups (up to 200 °C) was identified as the factor responsible for the high curing temperature of the novolac resin containing boric acid.

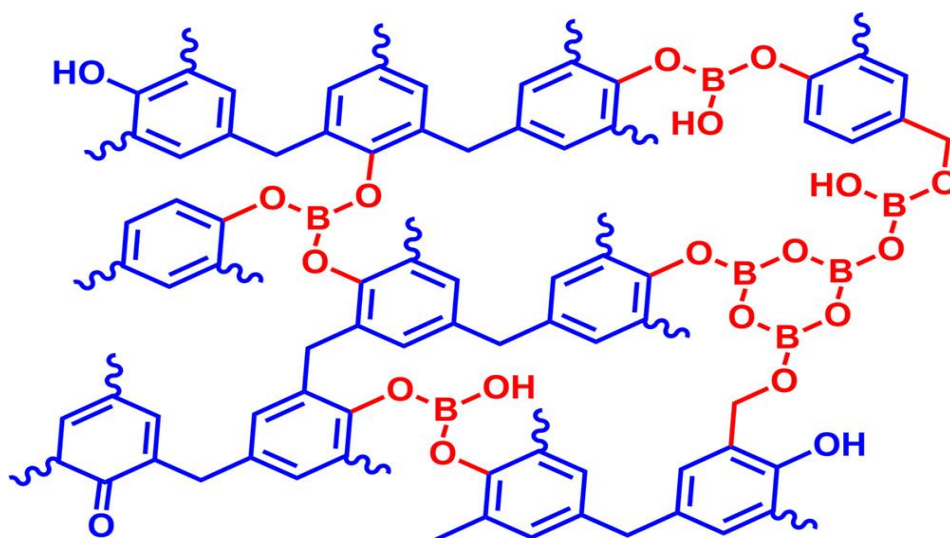


Figure 2.20: Possible structure of cured phenolic resin modified with boric acid [101].

The thermal degradation of cured boric acid-modified phenolic resin was studied by Wang et al. [101]. The essential stages and findings were discussed below. Similarly, the structural transformation that took place during the pyrolysis was represented in Figure 2.21.

- i. At 220 °C: The main product generated at this stage was H<sub>2</sub>O due to moisture evaporation and condensation reactions from residual methylol, B–OH and phenolic hydroxyl groups.
- ii. At 400 °C: Additional cross-linking between O–H groups and aromatic C–H occurred at this temperature. More so, the initially formed phenyl borates decomposed to form B<sub>2</sub>O<sub>3</sub>. The XPS analysis showed a reduction from 85.78 % to 31.05 % in the percentage area of the B–O bond corresponding to the borate compound. Also, the one belonging to B<sub>2</sub>O<sub>3</sub> increases from 4.40 % to 47.10 %.
- iii. Between 400–800 °C: This temperature range was characterized by polymeric network collapse to form polyaromatic domains as well as small volatile molecules, such as CO, CO<sub>2</sub>, H<sub>2</sub>O, and phenol. Furthermore, initial char formation and bonds breaking between aromatic rings and methylene bridges took place.
- iv. Above 800 °C: The reaction at temperatures higher than 800 °C was characterized mainly by dehydrogenation and carbonization. Moreover, the volatilization of B<sub>2</sub>O<sub>3</sub> was observed to begin at this stage.

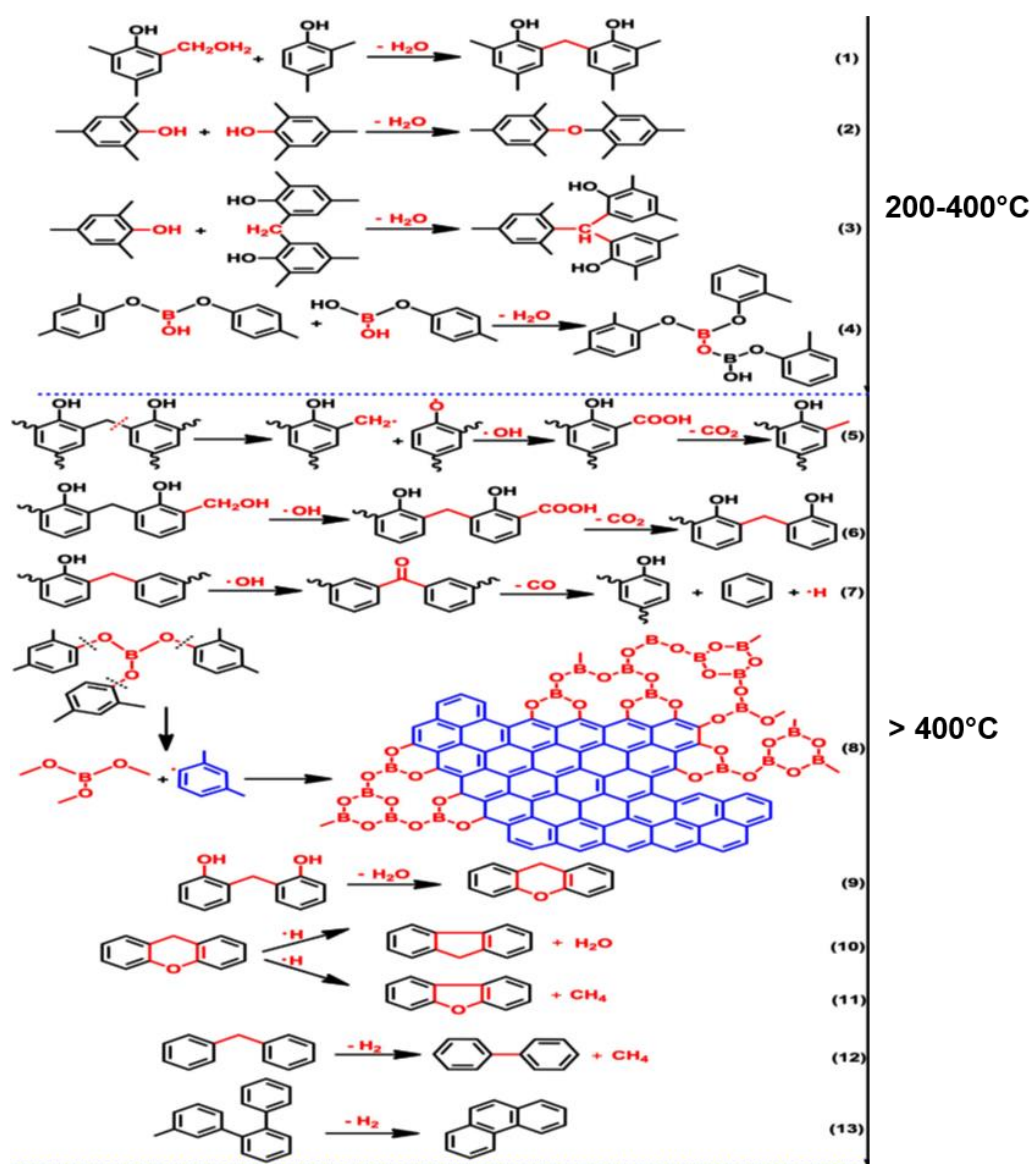


Figure 2.21: Pyrolysis process of boric acid-modified novolac resin [101].

Generally, the role of boron and its compounds on the characteristic of carbon derived from phenolic resins was captured by the studies outlined below. It is important to note that some of these works were not explicitly designed to investigate catalytic graphitization of resin nor intended for CCRs production. The primary objective of most of the published studies on the use of boron-based additives involved the development of carbon-carbon or ablative composites with improved thermal resistance. Hence, the goal was not to attain maximum production of crystalline carbons. Nevertheless, the articles are relevant as they

provided insight on several factors that can influence the generation of graphitic carbon from such modified resins.

Oya et al. [20], studied the catalytic graphitization of carbons derived from a non-graphitizing phenol-formaldehyde resin containing 1-10 wt% elemental boron at different temperatures up to 2600 °C. Homogeneous graphitization of the entire carbon was observed to begin at 1800 °C when 1 wt% boron was added to the initially carbonized resin (at 800 °C). At that temperature, turbostratic carbon was not detected. Furthermore, higher heat treatment temperature and boron's content also enhanced the homogenous effect. The authors attributed the attained result to increase in boron vapour pressure at the elevated pyrolysis temperatures, which made it easier for boron to be deposited on the carbon surface.

Liu et al. [122] mixed phenolic resin with boric acid terminated hyperbranched polyborate. The carbonization product was characterized via XRD, Raman spectroscopy and thermogravimetric techniques. Compared to the unmodified resin, the interlayer spacing of the carbons derived from the modified resin decreased (from 0.3802 nm to 0.3429 nm) while the crystallite height increased (from 4.6 nm to 8.6 nm) due to boron's incorporation during pyrolysis. The XPS analysis of the cured modified resin revealed the presence of B-C and B-O linkages. These bonds indicated that boron atoms were introduced into the carbonized resin structure. The research findings led to the conclusion that the boron compound can promote phenolic resin's graphitization, yielding carbon with improved thermal stability.

Wang et al. [118], added phenylboronic acid (PBA) to phenolic resin and studied its effect on carbon yield and graphitic carbon generation during pyrolysis. Their findings revealed that the presence of this compound promoted crystallization of the carbonized resin. FTIR, XPS and NMR characterizations show the formation and eventual cleavage of B-C and B-O-C bonds during pyrolysis coupled with boron incorporation into the carbon lattice structure. From the Raman measurement, the intensity ratio ( $I_D/I_G$ ) of the carbon sample derived from the formulation containing 10 wt% phenylboronic acid decreased from 2.13 (for the plain resin) to 1.93. Moreover, the crystallite height of the pyrolyzed

product increased to 1.23 nm (compared to that of the plain resin which was 0.81 nm) and the interlayer spacing decrease to 0.3425 nm (compared to that of the plain resin which is 0.3807 nm). These parameters suggest the graphitization of the resulting carbon. Finally, an increase in carbon yield of up to 76.4 % (about 13.4 % more than PR) was also attained.

Wang et al. [101], investigated the chemical evolution that occurred during the pyrolysis of boric acid-modified phenolic resin as a function of temperature. Firstly, the addition of boric acid led to increased carbon yield. This was attributed to the formation and decomposition of phenylborate during carbonization. The cleavage of O–C bonds from this compound during pyrolysis led to boron oxide film production, which covers the surface of the carbonized products and limits carbon oxides formation. Furthermore, boron's incorporation within the carbon structure was found to promote graphitization. At 1500 °C, the plain resin carbon has an interlayer spacing, crystallite height and an intensity ratio values ( $I_D/I_G$ ) of 0.3472 nm, 15.14 nm and 2.636 nm, respectively. The XRD analysis of samples derived from the resin formulation containing boric acid shows an increased crystallite height (15.39 nm), decreased interlayer spacing (0.3392 nm) and intensity ratio ( $I_D/I_G$ , 1.53 nm). The  $d_{002}$  of the generated crystalline carbon was close to that of graphite, which is 0.3354 nm.



The addition of hyperbranched polyborate (HBPB) to phenolic resin was studied with and without the addition of paraformaldehyde by Xu et al. [121]. Paraformaldehyde was introduced to remedy the deficiency of hydroxymethyl groups in hyperbranched polyborate-modified phenolic resin blends. Firstly, polyborate addition was found to improve carbon yield, which represented 71.3 % and 73.1 % at 800 °C for phenolic resin containing 10 and 20 wt% of this compound, respectively. The improvement was attributed to the combined effects of the excellent thermal stability of HBPB, the formation of  $BC_3$ , and the protection of the edges of the graphite microcrystallites by  $B_2O_3$ . Similarly, HBPB was found to promote graphitization of the phenolic resin carbons. The carbonization products have more tidily arranged graphitic structures. Furthermore, the carbon yield of the resin-polyborate formulation containing paraformaldehyde (75–80 % at 800 °C in  $N_2$ ) was higher than those without it.



The thermal stability of novolac resin containing hexamethylenetetramine (HMTA) and phenylboronic acid was studied by Yun et al. [127]. The char yield was found to increase by 5.3 % at 800 °C, 11.13 % at 1000 °C and 17.02 % at 1200 °C. From the XRD results, the authors attributed the peak at 28.1° to B<sub>2</sub>O<sub>3</sub> formation between 400 °C and 600 °C, which contributed to the obtained higher char yield during carbonization. Moreover, boron was also reported to have improved crystallinity and promoted crystalline carbon formation. Nevertheless, the XRD profiles depict a limited graphitization of the resulting carbons. Although the authors did not provide an explanation in their report, it may be due to the presence of HMTA and increased cross-linking at the early carbonization stages.

The yield and structural parameters of carbons derived from phenolic resins containing various boron source compounds are summarized in Table 2.7.

Table 2.7: Selected results on the effects of boron incorporation in phenolic resin [101, 118, 121, 122].

Boron Source	Quantity (wt%)	Results					
		800 °C	@ 1500 °C				
		Char yield (%)	d <sub>002</sub> (nm)	L <sub>c</sub> (nm)	L <sub>a</sub> (nm)	Intensity ratio (I <sub>D</sub> /I <sub>G</sub> )	
Phenylboronic acid (10 wt%) @ 1500 °C [118]	5-20	63.0	0.3807	0.81	1.54	2.13	
		76.4	0.3425	1.23	2.86	1.93	
Boric acid @ 1500 °C [101]	BPR-b (NK)	60.4	0.3472	15.14	2.64	1.88	
		70.5	0.3392	15.39	3.24	1.53	
Hyperbranched polyborate (10, 20, 80 wt %) @ 800 °C [121]	10-80	63.8	-	-	-	-	
		71.3					
		73.1					
		78.4					
Boric acid terminated hyperbranched polyborate @ 1050 °C [122]	10	-	0.3801	4.6	1.13	3.89	
			0.3429	8.6	2.83	1.55	
			Phenolic Resins			Modified Samples	
d <sub>002</sub> - interlayer spacing, L <sub>c</sub> -Crystallite height, L <sub>a</sub> -microcrystalline size, NK- not known							

The graphitizing effect of boron compounds can be examined from several perspectives and each of the following reaction pathways are interrelated:

- i. Formation-Decomposition: B-C bond is formed during carbonization of the cured modified resin at temperatures above 500 °C [101, 125]. The cleavage of boron-carbide phase during pyrolysis leads to graphitic carbon generation. Generally,  $sp^2$  carbons are more stable than  $sp^3$  ones and reordering of the atoms tends to crystalline carbons formation (the standard enthalpy change of graphite formation is 0 kJ/mol [15]).
- ii. Dissolution-Precipitation: The presence of boron compounds can lead to the formation of  $B_2O_3$  which melt at temperatures above 450 °C (melting point of  $B_2O_3$ ), act as a solvent for carbon and graphite-like carbon is formed by crystallization. During the process, the B-O-C bonds break above 800 °C [101, 118].
- iii. Incorporation of boron atoms via substitution during pyrolysis of the catalyzed resin resulted in the increased orderliness of non-crystalline carbon structure and promoted graphitization [101]. The boron atoms may slip within the layer of the pre-existing carbons without completely disrupting its structure [101, 128, 129].

Furthermore, the binding energy as shown in Table 2.8 of B-O-C and B-C bonds are less than C-C bonds. The lower energy value should favour the disruption and structuring that leads to graphitic carbon generation at a lower temperature.

Table 2.8: Binding energy of bonds formed during the pyrolysis of boron compounds-modified phenolic resin [101, 118, 125].

<b>Bonds</b>	<b>Binding energy (eV)</b>
C-C ( $sp^3$ )	284.8
C-C ( $sp^2$ )	284.3
B-C	189.1
B-O-C	190.3

## 2.6 Graphitization of novolac resin by ferrocene and its reaction pathway

Researchers have shown that ferrocene [ $\text{Fe}(\text{C}_5\text{H}_5)_2$ ] possesses a catalytic ability for the graphitization of several organic precursors [3, 50, 130]. Bitencourt et al. [17], obtained 33.1 % graphitic carbons from the pyrolysis of novolac resin containing 3 wt% of this additive after firing the formulation up to 1400 °C. The authors found that various processing parameters such as heating rate and temperature influenced the amount of generated graphitic carbon. Figure 2.22 captured the effect of an increasing amount of ferrocene and temperature on novolac resin graphitization. Figure 2.22c represent the macromolecular structure of ferrocene.

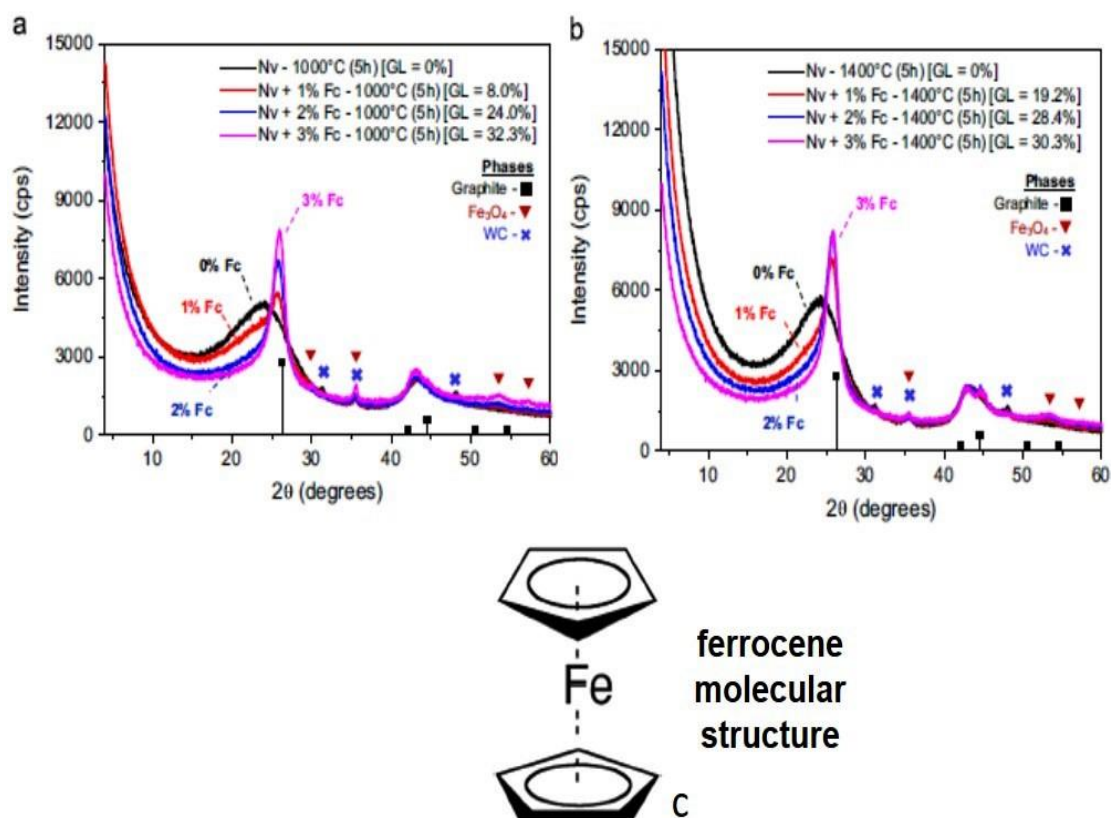


Figure 2.22: Graphitization of novolac resin containing ferrocene [17].

Similarly, Luz et al. [130], found that processing procedures (mixing techniques, curing sequence, and temperature) have a significant influence on the quantity of graphitic carbons derived from the pyrolysis of such modified resin.

The use of low energy mixing procedure led to a higher graphitization level. Stamatin et al. [131], catalyzed the pyrolysis of novolac resin (cured with HMTA) with ferrocene to develop carbon nanotubes and graphene sheets. According to the authors, ferrocene decomposition begins at 300-400 °C, leading to the generation of Fe and Fe<sub>3</sub>C nanoparticles (at temperature values up to 900 °C), which provide active sites for rearrangement of the amorphous carbon to graphene sheets. Furthermore, Bartha et al. [10], mentioned ferrocene among the list of graphitizing auxiliary (consisting of reducible organic compounds) that can be incorporated into phenolic resin as a binder for the development of shaped refractory bricks (such as MgO-C) with improved oxidation resistance.

Based on the considered literature, the following aspect will be important in this study to provide some necessary information to produce CCRs with improved chemical and thermomechanical properties.

1. The homogeneity of carbons derived from catalytic graphitization of phenolic resins containing boron source additives.
2. The reproducibility of the attained results.
3. The influence of the resin chemistry on the crystallization of carbons from the modified resins.
4. Understanding those factors that can influence the degree of graphitization.
5. Investigating other preparation and carbonization procedures that can be adopted for refractories production.
6. Synthesis and graphitization of low-cost phenolic resin products.

## **2.7 Characterization Techniques for evaluating graphitization degree in carbons**

The degree of orderliness that can be detected in carbon structure is usually affected by the type of equipment or techniques employed for the measurement. It is therefore appropriate to briefly consider the principal methods that are used to characterize this material and discuss the implications of each.

### 2.7.1 X-ray diffraction technique

X-ray diffraction (XRD) is based on the collection of diffracted rays from a cathode ray tube, which has been filtered to produce monochromatic radiation collimated to concentrate and focused on the sample under examination. The interaction between the incident rays and the material produced constructive interference when Bragg's law is satisfied.

The technique has been primarily and extensively used to investigate graphitization degree, determine interlayer spacing ( $d_{002}$ ), crystallite height ( $L_c$ ), crystal size ( $L_a$ ) and carbon atoms orientation. Two methods have been proposed to calculate the extent of crystallinity based on entirely disordered (turbostratic) stacking of perfect aromatic layers in graphitizable carbons as shown in equation 2.6 and 2.7. These mathematical expressions are used to determine graphitization degree [132] and graphitization level [17], respectively.

$$g(\%) = \left( \frac{0.3440 - d_{200}}{0.3440 - 0.3354} \right) * 100 \quad (2.6) \quad [132]$$

where  $g$  = graphitization degree, 0.3440 is interlayer spacing of fully non-graphitized carbon, 0.3354 is interlayer spacing of ideal graphite crystallite and  $d_{002}$  is the interlayer spacing derived from XRD measurement.

$$GL = \frac{\text{Graphitic carbon area}}{\text{Total area (graphitic carbon + non-graphitic carbon)}} \quad (2.7) \quad [17]$$

where  $GL$  = graphitization level

The  $L_c$  and  $L_a$  are determined using Scherer's equation according to Equation 2.8. The  $L_c$  can be measured from the width of the 002 and 004 planes, while  $L_a$  is based on that of the (10) and (11) reflections [97, 133].

$$L(c,a) = k\lambda\beta\cos\theta \quad (2.8) \quad [97, 133]$$

where  $k = 0.89$  for  $L_c$  and  $1.84$  for  $L_a$ ,  $\lambda$  = wavelength of the x-ray (0.154 nm),  $\beta$  = full width at half maximum

Furthermore, the interlayer spacing value along the 002 plane is determined from Bragg's equation (Equation 2.9) [118].

$$d_{002} = n\lambda / 2\sin\theta \quad (2.9) \quad [118]$$

where  $\theta$  = Bragg's diffraction angle,  $n$  = positive integer

Generally, increasing value of either  $L_c$  or  $L_a$  and decreasing value of  $d_{002}$  indicates higher graphitization degree [101].

The simulation of the fitting XRD profiles can be done with OriginPro or other peak analyzing software as shown in Figure 2.23.

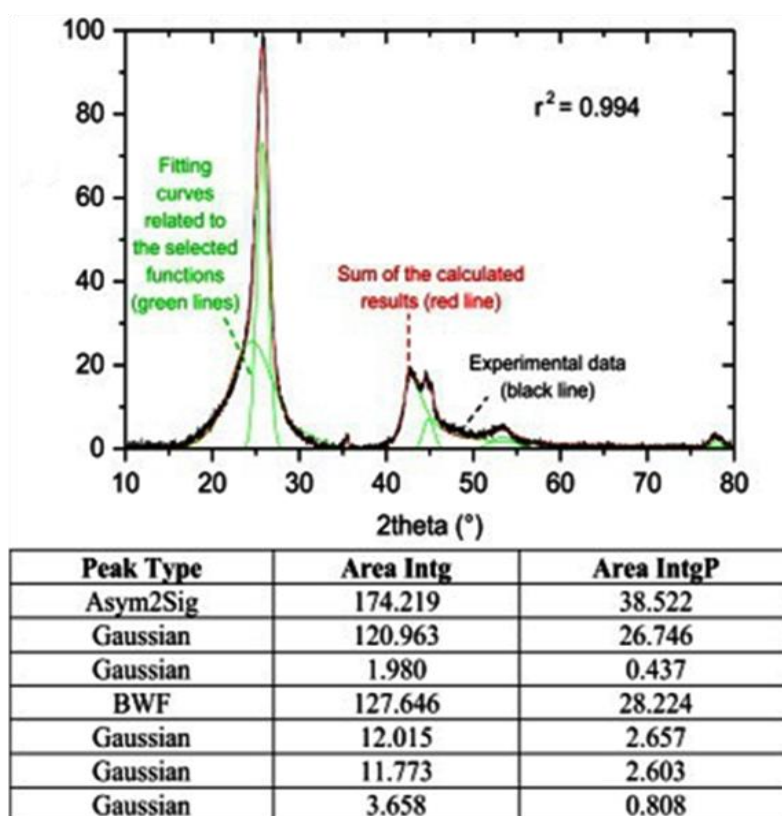


Figure 2.23: Example of the generated curve and data by OriginPro software.

## 2.7.2 Raman Spectroscopy

Raman spectroscopy (RS) is a technique based on inelastic scattering of monochromatic light, usually from a laser source. Inelastic scattering means that the frequency of photons in monochromatic light changes upon interaction with a

sample (Figure 2.24). For this measurement, a laser is focused on the sample and light emitted back is collected. When monochromatic radiation strikes the material, it interacts with its molecules and originates a scattered light in all directions. The frequency of much of this scattered radiation is the same as the source laser and constitutes Rayleigh scattering. Hence, the light emitted back is collected and filtered to remove the source laser wavelength. The remaining light is focused on a dispersive spectroscopy that separates the different energies of light before concentrating it on the detector that gives results in the appearance of a spectrum.

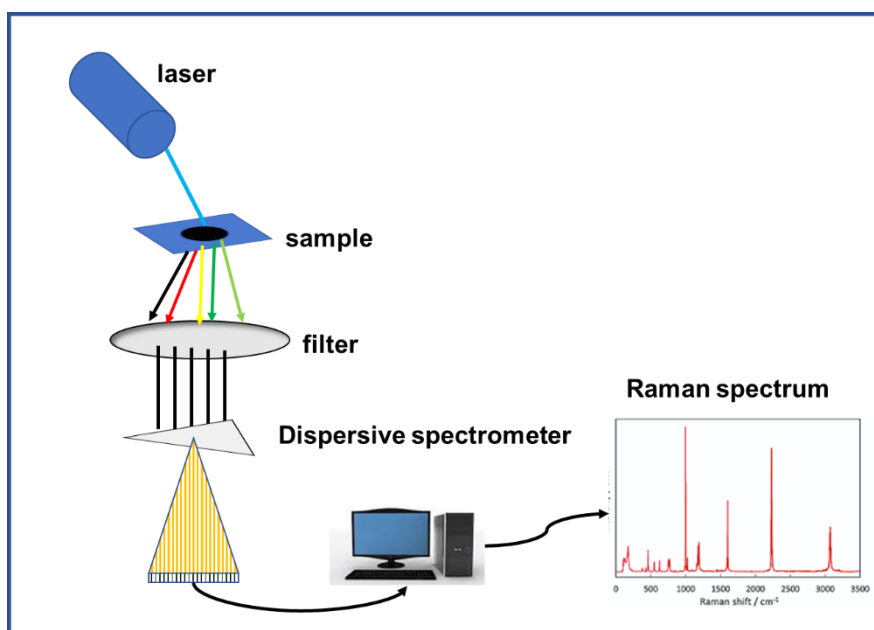


Figure 2.24: Scheme of Raman spectroscopy.

Raman spectroscopy is used to evaluate the extent of structural disorder in carbon products. Their spectra are divided into first-order and second-order regions [133, 134] as depicted in Figure 2.25. The first order region, commonly known as G-band mode (the  $E_{2g}$  vibration mode) is attributed to the stretching vibration in the aromatic layers and occurs at a frequency of  $\sim 1580\text{ cm}^{-1}$ . In perfect graphite, the G-band is the only one that can be found in the first-order region. For a less ordered carbon material, additional bands appear in the first-order region around  $1350\text{ cm}^{-1}$ ,  $1500\text{ cm}^{-1}$ , and  $1620\text{ cm}^{-1}$ . The  $1350\text{ cm}^{-1}$  peak, commonly called the defect band or D-band is frequently attributed to an  $A_{1g}$

mode or to the breakdown of translational and local lattice symmetries. The 1500  $\text{cm}^{-1}$  band is possibly due to “interstitials” such as residual  $\text{sp}^3$  carbons. This band is present only in poorly crystallized carbon materials. In certain instances, a peak is visible in the high frequencies zone at  $\sim 1620 \text{ cm}^{-1}$ . It is usually designated as  $\text{D}'$  [135]. The main band in the second-order spectrum is at  $\sim 2700 \text{ cm}^{-1}$  and is called  $\text{G}'$ -band. Raman feature at about  $2950 \text{ cm}^{-1}$  is associated with the  $\text{D} + \text{G}$  combination mode. Finally, the band at  $\sim 3240 \text{ cm}^{-1}$  is the second harmonic of the  $\text{D}'$  line [136].

The position and width of the  $\text{D}$  and  $\text{G}$ -bands have been proposed as indicators of the extent of carbon crystallization [137]. More so, the intensity ratio of the  $\text{D}$  band to that of the  $\text{G}$  band ( $I_{\text{D}}/I_{\text{G}}$ ) has been used as parameters for describing graphitization degree. This parameter (intensity ratio) generally decreases with an increase in the degree of structural orderliness [133].

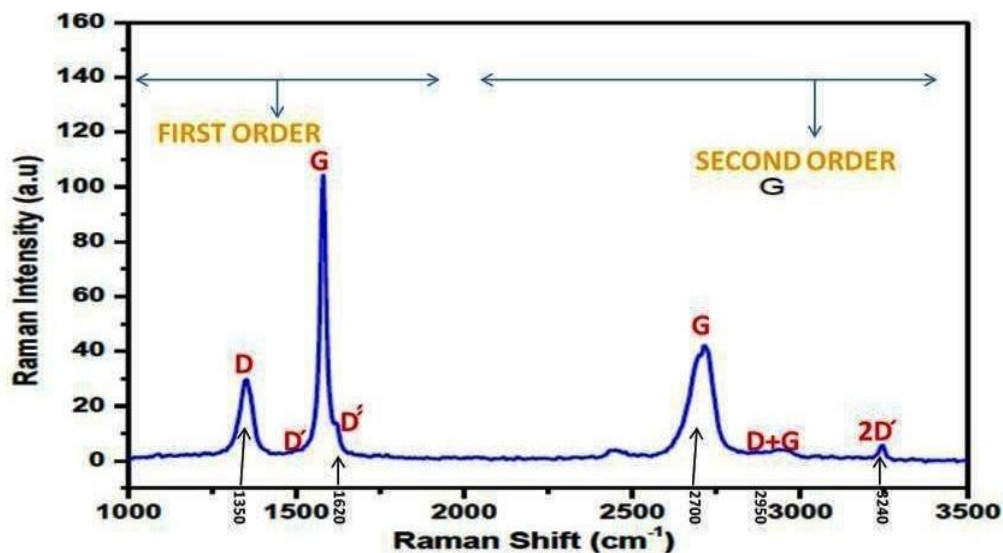


Figure 2.25: General description of carbon Raman spectra.

The  $L_a$  value can also be determined from the Raman intensities ratio ( $I_{\text{D}}/I_{\text{G}}$ ) using equation 2.10 developed by Cancado et al. [106, 133]. Nevertheless, discrepancies usually existed between the values obtained based on XRD and Raman analysis.



$$L_a(\text{nm}) = (2.4 \times 10^{-10}) \lambda_{\text{laser}}^4 \left(\frac{I_D}{I_G}\right)^{-1} \quad (2.10) \quad [106]$$

Notably, Cuesta et al. [137] and Vazquez-Santos et al. [133] compared the information provided by XRD and RS techniques using extensive set of solid carbons. The authors reported some discrepancies in the obtained values. For some measurements, they observed that the errors associated with Raman spectroscopic can be as high as  $\pm 100\%$ . For example, the  $L_a$  values calculated from the XRD profiles were smaller than those obtained based on Raman intensities ratio. They concluded that information provided by these methods should be considered as complementary rather than equivalent. However, XRD technique appears to present more reliable results.

The observed differences were attributed to the mechanism and mode of data acquisition by these techniques as listed below:

- i. XRD is tridimensional while RS is bi-dimensional.
- ii. XRD is based on diffraction in crystal while RS depends on molecular vibration, i.e., propagation of phonons.
- iii. Due to low laser penetration ( $\sim 0.1$  to  $0.2 \mu\text{m}$ ), RS probes only a small spot area and does not capture disorder contribution of the bulk. However, the XRD technique offers a higher depth of penetration ( $\sim 500 \mu\text{m}$ ) and is sensitive to a higher degree of order.
- iv. Unlike XRD, RS technique is insensitive to orientations but sensitive to changes in symmetry.

Some other techniques such as Differential Scanning Calorimetry (DSC) and thermogravimetric (TG), Fourier Transform Infrared spectrometry (FTIR) measurements are also relevant in studies related to carbonization of thermosetting resins.

### 2.7.3 Some other relevant techniques

DSC and TG equipment are used to study the thermal degradation and determine the oxidation resistance of pyrolytic carbons derived from organic precursors. DSC is a thermal analysis technique that measures samples (a reference and the one under investigation) heat flow as a function of temperature or time. It provides an opportunity for the determination of chemical reactions and physical transitions [138]. It is a widely used experimental tool for understanding the curing process in polymers. When a sample is heated, cooled and/or held isothermally, the equipment measures heat flow from or into the sample. The fundamental concept in this technique is that when a material goes through a physical change due to chemical reactions, it will take more or less heat to keep its temperature increasing at the same rate as the reference. This trend will determine whether the process is exothermic or endothermic. Moreover, the analysis can provide excellent information about glass transition temperature ( $T_g$ ), and cure kinetics (cure onset, cure heat, the maximum cure rate, cure completion and cure degree). On the other hand, thermogravimetric analysis (TGA) is a technique that measures the mass change of a sample while it is heated, cooled or held isothermally in a specific atmosphere. It is mainly used for quantitative analysis of products based on weight loss technique.

Fourier Transform Infrared spectrometry (FTIR) is an analytical, non-destructive and real-time measurement method for materials identification. This technique provides both quantitative and qualitative information about the examined sample [46]. The spectrum of the active substance is a characteristic fingerprint that differs for different molecule, bond strengths, atoms number, and material condition. In IR spectrometry, each chemical bond has a specific vibration frequency corresponding to an energy level. FTIR is primarily used to study the organic precursor structure, the evolution that occurs during its pyrolysis, as well as determine the chemical composition and purity level of the derived carbons. Therefore, the spectra analysis can provide an opportunity to determine the reactions (compounds formed) leading to graphitization.

Based on the literature, some principal absorption peaks pertaining to phenolic resins' FTIR spectra and their corresponding functional group were identified and presented in Table 2.9.

Table 2.9: IR bands and functional groups of cured phenolic resins.

<b>Position (cm<sup>-1</sup>)</b>	<b>Functional group</b>	<b>Reference</b>
3400	Phenolic –OH stretch	Liu 2002 et al. [139], Ida et al. [140]
2922	Aliphatic –CH <sub>2</sub> symmetric stretch	Theodoropoulou et al. [141], Ida et al. [140], Ertugrul et al. [142]
1610-1647	C=C aromatic ring stretching vibration	Wang et al. [101], Theodoropoulou et al. [141]
1470	–CH <sub>2</sub> deformation	Ertugrul et al. [142]
1450	C=C benzene ring obscured by –CH <sub>2</sub> - methylene bridge	Ida et al. [140]
1373	–OH in plane	Ertugrul et al. [142], Theodoropoulou et al. [141]
1226	Ph–OH	Wang et al. [101], Li et al., Pardini et al. [53], Wang et al. [125] <a href="http://webbook.nist.gov">http://webbook.nist.gov</a>
1120	C–O–C Ether bond symmetric vibration	Theodoropoulou et al. [141], Ertugrul et al. [142]
1064	C–O –CH <sub>2</sub> OH group stretching vibrations	Liu et al. [139], Ida et al. [140]
756-880	CH out-of-plane, substituted	Ertugrul et al. [142], Theodoropoulou et al. [141], Ida et al. [140]



### **3 MATERIALS AND METHODOLOGY**

This section outlines and discusses the materials and methodology employed during the course of this study. The experimental work was grouped into four stages involving: (i) graphitization of commercially available phenolic resin (novolac), (ii) synthesis and graphitization of phenolic resins (resole-type), (iii) synthesis and graphitization of lignin-modified phenolic resins, and (iv) evaluating the effect of in-situ graphitization on oxidation resistance and physicomechanical properties of CCRs using resin-bonded castables.

#### **3.1 Graphitization of commercial novolac type phenolic resin**

Boron oxide ( $B_2O_3$ ), boric acid ( $H_3BO_3$ ) and ferrocene ( $C_{10}H_{10}Fe$ ) were selected as the graphitizing agents for commercially available phenolic resin. To ensure proper comparison, the overall  $B_2O_3$  content, derived from boric acid and boron oxide in the formulations, was equivalent. The boron compounds were selected to find a cheaper alternative to ferrocene based on the results obtained in a previous study by Bitencourt et al. [17]. Consequently, emphasis was given to the boron source additives in this present investigation. The general overview of the experimental work carried out at this stage is depicted in Figure 3.1.

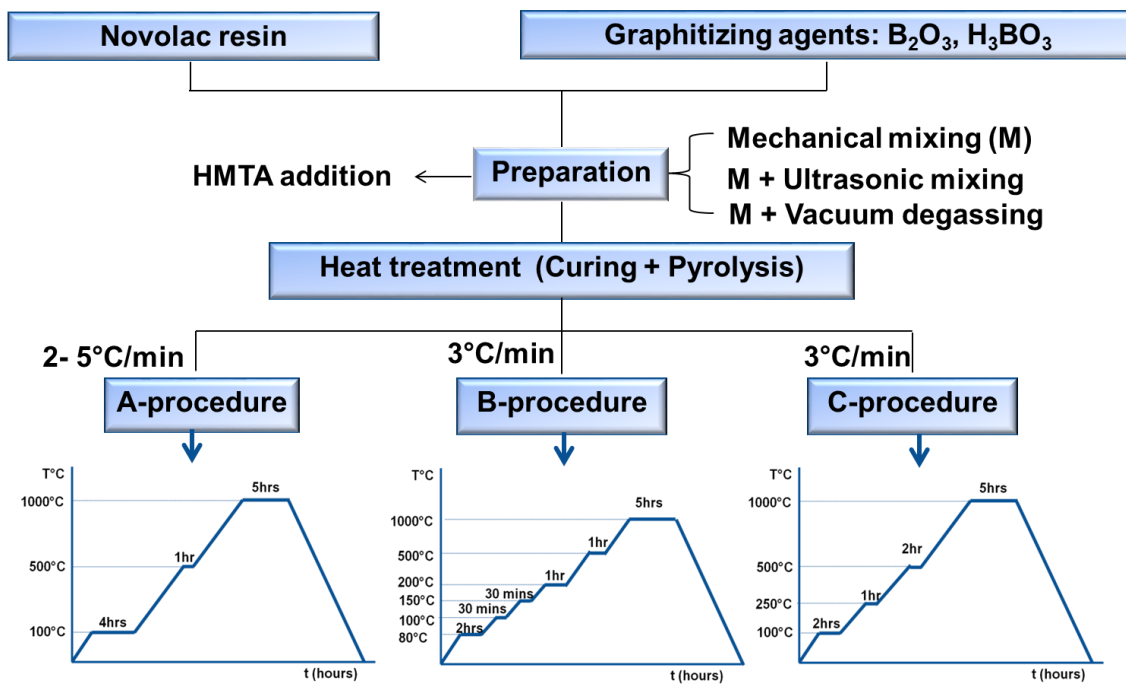


Figure 3.1: Description of the experiments involving novolac resin.

The carbonization procedures were chosen to promote curing and dispersion of the additives (< 500 °C), carbonization (at 500 °C) and induce graphitic generation during the final heat treatment stage of the pyrolysis (at 1000 °C). Regarding B and C- procedures, additional dwell time and steps during the initial stages of carbonization were introduced to evaluate how the different heating pathways will affect graphitization.

The information about the raw materials and evaluated compositions is presented in Table 3.1.

Table 3.1: General information about raw materials and samples description.

Materials	Main Features	Supplier
Commercial Novolac resin	Nv, Viscous Liquid (solvent = ethylene glycol) Density = 1.18 g/cm <sup>3</sup>	Dynea, Brazil
<b>Graphitizing agents:</b> Boron oxide, Boric acid, Ferrocene	B <sub>2</sub> O <sub>3</sub> , solid powder, (d <sub>50</sub> < 10 μm, 99 % purity)	RHI-Magnesita, SA
	H <sub>3</sub> BO <sub>3</sub> , solid powder, molecular weight = 61.83, Product code: A1025.01A4, (d <sub>90</sub> < 45 μm, 99 %)	Synth Chemical Co., SP-Brazil
	C <sub>10</sub> H <sub>10</sub> Fe, Ferrocene (150 < d < 70 μm, 98 % purity)	Aldrich, USA
Hexamethylenetetramine	HMTA, solid powder	Dynea, Brazil
<b>Evaluated Compositions</b>	<b>Description</b>	
Nv-HMTA (reference sample)	Nv + 10 wt% HMTA	
Nv-6B	Nv + 6 wt% B <sub>2</sub> O <sub>3</sub>	
Nv-10H	Nv + 10 wt% H <sub>3</sub> BO <sub>3</sub>	
Nv-HMTA-6B	Nv + 10 wt% HMTA + 6 wt% B <sub>2</sub> O <sub>3</sub>	
Nv-HMTA-10H	Nv + 10 wt% HMTA + 10 wt% H <sub>3</sub> BO <sub>3</sub>	
Nv-HMTA-3Fc	Nv + 10 wt% HMTA + 3 wt% Ferrocene	

The resin and graphitizing agents were mixed at ambient temperature with the aid of a mechanical stirrer (rotation speed of 300 rpm, Etica Scientific Equipment, Model: 105, No.: 0209) to achieve considerable homogenization of the compositions. After that, each of the prepared formulations was poured into alumina crucibles, covered with alumina disk, and embedded in a refractory box filled with coke to create a reducing environment during their pyrolysis. The samples' firing was done based on a controlled heating sequence and subsequent cooling procedures. Several processing parameters were investigated in the course of the experiments. The effect of additional ultrasonic

mixing, vacuum degassing, heating rates and heating routes on the process leading to graphitic carbon generation was investigated. The employed mixing techniques and heat treatment regimes are described in Table 3.2. Furthermore, the impact of hexamethylenetetramine (cross-linking agent commonly used during CCRs industrial production) on graphitization of the resin's formulations containing the boron source additives was examined. The resulting carbon samples were characterized according to the description in section 3.4.2.

Table 3.2: Details of the heating steps and mixing techniques carried out to induce graphitization.

<b>Designations</b>	<b>Heat Treatment Description</b>	<b>Heating rate</b>
A2-A5 procedure	100 °C/4h+500 °C/1h+1000 °C/5h (Note: the number after the letter describe the heating rate i.e., A3 implies that the formulation was subjected to thermal treatment using A-procedure at a heating rate of 3 °C/min)	2-5 °C/min
B3-procedure	80 °C/4h+100 °C/1h+150 °C/30min+500 °C/1h+1000 °C/5h	3 °C/min
C3-procedure	100 °C/2h+220 °C/1h+500 °C/2h+1000 °C/5h	3 °C/min
<b>Mixing Procedures</b>		<b>Description</b>
M		Mechanical mixing
M-V		Mechanical mixing + vacuum degassing
M-U		Mechanical mixing + ultrasonic mixing



### 3.2 Conventional resole and lignin-modified phenolic resins synthesis and graphitization

The laboratory products were synthesized to produce resole-type phenolic resins (including the lignin-modified ones). The conventional ones were produced based on 1.5 and 2.0 formaldehyde to phenol molar ratio (F:P). The lignin-modified ones were produced with up to 30 wt% lignin as phenol replacement based on 1.5 F:P. The general information about the raw materials that were used for the synthesis is presented in Table 3.3.

Table 3.3: General information about the materials used during the second experimental stage.

Raw materials		Supplier
Binder	Commercial Resole resin (Rs, Prefere 88 5000R)	Dynea (Brazil)
	*Phenol, C <sub>6</sub> H <sub>5</sub> OH, solid, molecular weight = 94.11 g/mol *Formaldehyde (37 wt%), CH <sub>2</sub> O, liquid, molecular weight = 30.03 g/mol **Kraft lignin	*Synth Chemical Co., SP-Brazil  **Fibria, Brazil
Catalyst	NH <sub>4</sub> OH, aqueous, molecular weight = 35.04 g/mol, 10 wt.% of phenol quantity	Synth Chemical Co., SP-Brazil
Graphitizing agents: Ferrocene, Boric acid, Boron oxide	Refer to Table 3.1	Refer to Table 3.1

The synthesis was carried out in a three-necked round bottom flask equipped with a Dean-stark system (for water removal), condenser, and thermometer (Figure 3.2). The mixture was heated while stirring under reflux with the aid of a hot plate magnetic stirrer.

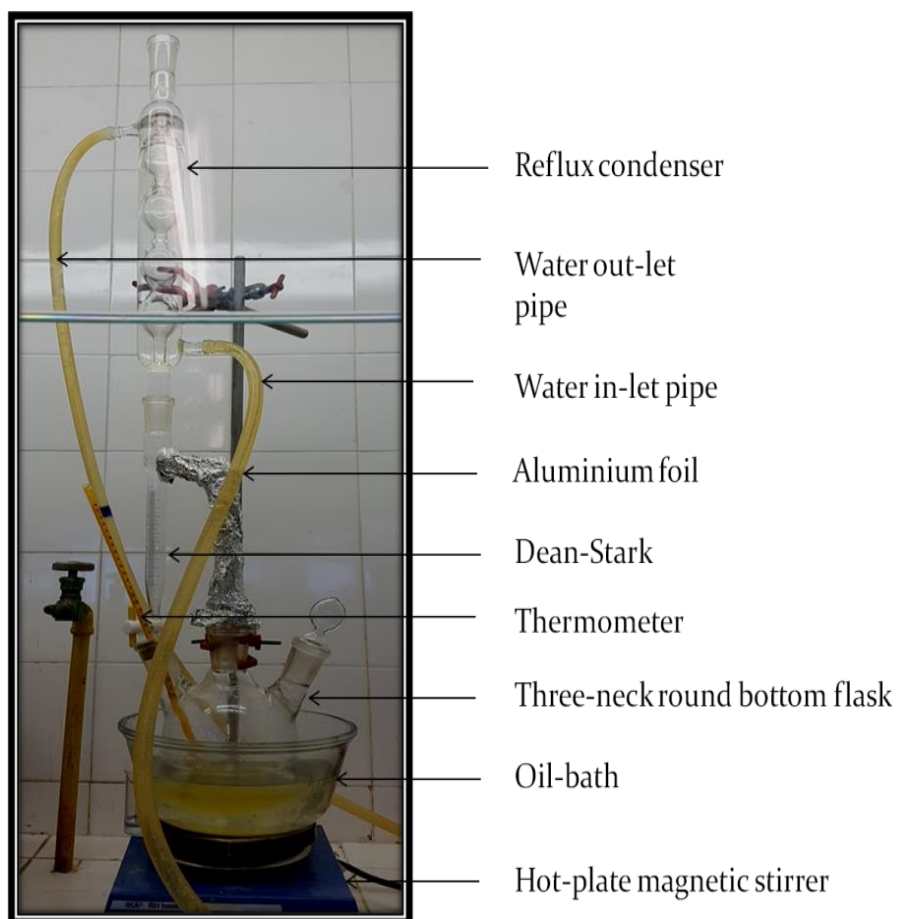


Figure 3.2: Experimental set-up for the production of resole and lignin-modified phenolic resin.

Thereafter, the synthesized resins were carbonized using the A3-procedure (Table 3.2) according to the description in section 3.1.

The investigated compositions and designations are described in Table 3.4.

Table 3.4: Description of investigated compositions and samples designations.

Sample Designation	Description
Rs	Commercial resole resin
1.5Rs	LSR with Formaldehyde: Phenol equal to 1.5
2Rs	LSR with Formaldehyde: Phenol equal to 2.0
1.5Rs-3Fc, 1.5Rs-4Fc, 1.5Rs-5Fc	1.5Rs + 3-5 wt% ferrocene
2Rs-3Fc, 2Rs-4Fc, 2Rs-5Fc	2Rs + 3-5 wt% ferrocene
1.5Rs-10H	1.5Rs + 10 wt% boric acid
2Rs-10H	2Rs + 10 wt% boric acid
1.5Rs-6B	1.5Rs + 6 wt% boron oxide
2Rs-6B	2Rs + 6 wt% boron oxide
10LPF	Lignin-phenol-formaldehyde resin synthesized with 10 wt% lignin as a substitute for phenol
20LPF	Lignin-phenol-formaldehyde resin synthesized with 20 wt% lignin as a substitute for phenol
30LPF	Lignin-phenol-formaldehyde resin synthesized with 30 wt% lignin as a substitute for phenol
10LPF-6B, 20LPF-6B, 30LPF-6B	10LPF+ 6 wt% boron oxide, 20LPF+ 6 wt% boron oxide, 30LPF+ 6 wt% boron oxide
10LPF-10H, 20LPF-10H, 30LPF-10H	10LPF+ 10 wt% boric acid, 20LPF+ 10 wt% boric acid, 30LPF+ 10 wt% boric acid
10LPF-3Fc, 10LPF-4Fc, 10LPF-5Fc	10LPF+ 3-5 wt% ferrocene
20LPF-3Fc, 20LPF-4Fc, 20LPF-5Fc	20LPF+ 3-5 wt% ferrocene
30LPF-3Fc, 30LPF-4Fc, 30LPF-5Fc	30LPF+ 3-5 wt% ferrocene

### 3.2.1 Conventional resole resins synthesis and graphitization

Regarding resole resin synthesis, the mixture of phenol (100 %), water and catalyst were heated up to  $60 \pm 5$  °C for 30 minutes. After that, formaldehyde (37 wt% solution in water) was added and the subsequent mixture heated to  $85 \pm 5$  °C for 30 minutes. The temperature was then reduced to 70 °C, and the reaction was allowed to proceed at that temperature until the required viscosity was attained. The molar ratio of formaldehyde to phenol (1.5 and 2.0) was varied during the synthesis. Moreover, during the initial experimental stages,  $\text{NH}_4\text{OH}$  and  $\text{NaOH}$  were investigated as catalyst for the synthesis. However, the former was eventually selected to eliminate the sodium-related compounds, which were detected in the carbon composition when the reaction was catalyzed with the latter.

Thereafter, the synthesized resins were mixed with the aid of a mechanical mixer (rotation speed of 300 rpm) for 10 minutes to achieve dispersion of the additives (3–5 wt% ferrocene, 6 wt% boron oxide and 10 wt% boric acid) within the resins. The prepared compositions were poured into alumina crucibles, covered with disk, embedded in a refractory box filled with coke and carbonized inside a muffle furnace. The step-wise pyrolysis procedure involved heating the samples from 30 °C to 100 °C and holding it at that temperature for 4 hours, followed by increasing the temperature to 500 °C for 1 hour, before finally heating them to 1000 °C and keeping at that temperature for 5 hours. After carbonization, the samples were cooled to room temperature ( $\sim 30$  °C) inside the muffle furnace. The laboratory synthesized resole carbons (without any additive) were used as reference samples.

The resulting carbon samples derived from the carbonized resins were characterized according to the description in section 3.4.2. The general overview of the experimental work carried out at this stage is presented in Figure 3.3.

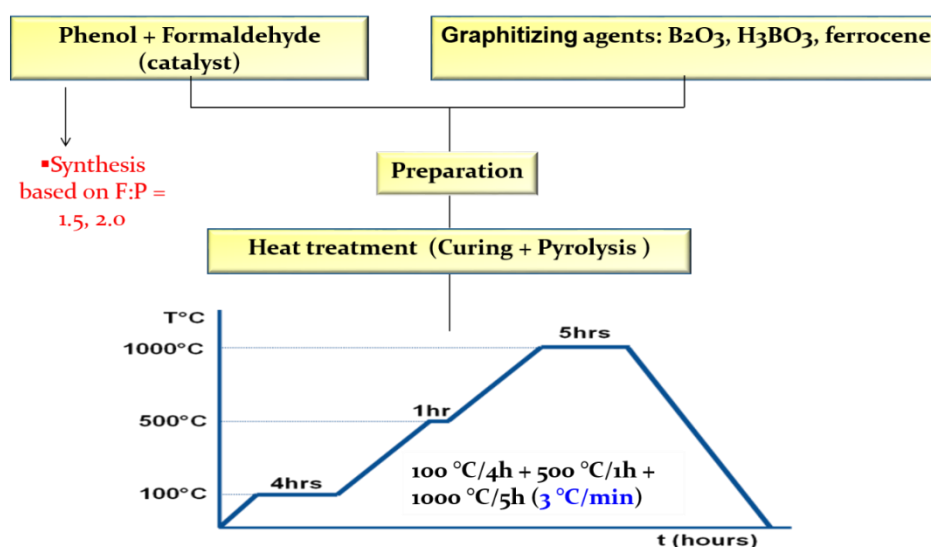


Figure 3.3: Description of the experiments involving resole resins.

### 3.2.2 Lignin-modified phenolic resins synthesis and graphitization

The lignin-modified phenolic resins were produced by substituting phenol for Kraft lignin during synthesis. Lignin-phenol-formaldehyde (LPF) resins were synthesized based on 1.5 formaldehyde to phenol molar ratio. The used lignin was initially heat-treated at 200 °C for 1 hour inside a muffle furnace to improve its reactivity. The modified resins' were produced according to the following procedure. Firstly, the solution mixture of phenol, water and NH<sub>4</sub>OH (catalyst) was heated up to 65 ± 5 °C with a hot-plate magnetic stirrer via an oil bath for 30 minutes inside the glassware. The amount of phenol used depends on the intended lignin to phenol weight percentage ratio. This reaction step was catalyzed by 70 % of the total amount of the catalyst (8.6 wt% of phenol quantity). After that, the required quantity of the heat-treated kraft lignin was added slowly to the mixture. The reaction was allowed to continue for another 30 minutes before adding the remaining NH<sub>4</sub>OH (3.7 wt% of phenol quantity) and formaldehyde (37 wt%). The synthesis then proceeded to completion at a maximum temperature of 75 ± 5 °C. The amount of lignin used for the preparation represents 10 wt% (10LPF), 20 wt% (20LPF) and 30 wt% (30LPF) of phenol, respectively.

Before carbonization, the lignin-modified resoles and the graphitizing agents (3-5 wt% ferrocene, 6 wt% boron oxide and 10 wt% boric acid) were mixed with the aid of a mechanical mixer (Etica Scientific Equipment, Model: 105, No.: 0209) to disperse the additives within the resin. The mixing was carried out at a rotation speed of 300 rpm for ten minutes at room temperature. Each of the additives was mixed separately to prepare mixtures containing either boron oxide, boric acid or ferrocene. The obtained formulations were poured into aluminium crucibles, covered with a lid and buried inside a refractory box containing coke. The heat treatment was done using a stepwise heating procedure, which involved firing the samples from 30 °C to 100 °C and keeping it at that temperature for 4 hours, followed by increasing the temperature to 500 °C and holding it there for 1 hour and finally raising it to 1000 °C and 1500 °C for 5 hours, respectively. The pyrolysis was carried out inside a muffle furnace at 3 °C/min heating rate. Figure 3.4 pointed out the experimental procedures.

The carbon samples derived from the carbonized resins were characterized according to the description in section 3.4.2.

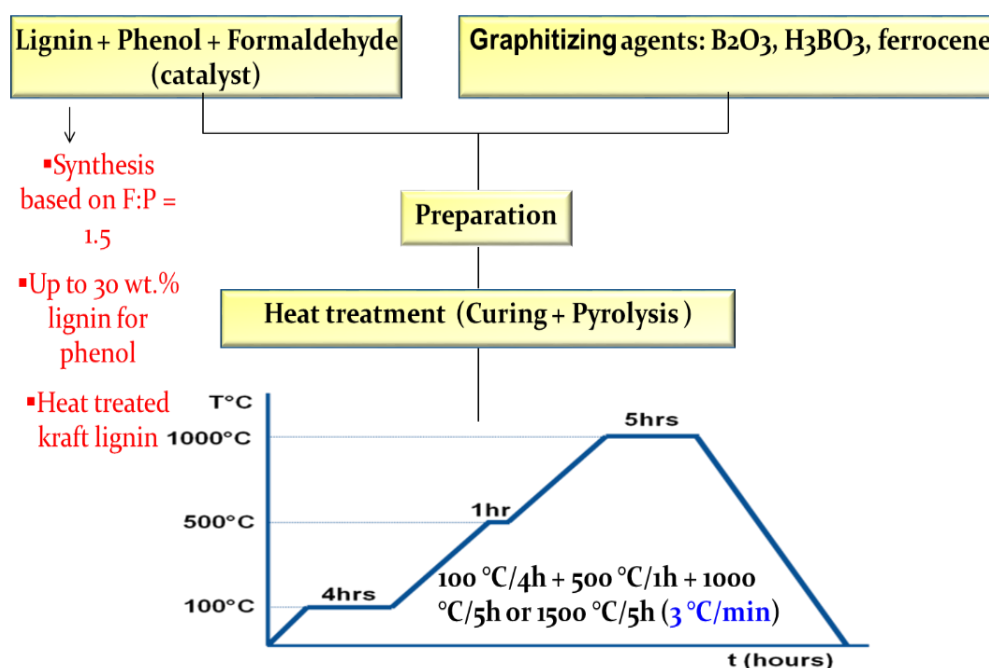


Figure 3.4: Description of the experiments involving lignin-modified resins.

### 3.3 Production of resin bonded Al<sub>2</sub>O<sub>3</sub>-MgO refractory castables

The final experimental work involved the preparation of carbon-containing refractory (CCR) castables using a selected resin formulation containing ferrocene as graphitizing agent. This aspect was designed to evaluate the effect of in-situ graphitization of the binder component on some physical and mechanical properties of the developed CCRs. The materials (refractory oxides, resin and graphitizing additive) used to produce the resin-bonded castables were enumerated in Table 3.5. To achieve a good vibratable flow, the refractory composition was optimized based on modified Andreassen particle model with a distribution coefficient (q) value of 0.26 [143].

Table 3.5: Information about raw materials used for the preparation of the resin-bonded castables.

Raw materials	Supplier	Weight (%)
Tabular alumina (6-3 µm)	Almatis	18
Tabular alumina (3-1 µm)	Almatis	12
Tabular alumina (1-0.5 µm)	Almatis	17
Tabular alumina (0.6-0.2 µm)	Almatis	9
Tabular alumina (0.2-0 µm)	Almatis	18
Tabular alumina (< 45 µm)	Almatis	5
Calcined alumina CL370 ()	Almatis	4
Reactive alumina CT3000SG (< 15 µm)	Almatis	2
Dead-burnt MgO (< 212 µm)	RHI-Magnesita	4
Resin (Prefere 88 5000 R)	Dynea (Brazil)	7
Additive	ferrocene	4

The formulations were properly mixed and homogenized with a rheometer mixer before the samples were cast inside cylindrical aluminium moulds and vibrated at 40 Hz. The prepared castables were dried at 50 °C for 24 hours or 48 hours or 72 hours and cured at 110 °C for another 24 hours. Thereafter, the

samples were demoulded and heat-treated at 500 °C for 1 hour and 1500 °C for 5 hours inside a refractory box filled with coke to create a reducing environment at 3 °C/min heating rate.

### **3.4 Characterization techniques employed during the study**

Several characterization tools were employed during the experimental study. This section identifies and discusses these techniques as it applies to the evaluated materials. The investigation was divided into three sections, related to:

- a) the resin and lignin samples,
- b) the carbon samples (from the resins) and graphitization mechanism study, and
- c) castables prepared based on in-situ graphitization of the selected binder material.

#### **3.4.1 Characterization techniques associated with lignin and the resins**

The physical and chemical properties of the binder (resins) and lignin material were measured as highlighted below.

##### **3.4.1.1 Viscosity measurement**

The resins shear viscosity with and without the graphitizing additives was measured with a ThermoHaake Rheostress 300 equipment under different shear rates. The analysis was conducted with a 41 mm cylindrical plate, at a constant gap of 3 mm under an isothermal condition at 30 °C.



#### **3.4.1.2 Fourier Transform Infrared Measurement of the resins and lignin material**

Nicolet 6700 spectrometer was employed to identify the functional groups present in the resins and lignin structure. The spectra were obtained at 2  $\text{cm}^{-1}$  resolution and 32 accumulations between 400 and 4000  $\text{cm}^{-1}$ . No sample preparation was done before the analysis.

#### **3.4.1.3 Molecular weights measurement of the lignin samples**

The effect of heat treatment on the as-received Kraft lignin molecular weight distribution was determined. For the measurement, 100 mg of each sample was weighed and dissolved in 2 ml of pyridine solution and acetic anhydride (1: 1 v/v) at 105 °C for 2h. The acetylated material was precipitated in 30 ml of distilled water and centrifuged at 7500 rpm for 15 min. Thereafter, the samples were dissolved in tetrahydrofuran (THF) in a 1:100 mass ratio and analyzed by an Agilent Technologies 1260 Infinity II Gel Permeability Chromatography (GPC) equipment. The chromatographic run was done at 12 minutes permeation time, 1 ml/min solvent flow, 30 °C column temperature, 40 °C sensor temperature and 5-20 bar pressure.

#### **3.4.2 Characterization techniques associated with the study of carbons derived from the resins and graphitization mechanism**

This section discussed the characterization techniques associated with the carbon samples and carbonization process. The analyses were mainly done to:

- a) characterize the carbons derived from the resins, and
- b) study the graphitization mechanism.

### 3.4.2.1 X-ray Diffraction (XRD) analysis

The carbon samples obtained from the plain and modified resins were ground in AMEF vibratory mill (AMP1-M) at initial experimental stage and later with a glass mortar and pestle (to eliminate the impurities introduced by the grinding mill) before characterization via X-Ray Diffraction (XRD) technique. The analysis was carried out with Rigaku Geigerflex equipment with graphite monochromator (Part 1 of this report) and Shimadzu X-ray diffraction equipment (LabX XRD-6000) under CuK $\alpha$  radiation [ $\lambda = 1.5418 \text{ \AA}$ , scanning step =  $0.032^\circ$ ] to determine the amount of generated graphitic carbon (graphitization level) and for phase determination. The phases were identified using crystallographic search-match software.

OriginPro lab-9 software (a peak analyzer tool) was used to analyze the XRD pattern for graphitization level (GL) calculation according to Bitencourt et al., [17] description. The tool was used to simulate regions of the diffractogram related to carbons and non-carbon phases to quantify their areas, respectively. Before iterations, the following mathematical functions were defined for the different peaks: (i) Gaussian function for graphitic and crystalline phases (ii) asymmetric double sigmoidal (Asym2Sig) function for the peak at  $\sim 24^\circ$ . During the iterations, functions such as half-width and peak position were adjusted or fixed to avoid unrealistic adjustment during simulation and to attain the best fit, which is defined by the coefficient of determination ( $R^2$ ) value as described in Figure 3.5. For error minimization, the XRD profiles background noise was subtracted using a DIFFRACplusEVE software before the analysis.

After the simulation, the graphitization level was calculated using equation 3.1. The area related to minor peaks associated with the presence of non-carbon materials were not considered in the GL determination.

Graphitization level (GL)

$$= \frac{\text{Graphitic carbon area}}{\text{Total area}(\text{graphitic carbon} + \text{non-graphitic carbon})} \quad (3.1)$$

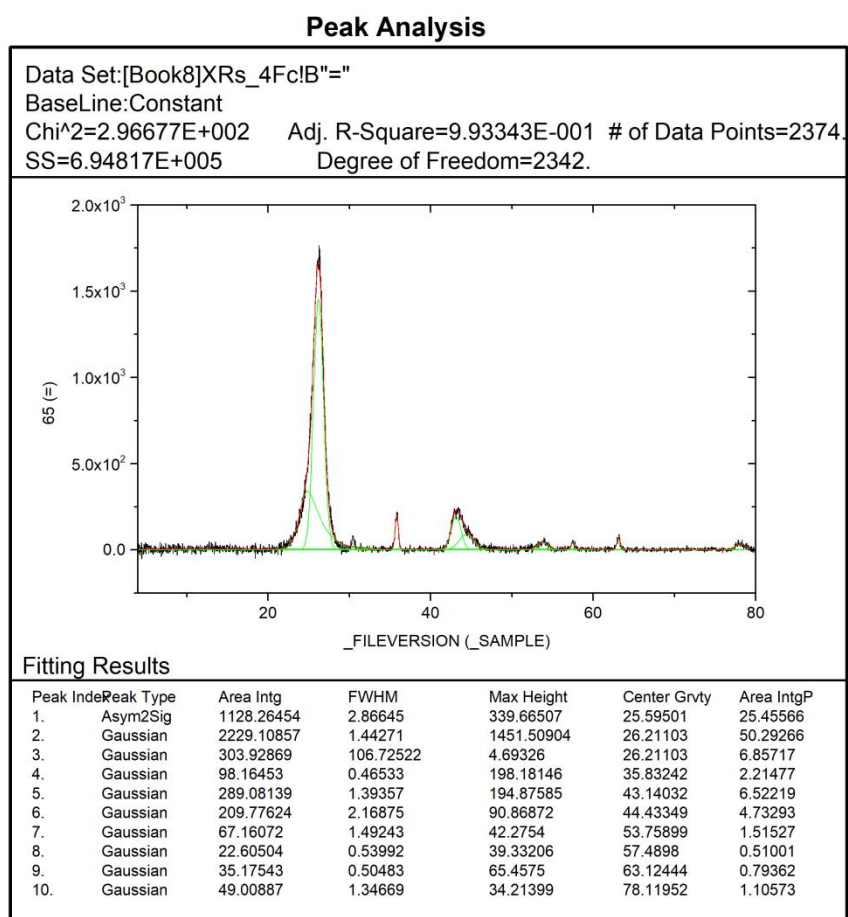


Figure 3.5: Example of the simulation report generated by OriginPro software

Furthermore, Originpro 9 software was used for peak deconvolution to determine the interlayer spacing, crystallite height and crystallite size. These parameters were obtained using equation 3.2 and 3.3.

$$n\lambda = d_{200} 2 \sin \theta \quad (3.2)$$

$$k\lambda = L_{c,a} \beta \cos \theta \quad (3.3)$$

where  $n$  = positive integer,  $d_{200}$  (nm) = interlayer spacing,  $\theta$  = incident angle,  $L_c$  (nm) = crystallite height,  $L_a$  (nm) = crystallite height,  $\beta$  = full width at half maximum,  $\lambda$  = wavelength = 0.154 nm,  $k$  = 0.89 for  $L_c$  and 1.84 for  $L_a$

### 3.4.2.2 Raman Spectroscopy analysis

Labran HR equipment was used to carry out Raman spectroscopy measurements of carbons derived from the resin formulations containing boron oxide, boric acid and ferrocene. The analysis was done to complement the primary XRD results but was not the primary characterization technique used to detect the presence of graphitic carbon in this study. The measurement was conducted at room temperature under a He-Ne laser with a nominal wavelength of 632.8 nm, at 17  $\mu$ W incident beam and an integration time of 30 s for good counting rates.

Adopting the approach put forward by Vázquez-Santos et al. [133], the crystallite size ( $L_a$ ) was calculated using equation 3.4.

$$L_a(\text{nm}) = (2.4 * 10^{-10}) \lambda_{laser}^4 \left( \frac{I_D}{I_G} \right)^{-1} \quad (3.4)$$

where  $\lambda = 632.8$  nm,  $I_D$  = intensity of the D–peak and  $I_G$  = intensity of the G–peak

### 3.4.2.3 Thermogravimetric analysis

A NETZSCH STA 449F3 (Netzsch Inc., Germany)-type TGA/DSC analyzer was used to determine the oxidation resistance of carbons obtained after the resins (with and without the various additives) pyrolysis. The apparatus detects mass loss with a resolution of 0.001g as a function of temperature and time and heat flow with 0.0001 mW/mg resolution. Before the measurement, the ground sample was evenly distributed in an alumina sample pan. The analysis was carried out in an oxidizing environment (with synthetic air (80 % N<sub>2</sub>, 20 % O<sub>2</sub>) at 50 cm<sup>3</sup>/min flow rate) starting from 30 °C to 1000 °C  $\pm$  10 °C at a heating rate of 10 °C/min. The carbon loss and oxidation initiation temperature of the samples were extracted from the non-isothermal TGA curve. Information from the DSC curves provided insight into the two principal reactions that occur during the measurements.

The thermogravimetric (TG) curves were normalized to eliminate the effect of non-carbon material described by the initial mass loss between 30 °C to ~150 °C. From the non-isothermal profile, the inflection point temperature, which represents the onset of carbon oxidation ( $T_i$ ), mass at the onset of carbon oxidation ( $MO_i$ ) and the final residual mass ( $RM_f$ ) was determined as depicted in Figure 3.6. To obtain the actual carbon loss (designated as “X” in Fig. 1),  $RM_f$  was subtracted from  $MO_i$ .

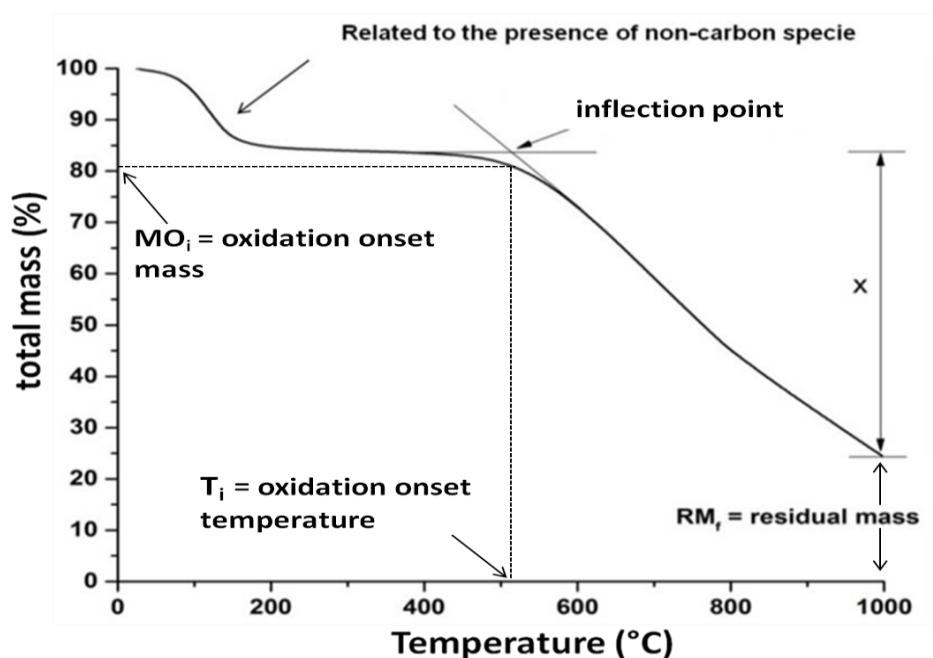


Figure 3.6: TG profile pointing out parameters used to determine the actual carbon loss of the prepared samples.

#### 3.4.2.4 Microstructural analysis

Philips XL-30 FEG scanning electron microscope with EDS detector and FEI Tecnai G2 F20 transmission electron microscope (TEM) were used to obtain microstructural information, chemical composition, lattice resolution imaging and selected area electron diffraction (SAED) pattern of the amorphous and graphitized carbon samples derived from the plain and modified resin. The images and SAED patterns were evaluated using GATAN DigitalMicrograph

software. Regarding the TEM measurements, a small quantity of the powder carbon sample was dispersed inside isopropanol and sonicated for 10 minutes. Thereafter, a drop of the suspension was pipetted and placed on the carbon-coated copper grid and the solvent was allowed to evaporate while the particles settled.

#### **3.4.2.5 Graphitization mechanism study by X-ray Photoelectron Spectrometer (XPS)**

A Thermo Scientific™ K-alpha X-ray Photoelectron Spectroscopy (Al K $\alpha$  radiation), which is a fully integrated, monochromated (using quartz crystal) small-spot system with a detection limit > 0.05 % was used to study the chemical evolution during pyrolysis. The examined samples were prepared to reflect the different carbonization stages according to the sequential heat treatment procedure that presents the best graphitization level. Samples were heated up to 300 °C (30 °C + 100 °C/4h + 300 °C), 500 °C (30 °C + 100 °C/4h + 500 °C/1h), 800 °C (30 °C + 100 °C/4h + 500 °C/1h + 800 °C), and 1000 °C (30 °C to 100 °C/5h to 500 °C/1h+1000 °C/1h and 30 °C to 100 °C/4h to 500 °C/1h+1000 °C/4h) at 3 °C/min heating rate, inside a muffle furnace and a reducing environment. The investigated resin formulations contain either boric acid, boron oxide or ferrocene additives. The equipment analyzed the samples' composition, quantifies the elements present and detect their chemical state at the different reaction stages. Peak deconvolution and curve fitting (data analysis) was done with Avantage software to quantify the elements chemical states from the overlapping peaks.

#### **3.4.2.6 Graphitization mechanism determination by Fourier Transform Infrared Spectroscopy measurements**

Varian 640-IR spectrometer was used to study the chemical evolution that occurs during thermal cross-linking, carbonization and graphitization stages of the evaluated resin formulations. The FTIR spectra were recorded between 400

and  $4000\text{ cm}^{-1}$  with 64 accumulations and  $4\text{ cm}^{-1}$  resolution using a standard KBr method. For this analysis, the samples and KBr powder were dried in an oven at  $110\text{ }^{\circ}\text{C}$  for 24 hours to remove air and moisture. After that, about 200 mg of fine KBr was mixed with 2 mg of the carbon samples, pulverized and then pressed in a die to form transparent pellets for the characterization.

### 3.4.3 Characterization of the CCR ( $\text{Al}_2\text{O}_3\text{-MgO-C}$ ) castables

The thermomechanical performance of the resin bonded castables developed based on in-situ graphitization of the binder component was analyzed and compared with a reference composition. A minimum of three samples was used for each test. The measured properties were determined as discussed below.

#### 3.4.3.1 Apparent porosity (AP) and Bulk density Measurements

Apparent porosity (AP) is defined as the ratio of open pores to its bulk volume. Closed pores, unlike open pores, are those that are not penetrated by the immersion liquid. The determination was carried out for both the cured (dried at temperatures up to  $110\text{ }^{\circ}\text{C}$  for 24 hours) and fired samples. AP of the CCRs castables was determined by ASTM C830-00 [144], using kerosene as the immersion liquid (equation 3.5). For the measurement, the sample dry weight ( $W_1$ ) was taken before being immersed in kerosene inside a vacuum desiccator under reduced pressure of 22 mmHg for 90 minutes. Each test specimen was then suspended in the immersion liquid to obtain the suspended weight ( $W_2$ ). Finally, the samples were slowly lifted from the immersion liquid by means of a sling and the weight of the soaked test piece ( $W_3$ ) was obtained.

$$AP (\%) = \left( \frac{W_3 - W_1}{W_3 - W_2} \right) \times 100 \quad (3.5)$$

where,

$W_1$  = dry weight

$W_2$  = suspended weight

$W_3$  = soaked weight

Moreover, the bulk density (BD), which is the ratio of the dry weight to the bulk volume of the porous material was determined using equation 3.6.

$$BD (\%) = \left( \frac{W_1}{W_3 - W_2} \right) \times \text{liquid density at ambient temperature} \quad (3.6)$$

Each AP and BD values represent the average of at least three samples.

### 3.4.3.2 Cold Crushing Strength (CCS) Measurement

Cold crushing strength (equation 3.7) of the developed refractories was measured as described by ASTM C133-97 [145], with a standard hydraulic compression testing machine (EMIC DL 60000, 600 kN). At least, three samples were used for each measurement.

$$CCS (MPa) = \frac{P}{A} \quad (3.7)$$

where,

P = total maximum load indicated by the testing machine (N),

A = average of the areas of the top and bottom of the specimen perpendicular to the line of application of the load (mm<sup>2</sup>).

### 3.4.3.3 Oxidation Resistance Measurements

For oxidation resistance test, cylindrical samples from the developed CCRs was fired in an electrically heated furnace (heating rate of 5 °C/min) under an ambient condition at 1000 °C for 1 hour. The furnace was allowed to cool down at the same rate. The samples' oxidation resistance was measured via weight loss technique and oxidation index determination. For the first method, the samples weights before and after oxidation were determined and oxidation loss



was calculated using equation 3.8. The weight loss was assumed to be due to carbon loss.

$$\text{oxidation loss} = \left( \frac{\text{initial weight} - \text{final weight}}{\text{initial weight}} \right) \times 100 \quad (3.8)$$

Subsequently, the fired samples were cut horizontally into two pieces. The diameter of the remaining black surface was then measured at eight different locations. The average value of this measurement was used to determine the oxidation index according to equation 3.9. Three samples per each composition was used for the investigations.

$$\text{oxidation index} = \left( \frac{\text{oxidized diameter}}{\text{total diameter}} \right) \times 100 \quad (3.9)$$



## 4 RESULTS AND DISCUSSION

The experimental results are presented in four parts for better comprehension of the write-up. Each segment discussed the research associated with:

- a) commercial phenolic resin,
- b) laboratory synthesized conventional resins,
- c) laboratory synthesized lignin-modified resins, and
- d) resin-bonded carbon-containing refractory castables, respectively.

### 4.1 Part 1: Catalytic graphitization of commercial novolac resin by boric acid, boron oxide and ferrocene

This section discussed the results on graphitization of commercial novolac resin (Nv) using conditions that can be adopted for carbon-containing refractories (CCRs) production. The effect of boron oxide and boric acid (graphitizing agents), hexamethylenetetramine (cross-linking additive) and the influence of some processing parameters (mixing technique, vacuum degassing, and heating procedure) on the amount of generated graphitic carbon was presented. X-ray diffraction (XRD) equipment and Raman spectrometer (to complement) were selected to evaluate the graphitization level and crystal parameters of the carbon samples. The oxidation resistance of the derived carbons was studied with the aid of thermogravimetric (TGA) and differential scanning calorimetry (DSC) equipment. Chemical changes that occur during pyrolysis of the resin formulations were investigated via Fourier Transform Infrared (FTIR) spectroscopy and X-ray Photoelectron Spectroscopy (XPS). Moreover, an investigation on the effect of different heating procedures on the graphitization of novolac resin containing ferrocene formulation was also reported.

#### 4.1.1 Structure of carbons derived from novolac resin formulations containing boric acid and boron oxide

The crystallinity and structural orderliness of carbonized novolac resin containing boron compounds ( $\text{H}_3\text{BO}_3$ ,  $\text{B}_2\text{O}_3$ ) samples were studied using X-ray diffraction technique. Firstly, a reference carbon sample was prepared from a mixture of novolac resin and 10 wt% HMTA after pyrolysis via the A3-procedure (see Table 3.2). This is the typical resin formulation that is used as a binder during industrial production of carbon-containing refractories. Figure 4.1 shows the XRD pattern of the derived pyrolytic carbon. A low-intensity broad hump across  $20^\circ$  and  $30^\circ$  near the 002 plane of graphitic structure characterized the profile. The peak at  $\sim 43^\circ$  corresponds to 100 in-plane symmetry for non-graphitic carbon structure. This is the usual diffractogram of  $\text{sp}^3$ -hybridized carbon with an amorphous structural arrangement based on a rigid structure that limits the rotation of atoms to graphene layers during pyrolysis [141]. Similarly, carbonized novolac resin (Nv) without HMTA addition presents the same XRD pattern. Based on this result, graphitization of plain Nv was not favoured at  $1000^\circ\text{C}$ .

Previous research findings have shown that higher processing temperatures ( $1650\text{-}1750^\circ\text{C}$ ) used in steelmaking is not sufficient for crystallization of carbon from such organic precursors [3]. In fact, the highly cross-linked nature of Nv carbon should inhibit thermal ordering even at temperatures up to  $3000^\circ\text{C}$  [9]. The additional peaks observed at  $31.5^\circ$ ,  $35.5^\circ$  and  $48^\circ$  (Figure 4.1) are related to tungsten carbide contamination from the grinding equipment lining material that was used for samples preparation prior to analysis.

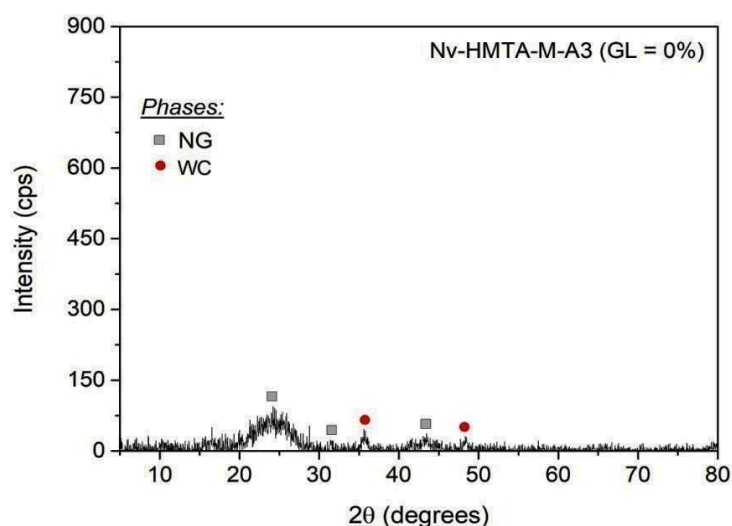


Figure 4.1: X-ray diffraction pattern of novolac resin + 10 wt% HMTA (reference composition) after firing at 1000 °C for 5h using A3-procedure (NG = non-graphitic, WC = tungsten carbide, GL = graphitization level, M = mechanical mixing, Nv = novolac resin).

Despite the non-graphitizing characteristic of novolac resin (as observed in Figure 4.1), the XRD profiles of carbons from the modified resin (containing  $B_2O_3$  or  $H_3BO_3$ ) show a transition from highly amorphous to graphitic ones. The diffractograms of Nv-6B-M-A3 (Figure 4.2a) and Nv-10H-M-A3 (Figure 4.2b) show an asymmetric 002 peak at  $\sim 26^\circ$ , which is sharper with increased intensity due to graphene layers stacking. The intensity and width of the peak at  $\sim 26^\circ$  are generally used to explain carbon crystallization [17, 101, 119]. The graphitization level (GL) of Nv-6B-M-A3 and Nv-10H-M-A3 samples was calculated to be 49 % and 69 %, respectively (Figure 4.2a and 4.2b). These results agree with observations by other researchers that the incorporation of boron enhances the crystallization of pyrolyzed organic precursors [101, 146]. Additionally, they are significant as graphitization is usually not achieved at such temperatures (1000 °C). A new distinct peak (at  $\sim 28^\circ$ ) corresponding to the  $B_2O_3$  phase was also identified in the Nv-10H-M-A3 composition (Figure 4.2b). Although some authors [101, 121, 147] reported the volatilization of boron oxide after heating at 1000 °C, its presence suggested that oxygen may have partially participated in the pyrolysis because coke (instead inert gas) was used to create the reducing

environment during the samples' treatment [17]. More so, oxygen is part of the carbonization products and it is therefore difficult to completely eliminate this gas during the pyrolysis operation. However, as this phase was only detected in compositions prepared from boric acid-catalyzed resin, its presence may also be attributed to the additional reaction-step involving initial formation and decomposition of phenylborate (formed during the curing of novolac resin [101]) to boron oxide at 400 °C.

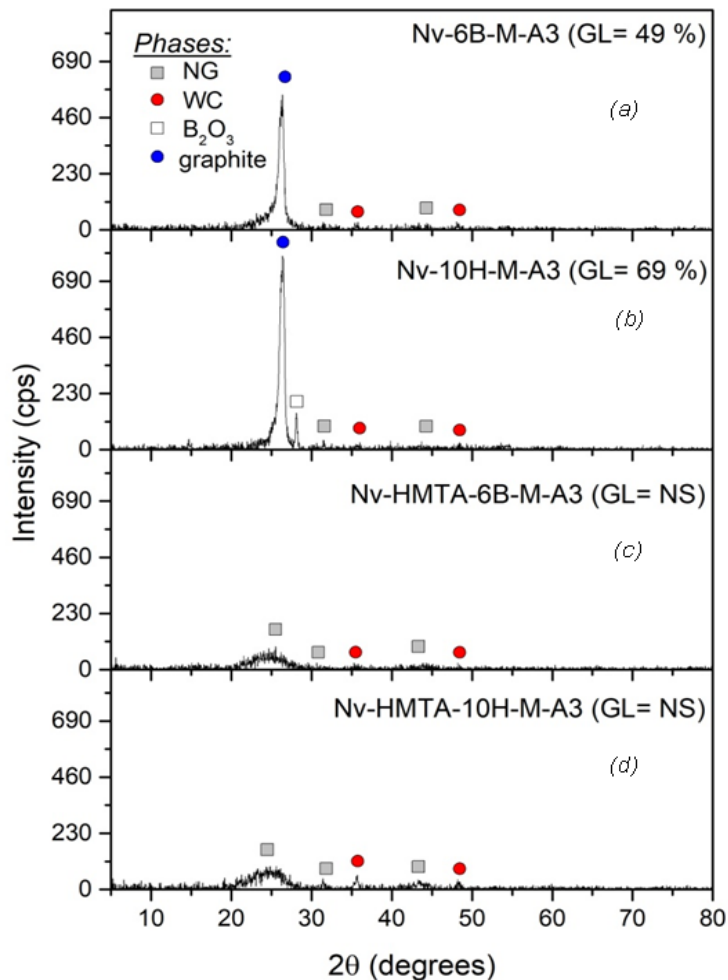


Figure 4.2: XRD profiles showing the effect of boron-based additives on graphitization of a commercial novolac resin (with and without 10 wt% HMTA) after firing at 1000 °C for 5h under reducing atmosphere. GL = graphitization level, NS = not significant, A3 = heating procedure at 3 °C/min, M = mechanical mixing, NG = non-graphitic, WC = tungsten carbide, 6B = 6 wt%  $B_2O_3$ , 10H = 10 wt%  $H_3BO_3$ , HMTA = 10 wt% hexamethylenetetramine, Nv = novolac resin.

The presence of  $B_2O_3$  may be beneficial in the refractory formulation (such as MgO-C), as it can lead to the formation of a low melting phase ( $3MgO.B_2O_3$ ) that can block open pores and coat the carbon surface, thus suppressing oxidation. Nevertheless, this benefit will be at the expense of hot mechanical strength.

Besides that, the influence of HMTA (which is a hardening agent used in the development of resin-bonded refractories to increase its amount of fixed carbon yield [7]) addition to the boron compound modified resin formulations, was also evaluated. By incorporating 10 wt% HMTA to the boron oxide or boric acid-modified resin, graphitization was inhibited (Figure 4.2c and 4.2d). Heteroatoms, such as nitrogen and its functional groups (present in HMTA), typically enhance reactivity and atoms cross-linking [148]. These reactions significantly reduced the graphitizability of the resultant carbons and prevented reconstructive transformation necessary for graphite generation. The results suggest that to achieve an ordered arrangement, atoms' binding energy must be much weaker to allow carbon nuclei formed during the initial stages of carbonization to remain relatively mobile [55, 97, 98]. This inference was similar to the observation made by Kipling et al. [94, 149, 150] regarding factors that can influence the graphitization of polymers. The authors found that substantial cross-linking during the curing stages prevented crystallization of the resulting carbon. Moreover, the XRD profiles of the samples were similar to those obtained by Yun et al. [127], with a novolac composition containing 12 wt% HMTA and phenylboronic acid.

The experiments and XRD analysis were repeated six times for each composition to ascertain reproducibility of the obtained results using the mixtures that presented the best graphitization level. The calculated GL values for Nv-6B-M-A3 and Nv-10H-M-A3 are  $47 \pm 10$  and  $49 \pm 12$ , respectively. Most related studies published in the literature overlooked this important aspect. Therefore, based on the experimental results, the following conclusion and inferences were made:

- i. The addition of boron-containing compounds such as  $B_2O_3$  and  $H_3BO_3$  to novolac resin leads to its graphitization at 1000 °C.

- ii. Graphitization of the boron-catalyzed novolac samples at 1000 °C takes place in a heterogeneous manner. The selected additives caused partial acceleration of the carbon matrix crystallization, producing carbons consisting of different phases (i.e. graphitic and non-graphitic components).
- iii. The average GL value ( $GL_a$ ) for Nv-10H-M-A3 is ~8 % less than the one obtained by Luz et al. [130] that used similar composition and experimental procedure. The calculated standard deviation results for this property indicate the heterogeneity of the attained samples.

The following are some likely reasons for the heterogeneous graphitization/limited reproducibility detected in the samples:

- i. The agglomeration of additives as a result of their susceptibility to hydration (water vapour is released during the heat treatment process [92]) and the natural tendency for particles coagulation [124, 151] can lead to heterogeneous graphitization and non-uniform distribution of the crystalline phase. This observation agrees with the study carried out by Wang et al. [124], where  $B_4C$  particles were dispersed in a phenolic resin with the aid of a powerful mixing device for 40 minutes. The inhomogeneous distribution and additive accumulation (even after heat treating the sample up to 300 °C) was attributed to the relatively high viscosity of the resin and difference in the physical properties of both materials [124].
- ii. The incorporation of boron atoms or non-uniform distribution of residual  $B_2O_3$  in the carbon matrix might lead to a peak broadening effect. As pointed out by Davor and Balzar, any lattice imperfection such as the presence of vacancies, dislocation, interstitial and similar defects can cause X-ray diffraction line broadening [152].
- iii. Temperature is a crucial factor in thermosetting resin graphitization. As observed by Franklin [153], homogenous graphitization is a function of cross-linking developed between the carbon atoms (during the curing stage) and temperature at which pyrolysis was carried out. These observations agree with the results by Oya et al. [20]. The authors reported that uniform and



continuous graphitization of carbons derived from phenolic resin catalyzed with boron only begins at 1800 °C. Hence, to achieve continuous carbon crystallization, the pyrolysis temperature must provide sufficient energy to break maximum number of bonds.

- iv. Another likely cause is the preferential graphitization originating from B–O–C sites with lower binding energy than C–C bonds (B–O–C band was detected in the FTIR profile of samples heat-treated up to 230 °C or 500 °C). This type of mechanism has been observed in graphitization of thermosetting resin under high pressure such as 1000 MPa. At that instant, heterogeneous crystallization was ascribed to the internal stress generated through anisotropic thermal expansion of carbon crystallites, concentrated at certain sites where graphitization proceeds preferentially in order to release the stress [154]. Such preferred graphitization of carbons derived from phenolic resins around pores was also implied in a study by Kamiya and Suzuki [104]. Microstructural examination shows packets of carbons around pores formed during the hardening and carbonization process. The concept suggests that increasing the amount of graphitizing agents may enhance the homogeneity/graphitization level. However, the fact that boric acid is sometimes used as a catalyst and hardening agent for thermosetting resin, such as novolac in the foundry industry, may not allow unlimited additions [151].

From the XRD characterization, structural features such as crystallite height ( $L_c$ ) and interlayer spacing ( $d_{002}$ ) of the graphitized carbons were determined using Scherrer's (equation 3.2) and Bragg's (equation 3.3) equations, respectively. Both parameters have been used to describe the degree of carbon crystallization, where an increasing  $L_c$  and decreasing  $d_{002}$  (tending towards 0.3354 nm, which is graphite's  $d_{002}$  value) indicate a higher graphitization level [101]. As mentioned earlier, OriginPro lab-9 software was used for the diffractogram deconvolution in the 20–32° of the  $2\theta$  region. To determine these parameters, the humps were fitted using Gaussian peaks. Table 4.1 shows the obtained results. As expected, a range of values was obtained for both evaluated properties due to the heterogeneous nature of the compositions. The carbon

interlayer spacing values are within 0.3372-0.3427 nm range and the crystallite heights are in the 7-12 nm one. These numbers are within those obtained in the literature for carbonized novolac resin modified with boron-containing compounds [101, 119, 122, 130], which suggests a random combination of graphitic and turbostratic stacking [155].

Table 4.1: Crystal parameters of pyrolytic carbon samples fired at 1000 °C for 5h under reducing atmosphere (for the composition without HMTA, the results represent the average and standard deviation of 6 measurements in 3 different batches).

Samples	$L_c$ (nm)	$d_{002}$ (nm)
Nv-HMTA-M-A3	1.69	0.3629 – 0.3742
Nv-HMTA-6B-M-A3	2.06 – 2.78	0.3604 – 0.3606
Nv-HMTA-10H-M-A3	2.96 – 3.01	0.3608 – 0.3610
Nv-6B-M-A3	$9.39 \pm 2.39$	$0.3406 \pm 0.002$
Nv-10H-M-A3	$10.66 \pm 2.09$	$0.3382 \pm 0.001$

A significant increase in  $L_c$  detected in some of the compositions show that boron catalyzed the process resulting in some degree of orderliness [90]. As reported by some authors [101, 156], the incorporation of boron can bring about change in  $\pi$ -electron density, which could result in reduced interlayer spacing and increased crystallite height. Specifically, the presence of boron in the carbon matrix can lead to electron deficiency and more attractive interaction between the  $\pi$ -electron clouds of adjacent graphitic layers allowing them to come closer together [122, 157]. Boron atoms have the ability to intercalate carbons during pyrolysis of the catalyzed resin [128, 158]. Their enhanced diffusivity also allows them to act as vacancies in carbon structure, which favours the growth of  $L_c$  and reduced  $d_{002}$  [146]. Furthermore, as the growth of crystals in the c-direction requires proper planer stacking, there is an agreement between the increased values of  $L_c$  (compared to the reference composition) and those of  $d_{002}$  with estimations closer to graphene layers [133].

It is important to highlight that the effect of grinding time (using a WC lined mill) when preparing the samples for XRD analysis was studied as an alternative way to adequately quantify the amount of generated graphitic carbon. For this measurement, the samples were ground at different times up to 120 s. Homogeneity of the analyzed samples effectively improved with increased milling time (~3 % difference in graphitization level values at 120 s grinding time). Nevertheless, the process also caused significant amorphization. Notably, the peak intensity at 31.5°, 35.5° and 48° related to tungsten carbide contaminant from the grinding equipment lining material also increased with prolonged milling. Consequently, this preparation route for XRD analysis was considered not reliable compared to determining the average graphitization level. Moreover, the  $GL_a$  values provide a basis to identify other factors that can influence the catalyzed resin graphitization.

The role of lower HMTA additions (1 and 5 wt%) on the resin catalytic graphitization was further investigated using 2, 4, 5 °C/min heating rates (designated as A2, A4 and A5 and described in Table 3.2). The investigation was done to ascertain if a lesser quantity of HMTA under different heating procedures would remove the barrier to crystalline carbon generation for compositions containing the crosslinking additives. A broad hump between 20° and 30° characterized the diffractograms of Nv-6B-M and Nv-10H-M's formulation containing 1 or 5 wt% HMTA (Figure 4.3). As pointed out earlier, the enhanced reactivity provided by HMTA additions led to higher bond cross-linkage, which prevented fusion and carbon atoms rotation during pyrolysis. A little addition of 1 wt% HMTA was enough to inhibit the carbons crystallization. Besides, changing the heating rate did not significantly lead to graphitic carbon generation, except for the boron oxide modified resin containing 1 wt% HMTA that was pyrolyzed using the A4-procedure (Figure 4.3b). The carbon derived from this formulation has a low-intensity peak at ~26°. More so, the profile depicted that the varied parameters were more pronounced with 5 wt% HMTA addition and increased heat treatment time (2 °C/min). This observation was based on the reduced intensity and increased hump base width typified by the samples diffractogram.

Furthermore, the hump at  $\sim 43^\circ$  further confirmed the non-graphitic nature of the carbon samples [159].

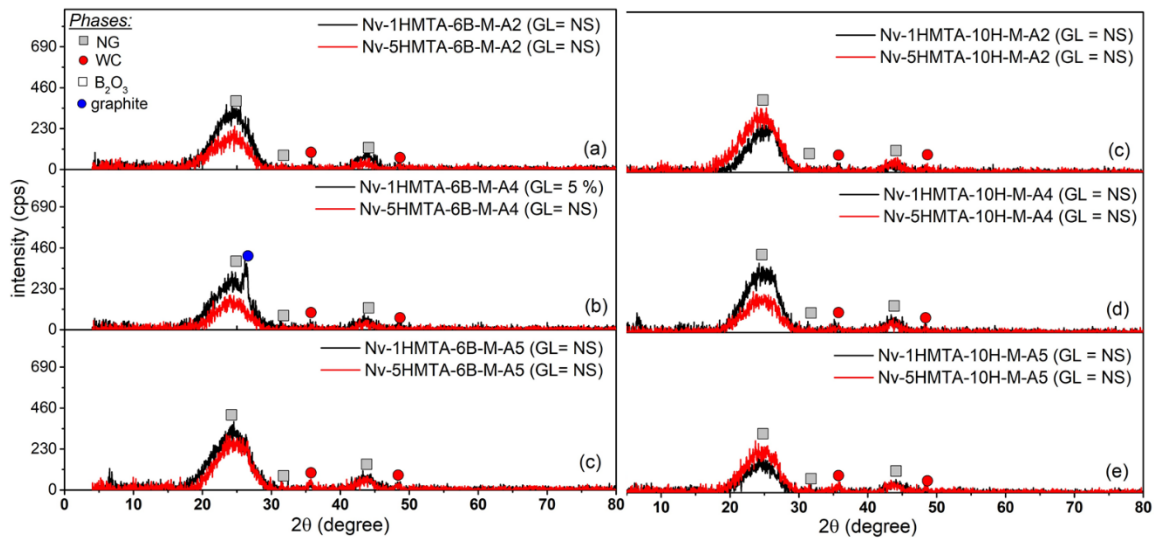


Figure 4.3: XRD profiles of the evaluated compositions showing the effect of HMTA additions on catalytic graphitization of novolac resin: (a) with boron oxide (b) boric acid as the graphitizing agents after firing at  $1000^\circ\text{C}$  for 5h under reducing atmosphere. GL = graphitization level, NS = not significant, M = mechanical mixing, NG = non-graphitic, WC = tungsten carbide, 6B = 6 wt%  $\text{B}_2\text{O}_3$ , 10H = 10 wt%  $\text{H}_3\text{BO}_3$ , 1HMTA = 1 wt% hexamethylenetetramine, 5HMTA = 5 wt% hexamethylenetetramine, Nv = novolac resin.

#### 4.1.2 Influence of processing parameters on the catalytic graphitization of novolac resin containing boron source compounds

Based on the attained results, an attempt was made to study the influence of other processing parameters on the graphitization behaviour of the modified novolac resin. Taking this into consideration, the use of ultrasonic mixing, vacuum degassing, heating rates and heat treatment sequence were investigated. Higher mixing speed and time were not analyzed in this study based on the observation of other researchers that: (i) prolonged mixing/agitation may lead to heat generation, which most likely limits the graphitization degree of resins [130], (ii)

particle agglomeration can be detected even after prolonged mixing (40 minutes) of phenolic resin and boron carbide additives at room temperature [124].

Research studies have shown that to achieve effective crystallization of carbon derived from phenolic resins, the additives should be properly dispersed within the composition's matrix [17]. Based on this information, ultrasonic mixing was incorporated into the preparation procedures. Compared to the samples prepared with only mechanical mixing (Figure 4.2), Nv-6B-M-U-A3 and Nv-10H-M-U-A3 presented limited graphitization, which represents an average GL reduction of about ~54 %, respectively (Figure 4.4a and 4.4b). Such a performance indicated that this preparation procedure (mechanical + ultrasonic mixing) might have a negative impact on graphitization.

Additionally, a broad hump associated with disordered carbon phase showed up at  $\sim 24^\circ$  in Figure 4.4. The stronger atomic linkages resulting from increased chemical reactions during sonication hindered ordered structuring of the resultant bonds. Typically, the additional mixing technique can induce high energy chemical reactions due to formation, growth and collapse of bubbles, which favours the release of instantaneous pressure, high-intensity local heating that can promote increased cross-linking density [160, 161]. Consequently, because the carbon network was tightly held, limited rotation hindered the maximum generation of graphitic carbon. No significant change took place in the composition containing 10 wt% HMTA, as the presence of HMTA still prevented carbon crystallization (Figure 4.4c).

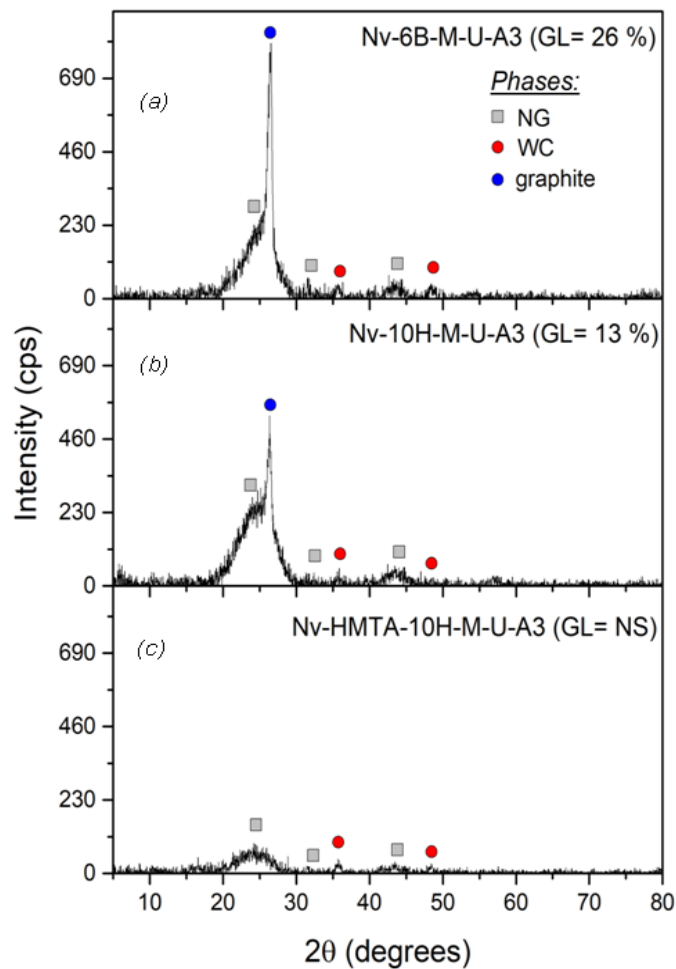


Figure 4.4: XRD profiles of the prepared samples showing the effect of additional ultrasonic mixing on catalytic graphitization of novolac resin after firing at 1000 °C for 5h under reducing atmosphere. GL = graphitization level, NS = not significant, A3 = heating procedure at 3 °C/min, M = mechanical mixing, U = ultrasonic mixing, NG = non-graphitic, WC = tungsten carbide, 6B = 6 wt% B<sub>2</sub>O<sub>3</sub>, 10H = 10 wt% H<sub>3</sub>BO<sub>3</sub>, HMTA = 10 wt% hexamethylenetetramine, Nv = novolac resin.

To ascertain the drawn conclusion, the analysis was repeated with the same batch of samples as shown in Table 4.2. Furthermore, introducing the additional mixing technique did not diminish the heterogeneity detected in the prepared compositions.

Table 4.2: Comparison of the average graphitization level ( $GL_a$ ) for samples prepared with mechanical mixing or with mechanical + ultrasonic mixing. All materials were fired up to 1000 °C for 5h and under reducing atmosphere.

<b>Samples</b>	<b><math>GL_a</math> (%)</b>
Nv-6B-M-A3	$47 \pm 10$
Nv-6B-M-U-A3	$21 \pm 7$
Nv-10H-M-A3	$49 \pm 12$
Nv-10H-M-U-A3	$19 \pm 9$
Nv-HMTA-10H-M-A3	NS
Nv-HMTA-10H-M-U-A3	NS
<i>*NS = not significant</i>	

Degassing the resin-additive compositions prior to pyrolysis produced a similar effect to using ultrasonic mixing. The GL value of novolac resin catalyzed with boron oxide or boric acid significantly decreased with the removal of entrapped gas from the formulations (Figure 4.5a and 4.5b). Compared to Nv-6B-M-A3 and Nv-10H-M-A3 (Figure 4.2), GL values of Nv-6B-M-V-A3 and Nv-10H-M-V-A3 showed an average reduction of 52 % and 63 %, respectively. According to Pilkenton et al. [162], the presence of oxygen in an organic precursor will inhibit free-radical polymerization by reacting to form stable peroxy radicals, which restrict the degree of conversion and amount of cross-linking network. The aforementioned process can occur at several steps in the reaction sequence leading to an extension in the induction time needed for the completion of polymerization (as they do not readily reinitiate the process). Consequently, the incorporation of vacuum degassing favours increased cross-linking amid curing, which eventually limits the rotation of atoms to graphene layers during carbonization [94].

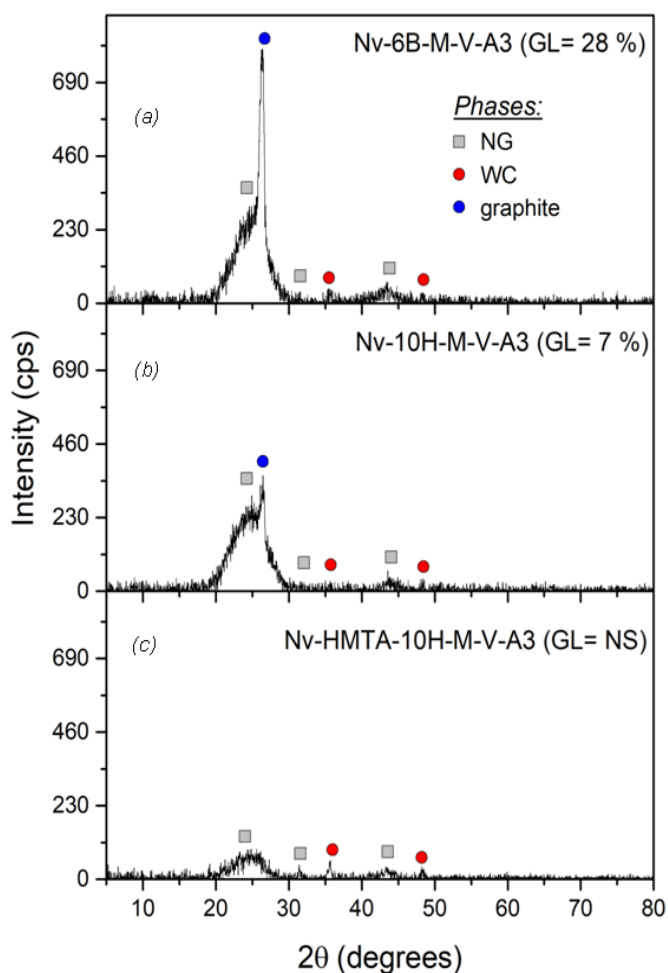


Figure 4.5: XRD profiles of the prepared samples showing the effect of vacuum degassing on catalytic graphitization of novolac resin after firing at 1000 °C for 5h under reducing atmosphere. GL = graphitization level, NS = not significant, A3 = heating procedure at 3 °C/min, M = mechanical mixing, V = vacuum degassing, NG = non-graphitic, WC = tungsten carbide, 6B = 6 wt% B<sub>2</sub>O<sub>3</sub>, 10H = 10 wt% H<sub>3</sub>BO<sub>3</sub>, HMTA = 10 wt% hexamethylenetetramine).

Additionally, the effect of degasification appears to be more significant when boric acid (compared to boron oxide) was the graphitizing agent. The intermolecular hydrogen bond between H<sub>3</sub>BO<sub>3</sub> and novolac resin may enhance the cross-linkage's effect during the chemical reactions. Besides, with and without the introduction of vacuum degassing, the presence of HMTA in boric acid-catalyzed resin hindered its graphitization (Figure 4.5c). The results further justify the role of the atoms' binding energy on the ordered rearrangement of carbonized



resin [17, 149, 163]. Consequently, all factors that favour substantial bonding during the curing stage may inhibit the generation of graphitic carbons from  $B_2O_3$  or  $H_3BO_3$  catalyzed resin. Moreover, the results suggest that the initial presence of oxygen may not prevent crystalline carbon formation when CCR bricks are fired. The average graphitization results ( $GL_a$ ) of the carbons derived from the compositions prepared with and without the degassing step are presented in Table 4.3.

Table 4.3: Comparison of the average graphitization level ( $GL_a$ ) for samples prepared with mechanical mixing and with or without applying vacuum degassing during the processing steps. All materials were fired up to 1000 °C for 5h and under reducing atmosphere.

<b>Samples</b>	<b><math>GL_a</math> (%)</b>
Nv-6B-M-A3	47 ± 10
Nv-6B-M-V-A3	22 ± 9
Nv-10H-M-A3	49 ± 12
Nv-10H-M-V-A3	15 ± 11
Nv-HMTA-10H-M-A3	NS
Nv-HMTA-10H-M-V-A3	NS
<i>*NS = not significant</i>	

Generally, heating rate influences the course of chemical reaction and diffusion process. Hence, its role on graphitization of the catalyzed resin was investigated. Table 3.2 describes the selected firing procedures designated as A2, A3, A4 and A5. The phase evolution of Nv-6B-M and Nv-10H-M compositions under 2–5 °C/min heating rates was described in Figure 4.6. The hump at ~ 26° related to the crystalline phase appeared whereas the amorphous one (near the 002 plane of the graphitic structure) decreased as the heating rate increased from 2 to 3 °C/min (Figure 4.6b and 4.6c). These patterns represent a transition from amorphous to graphitic carbons. In principle, because the pyrolysis operation involves the formation and breaking of bonds, the heating sequence may

influence the atoms' binding energy. Therefore, a decrease in the GL values below 3 °C/min may be attributed to the higher cross-linking induced by prolonged HTT during the pre-pyrolysis stage. The strong chemical bonding limits the fusion and the rotation of the atoms during heat treatment [150]. Besides, the use of 4 and 5 °C/min heating rates (Figure 4.6d and 4.6e) restricted catalytic additive diffusion and minimized bond-breaking due to the shorter HTT applied during the pyrolysis operation, which resulted in limited carbon crystallization [17, 164].

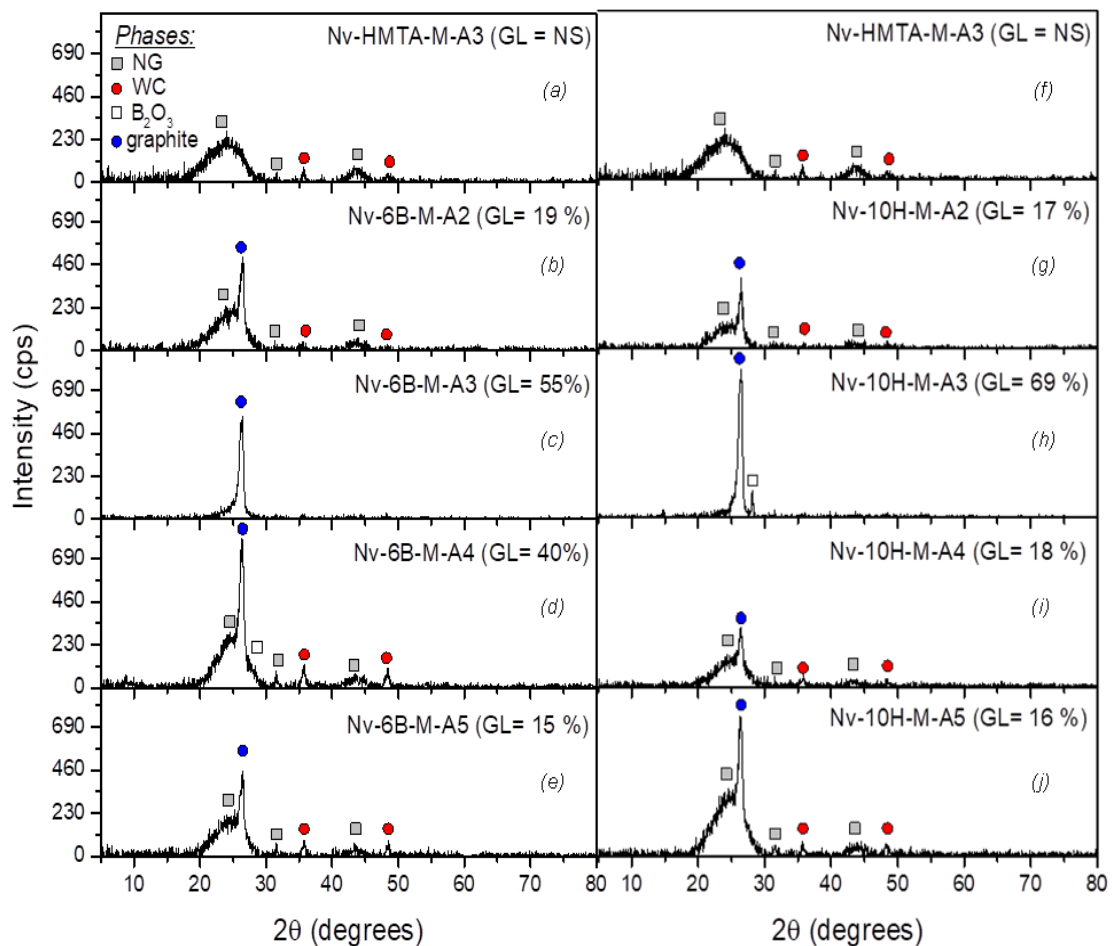


Figure 4.6: Effect of heating rates on graphitization of carbonized novolac resin containing: (b-e) boron oxide or (g-j) boric acid as graphitizing agent and (a, f) reference composition. GL = graphitization level, NS = not significant, M = mechanical mixing, NG = non-graphitic, WC = tungsten carbide, 6B = 6 wt%  $B_2O_3$ , 10H = 10 wt%  $H_3BO_3$ , HMTA = 10 wt% hexamethylenetetramine.

The XRD profiles of the pyrolytic carbons derived from boric acid-catalyzed resin show a similar GL evolution (Figure 4.6g – 4.6j). The 3 °C/min heating rate also seems to be the most favourable condition for its catalytic graphitization. The results indicate that any adopted protocol must: (i) not generate substantial cross-linking during pre-pyrolysis stages, (ii) provide enough time for the graphitizing agents to act and, (iii) ensure maximum bond cleavage and atom rearrangement to develop a more ordered structure from the amorphous carbons. Table 4.4 compares the samples' GL values for the different heating rates.

Table 4.4: Comparison of graphitization level for the prepared samples produced using different heating rates.

<b>Samples</b>	<b>GL<sub>a</sub> (%)</b>
Nv-HMTA-M-A3	NS
Nv-6B-M-A2	19
Nv-6B-M-A3	47 ± 10
Nv-6B-M-A4	40
Nv-6B-M-A5	15
Nv-10H-M-A2	17
Nv-10H-M-A3	49 ± 12
Nv-10H-M-A4	18
Nv-10H-M-A5	16
<i>*NS = not significant</i>	

To find other factors that might influence or induce Nv graphitization, the effect of different treatment pathways, i.e. B3 and C3–procedure (see Table 3.2 for heating procedure description) was also evaluated. The selected procedures provided information on the role of the heating sequence and increased HTT during curing (below 500 °C) on the carbon crystallization. The peak's intensity at ~26° decreased for samples produced via B3 and C3 treatments (Figure 4.7).

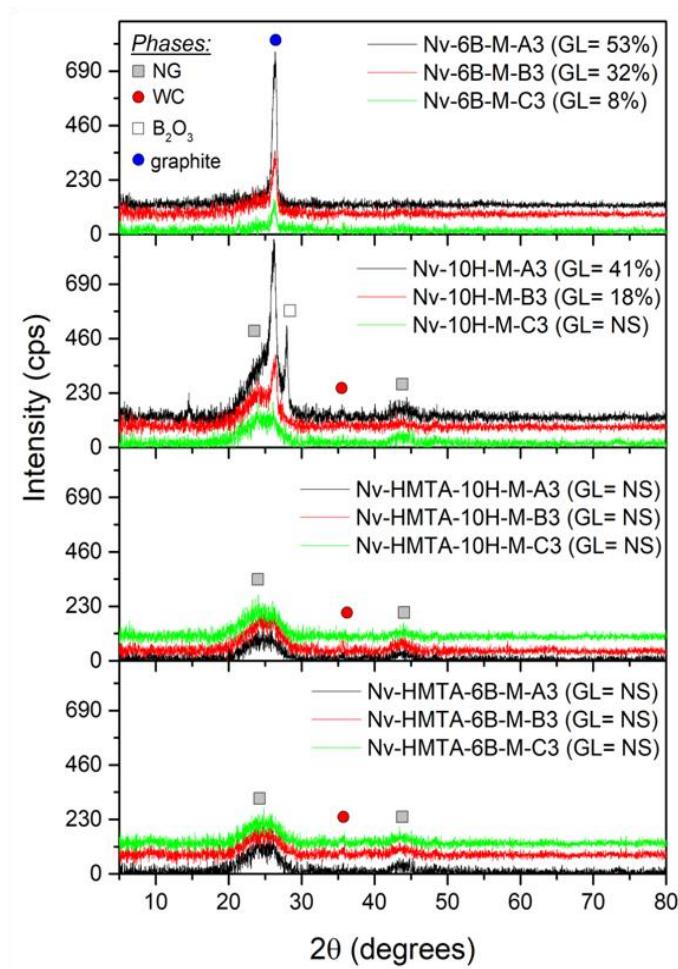


Figure 4.7: XRD profiles of the evaluated compositions showing the effect of different heat treatment sequence on graphitization of catalyzed novolac resin after firing at 1000 °C for 5h under reducing atmosphere. GL = graphitization level, NS = not significant, M = mechanical mixing, NG = non-graphitic, WC = tungsten carbide, 6B = 6 wt% B<sub>2</sub>O<sub>3</sub>, 10H = 10 wt% H<sub>3</sub>BO<sub>3</sub>, HMTA = 10 wt% hexamethylenetetramine.

Compared to Nv-6B-M-A3 (GL = 54 %), the GL of Nv-6B-M-B3 and Nv-6B-M-C3 decreased to 32 % and 8 %, respectively. Similarly, Nv-10H-M-B3 compared to Nv-10H-M-A3 shows a reduction of about 23 % of this property, whereas the GL of Nv-10H-M-C3 becomes insignificant.

The results show that using additional dwell time during the curing stages was not suitable for maximum generation of graphitic carbon. Typically, cross-linking degree of resin containing additives depends on specific formulation, cross-linking system, temperature condition, curing time, etc. [165-167]. Both the

B3 and C3-procedure might have induced stronger bonding, which gave rise to a three-dimensional structure, lower disruption, structuring and maximum graphitization of the catalyzed resin. In a previous study, Liu et al. [139] clearly show, by measuring the glass transition temperature, that cross-linking degree in boric acid-catalyzed resin increased with prolonged curing time. A similar pattern was pointed out by Luz et al. [130] as the use of a slow curing step resulted in a lower graphitization level for novolac resin composition containing 10 wt% boric acid. Both mentioned experimental results justify the explanation provided earlier. Consequently, heating sequence was identified as another factor that can affect graphitic carbon generation from  $B_2O_3$  or  $H_3BO_3$ -modified novolac resin. Regarding Nv-HMTA-10H composition, no significant phase transition was detected as a result of a change in the heating procedures (although the intensity of the broad hump decreases with the B3 or C3-procedure). The GL values are presented in Table 4.5.

Table 4.5: Comparison of graphitization level for samples produced using the different heating sequence.

<b>Samples</b>	<b>GL (%)</b>
Nv-6B-M-A3	47 ± 10
Nv-6B-M-B3	31
Nv-6B-M-C3	8
Nv-10H-M-A3	49 ± 12
Nv-10H-M-B3	18
Nv-10H-M-C3	NS
Nv-HMTA-10H-M-A3	NS
Nv-HMTA-10H-M-B3	NS
Nv-HMTA-10H-M-C3	NS
Nv-HMTA-6B-M-A3	NS
Nv-HMTA-6B-M-B3	NS
Nv-HMTA-6B-M-C3	NS
<i>*NS = not significant.</i>	

### 4.1.3 Raman spectra of some selected carbon samples from novolac resin containing boric acid and boron oxide

In this study, some of the carbon samples were chosen for investigation by Raman spectroscopic. The Raman spectra of carbons derived from novolac resin containing boric acid or boron oxide after carbonization using A3- and B3-procedures were presented in Figure 4.8 (refer to Table 3.2 for heat treatment description). The results from this analysis were compared with the deductions based on the XRD technique. The most prominent features of the first-order Raman spectra are the G-band, which appears at  $\sim 1580\text{ cm}^{-1}$  for crystalline carbon phase and the D-band at about  $\sim 1350\text{ cm}^{-1}$  for amorphous or non-crystalline phase [168]. The intensity ratio [ $I_g/(I_d+I_g)$ ], the G-band width (FWHM) and the calculated crystallite size values (Table 4.6) were related with graphitization degree in accordance with previous studies [133, 137]. The Raman spectra deconvolution was done with the help of OriginPro software after the peaks were fitted with Gaussian function. Figure 4.8a shows the Raman spectra of carbons derived from novolac resin containing boric acid (Nv-10H-M-A3 and Nv-10H-M-B3). A comparison of both heating procedures shows that the product obtained from the formulation subjected to the A3-procedure have higher intensity-ratio and lower G-band width value compared to the ones derived from the B3-procedure (Table 4.6). Moreover, the occurrence of the band at  $2700\text{ cm}^{-1}$  ( $G'$ ), in the second-order spectrum of Nv-10H-M-A3 sample supported the assertion that the A3-procedure favours better graphitic carbon generation [133]. This band is a Raman-allowed mode for  $sp^2$  carbons and indicated 3D order [169]. Consequently, this submission agrees with the deductions from the XRD technique. Similarly, the intensity-ratio for Nv-6B-M-A3 was slightly higher than that of Nv-6B-M-B3 and has the most narrowed G-band width (Figure 4.8b).

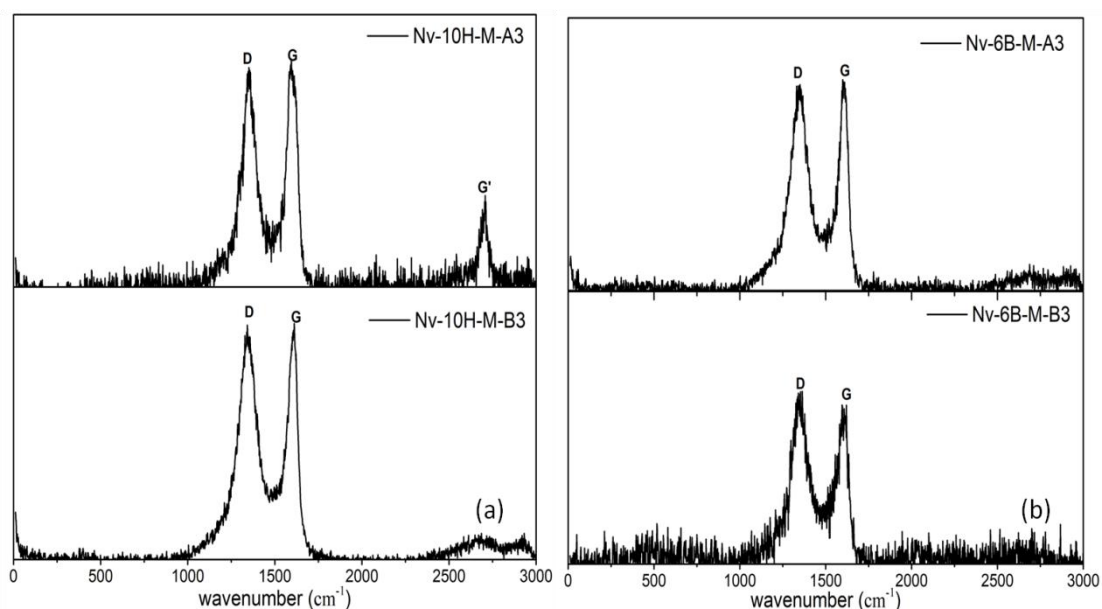


Figure 4.8: Raman spectra of selected carbon based on differences in heating sequence: carbons from novolac resin containing (a) 10 wt% boric acid (b) 6 wt% boron oxide.

The crystallite size ( $L_a$ ) was calculated using equation 3.5 and their values are presented in Table 4.6. The XRD technique did not provide information that can aid in the  $L_a$  values determination. Consequently, regarding this parameter, it was not possible to make a comparison.

Table 4.6: Raman and XRD parameters

<b>Samples</b>	<b>R-ratio [<math>I_D/(I_D+I_G)</math>] (%)</b>	<b>G-band width (<math>\text{cm}^{-1}</math>)</b>	<b><math>L_a</math> (nm)</b>	<b>GL (%)</b>
Nv-10H-M-A3	37.44	96	11.50	49 $\pm$ 12
Nv-10H-M-B3	33.17	92	9.61	18
Nv-6B-M-A3	35.82	79	9.94	47 $\pm$ 10
Nv-6B-M-B3	33.99	95	11.10	32

Nevertheless, XRD technique was selected for subsequent analysis on the derived carbons structural organization due to access to the equipment and reliability issues that were enumerated in the section 2.7.2.

#### 4.1.4 Chemical evolution during pyrolysis of novolac resins containing boric acid or boron oxide

The FTIR spectra presented in this section were recorded via a Varian 640-IR spectrometer between 400 and 4000  $\text{cm}^{-1}$  using the standard KBr method, as described in section 3.3.4.

Figure 4.9 represents the spectra contours of the boron compound additives (i.e.,  $\text{H}_3\text{BO}_3$  and  $\text{B}_2\text{O}_3$ ). As a result of hydrogen atoms orientation relative to the  $\text{B}_3\text{O}_3(\text{O}^-)_3$  backbone, boric acid has low symmetry [170]. Its molecules can be classified into hydrogen atoms and  $\text{B}_3\text{O}_3(\text{O}^-)_3$  skeleton motions [170, 171]. Many broad bands, which correspond to different structure-forming OH groups characterized the boric acid spectrum [171]. The band at 650  $\text{cm}^{-1}$ , 1195  $\text{cm}^{-1}$ , and 1460  $\text{cm}^{-1}$  are found in boric acid [172]. The band at 650  $\text{cm}^{-1}$  was due to the deformation of B–O bond atoms vibrations. According to Medvedev et al. [172], the weak band at ~940  $\text{cm}^{-1}$  may be due to the presence of metaboric acid. The band at 1020  $\text{cm}^{-1}$  indicates the presence of structure-forming  $[\text{BO}_4]$  groups [172, 173]. The peak at 1390  $\text{cm}^{-1}$  was due to  $\text{B}(\text{O}^-)_3$  bond vibration in  $[\text{BO}_3]$  or  $\text{B}_3^{10}\text{O}_3(\text{OH})_3$  groups [172]. The band at 1632  $\text{cm}^{-1}$  corresponds to water molecule vibration. When boron oxide spectrum was superimposed on boric acid, similar peaks were present. The only identified difference was in their bands' area and intensity. For example, the spectrum peak area at ~3200  $\text{cm}^{-1}$  belonging to the OH group of boron oxide was higher than that of boric acid, which may be due to its higher hygroscopic characteristic compared to boric acid.



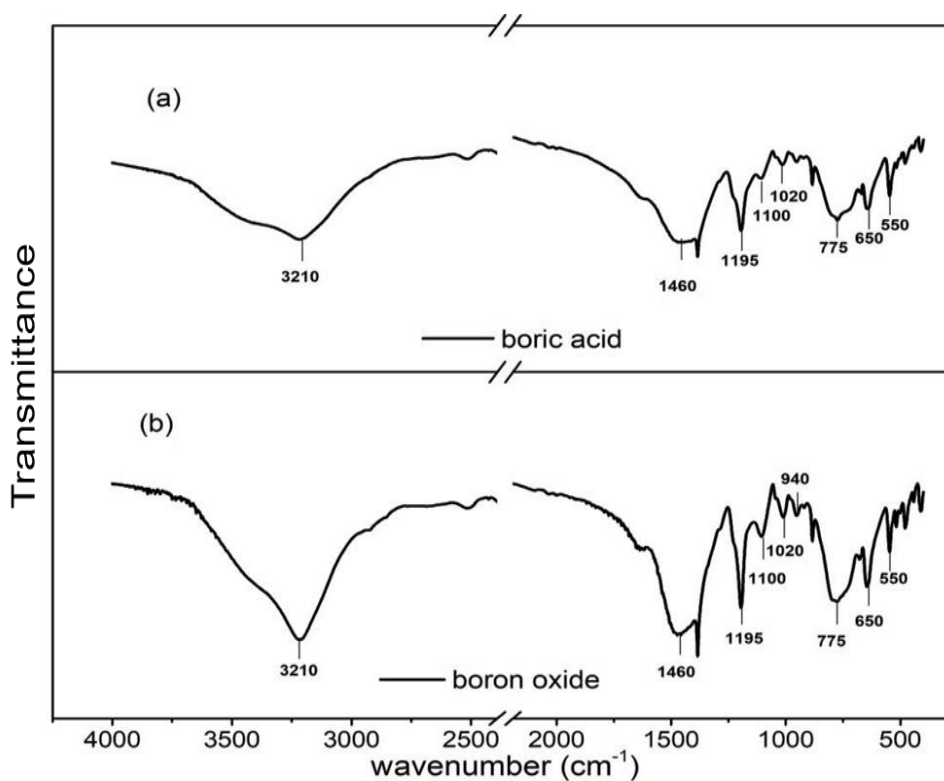


Figure 4.9: FTIR spectra of the graphitizing agents: (a) boric acid (b) boron oxide.

The characteristic bands detected in plain novolac resin were assigned based on literature review and IR spectra database as shown in Table 4.7. As expected, the peaks assigned to the various chemical groups varied slightly in the literature. The spectra in the wavelength range from 400 – 4000  $\text{cm}^{-1}$  are shown in Figure 4.10. The peaks at 755  $\text{cm}^{-1}$ , 815  $\text{cm}^{-1}$ , and 890  $\text{cm}^{-1}$  correspond to C–H vibrations while the ones at 1050  $\text{cm}^{-1}$  and 1064  $\text{cm}^{-1}$  correspond to the C–O stretching vibrations of  $\text{CH}_2\text{OH}$  group. The bands, which correspond to C–O–C aliphatic ether and an asymmetric stretch of phenol were detected at 1125  $\text{cm}^{-1}$  and 1230  $\text{cm}^{-1}$ , respectively. The width of the band at 1355  $\text{cm}^{-1}$  and 3300  $\text{cm}^{-1}$  indicated that these wavenumbers are due to O–H bond vibration. Additional peaks, which correspond to C=C aromatic ring vibration were detected at 1510, 1595 and 1645  $\text{cm}^{-1}$ . The one at 2929  $\text{cm}^{-1}$  was assigned to aliphatic – $\text{CH}_2$  in-phase stretch.

Table 4.7: IR bands detected in the plain and cured novolac resin

Peaks (cm <sup>-1</sup> )	Functional group	Reference
3300	Phenolic —OH stretch	Liu 2002 et al. [139], Ida et al. [140]
2929	Aliphatic —CH <sub>2</sub> in-phase stretch	Theodoropoulou et al. [141], Ida et al. [140], Ertugrul et al. [142]
2865	Out of phase stretching of CH <sub>2</sub>	Ida et al. [140]
1645	C=C stretching vibration of aromatic ring	Wang et al. [101], Theodoropoulou et al. [141]
1595	C=C stretching vibration of aromatic ring	Ida et al. [140]
1510	C=C aromatic ring	Ida et al. [140]
1440	C=C benzene ring obscured by —CH <sub>2</sub> - methylene bridge	Ida et al. [140]
1355	OH in-plane	Ida et al. [140]
1230	the asymmetric stretch of phenolic C—C—OH	Wang et al. [101], Kawamoto et al. [53], Wang et al. [125], Ida et al. [140]
1125	stretching vibration of C—O—C aliphatic ether	Ida et al. [140], Theodoropoulou et al. [141], Ertugrul et al. [142]
1064	C—O stretching vibrations of CH <sub>2</sub> OH group	Liu et al. [139], Ida et al. [140]
1050	C—O stretching vibrations of CH <sub>2</sub> OH group	Liu et al. [139], Ida et al. [140]
890	CH out-of-plane, isolated	Ida et al. [140]
815	CH out-of-plane, substituted	Ertugrul et al. [142], Theodoropoulou et al. [141], Ida et al. [140]
755	CH out of plane, ortho-substituted	Ida et al. [140]

Figure 4.10a shows that the band at  $3300\text{ cm}^{-1}$  belonging to phenolic hydroxyl group vibration of the plain resin and mostly all the other peaks became weaker with increased heat treatment temperature up to  $230\text{ }^{\circ}\text{C}/1\text{h}$ . However, no new peak was detected after pyrolysis up to that temperature. This type of chemical evolution suggests that decomposition and thermal cross-linking process led to char formation [174, 175]. The thermal degradation process resulting in the production of glassy/non-graphitic carbon should proceed according to the order proposed by Lee [51].

Typically, glassy carbons derived from plain novolac resin consist of 6 member  $\text{sp}^2$  bonded cyclic structures, which are held tightly within a network of  $\text{sp}^3$  crosslink [51] that does not permit reorganization or rotation necessary for graphitization (Figure 4.10b). Both inert pyrolysis and to a limited extent oxidation/combustion coexist during the thermal decomposition process due to reaction water, absorbed moisture and hydroxyl groups present in the resin's structure [51]. However, the oxidation reaction is limited to the effect of generated oxygen radicals on their way out of the polymer sites for inert pyrolytic decomposition.

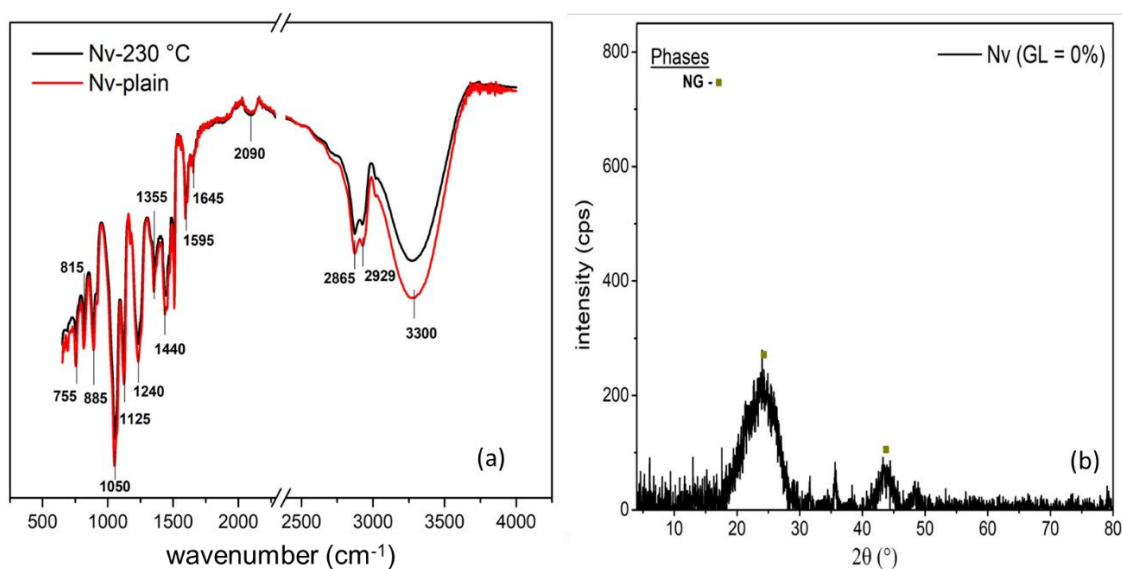


Figure 4.10: (a) FTIR spectra of plain and cured novolac resin at  $230\text{ }^{\circ}\text{C}$ , (b) X-ray diffraction pattern of carbon derived from the plain novolac resin at  $1000\text{ }^{\circ}\text{C}/5\text{h}$ .

As mentioned earlier, HMTA is usually added to novolac resin for use as a binder during the industrial preparation of carbon-containing refractories. Based on this information, a reference composition containing 10 wt% HMTA (Nv-HMTA) was also heat-treated up to 230 °C/1h. The spectrum of the cured reference novolac resin was presented in Figure 4.11a. Although no new functional group (compared to the plain novolac sample) was detected, some minor peaks shift occurred. Figure 4.11b shows the diffraction pattern of the derived  $sp^3$ -hybridized carbon with an amorphous structural arrangement due to the atoms limited rotation during carbonization [176].

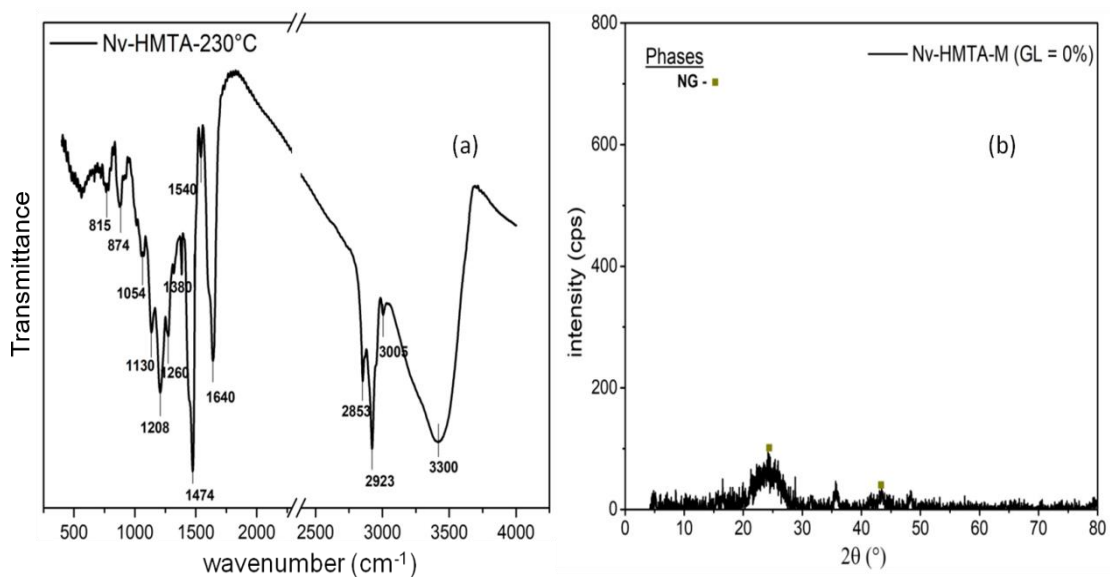


Figure 4.11: (a) Novolac resin + 10 wt% HMTA (reference composition) heat-treated up to 230 °C, (b) X-ray diffraction pattern of reference composition after firing up to 1000 °C and a hold time of 5h. GL = graphitization level, NG = non-graphitic.

FTIR spectroscopy was used to study the chemical evolution that occurs during the thermal cross-linking (100 °C/4h + 230 °C/1h), carbonization (100 °C/4h + 230 °C/1h + 500 °C/1h) and graphitization (100 °C/4h + 230 °C/1h + 500 °C/1h + 1000 °C/5h) stages of boron compound modified-novolac resin formulations in accordance with the encapsulated heating sequence. These procedures were selected based on the firing route that led to maximum graphitic carbon generation. The peaks detected in the novolac resin containing the boron

source additives (boric acid and boron oxide) were assigned as shown in Table 4.8.

The chemical changes that occur when Nv-10H formulation (novolac resin + 10 wt% boric acid) was subjected to thermal treatment up to 230 °C, 500 °C and 1000 °C were depicted by the spectra in Figure 4.12a.

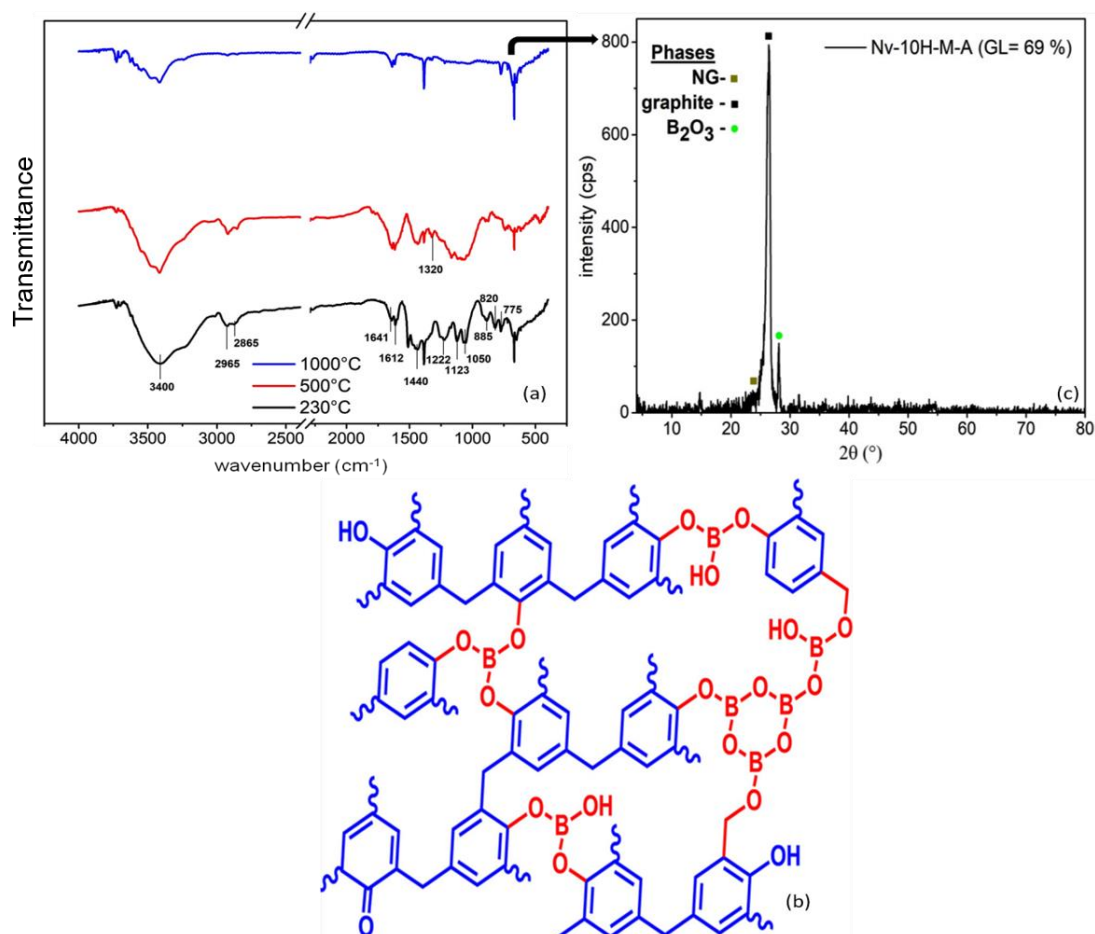


Figure 4.12: (a) FTIR spectra of novolac resin composition containing 10 wt% boric acid, heated up to 230 °C/1h, 500 °C/1h and 1000 °C/5h, (b) Structural representation of cured boric acid-modified novolac resin [101], (c) XRD diffraction pattern of carbon derived from novolac resin containing 10 wt% boric acid. GL = graphitization level, NG = non-graphitic.

Compared to the unmodified cured resin some new peaks were detected at 885  $\text{cm}^{-1}$  and 1440  $\text{cm}^{-1}$ , which correspond to B–O vibration attributed to phenylborate formation, as shown in Figure 4.12b [101, 125] at 230 °C. The peak

intensity at  $885\text{ cm}^{-1}$  decreased with increasing treatment temperature (it was still detected at  $500\text{ }^{\circ}\text{C}$ ) and disappeared at  $1000\text{ }^{\circ}\text{C}$ . This observation suggested that B–O–B formation and dissociation was gradual and a function of increasing temperature [88]. According to Ertugrul et al. [142], this reaction depends on production route and time. Furthermore, this bond indicates that a chemical reaction between the additive and resin occurred at an early stage ( $230\text{ }^{\circ}\text{C}$ ). Wang et al. [101], observed that higher temperature up to  $200\text{ }^{\circ}\text{C}$  was required to initiate a reaction between B–OH and phenolic hydroxyl group to form phenylborate. Similarly, Liu et al. [139] attributed borate formation to the reaction of phenol and benzyl hydroxyl groups with boric acid. Moreover, the band assigned to the stretching vibration of the B–O–C group appears at  $\sim 1320\text{ cm}^{-1}$  after thermal treatment up to  $500\text{ }^{\circ}\text{C}$ . This peak was not detected at  $230\text{ }^{\circ}\text{C}$  and after the pyrolysis process at  $1000\text{ }^{\circ}\text{C}$ . The B–O–C bond has lesser binding energy ( $190.2\text{ eV}$  [101]) compared to plain C–C ( $284.8\text{ eV}$ ) ones, which characterized the uncatalyzed resin. Hence, B–O–C transition supports the assertion that its formation and cleavage plays a significant role in the catalytic graphitization of novolac resin containing boron-based additives [101, 176]. The weakest bond in the polymer chain (at this instance, B–O–C) can lead to chain cleavage, which permits disruption and structuring during pyrolysis that favours crystalline carbon generation at a lower temperature such as  $1000\text{ }^{\circ}\text{C}$  (as seen by the sharpness and intensity of the peak at  $26^{\circ}$ , Figure 4.12c). Moreover, the cleavage of this bond should lead to boron's addition to the carbon's structure. Boron atoms due to their enhanced diffusivity can intercalate carbon atoms during the pyrolysis operation and change the  $\pi$ -electron density [128, 158].

The medium bands intensities between  $1617\text{-}1647\text{ cm}^{-1}$  were assigned to C=C vibration stretching of the aromatic ring [139, 142]. As the process proceeded, phenol hydroxyl and benzyl hydroxyl absorption bands decreased due to borate formation and water evolution [101] as observed by a decrease in the –OH band percentage area with increasing heat treatment temperature. This consideration agrees with Jiang et al. [177] and Wang et al. [101] submission that water evolution and additional intermolecular cross-linking takes place at the early stages of pyrolysis. The produced water can be attributed to hydroxyl link

cleavage and the reaction between B–OH and phenolic hydroxyl groups [51, 101]. The decrease with the firing temperature in the absorption peak intensity at  $820\text{ cm}^{-1}$ , which corresponds to C–H flexural vibration of benzene ring shows the volatilization of methyl and phenol derivatives. In addition, dehydrogenation and carbonization reaction appears to be more pronounced above  $500\text{ }^{\circ}\text{C}$ .

Table 4.8: FTIR spectra of novolac resin containing boron source additives heat treated up to  $230\text{ }^{\circ}\text{C}$ ,  $500\text{ }^{\circ}\text{C}$ , and  $1000\text{ }^{\circ}\text{C}$ .

Peaks ( $\text{cm}^{-1}$ )	Functional group	Reference
3350-3400	Phenolic –OH stretch	See Table 4.7
2925	Aliphatic –CH <sub>2</sub> in-phase stretch	See Table 4.7
1890, 875	B–O bond	Medvedev et al. [172], Ertugrul et al. [142], <a href="http://webbook.nist.gov">http://webbook.nist.gov</a>
1600-1650	C=C stretching vibration of aromatic ring	See Table 4.7
1510-1550	C=C aromatic ring	See Table 4.7
1430	B–O–B	Liu et al. [139], Wang et al. [101], <a href="http://webbook.nist.gov">http://webbook.nist.gov</a>
1380	OH in-plane	Ida et al. [140]
1310-1350	B–O–C	Wang et al. [101], <a href="http://webbook.nist.gov">http://webbook.nist.gov</a>
1222	the asymmetric stretch of phenolic C–C–OH	See Table 4.7
1120-1125	stretching vibration of C–O–C aliphatic ether	See Table 4.7
1050	single bond C–O stretching vibrations of CH <sub>2</sub> OH group	See Table 4.7
885	B–O bond belonging to boron source additives	Wang et al. [101]

815	CH out-of-plane, substituted	See Table 4.7
≤750	CH out-of-plane, substituted, ortho-substituted	See Table 4.7

Furthermore, XPS analyses were conducted to assess the chemical transformation (especially the bonds formed) occurring during carbonization of the boric acid-modified novolac resin. Nv-10H formulation full spectra after sequential heat treatment up to 300 °C (30 °C + 100 °C/4h + 300 °C), 500 °C (30 °C + 100 °C/4h + 500 °C/1h), and 1000 °C (30 °C + 100 °C/5h + 500 °C/1h + 1000 °C/1h and 30 °C to 100 °C/4h + 500 °C/1h + 1000 °C/5h) are shown in Figure 4.13. Firstly, the decreasing values of B1s peak at higher heat treatment temperatures (starting from 500 °C) may be due to B<sub>2</sub>O<sub>3</sub> volatilization, whereas the increasing peak intensity of C1s peaks can be attributed to dehydration and dehydrogenation reaction. The degradation process of cured phenolic resin with or without additives has been observed to involve the loss of moisture and lower molecular weight compounds [51, 101, 178]. For example, at 1000 °C, the percentage area corresponding to oxygen has significantly decreased relative to carbon due to dehydrogenation and water evolution. Nevertheless, some amount of oxygen (~7 %) was still detected in the carbonized samples after firing at 1000 °C/5h. This observation agrees with the FTIR results.



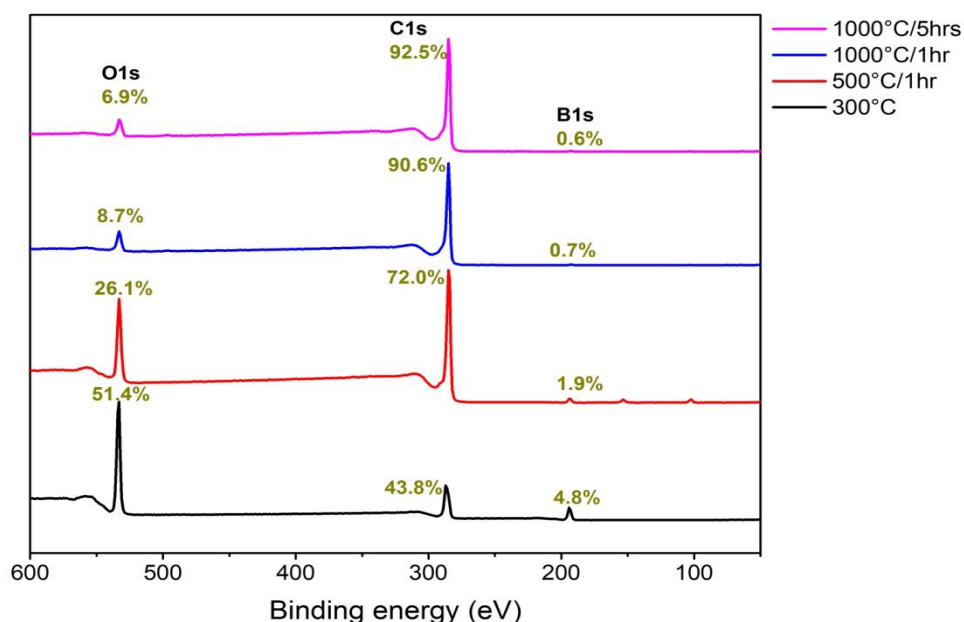


Figure 4.13: XPS spectra of cured and heat-treated novolac resin containing 10 wt% boric acid.

The B1s high-resolution spectra are shown in Figure 14a-d. The peaks correspond to B–O at ~190.7 eV, B–O–C at ~192.2 eV, B–O–B at ~193.4 eV, and ~B–OH (194.7 eV). At 300 °C, the B–O–B bond has the highest percentage area (78 %), followed by B–O–C peak, which is ~11 % (Figure 4.14a). The profile depicts the onset of phenyl borate formation in-line with the submission of Wang et al. [101]. This observation is in-line with the deduction from FTIR analysis. The peak ascribed to B–OH bond, was not detected at 500 °C, which suggests that the additive might have reacted completely with the resin. Moreover, the percentage area of B–O–B linkage decreased, whereas that of B–O–C increased heat treatment. The main peaks detected at the final pyrolysis stages (1000 °C/1h and 1000 °C/5h) were B–O–C and B–O, as B–O–B percentage decreased. The B–O linkage may arise from the B–O–C bond decomposition. As observed earlier, the lower binding energy of this bond (compared to plain C–C) should facilitate atoms' rotation and rearrangement that led to graphitic carbon generation during carbonization of phenolic resin containing boric acid.

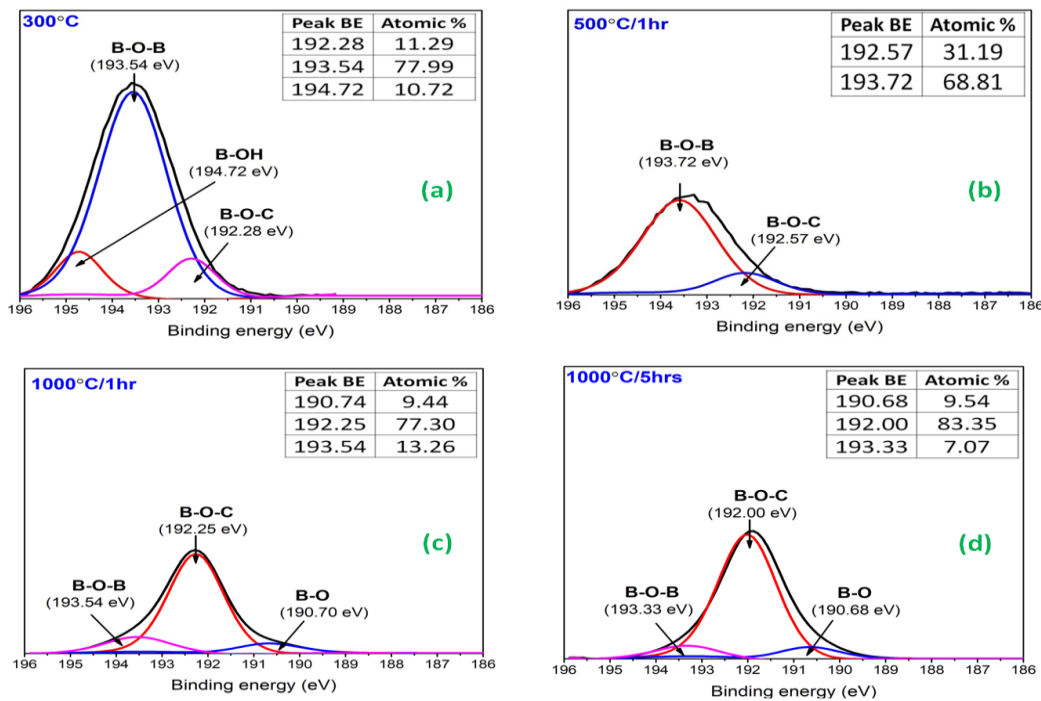


Figure 4.14: B1s high-resolution spectra of cured and heat-treated novolac resin containing 10 wt% boric acid.

Meanwhile, the high-resolution C1s spectra show the evolution of different types of carbon-based functional groups, i.e. C–C, C–O–C, C=O at each carbonization stages. The peaks at 284.4 eV was assigned to C–C, at 286.2 eV to C–O–C, at 287.9 to C=O (carbonyl) and 289.2 eV to C=O (carboxyl) functionalities [125, 179] as shown in Figure 4.15. The relative percentage of these bonds changed at the different pyrolysis stages in a manner that depicts decomposition and degradation reaction. Moreover, the percentage area of C–C bond increased at 500 °C, indicating that significant carbonization reaction took place at that temperature.

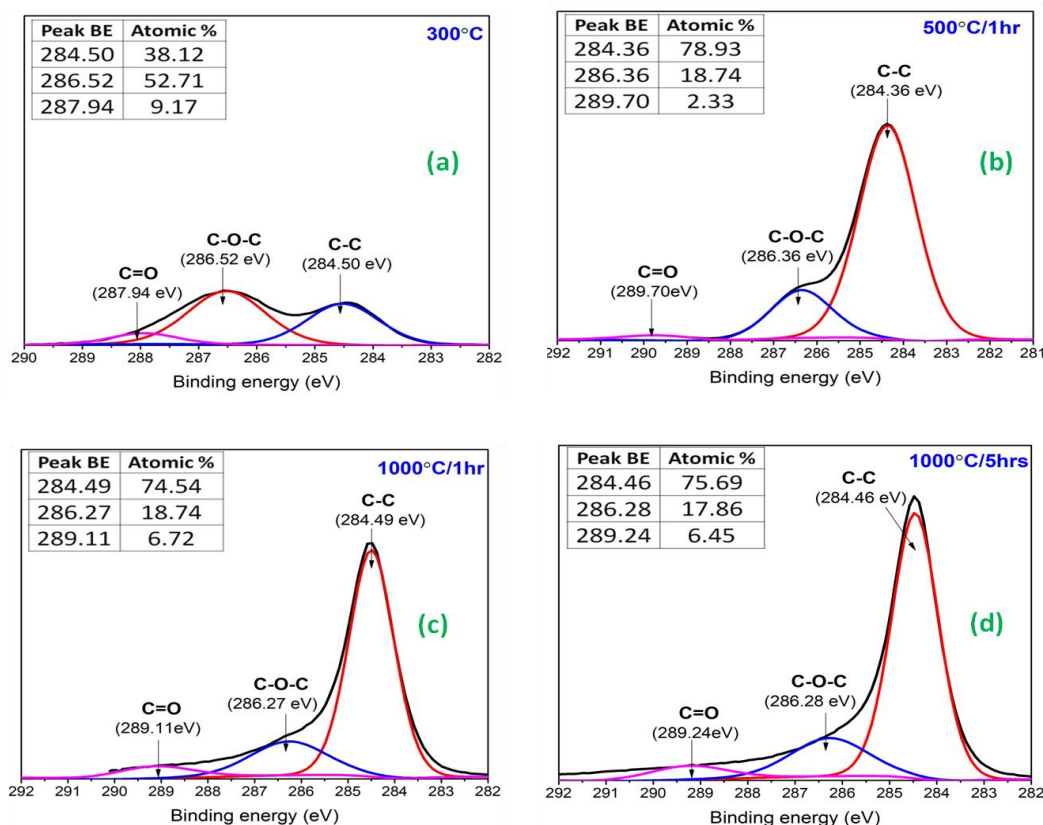


Figure 4.15: C1s high-resolution spectra of cured and heat-treated novolac resin containing 10 wt% boric acid.

Similarly, the phenolic resin formulation containing boron oxide additive was examined at the different carbonization stages using FTIR and XPS equipment. The chemical evolution followed the same pattern as the above discussed boric acid-modified resin.

The FTIR spectra showing chemical evolution during pyrolysis of boron oxide-modified novolac resin are shown in Figure 4.16a. The likely structure of the cured sample [125] and diffractogram of the derived carbon were presented in Figure 4.16b and 4.16c, respectively. Firstly, B–O–C bond (at  $1330\text{ cm}^{-1}$ ) was detected earlier at  $230\text{ °C}$  at this instance. The reasons for the observed change (compared to boric acid containing resin formulation) may be due to boron oxide smaller particles size ( $d_{50} < 10\text{ }\mu\text{m}$ ) compared to boric acid ( $d_{50} < 45\text{ }\mu\text{m}$ ), which should promote a more rapid reaction. The band due to phenyl borate formation was detected at  $1430\text{ cm}^{-1}$ .

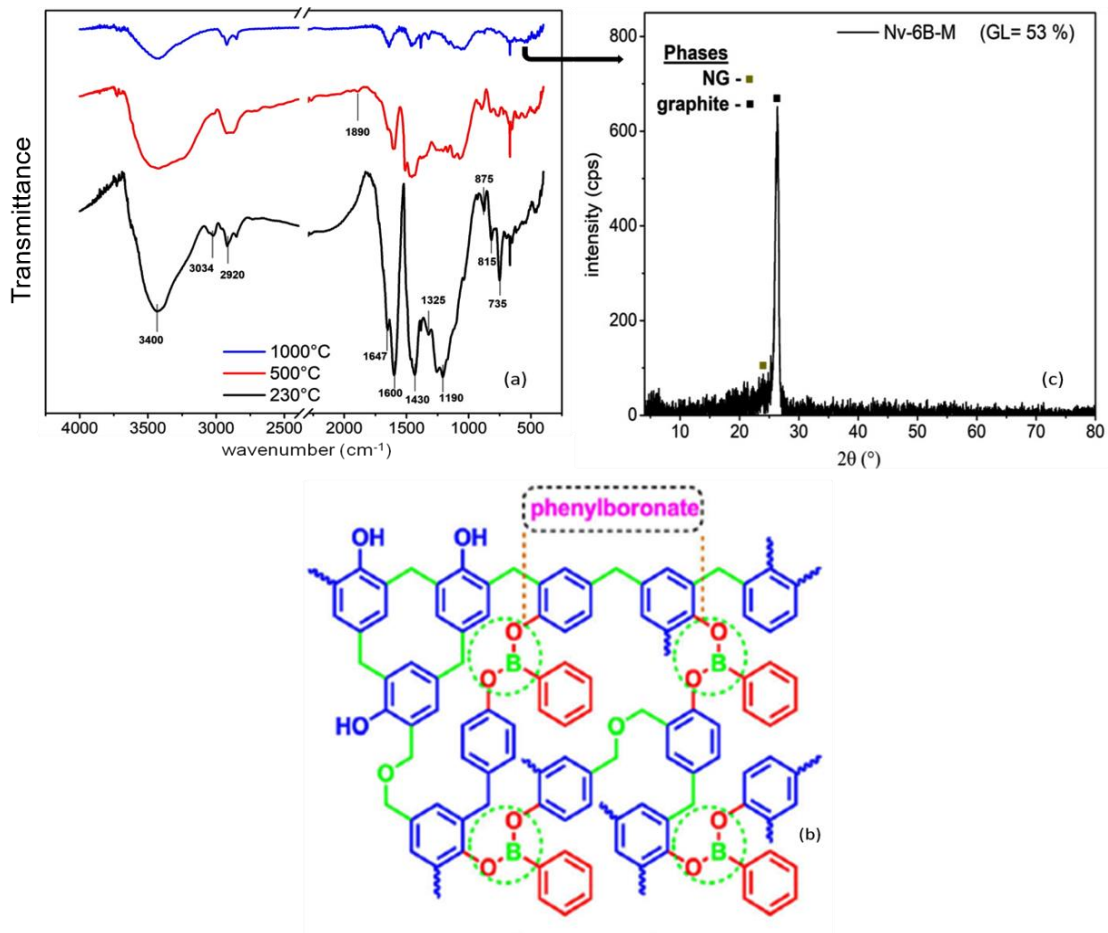


Figure 4.16: (a) FTIR spectra of novolac resin composition containing 6 wt% boron oxide heat treated up to 230 °C/1h, 500 °C/1h and 1000 °C/5h (b) Structural representation of cured boron oxide-modified novolac resin [125], (c) XRD diffraction pattern of carbon derived from novolac resin containing 6 wt% boron oxide. GL = graphitization level, NG = non-graphitic.

Furthermore, the full XPS spectra of novolac resin containing 6 wt% boron oxide after heat treatment up to 300 °C, 500 °C and 1000 °C were shown in Figure 4.17. The chemical state evolution followed a similar pattern like that of boric acid-modified novolac resin, although the percentage area of oxygen peak was higher than the Nv-10H formulation after pyrolysis at 1000 °C. This observation suggests that boric acid addition can promote increased carbon yield than boron oxide. The B1s peak after pyrolysis at 1000 °C for 1 hour compared to after 5 hours has a slightly lesser value. The observation infers a non-homogeneous distribution of

the boron related signals in the carbon composition and agrees with finding based on the carbon samples XRD analysis.

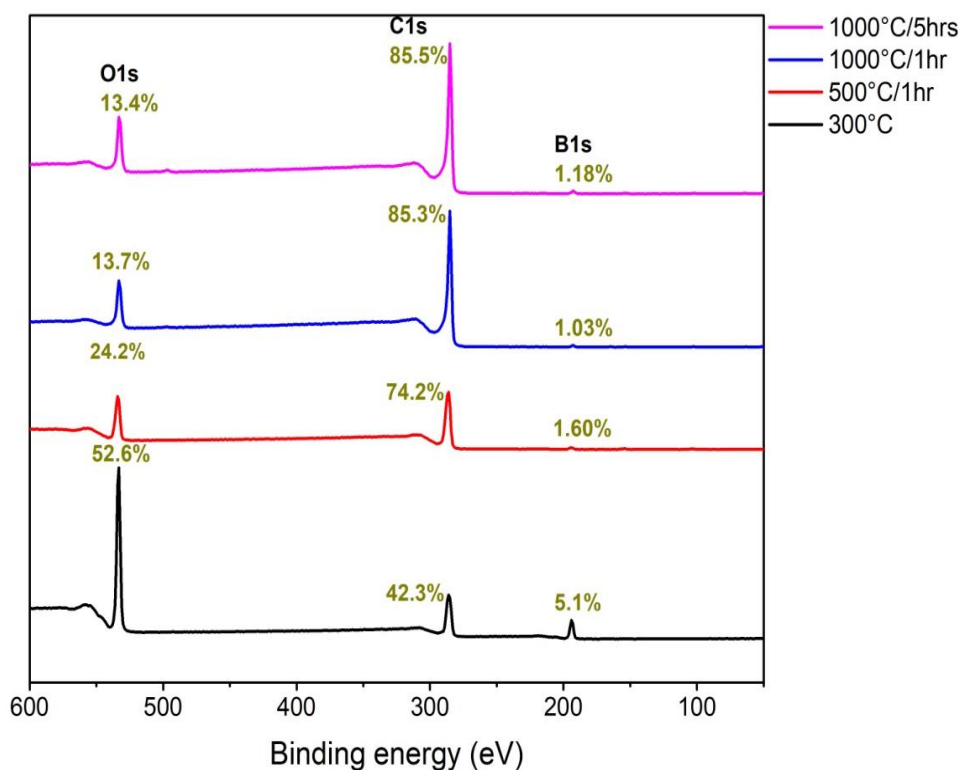


Figure 4.17: XPS spectra of cured and heat-treated novolac resin containing 6 wt% boron oxide.

The high-resolution B1s spectra at the different heat treatment temperature stages were shown in Figure 4.18. The chemical transformation was similar to the boric acid-modified novolac resin, although the B–O signal was detected earlier at 500 °C. As observed earlier, boron oxide smaller particle size (compared to boric acid) may be responsible for the increased reaction speed. The primary bond detected at 1000 °C is B–O–C. As mentioned earlier, in addition to facilitating carbon rotation during pyrolysis, B–O–C dissociation can lead to boron atom introduction and intercalation within the carbon structure, which should also promote its graphitization.

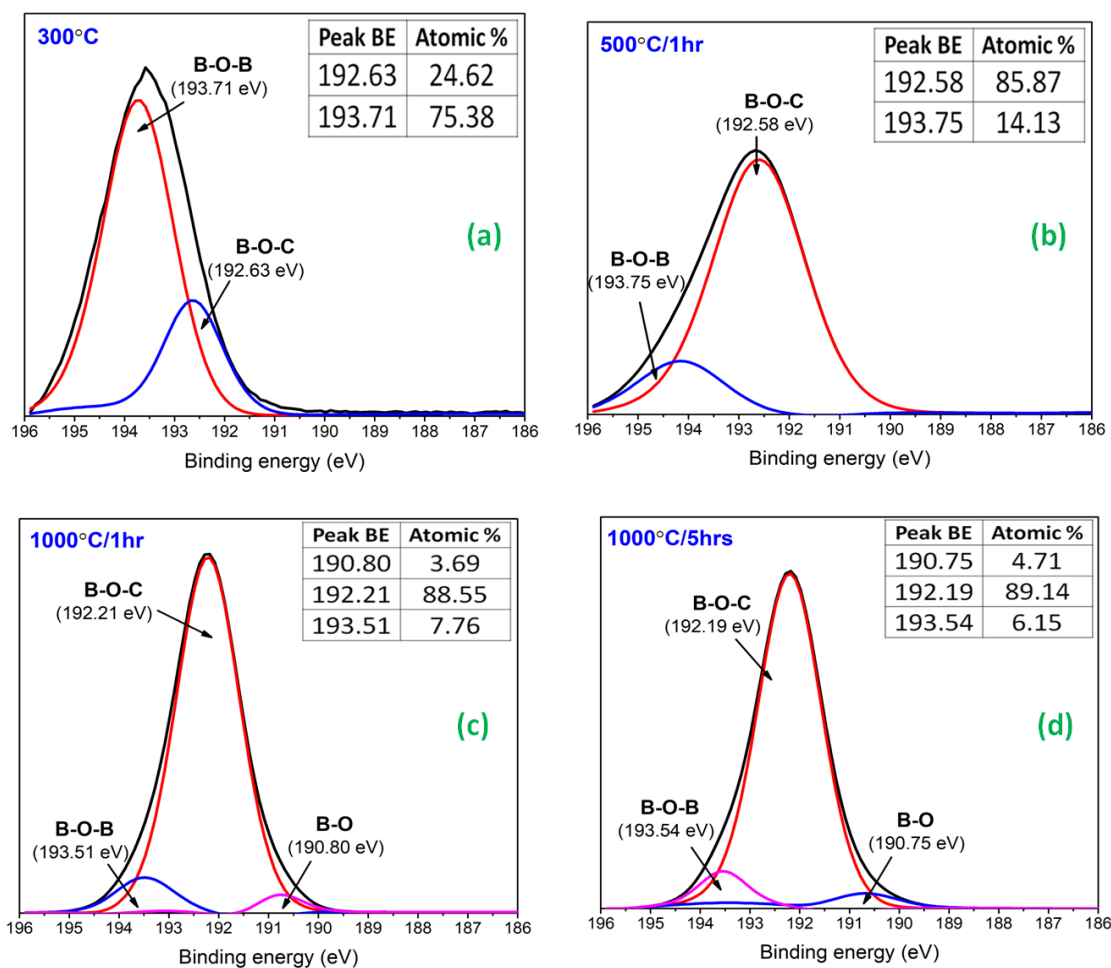


Figure 4.18: B1s high-resolution spectra of cured and heat-treated novolac resin containing 6 wt% boron oxide: (a) 300 °C, (b) 500 °C, (c) 1000 °C/1h, (d) 1000 °C/5h.

The C1s spectra at the different heat treatment temperatures further attest to carbon functional groups' evolution during the carbonization process as shown in Figure 4.19. The profile transformation was also similar to the boric acid-modified resin showing degradation reaction and the presence of a significant amount of oxygen after carbonization at 1000 °C.

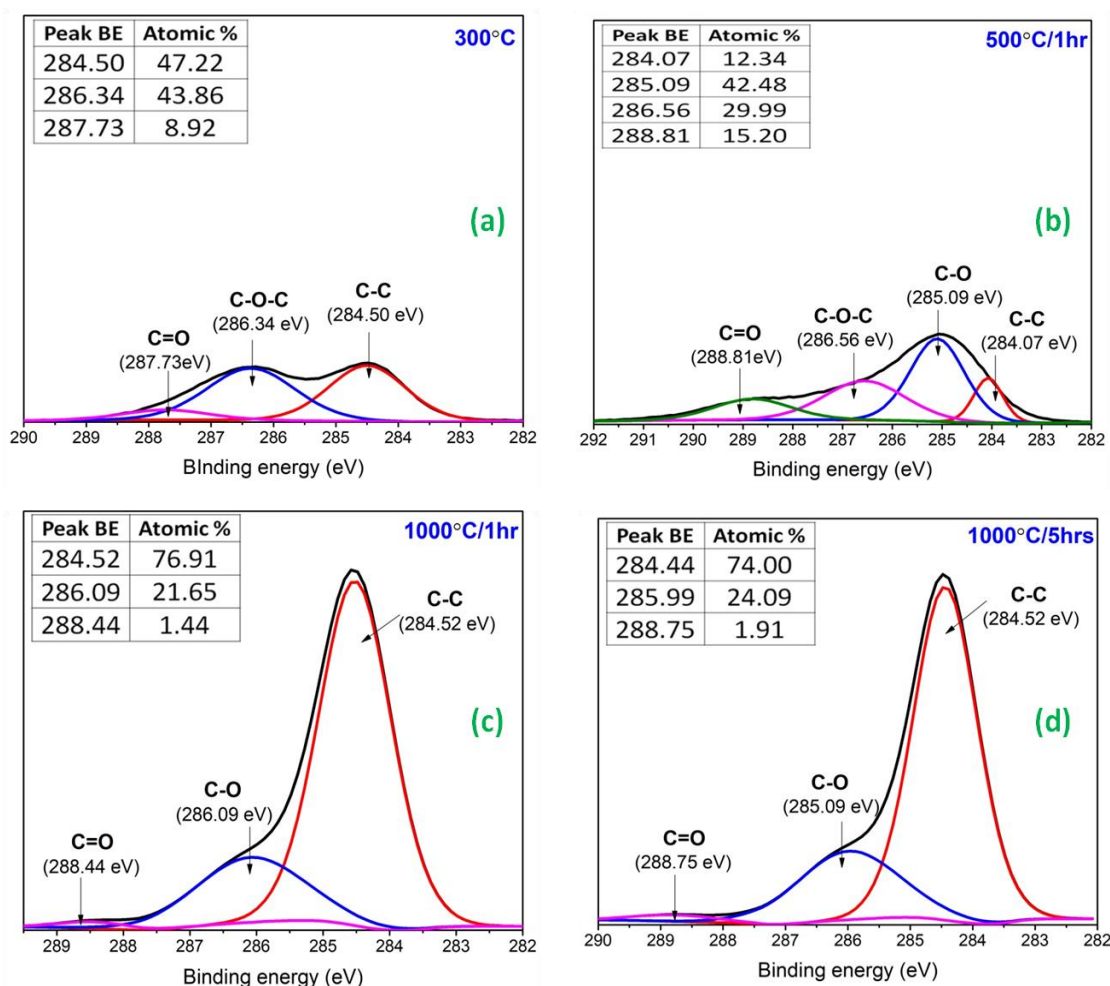


Figure 4.19: C1s high-resolution spectra of cured and heat-treated novolac resin containing 6 wt% boron oxide: (a) 300 °C, (b) 500 °C, (c) 1000 °C/1h, (d) 1000 °C/5h.

#### 4.1.5 Oxidation resistance of carbons derived from novolac resin containing boron compounds additives after carbonization using A3-procedure

Figure 4.20a typified the oxidation behaviour of carbons derived from the novolac resin (reference formulation containing 10 wt% HMTA) and the modified-resins. Firstly, the TG curves indicate the presence of non-carbon materials in the samples' composition (as seen by the initial mass loss between ~50 and 150 °C). The endothermic region in the DSC curves, within that same temperature range



(Figure 4.20b), confirmed this observation as indicated by the FTIR and XPS spectra (Figure 4.12a and 4.16a), which showed the presence of –OH group and retained oxygen in the derived carbon composition. The results also support findings from the literature that significant amount of oxygen, carbon oxides and other impurities are present after pyrolysis of phenolic resins containing additives at 1000 °C [101, 180, 181]. For example, carbons derived from the pyrolysis of boric acid-modified novolac resin at 1000 °C was reported to contain about 7 % oxygen by Wang et al. [101]. Nevertheless, all non-carbon species will be removed with increased carbonization temperature [19]. More so, the amount of the non-carbon material differs per composition (based on the TG curves), which may not be unconnected with the difference in the resin formulations starting components. Consequently, to enable proper estimation of carbon loss, the TG-curves were normalized, and the actual carbon loss was determined from the oxidation initiation point as explained in “Section 3.4.2.3”. The data presented in Table 4.9 represent the average values of three analyses carried out on the same sample batch. By going through this route, the oxidation rate of the different carbon samples was found to differ as a function of the starting resin formulations. Compared to Nv-HMTA-M (74 %), the carbon loss of Nv-6B-M and Nv-10H-M samples was of  $50 \pm 5$  % and  $48 \pm 3$  %, respectively. These values indicate a significant improvement in the oxidation resistance of the graphitized carbons. The chemical and structural features of plain novolac resin compel it to yield glassy carbon during carbonization. Due to their isotropic structure, such carbons are more susceptible to oxidation. However, the structuring that took place during pyrolysis of the modified resin led to a reduction in the amount of edge site atoms (which are more reactive than those of basal plane), reduced interlayer spacing and induced anisotropic characteristic, which was beneficial for improved oxidation resistance [113-115]. Moreover, the rate controlling-step during carbon high-temperature oxidation is believed to depend on oxygen transport through the solid boundary layer [182]. Apart from these, the presence of  $B_2O_3$  detected in the sample’s composition will also protect the carbon microcrystallites edges against rapid loss [121]. Therefore, the attained thermal stability in an oxidizing environment may be attributed to the protective coating formed on the carbon



surface and ordered atomic arrangement. Nevertheless, carbons derived from the boron compounds-modified resin containing 10 wt% HMTA (especially for the formulation containing boric acid) show greater oxidation stability although graphitic carbon was not detected in their composition. According to Edward et al. [163], the macromolecular (polymeric) structure of non-graphitizing materials remains during heat treatment, losing only small molecules by degradation and developing even more cross-linking during pyrolysis. Invariably, increased bond strength and presence of inclusion that can acts as a protective oxide in addition to minimal restructuring may have resulted in the better oxidation resistance. The results obtained regarding this formulations show that optimal cross-linking of the novolac resin during the curing stage and the presence of boron oxide in the amorphous carbon can also improve carbons' oxidation stability [1, 183].

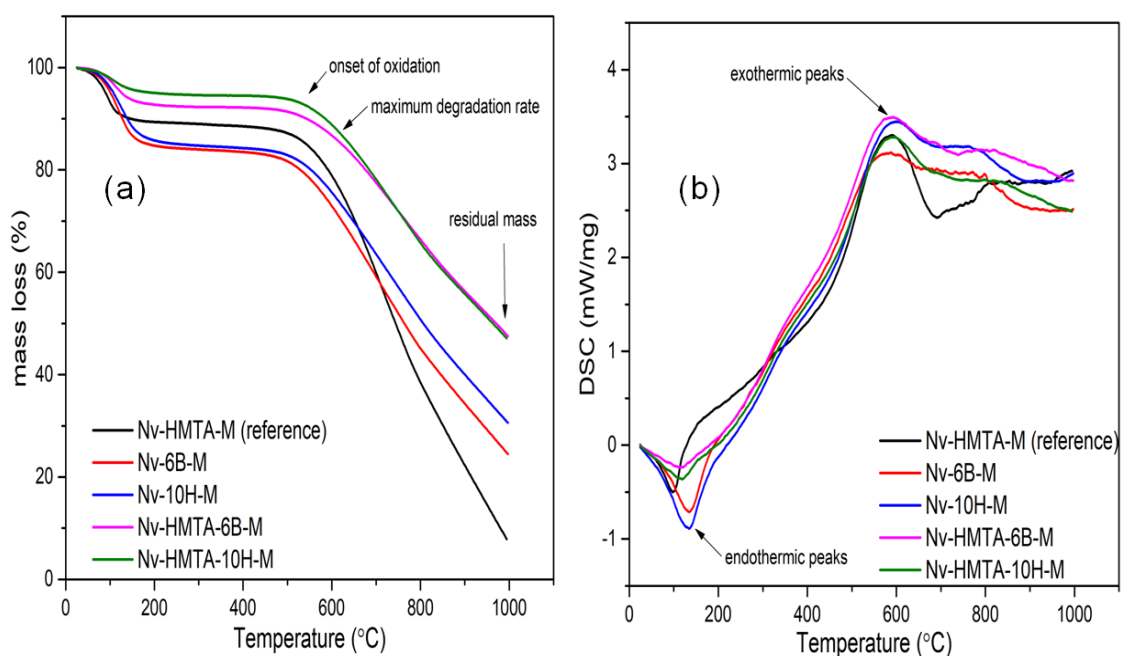


Figure 4.20: (a) Descriptive TG curves (b) Descriptive DSC curves of carbons derived boron catalyzed novolac resin.

Table 4.9: Effect of graphitization, increased addition of HMTA and preparation procedure on the carbons' oxidation resistance.

Sample	Carbon loss (%)	Onset of Oxidation (T <sub>i</sub> )	GL(%)
Nv-HMTA-M	74	582	0
Nv-6B-M	50 ± 5	525 ± 12	47 ± 12
Nv-10H-M	48 ± 3	535 ± 12	49 ± 12
Nv-10HMTA-6B-M	46 ± 4	574 ± 4	0
Nv-10HMTA-10H-M	40 ± 3	566 ± 6	0
Nv-11HMTA-10H-M	40	573	0
Nv-12HMTA-10H-M	35	572	0
Nv-13HMTA-10H-M	36	572	0
Preparation procedure: Ultrasonic mixing incorporation			
Nv-6B-M-U	49	543	26
Nv-10H-M-U	37	540	13
Preparation procedure: Vacuum degassing incorporation			
Nv-6B-M-V	51	533	28
Nv-10H-M-V	50	527	7
GL – Graphitization level			

To ascertain these deductions, more HMTA (11- 13 wt%) was added to the boron compounds-modified resin. The results further show that:

1. The increased amount of HMTA in the starting formulation of the modified resin can reduce the carbon's reactivity in air and oxidation is not only a function of crystallization.
2. The presence of HMTA also plays a significant role on the oxidation onset temperature. Carbons derived from the compositions containing the cross-linking agent have higher T<sub>i</sub> values. For example, the T<sub>i</sub> for Nv + HMTA (reference) was 582 °C (the highest recorded value for all the investigated composition) compared to 535 °C of Nv-10H-M. Nevertheless, the overall performance of carbons derived from this formulation further indicated that

other factors including graphitization and composition affect their stability at high temperature in an oxidizing environment.

The amount of carbon loss for Nv-6B-M-U and Nv-10H-M-U (based on the introduction of additional ultrasonic mixing) was 49 % and 37 %, respectively. Similarly, the values of 49 % and 50 % loss were obtained for Nv-6B-M-V and Nv-10H-M-V carbons (based on additional vacuum degassing after mechanical mixing), respectively. These numbers are close to those of Nv-6B-M (~50 %) and Nv-10H-M (~48 %). As explained earlier, the additional mixing technique induces high energy chemical reactions due to the formation, growth, and collapse of bubbles, which promoted high-intensity local heating that resulted to increased cross-linking during the curing stage [160, 161]. The presence of oxygen in organic precursors usually led to the formation of stable peroxide that can limit conversion degree at the initial stages of carbonization [162, 176]. Consequently, the degasification process promoted free-radical polymerization and increased cross-linking network, which led to a significant reduction of the attained graphitization level of these samples. However, this reaction that limits the amount of generated graphitic carbon, promoted increased cross-linking, which can also improve the oxidation resistance of such pyrolytic carbons. These observations agree with the submission of Ruff et al. [184] that carbons' oxidation is influenced by several factors, which include the extent and accessibility of its surface, bond strength and composition.

Based on the combination of these controlling factors, it was not easy to establish a direct relationship between the carbon's crystallization and oxidation resistance. Consequently, a combination of several characterization techniques may be required to establish a correlation between graphitization and carbons stability at high temperature in an oxidizing environment.

#### **4.1.6 Catalytic graphitization of novolac resin by ferrocene**

Bitencourt et al. [17] had studied the role of various processing parameters on the graphitization of novolac resin containing 3 wt% ferrocene (Nv-3Fc). In this

study, the effect of different heating sequences (which were not previously evaluated in that study) on the crystallization process was examined. The difference in the heating procedures was primarily at the curing stage with more steps and time introduced for the B and C-procedures (see Table 3.2). The evaluated novolac-ferrocene formulation containing 10 wt% HMTA was reported by Bitencourt et al. [17] to present the best graphitization level. Firstly, only ~2 % variation in GL values was attained under the same experimental conditions (sample Nv-3Fc-HMTA-M-A3) that was used in the earlier study. Regarding this composition, this observation suggests results reproducibility. Moreover, changes in the heat treatment procedure did not have any significant effect (~1 % variation) on the derived carbons crystallization (Figure 4.21). The attained results may not be unconnected with the mechanism leading to graphitic carbon generation during the pyrolysis operation. Based on previous studies [10, 17, 131], the following explanation was provided to explain the mechanism involved in Nv-Fc graphitization. During thermal treatment of this formulation, Fc decomposes at around 900 °C to Fe and Fe<sub>3</sub>C nanoparticles and provide active sites for the rearrangement of the amorphous carbon to graphene sheets. This implies that the reactions that led to graphitic carbon production begin at a later stage of carbonization. This proposition was supported by the XPS analysis carried out in the subsequent stage (Part 2) of the present study. Consequently, unlike with boron source catalyzed resin, the process leading to graphitic carbon's generation occurs at high temperature and does not significantly depend on changes that occur during the curing stage. It is also more likely that the additive did not participate in any chemical reaction until the later stages of carbonization.

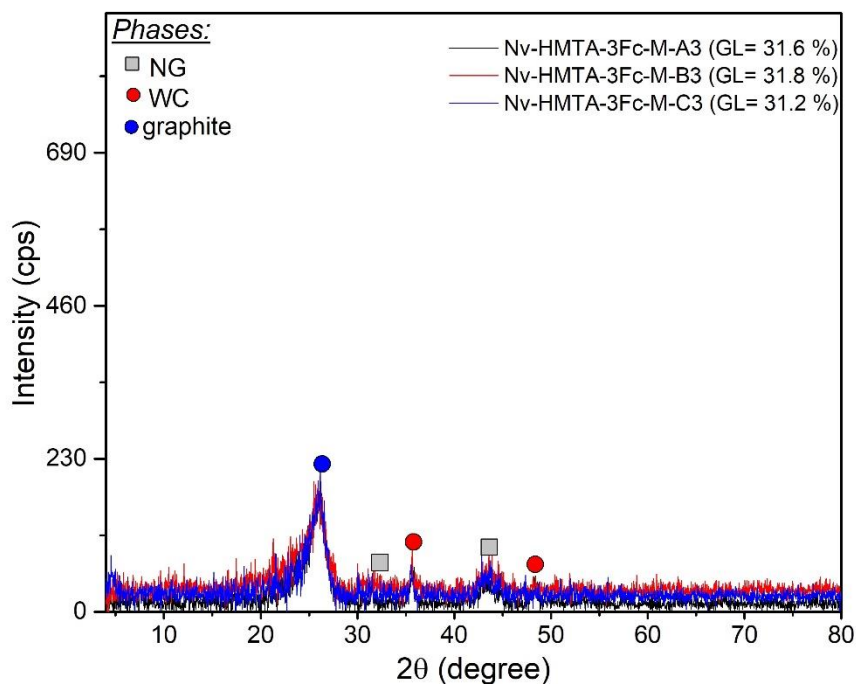


Figure 4.21: XRD profiles showing the effect of different heat treatment sequence on graphitization of catalyzed novolac resin by ferrocene. GL = graphitization level; M = mechanical mixing; NG = non-graphitic; WC = tungsten carbide; HMTA = 10 wt% hexamethylenetetramine; 3Fc = 3 wt% ferrocene; A3, B3, C3 = heating procedures.

Furthermore, some samples were selected for Raman spectroscopic analysis. Figure 4.22 shows the Raman profile of carbons derived from the resin formulation after A3 and B3–thermal treatment procedures. The analysis suggested that B3-procedure favours better crystalline carbons generation. The attained intensity-ratio, which was 41 % for Nv-3Fc-M-B3 is significantly higher than that of Nv-3Fc-M-A3 (35 %). More so the first overtone peak at  $2700\text{ cm}^{-1}$  was detected in Nv-3Fc-M-B3 spectrum. However, the G-band widths of both samples were very close. Based on the XRD result, change in the heating sequence did not lead to any significant difference in the amount of generated graphite-like phase regarding this formulation. Consequently, some discrepancy can be said to exist between both techniques at this instance. The intensity ratio, G-band width and  $L_a$  values of the carbon samples are presented in Table 4.10.

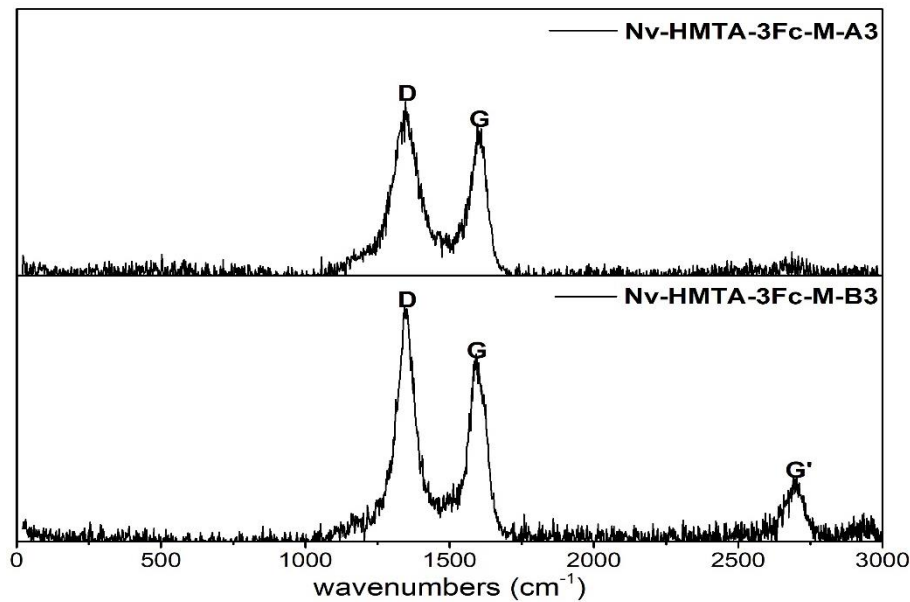


Figure 4.22: Raman spectra of selected carbons derived from novolac resin containing 3 wt% ferrocene and 10 wt% HMTA based on two different heating sequence.

Table 4.10: Raman and XRD parameters

<b>Samples</b>	<b>R-ratio [<math>I_g/(I_d+I_g)</math>] (%)</b>	<b>G-band width (<math>\text{cm}^{-1}</math>)</b>	<b><math>L_a</math> (nm)</b>	<b>GL (%) - XRD analysis</b>
Nv-3Fc-M-A3	35	77	10.58	32
Nv-3Fc-M-B3	41	75	13.64	32

Based on the results attained at this stage of the experimental the following principal conclusions can be made:

1. Boron source additives are cheaper alternative to ferrocene for the graphitization of novolac resin.
2. Processing parameters such heating sequence and rates as well as the preparation procedure affected the amount of generated graphitic carbon during carbonization of novolac resin containing the boron source additives:

3. The degree of crosslinking during the initial stages of carbonization plays significant role the graphitization of novolac resin by boron oxide and boric acid.
4. The formation of B-O-C bonds permits bond breaking/rotation that is necessary for graphitic generation.
5. Several factors including atoms arrangement, bond strength and composition were found to influence the oxidation resistance of carbons derived from phenolic resins.

However, it was not yet clear what role the resin chemistry will has on the graphitization of phenolic resins. More so, since the investigated resin is a commercial product there was no adequate information that can help establish a relationship between how the resin preparation procedure can influence amount of generated graphitic carbon by the selected graphitizing additives. All this necessitated the development of the second experimental stage.

#### **4.2 Part 2: Synthesis and graphitization of resole resin by ferrocene and boron compounds additives**

The present section focused on the structure and oxidation resistance of carbons derived from commercial (Rs), and laboratory synthesized resoles (LSRs) containing either ferrocene, boric acid, boron oxide or combination of these additives. The laboratory prepared resins were based on formaldehyde and phenol molar ratio equal to 1.5 (1.5Rs) and 2.0 (2Rs). The experimental conditions were based on the results attained in the previous study and involved mechanical mixing of the formulations and the use of A3-heating procedure. The resins' chemical structure was studied with the aid of Fourier Transform InfraRed-Attenuated Total Reflection (FTIR-ATR) spectroscopy. The carbon samples were characterized with an X-ray diffraction (XRD) equipment to determine the amount of generated graphitic carbon and measured structural parameters such as interlayer spacing ( $d_{002}$ ) and crystallite height ( $L_c$ ). The results show that ferrocene (unlike the boron source compounds) is an excellent additive for crystallizing resoles carbon. The highest graphitization level of 71 % was obtained when 1.5Rs resin containing 5 wt% ferrocene was subjected to a stepwise heat treatment procedure at 3 °C/min. Microstructural images from Transmission Electron Microscope (TEM) corroborate information derived from the XRD technique as the carbon microstructure revealed the presence of fringes. The carbons' reactivity in an oxidizing environment was also determined by thermogravimetric analyzer (TGA) equipment. Several factors such as bond strength, atoms organization and composition were found to control the oxidation resistance of the derived carbons. Besides, rheology measurement was obtained for the plain and formulated resins to determine their flow behaviour under isothermal condition. Based on the rheology measurement, the additive incorporation will not affect the resin near-Newtonian fluid behaviour nor limit processability during refractory production.



#### 4.2.1 Viscosity of the plain and modified resoles

The viscosity-shear rate curves at 30 °C of Rs and 1.5Rs resoles formulations containing the graphitizing additives were shown in Figure 4.23. The 1.5Rs resole was selected for this measurement since its formulations yield the highest amount of graphitic carbons after pyrolysis at 1000 °C for 5 hours. The plain and modified commercial and LSR resins show near Newtonian fluid characteristic (i.e., the stress rate to shear rate was constant and independent of shear load duration) under the test conditions. Compared to 1.5Rs, the commercial product (Rs) has the highest viscosity. However, with the addition of either 5 wt% ferrocene, 6 wt% boron oxide or 10 wt% boric acid, the LSR product became more viscous and attained a status close to the commercial one. Nevertheless, when 5 wt% ferrocene was added to the commercial product, its viscosity slightly reduced. This information assures that the inclusion of these substances by mechanical mixing will not limit processability during the refractory production. The formulations viscosity should provide ease of processing, excellent wettability and penetration into the refractory materials.

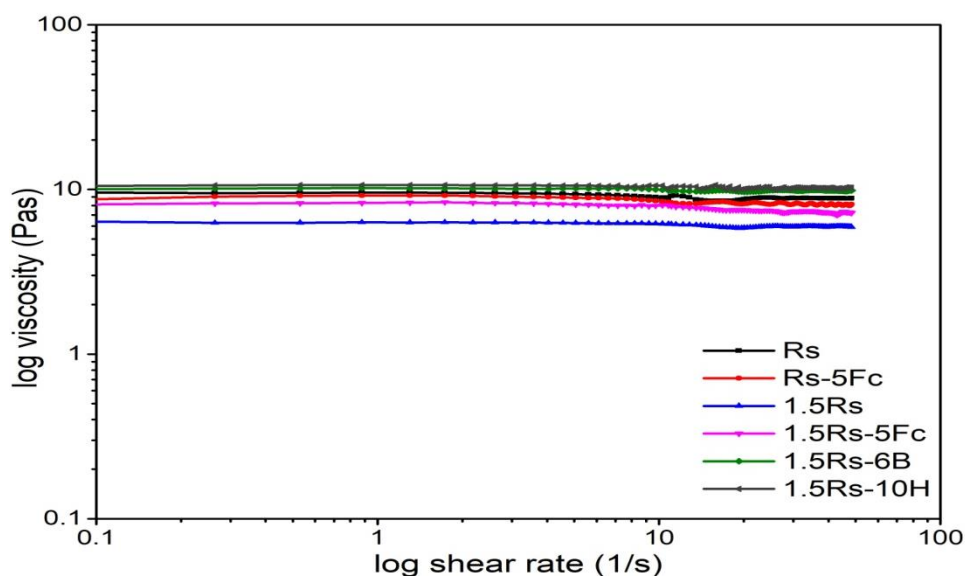


Figure 4.23: Viscosity of commercial and LSR resin with and without ferrocene, boron oxide and boric acid additions at 30 °C.

#### 4.2.2 FTIR-ATR analysis of commercial and laboratory synthesized resole resins

Figure 4.24 shows the spectra in 400 – 4000  $\text{cm}^{-1}$  wavenumber range of the commercial and LSRs. The peaks at 511  $\text{cm}^{-1}$ , 691  $\text{cm}^{-1}$ , 754  $\text{cm}^{-1}$ , 826  $\text{cm}^{-1}$ , and 888  $\text{cm}^{-1}$  were assigned to C-H vibrations [185]. The peak at 754  $\text{cm}^{-1}$  and 826  $\text{cm}^{-1}$  correspond to CH out-of-plane, ortho-substituted and para-substituted positions, respectively [140]. The proportion of the ortho and para linkages was determined from the absorbance intensities of these peaks, which were measured with the aid of spectragraphy 1.1.1 software. The peaks finding threshold was set at 5.0 % of visible spectrum ordinate and the obtained results are presented in Table 4.11. The analysis shows that 1.5Rs has the highest percentage of para links (39 %), whereas values for the commercial and 2Rs products are 34 % and 33 %, respectively. This observation was later related to the attained graphitization level after pyrolysis of the respective resin formulations. The peaks at 1018  $\text{cm}^{-1}$  and 1116  $\text{cm}^{-1}$  were assigned to the C-O vibrations of  $\text{CH}_2\text{OH}$  group. The band that corresponds to the asymmetric stretch of phenol was detected at 1233  $\text{cm}^{-1}$ . The width of the band at 1371  $\text{cm}^{-1}$  and 3320  $\text{cm}^{-1}$  indicated that these peaks were due to OH bond vibration related to the aromatic ring [140]. The peaks at 1452  $\text{cm}^{-1}$  and 1597  $\text{cm}^{-1}$  correspond to C=C aromatic ring vibration [140, 185]. Besides, the peak at 2880  $\text{cm}^{-1}$  was due to aliphatic  $\text{CH}_2$  in-phase stretch [140]. All the functional groups were the same for both the commercial resole and laboratory synthesized ones. However, the integration by area of the OH band represents 45.8  $\text{cm}^2$ , 48.9  $\text{cm}^2$ , and 45.0  $\text{cm}^2$  for the Rs, 1.5Rs, and 2Rs resins, respectively (based on individual baseline). This difference can may be related to the amount of phenol used for the synthesis. Moreover, the peak intensity of each resin differs, especially the one at 511  $\text{cm}^{-1}$ , which has the highest value in 1.5Rs sample. This observation can be related to the functional groups' concentration in the individual resins.

Table 4.11: Peaks absorbance intensity of ortho and para linkages

Peaks position (cm <sup>-1</sup> )	Rs	1.5Rs	2Rs
	Absorbance	Absorbance	Absorbance
754	0.19011	0.28527	0.20185
826	0.09996	0.18064	0.10378
Para links proportion (%)	34	39	33

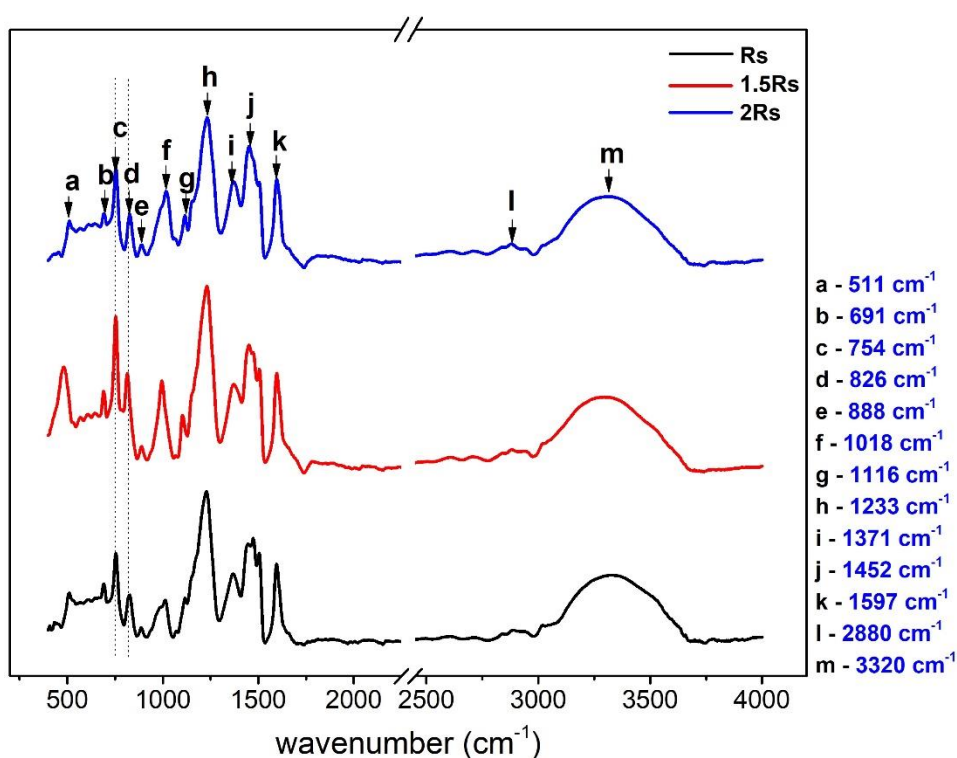


Figure 4.24: FTIR-ATR spectra of commercial and the laboratory synthesized resole resins.

### 4.2.3 Graphitization of commercial and laboratory synthesized resoles containing ferrocene

The diffractograms of the resulting carbons from unmodified resole resins (both commercial and laboratory synthesized ones) show a low-intensity hump between 20-30° and ~43° (Figure 4.25). The profiles indicate a disordered atomic

arrangement after pyrolysis at 1000 °C for 5 hours. This XRD pattern is peculiar to  $sp^3$ -hybridized carbons associated with an amorphous structural arrangement without a long range of carbon layer orientation [176]. Resole resins are non-graphitizable organic precursors since the process leading to carbon formation is mainly a solid-state reaction that does not include semi-liquid phase formation during their pyrolysis. The resins produced glassy carbons in which randomly spaced regions of 6 member  $sp^2$  bonded cyclic structures of the resulting carbons are held tightly within a network of  $sp^3$  crosslink [51]. This type of rigid structure does not permit the reorganization needed for carbons graphitization. The presence of  $\pi$ -bonds can also inhibit the required atoms' rotation necessary for crystalline carbon generation [176]. As mentioned earlier, the disordered organization of carbons derived from plain phenolic resins does not change when heated up to 3000 °C due to their highly cross-linked nature [9]. Consequently, the carbonization product was still isotropic and possessed distinct properties different from graphite.

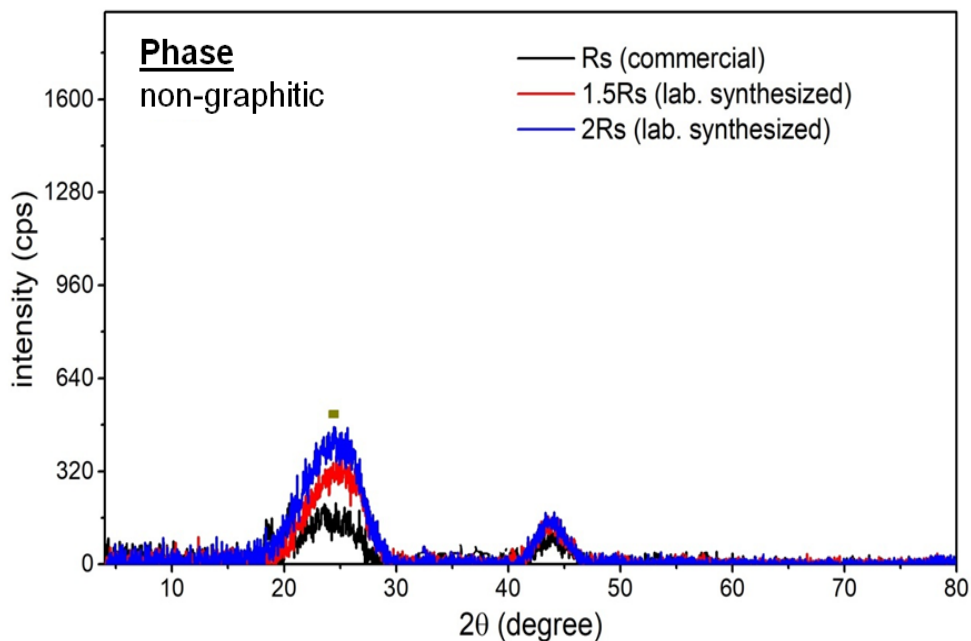


Figure 4.25: X-ray Diffraction pattern of uncatalyzed resole resin after carbonization at 1000 °C.

Figure 4.26 shows the effect of ferrocene addition (3-5 wt%) to resoles on the crystallization of carbons derived from these formulations after heat treatment up to 1000 °C for 5 hours. The diffraction peak at  $\sim 26^\circ$  and  $54^\circ$  represent an asymmetric 002 and 004 plane, which corresponds to graphene layers. The intensity, sharpness and integrated area value of these peaks relative to the non-graphitic ones have been used to describe the extent of graphitization [17, 101, 119, 176]. Firstly, the commercial resin containing 3 wt% Fc was selected to investigate the most suitable heating rate (3-5 °C/min) for the pyrolysis operation. Regardless of the heating rates used, the presence of ferrocene led to the crystallization of the carbonized resole (Figure 4.26a). However, the best GL value (61 %) was attained with the use of 3 °C/min (Rs-3Fc-A3). This heating rate appears to provide sufficient time for ferrocene to act as well as facilitated the carbon atoms bond disruption and rearrangement necessary for graphitic carbon generation during the carbonization process. 1.5Rs and 2Rs were formulated in the laboratory to have control over the resin chemistry and find other factors that can influence the amount of generated turbostratic carbon. These resins were subjected to the same stepwise heat treatment procedure using the heating rate that presented the best result with the commercial resin (i.e., 3 °C/min). Furthermore, 3, 4 and 5 wt% of ferrocene (compared to the weight of resin) were added to the synthesized products. 1.5Rs resin (formaldehyde to phenol ratio = 1.5) generated the highest amount of crystalline carbons during pyrolysis and the carbonized products prepared with 3-5 wt% Fc presented 64 %, 66 % and 71 % graphitization level, respectively (Figure 4.26b). These values were higher than those attained with pyrolytic carbons from 2Rs formulations containing the same amount of additive under similar experimental conditions (Figure 4.26c). The higher formaldehyde ratio with more methyl functional group and a corresponding methylene bridge implied higher cross-linking during the curing stage [186]. Consequently, the high degree of bonding at the initial stage of pyrolysis limit the graphitization of the resulting carbons [176]. This observation explained why 1.5Rs formulations were more susceptible to graphitization. Besides, the FTIR analysis suggested that para linkages during the curing stage may be beneficial to graphitization (as observed with 1.5Rs). Moreover, the peak corresponding to

$\text{Fe}_3\text{C}$  phase suggests that this compound may have acted as a site for crystalline carbon generation during the pyrolysis operation. The results also agree with previous research studies involving the use of ferrocene as a graphitizing agent [3, 50].

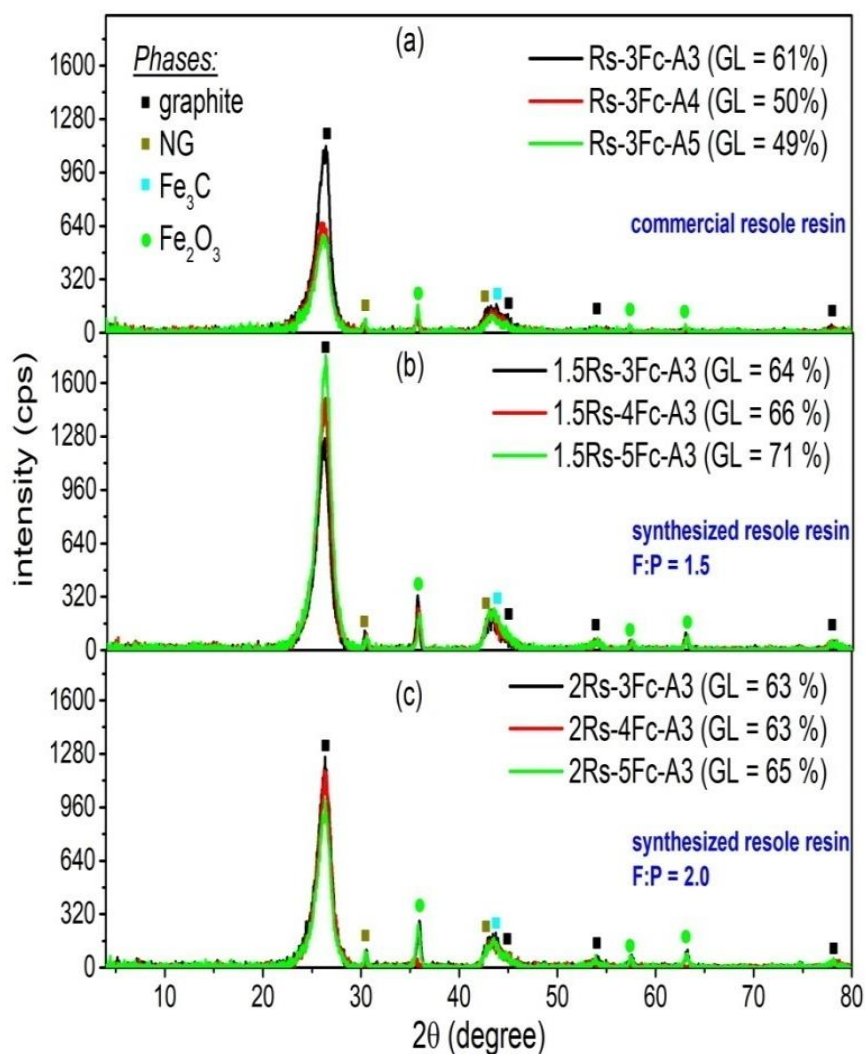


Figure 4.26: XRD profiles showing the effect of ferrocene additions on the graphitization of carbonized resole resins after 1000 °C. NG implies non-graphitic.

Table 4.12 shows the structural characteristics (i.e., interlayer spacing ( $d_{002}$ ), and crystallite height ( $L_c$ )) of the derived carbons. The parameters described the crystallization degree of carbons derived from these organic

precursor formulations. Usually, lower interlayer spacing (close to that of graphite, whose value is 0.3352 nm) and higher crystallite height values represent greater graphitization degree. As observed earlier, the 3 °C/min heating rate led to the best graphitization level and present the smallest values of  $d_{002}$  (0.3384 nm) and the highest of  $L_c$  (6.65 nm) for the commercial resin formulation containing 3 wt% ferrocene. Regarding the laboratory synthesized products, there was no specific trend in their  $L_c$  values (which have values in the range 6.31 nm-7.36 nm) with respect to the starting resin formulations (amount of added ferrocene). Also, the  $d_{002}$  of these carbons (LSR carbons) were very close irrespective of the amount of ferrocene used. Nevertheless, the reduced  $d_{002}$  and increased  $L_c$  values further showed that the addition of this additive to the resole-type phenolic resins before pyrolysis led to an ordered arrangement of the derived carbon atoms.

Table 4.12: Structural parameters of carbon samples derived after pyrolysis of commercial and LSRs at 1000 °C for 5h.

Samples	Interlayer spacing	Crystallite height
	$d_{002}$ (nm)	$L_c$ (nm)
Rs-A3 (from commercial resole)	0.3658	1.65
1.5Rs-A3 (from LSR)	0.3656	1.38
2Rs-A3 (from LSR)	0.3657	1.32
Rs-3Fc-A3	0.3384	6.65
Rs-3Fc-A4	0.3405	5.42
Rs-3Fc-A5	0.3395	5.85
1.5Rs-3Fc-A3	0.3391	6.47
1.5Rs-4Fc-A3	0.3393	6.42
1.5Rs-5Fc-A3	0.3398	6.87
2Rs-3Fc-A3	0.3379	6.31
2Rs-4Fc-A3	0.3377	7.36
2Rs-5Fc-A3	0.3381	6.73

#### 4.2.4 Microstructural analysis

Microstructural analysis was conducted to compare the structural arrangement of disordered carbon atoms from the unmodified resin (Rs-A3) and the graphitic ones from 1.5Rs-5Fc-A3 with the highest GL (Figure 4.27). The high-resolution transmission electron microscope (HRTEM) images show a distinct structural difference between both carbons. The image obtained for Rs-A3 indicates an irregular structural arrangement (Figure 4.27a), whereas the presence of fringes attested to the crystalline nature of 1.5Rs-5Fc-A3 carbon (Figure 4.27b). Lattice lines corresponding to 002 plane were more pronounced although there was evidence of different orientation as well. This ordered arrangement covers a significant portion of the sample microstructure. From the HRTEM image, interplanar spacing (i.e., the spacing between the fringes) corresponding to 002 lattice plane orientation was determined to be  $\sim 0.341$  nm. The stacked plane thickness was  $0.2235 \pm 0.001$  nm. The crystalline carbon HRTEM image also shows evidence of partial graphitization (as seen by the indicated amorphous region, Figure 4.27b). Some further information was obtained from the selected area electron diffraction (SAED) analysis. The Rs carbons have two different circles at 0.2132 nm and 0.1154 nm (Figure 4.27c). Regarding the graphitized sample (1.5Rs-5Fc-A3), the individual spots that represent the lattice plane distance corresponding to the  $2\theta$  values of the XRD were barely visible in the paired arc. This characteristic is peculiar to polycrystalline materials without preferred stacking orientations and indicates a short-range order close to that of graphite. The  $d_{002}$  value determined based on SAED analysis was 0.3384 nm (Figure 4.27d). Compared to Rs-A3, 1.5Rs-5Fc-A3 TEM image shows evidence of stacked graphene sheet layers and the presence of  $\text{Fe}_2\text{O}_3$  phase (Figure 4.27e and 4.27f). These carbon features should improve the thermomechanical performance of CCRs bricks developed based on ferrocene addition to the resin binder.

The EDS analysis of Rs-A3 and 1.5Rs-5Fc-A3 show that a significant amount of oxygen is still present after carbonization at 1000 °C (Figure 4.27g and 4.27h). This observation matches those of other researchers regarding the composition of carbons derived from pyrolyzed phenolic resins [101, 180, 181].



At this instance, up to 12 % and 10 % oxygen was detected in the carbon samples derived from the plain and modified resin, respectively. Also, Figure 4.27h shows the presence of about 4.31 % Fe in the ferrocene-containing carbon composition after pyrolysis at 1000 °C. This information agrees with the XRD results and the proposition that Fe and Fe<sub>3</sub>C may have acted as active sites for structural rearrangement that led to the attained graphitization [17]. Other authors have suggested that this compound (formed at 900 °C) may be responsible for the rearrangement of amorphous carbons to graphene sheets during the pyrolysis operation [10, 17, 131]. It implied that the reactions that led to graphitic carbon generation begin at a later stage of carbonization.

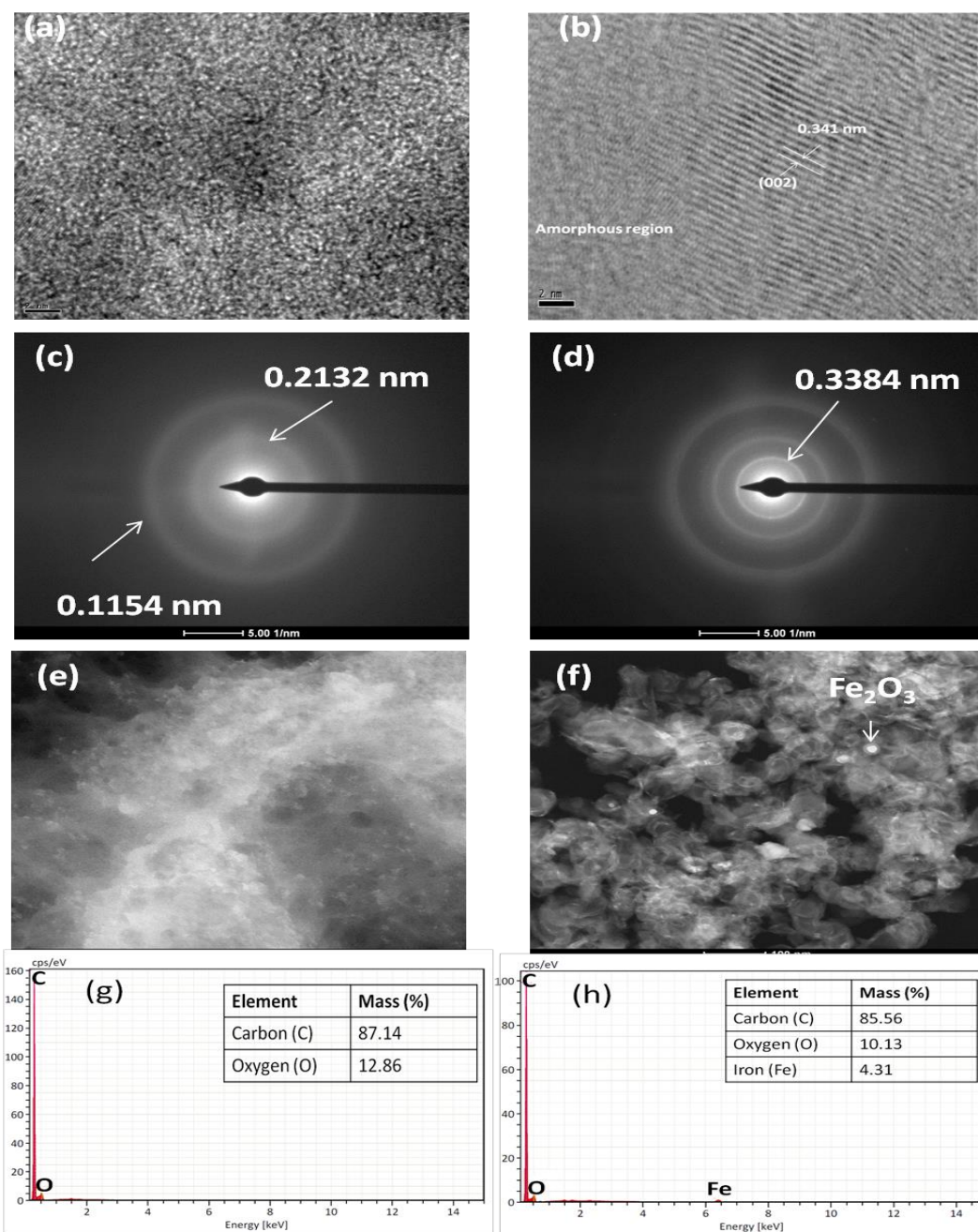


Figure 4.27: Microstructural and chemical information of carbons derived from Rs and 1.5Rs-5Fc formulations after thermal treatment at 1000 °C for 5 hours under reducing atmosphere: HRTEM images of (a) Rs-A3 and (b) 1.5Rs-5Fc-A3. SAED images of (c) Rs-A3 and (d) 1.5Rs-5Fc-A3. TEM images of (e) Rs-A3 and (f) 1.5Rs-5Fc-A3. Chemical composition of (g) Rs-A3, and (h) Rs-A3 1.5Rs-5Fc-A3. A3 = heating procedure at 3 °C/min.

#### 4.2.5 Chemical changes during the pyrolysis of resole containing ferrocene

The high-resolution C1s profiles of 1.5Rs-5Fc formulation subjected to heat treatment at temperatures up to 300 °C, 500 °C, 800 °C and 1000 °C (based on A3-heat treatment procedure) are shown in Figure 4.28a-e. The spectra indicate the presence of different types of carbon functional groups, i.e., C–C, C–O–C, C=O. The peaks at ~284.6 eV were assigned to C–C, at ~286.2 eV, C–O–C, at ~287.9, C=O (carbonyl) and ~289.2 eV to O–C=O (carboxyl) functionalities [125, 179]. The relative percentage changes in the functional groups during the heating process were also presented. The degradation and dehydration reaction during the pyrolysis operation led to the formation of compounds such as CO<sub>2</sub>, methanol, phenol, and water [51]. The release of these substances was responsible for the shift and evolution of the C1s spectra. Nevertheless, some amount of oxygen was still present in the carbonized structure after pyrolysis at 1000 °C. The large full width at half maximum (FWHM) values in Figure 4.28a-d, which are 1.53 eV, 1.44 eV, 1.36 eV, and 1.35 eV, respectively, suggested that the peak assigned to C–C bonds is the combination of C–C/C=C signal.

Moreover, the binding energy of the C–C bonds slightly shifted towards a lower binding energy value (284.3 eV) with a more narrowed width (0.96 eV), indicating the graphitization of these carbon samples after pyrolysis at 1000 °C for 5 hours (Figure 4.28e).

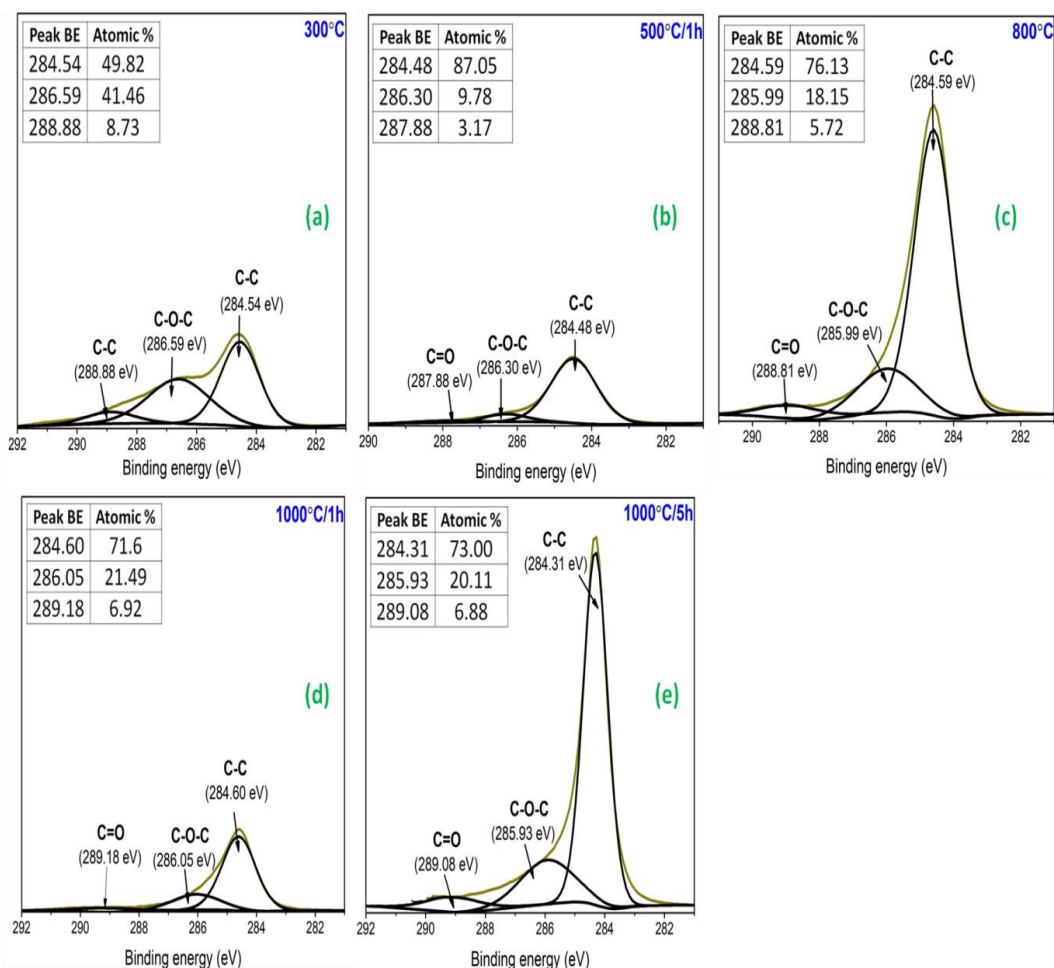


Figure 4.28: The XPS C1s spectra of 1.5Rs-5Fc formulation as a function of heat treatment temperatures. BE = Binding Energy.

The fitted Fe2p spectra of 1.5Rs-5Fc heat-treated samples are presented in Figure 4.29a-e. The profiles were characterized with a doublet of Fe<sup>2+</sup> and Fe<sup>3+</sup> oxides (Fe2p<sub>3/2</sub> and Fe2p<sub>1/2</sub>), as well as the oxides shake-up satellites. Also, the presence of Fe<sub>3</sub>C was detected at temperatures of 800 °C and 1000 °C/5hours. The binding energy values were assigned in line with studies, which involved Fe2p profile deconvolution [187-189]. Based on the transition of Fe2p profile, it is not clear whether there was a chemical reaction between the resin and ferrocene during the heat treatment process or if the various oxide species were due to the additive decomposition. The lack of clarity on the issue is because ferrocene is an organometallic material. Nevertheless, the solubility of carbon in iron may have consequently led to crystalline carbon generation with Fe<sub>3</sub>C acting as active

sites. Moreover,  $\text{Fe}_2\text{O}_3$  appears to be the predominant oxide after the pyrolysis operation at 1000 °C. This observation agrees with the XRD results.

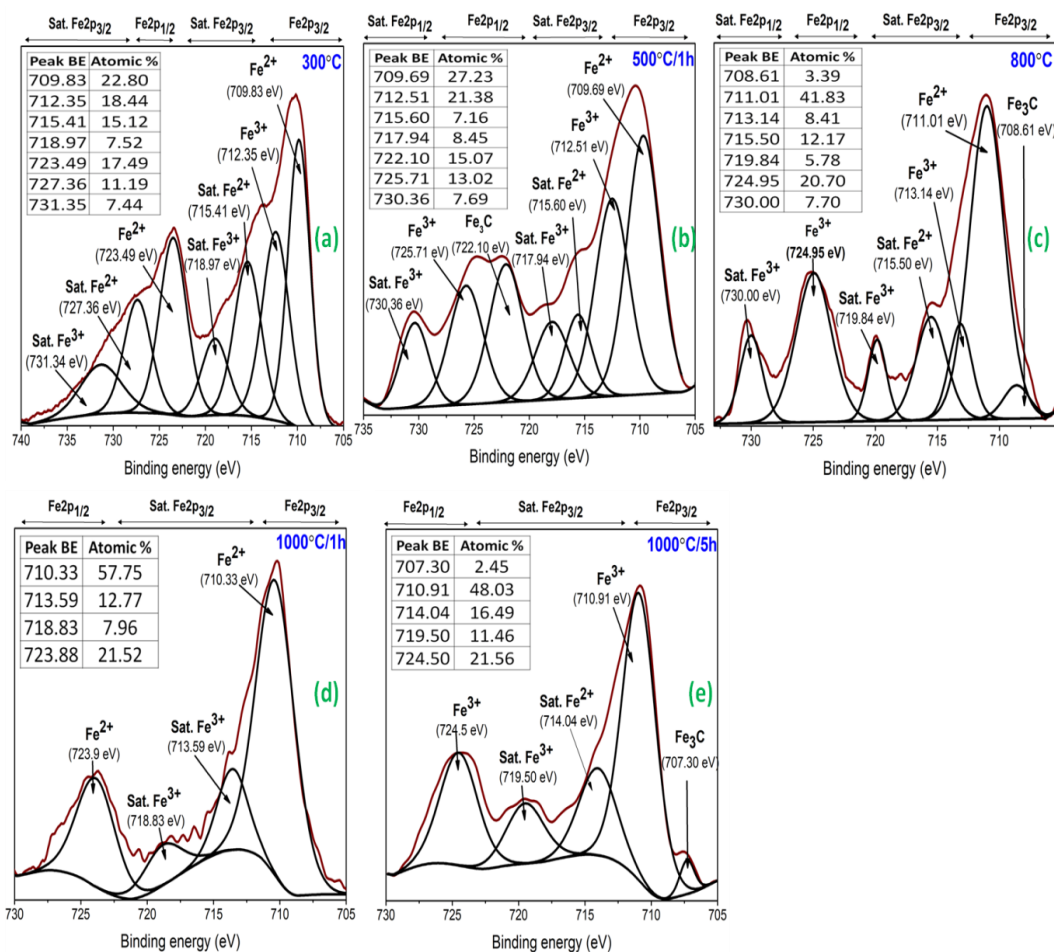


Figure 4.29: The XPS Fe2p spectra of 1.5Rs-5Fc formulation as a function of heat treatment temperatures. BE = Binding Energy.

#### 4.2.6 Oxidation resistance of carbons derived from modified and unmodified phenol-formaldehyde resin

The TG curves in Figure 4.30 described the carbon samples (obtained after the plain and ferrocene-containing resin up to 1000 °C at 3 °C/min) reactivity in an oxidizing environment and at elevated temperatures up to 1000 °C.

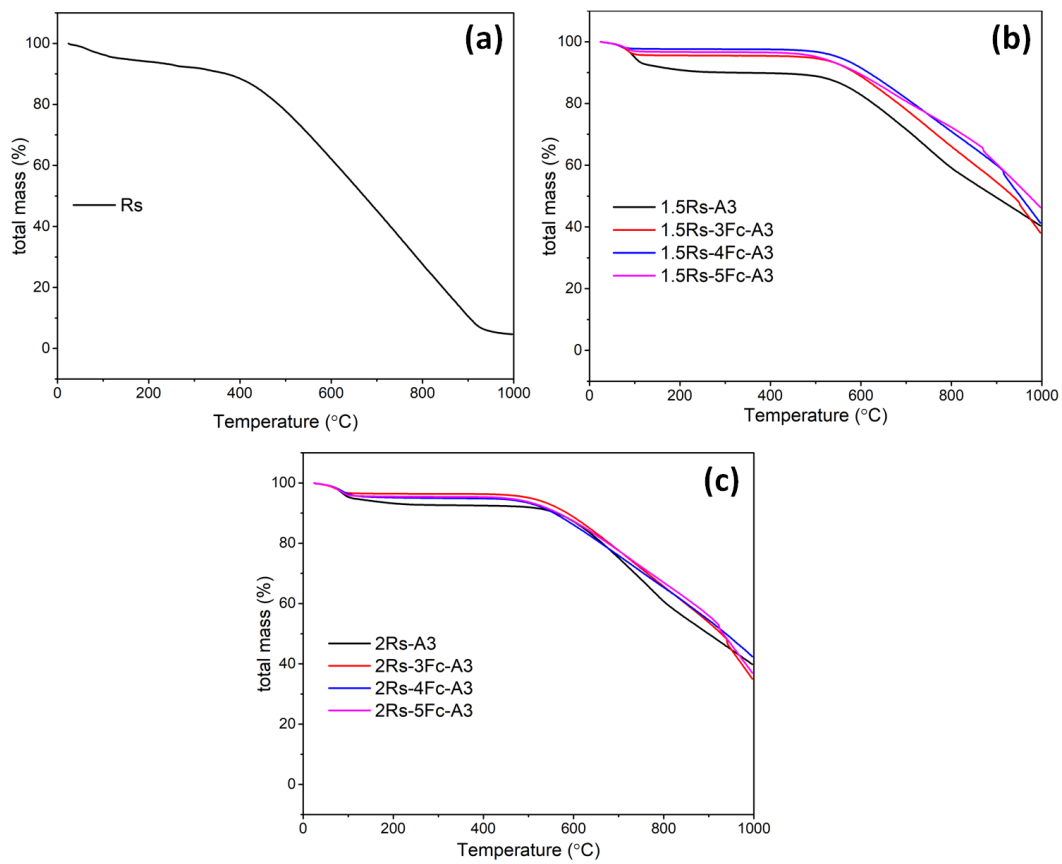


Figure 4.30: TG curves of carbons derived from (a) plain commercial resin (b) plain and modified 1.5Rs resin (c) plain and modified 2Rs during oxidation resistance measurement.

From these curves, the carbon oxidation initiation temperature ( $T_i$ ) and mass loss were determined as described in Section 3.4.2.3 and the results presented in Table 4.13.

Table 4.13: Effect of graphitization and composition on oxidation stability of resole resin carbons

Samples	Carbon loss (%)	T <sub>i</sub> (°C)	GL
Rs-A3	80.79	437.9	0
1.5Rs-A3	55.98	561.9	0
2Rs-A3	53.42	584.8	0
1.5Rs-3Fc-A3	55.55	551.9	64
1.5Rs-4Fc-A3	54.06	541.3	66
1.5Rs-5Fc-A3	48.17	522.3	71
2Rs-3Fc-A3	58.89	537.4	63
2Rs-4Fc-A3	50.45	530.6	63
2Rs-5Fc-A3	55.82	518.3	65
1.5Rs-6B-A3	41.22	535.1	0
1.5Rs-10H-A3	32.61	529.5	0
2Rs-6B-A3	42.43	548.9	0
2Rs-10H-A3	38.19	531.4	0

An attempt was made to ascertain the relationship between the attained graphitization level (GL) of the formulations starting composition and oxidation resistance of the derived carbon samples. Regarding this comparison, the carbon samples were grouped into different categories according to the several factors that appear to control their reactivity in the synthetic air.

- i. Carbons derived from the commercial resin without the additions of any additive (Rs) has the lowest oxidation initiation temperature (compared to others, Figure 4.30a), 0 % graphitization level and possesses the least oxidation resistance with 81 % carbon loss at 1000 °C. Generally, the isotropic nature, high surface area and high amount of edge carbon atoms in their structure promoted high oxidation rate in air. The lack of detailed information regarding the resin chemistry does not permit a thorough understanding of why the carbon exhibited the smallest thermal stability in

- air. However, the disordered arrangement of its atom, as depicted by the TEM image, will reduce its thermal stability in an oxidizing environment. This characteristic will limit CCRs service life and performance [190].
- ii. 1.5Rs-A3 and 2Rs-A3 (derived from the unmodified LSR resins) show improved oxidation resistance than that of the commercial one (Figure 4.30b). The carbons derived from these resins have non-crystalline characteristic but also higher  $T_i$  than the commercial resin carbons and those derived from the formulations containing ferrocene, which are graphitic. Interestingly, their overall performance in the oxidizing environment was similar to the graphitized ones. These observations suggest that other factors such as bond strength play a significant role in the process. Although it is not yet conclusive, the reactivity of the glassy carbon can be affected by atoms bond strength. As mentioned, the  $T_i$  values of 1.5Rs-A3 and 2Rs-A3 were significantly higher than Rs-A3 (from the commercial resin). Their oxidation initiation temperatures were 562 °C and 585 °C, respectively, compared to 438 °C, which was obtained for Rs-A3. The  $T_i$  values may be related to a combination of factors especially bond strength, which should significantly influence it, as oxidation comprises a bond breaking and forming reactions. Edward et al. [163] reported that the macromolecular structure of non-graphitizing polymeric materials is not only preserved but they developed even greater bonding during pyrolysis. Consequently, the oxidation of 2Rs carbon, which has stronger cross-linking due to the formation of more methylene bridges during the curing stage started at a higher temperature compared to 1.5Rs-A3.
  - iii. This section discusses the oxidation resistance of carbon derived from resole formulations containing ferrocene (Figure 4.30c) with a high amount of graphitic structure in their composition. The attained structural rearrangement during pyrolysis should lead to a reduction in the number of edge atoms and improved oxidation resistance. As seen from Table 4.13, the  $T_i$  values of these carbon samples were lower than those derived from the unmodified resins, which implied that oxidation began at a lower



temperature or earlier. The crystallization of resole resin carbon requires minimum cross-linking during the curing stage and the graphitization of the formulations containing ferrocene produce carbons (i.e.  $sp^2$  carbon) with a slightly lower binding energy. Hence, their oxidation onset temperature was lower (as expected) than those of the plain resin carbon. Nevertheless, due to the ordered structure associated with the generated carbon, the overall carbon loss was almost the same as those derived from the plain resins. At this instance, crystallinity seems to be the responsible controlling factor for their overall stability in the high-temperature oxidizing environment. This type of trend is similar to what was observed in previous experiments. Consequently, the advantages associated with the binder graphitization in carbon-containing refractories may be better related to improved thermomechanical properties such as hot modulus of elasticity as reported by Jansen [3].

Furthermore, to determine the role of graphitization, the carbon loss percentage from  $T_i$  to 800 °C and from 800 °C to 1000 °C was compared, as shown in Table 4.14. The analysis assumed two parameters as the oxidation rate-controlling factors, namely, atoms bond strength and organization. The carbon loss per minute at the lower temperature region ( $T_i$ -800 °C) of the graphitized samples (i.e., 1.5Rs-A3 and 2Rs-A3) was lower compared to the non-graphitic ones. At higher temperature region, the glassy carbon derived from the unmodified resin exhibited lower carbon loss rate. This pattern suggests that atoms arrangement presents a significant role at the beginning of oxidation when lower energy was available for bond breaking. However, bond strength may be the controlling factor at more elevated temperatures and the onset of oxidation.

Table 4.14: Carbon loss at different temperature range

Samples	T <sub>i</sub> -800 °C			800 °C-1000 °C		
	Carbon loss (%)	Time (minutes)	Loss per minute	Carbon loss (%)	Time (minutes)	Loss per minute
1.5Rs-A3	58.8	23.81	2.47	41.2	20	2.06
2Rs-A3	57.0	21.52	2.65	43.0	20	2.15
1.5Rs-3Fc-A3	48.9	24.81	1.97	51.1	20	2.56
1.5Rs-4Fc-A3	44.4	25.87	1.72	55.6	20	2.78
1.5Rs-5Fc-A3	45.8	27.77	1.65	54.2	20	2.71
2Rs-3Fc-A3	49.8	26.26	1.89	50.2	20	2.51
2Rs-4Fc-A3	53.9	26.94	2.00	46.1	20	2.31
2Rs-5Fc-A3	46.4	28.17	1.65	53.6	20	2.68

Another important aspect is the oxidation reaction direction, either in the a-axis or basal plane one of the carbon particles. As expected, if reactivity is more pronounced in the a-direction, crystallization will be the controlling factor and the carbon loss rate in the basal plane-direction should depend more on bond strength (due to strong covalent bond). Considering that edge site atoms are more reactive than those of basal plane, graphitization, which favours the reduction of the former should lead to improved oxidation resistance in the a-direction [113-115]. On the other hand, lower carbon loss will occur if oxidation proceeds in the c-direction due to the strong covalent bond within their atoms. The oxidation of plain graphite crystals followed a well-defined crystallographic plane along the polar edges of graphene layers due to oxygen chemisorption.

However, pyrolytic carbon from phenolic resin oxidized more in the c-direction [130, 191]. These observations further explained why the overall performance of the graphitized and non-graphitic carbons in a high-temperature oxidizing environment might appear similar.

Generally, the results show that several factors including atoms bond strength and atomic arrangement control the oxidation resistance of pyrolytic carbons derived from either the plain or modified resins. These observations agree with Chang et al. and Ruff et al. assumption [184, 191] that carbon oxidation is influenced by several factors that include the extent and accessibility of its surface, bond strength of its atoms and the composition.

#### **4.2.7 Role of boron oxide and boric acid on the atomic arrangement and oxidation resistance of carbon derived from resole resin**

The effect of boron source additives on the graphitization of resole resins was also studied. These additives were used based on the results attained in the initial section of this research (Part 1), which involved novolac resin (another phenolic resin type). At this instance, the carbonization of the modified resole resins (1.5Rs, 2Rs) did not lead to any noticeable crystallization of carbons from the resole type phenolic resin. Moreover, changes in the heating procedure did not produce any significant effect on the structural arrangement of the boron compounds-modified resole carbons after heat treatment up to 1000 °C (Figure 4.31a). The reason for the limited graphitization of resole carbons by boric acid or boron oxide may be related to the reaction during carbonization. Based on the previous results from FTIR and XPS analysis, the mechanism leading to graphitization of glassy carbons derived from phenolic resin (such as novolac) containing boron oxide or boric acid depends on the formation and cleavage of B-O-C bonds [178]. As mentioned earlier, the lower binding energy of this bond promotes the rearrangement necessary for graphitic carbon generation [176, 178]. However, a comparison between novolac and resole structure (Figure 4.31b1 and 4.31b2) shows that lesser number of C-positions are available in resole structure due to the presence of hydroxymethyl functional group. This functional

group may prevent the formation of a sufficient number of B-O-C bonds due to steric hindrance [192]. Consequently, the results suggest that the resin molecular structure plays a significant role in the graphitization of the boron compound-modified phenolic resins.

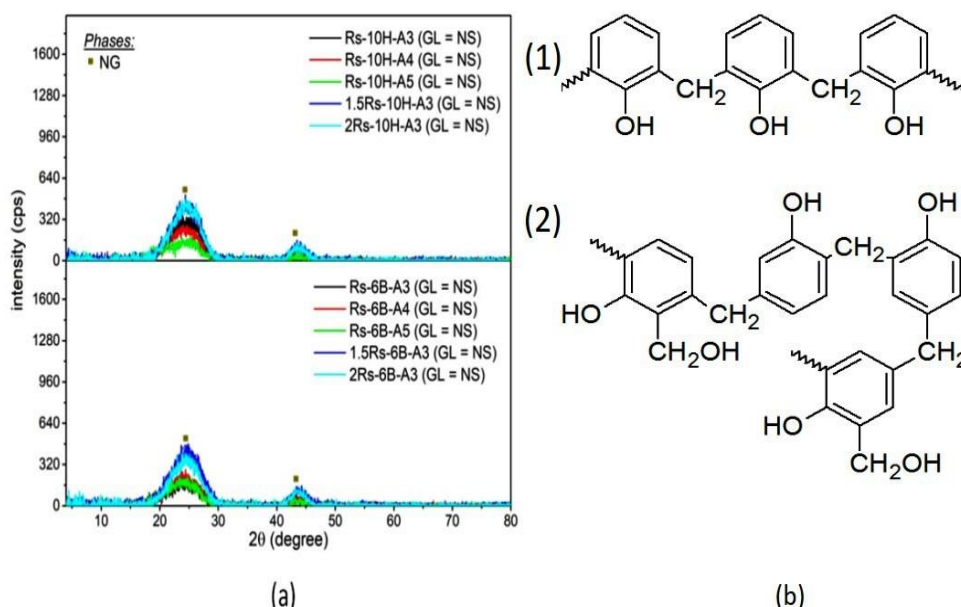


Figure 4.31: (a) XRD profiles showing the effect of boron compound additives on the graphitization of resole resin carbons, (b) structural description: (1) novolac resin (2) resole resin.

Nevertheless, the presence of these additives in the resin formulations provided another benefit regarding oxidation resistance of the derived carbons (Figure 4.32 and Table 4.15). Their carbons show excellent oxidation resistance. The presence of boron and oxygen (Figure 4.33) can lead to boron oxide formation, which will act as protective coating on the carbon surfaces at a temperature of  $\sim 450$  °C ( $B_2O_3$  melting point =  $\sim 450$  °C) and prevents rapid oxidation. These results agree with the earlier observations that the carbon's reactivity in an oxidizing environment depends on several factors including atoms arrangement, composition and bond strength.

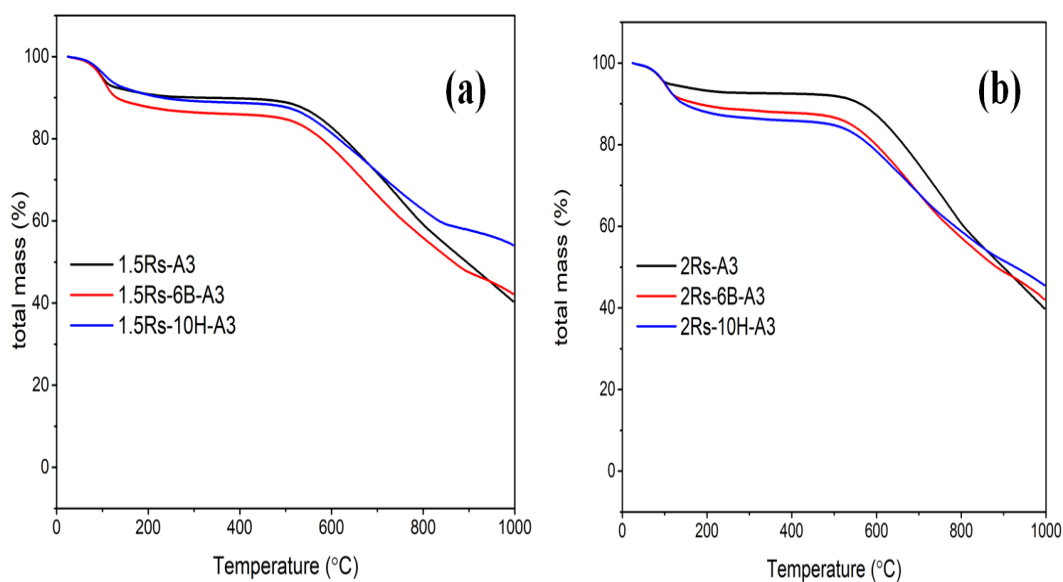


Figure 4.32: TG curves of carbons derived from (a) plain and boron compounds-modified 1.5Rs resin (b) plain and boron compounds-modified 2Rs during oxidation resistance measurement

Table 4.15: Effect of graphitization and composition on oxidation stability of resole resin carbons

Samples	Carbon loss (%)	$T_i$ (°C)	GL
1.5Rs-6B-A3	41.22	535.1	0
1.5Rs-10H-A3	32.61	529.5	0
2Rs-6B-A3	42.43	548.9	0
2Rs-10H-A3	38.19	531.4	0

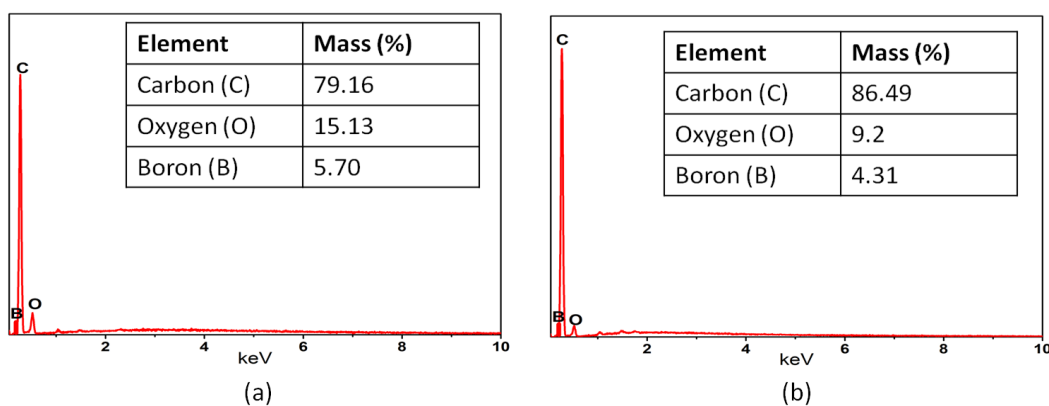


Figure 4.33: Chemical composition of carbons derived from boron compounds-modified resole resin based on EDS analysis (a) 1.5Rs + 10 wt% boron acid formulation (b) 1.5Rs + 6 wt% boron oxide formulation.

#### 4.2.8 Combined role of ferrocene and boron compounds on the atomic arrangement and oxidation resistance of carbon derived from resole resin

Earlier, the role of ferrocene addition on the graphitization of resole resins was discussed. Ferrocene presented good graphitizing ability for resole carbons. The best results were attained when this additive was added to the resin synthesized based on 1.5 formaldehyde and phenol molar ratio (1.5Rs). Considering the good oxidation resistance of carbons obtained from the formulations containing boron oxide and boric acid, the combined role of these compounds on the structural organization and thermal stability in air was investigated using 1.5Rs. The diffractograms of carbons derived from the resin composition containing either 6 wt% boron oxide or 10 wt% boric acid and 3 wt% ferrocene are shown in Figure 4.34. 1.5Rs-6B-3Fc and 1.5Rs-10H-3Fc have a graphitization level of 57 % and 65 %, respectively, compared to 64 % attained with the resin containing only 3 wt% ferrocene. Firstly, it can be seen that the addition of 6 wt% boron oxide slightly reduced the crystallinity obtained for 1.5Rs-3Fc formulation. However, the introduction of 10 wt% boric acid did not in any way limit the amount of generated graphitic carbon in the ferrocene-containing resin. The hardness of the three samples appears to differ, which make it difficult

to present samples of the same particle size range (without affecting the samples' crystallinity during grinding) for the XRD analysis. Nevertheless, this observation does not affect the overall calculated graphitization level that is based on the relative intensity area of the graphitic and non-graphitic phase.

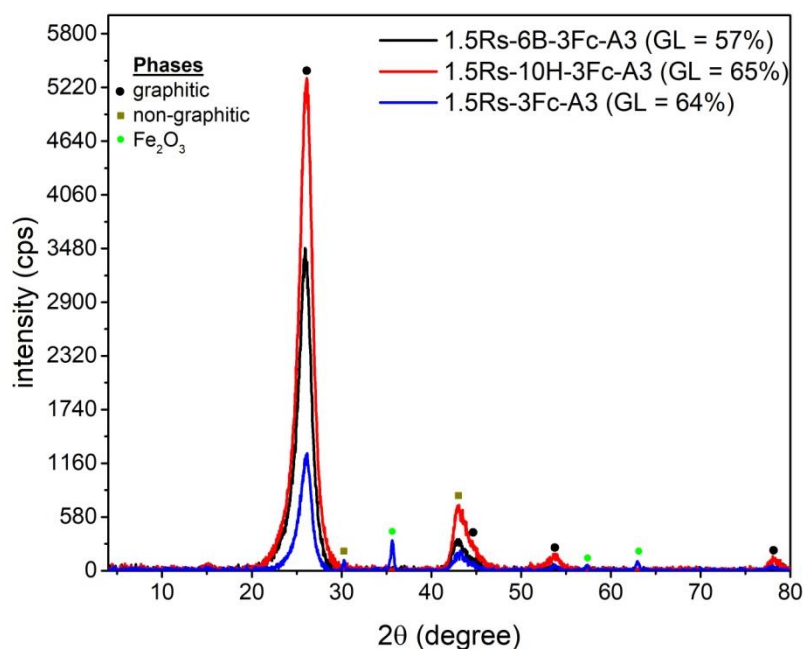


Figure 4.34: Diffractogram of carbons derived from resole resins containing boron compounds and ferrocene after pyrolysis at 1000 °C for 5 hours. 1.5Rs = resole resin with formaldehyde to phenol ratio of 1.5, 6B = 6 wt% boron oxide, 10H = 10 wt% boric acid, 3Fc = 3 wt% ferrocene.

The samples oxidation resistance values are presented in Table 4.16 and Figure 4.35. Compared to 1.5Rs-3Fc-A3 formulation, 1.5Rs-3Fc-10H-A3 has equally a good graphitization level and better stability in an oxidizing environment (with respect to the above formulations) during the thermogravimetric measurement at temperature up to 1000 °C. The attained result may not be unconnected to the combined effect of atoms ordering and composition due to graphitic carbon generation and presence of boron oxide coating, respectively.

Table 4.16: Oxidation resistance of carbons obtained from the formulations containing either the individual or combined additives.

Samples	Carbon loss (%)	T <sub>i</sub> (°C)	GL
1.5Rs-6B-A3	41.2	535	0
1.5Rs-10H-A3	32.6	530	0
1.5Rs-3Fc-A3	55.6	552	64
1.5Rs-3Fc-6B-A3	46.2	565	57
1.5Rs-3Fc-10H-A3	38.5	548	65

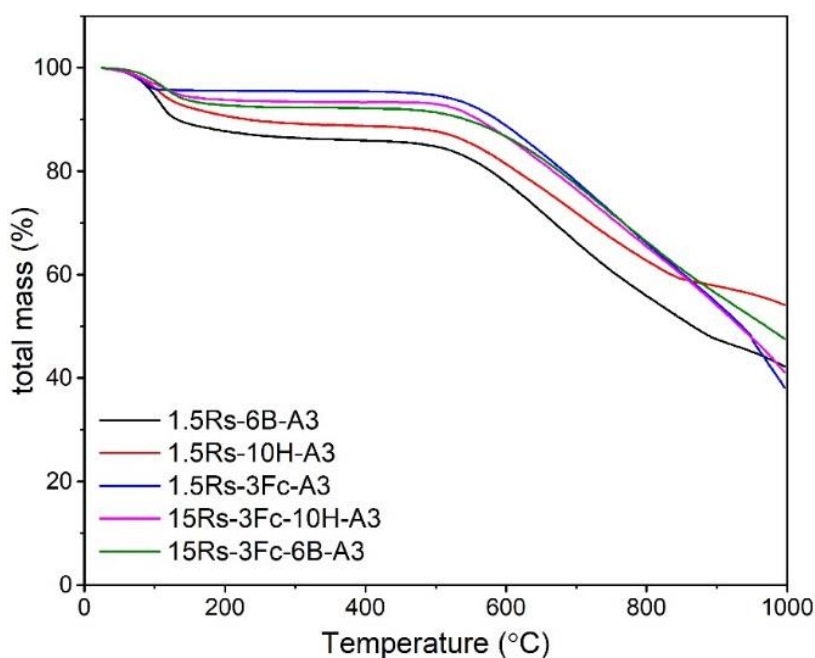


Figure 4.35: TG curves of carbons derived from resole containing ferrocene, boron oxide, boric acid or the combination of these additives.

Some of the principal conclusion of this stage experimental work are highlighted below:

1. Unlike the boron source additives, ferrocene presented the ability to induce graphitic carbon generation during pyrolysis of the resole resins.



2.  $\text{Fe}_3\text{C}$  appears to have acted as sites for graphitic carbon generation during carbonization of the investigated resins.
3. The degree of crosslinking degree and para linkages proportion also play a role in the generation of graphitic carbon from resole resins by ferrocene.
4. Several factors including atoms arrangement, bond strength and composition were found to influence the oxidation resistance of carbons derived from phenolic resins

Nevertheless, the proposed approach involving the use of a low-cost binder material such as lignin-modified phenolic resin has not been exploited. Ultimately, this will involve synthesis and graphitization of such lignin-phenol-formaldehyde resins. Consequently, the next stage of the present investigation addressed this aspect. Although several studies have been carried on the synthesis of lignin-modified phenolic resins, the aspect of graphitization has not yet investigated relative to their application as a binder for CCRs.

### **4.3 Part 3: Synthesis and graphitization of lignin-phenol-formaldehyde resins by ferrocene and boron compounds additives**

This section discussed lignin-phenol-formaldehyde (LPF) resins graphitization using ferrocene, boron oxide and boric acid. The modified resins were synthesized using thermally treated kraft lignin, based on 1.5 formaldehyde to phenol molar ratio. The synthesis was done with up to 30 wt% lignin as phenol replacement. The resins chemical structure was analyzed using Fourier Transform Infrared-Attenuated Total Reflection (FTIR-ATR) spectroscopy. The structural organization and oxidation resistance of carbons derived from the stepwise carbonization of plain LPF resins and the formulations containing the graphitizing additives were determined using X-ray Diffraction (XRD) and thermogravimetric analyzer (TGA) equipment, respectively. The results showed that ferrocene and the boron compounds could induce graphitic carbon generation during the pyrolysis of LPF resins at 1500 °C for 5 hours. The best graphitization level was achieved when 10 wt% boric acid was added to LPF resin produced with 20 wt% lignin. The sample synthesized with 30 wt% lignin present equally a good amount of graphitic carbon corresponding to 71 % graphitization level. However, no direct correlation was established between the thermal stability of the derived carbons in an oxidizing environment and the attained crystallinity values due to the several factors.

#### **4.3.1 FTIR-ATR analysis of the as-received and heat-treated lignin**

Figure 4.36 shows the spectra in the wavenumber range from 400 to 4000  $\text{cm}^{-1}$  of the as-received kraft lignin and the one heat-treated at 200 °C for 1 hour, which was done to enhance lignin reactivity during the synthesis reactions.

The spectra of both the untreated and treated samples were characterized with peaks at 650  $\text{cm}^{-1}$ , 821  $\text{cm}^{-1}$ , and 912  $\text{cm}^{-1}$ , which correspond to C–H vibration bonds of benzene rings. The one at 1030  $\text{cm}^{-1}$  matches with C–O bonds

stretching vibration caused by alcoholic ether groups. This peak may be explicitly assigned to the aliphatic C–O(Ar), aliphatic C–OH, and methylol C–OH in the syringyl unit of lignin [193]. The peak at  $1110\text{ cm}^{-1}$  belongs to the stretching vibration of the C–O bonds from ether linkages adsorption. Phenolic hydroxyl groups vibration of the lignin polymer structure belonging to guaiacyl and syringyl groups correspond to the peaks at  $1211\text{ cm}^{-1}$  and  $1325\text{ cm}^{-1}$ , respectively [194, 195]. Consequently, these profiles showed that the samples are rich in guaiacyl unit, making them suitable for phenolic resin production. The peaks at  $1456\text{ cm}^{-1}$  and the ones at  $1519\text{ cm}^{-1}$  and  $1600\text{ cm}^{-1}$  belong to  $-\text{OCH}_3$  in acetyl groups and C=C vibrations of the aromatic ring, respectively. The CH stretching vibration of the methoxyl group was observed at  $2833\text{ cm}^{-1}$  and  $2933\text{ cm}^{-1}$  [195]. The band at  $3460\text{ cm}^{-1}$  was ascribed to OH vibrations due to the alcoholic and phenolic hydroxyl groups. The units containing the free phenolic hydroxy groups are more susceptible to cleavage. No new functional group was detected after heating the lignin sample up to  $200\text{ }^\circ\text{C}$ . However, the peak intensity assigned to ether linkages at  $1110\text{ cm}^{-1}$  reduced due to ether bonds cleavage. Although some studies have attributed this peak to aromatic in-plane CH vibration [196, 197], other authors have suggested that it may be due to ether-type linkages [198-200] or a combination of both contributions [201]. However, the ease of synthesis which was observed during the resin production (compared to when the as-received kraft lignin was used during the initial experimental stages) attests that the peak is more likely due to ether linkages. The cracking of ether bonds has been observed to occur within the temperature range of  $200\text{ }^\circ\text{C}$  to  $400\text{ }^\circ\text{C}$  depending on the presence of phenolic (Ph) and non-phenolic (Non-Ph) dimers [202, 203]. The heterolysis cleavage of  $\alpha$ -ether bond in Ph compounds can form quinone methide intermediate which can result in a simultaneous homolytic cleavage of the  $\beta$ -ether bond at  $200\text{ }^\circ\text{C}$  [203]. The observation was also consistent with the results obtained by Nakamura et al [204].

Furthermore, there was no evidence of demethylation reaction, as the cleavage of O–CH<sub>3</sub> bond should produce a new OH group (as a result of the replacement of CH<sub>3</sub> by hydrogen), which will lead to increased intensity of the band between  $3200\text{ cm}^{-1}$  and  $3650\text{ cm}^{-1}$  [205]. Instead, the band intensity slightly

decreased. Also, the peak intensities at  $1456\text{ cm}^{-1}$ ,  $2839\text{ cm}^{-1}$  and  $2936\text{ cm}^{-1}$  that were attributed to methoxyl group also remain the same, confirming this assertion [198]. Consequently, the observed ease of synthesis that allows the lignin modified phenolic resins preparation was mainly due to ether cleavage. The peaks corresponding to phenolic hydroxyl groups' vibration of the guaiacyl and syringyl unit also decreased at the higher temperature ( $200\text{ }^{\circ}\text{C}$ ). This reduction may be ascribed to the decomposition of the phenolic groups [201]. Generally, lignin that is suitable for LPF development should be rich in OH group. However, the decrease in the intensities of peaks corresponding to  $-\text{OH}$  group has no pronounced effect on the resins' production because the employed synthesis sequence promoted phenolation reaction.

Finally, the peak intensity attributed to the C–H vibration bond at  $912\text{ cm}^{-1}$  reduced due to dehydration reaction at  $200\text{ }^{\circ}\text{C}$  [201]. Also, the one assigned to C–H vibration of the benzene ring decreased and shifted to  $635\text{ cm}^{-1}$ .

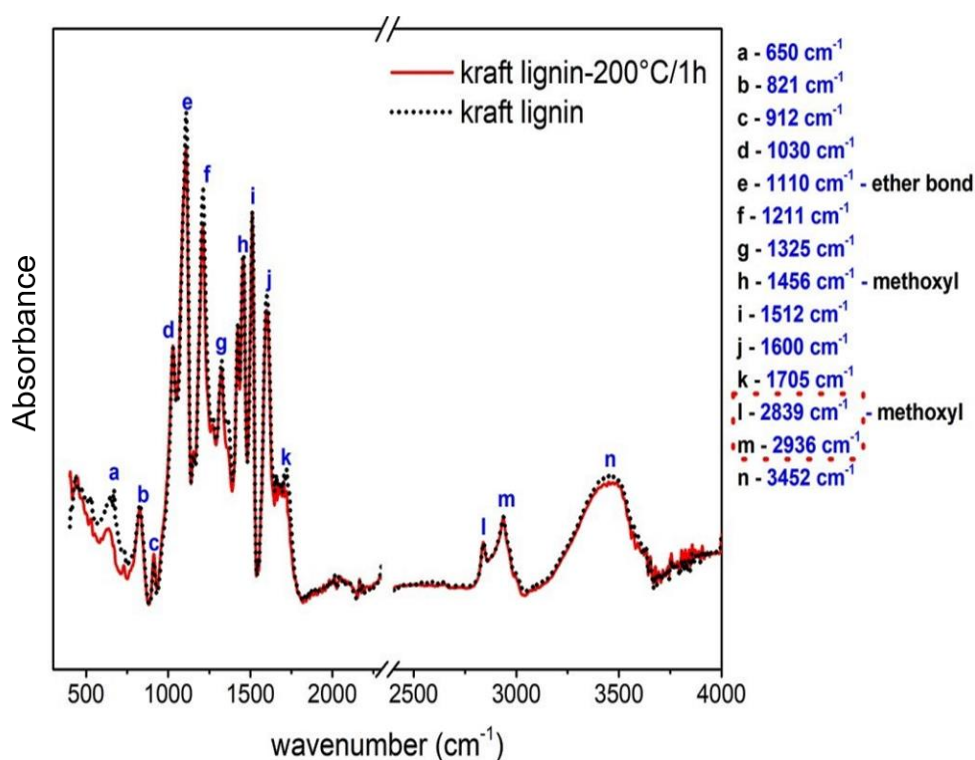


Figure 4.36: As-received and heat-treated kraft lignin samples spectra.

### 4.3.2 Glass transition temperature measurement

The thermal degradation of the as-received kraft lignin did not result in any significant effect on the glass transition temperature. The  $T_g$  values of the as-received sample and the one subjected to thermal treatment at 200 °C were determined to be 129.4 °C and 130.2 °C, respectively. These values are within the range of those that have been previously used for lignin-modified phenolic resins production [206, 207]. However, at 28 °C, the pH of the heat-treated sample was 5.2 compared to 4.5 of the as-received material and the former was also more miscible in water.

### 4.3.3 Molecular weight measurements

The average molecular weights and polydispersity (PD) of the as-received and thermally treated kraft lignin were determined using GPC technique and the results are presented in Table 4.17. The average molecular weight by number ( $M_n$ ) and weight ( $M_w$ ) values of the sample significantly reduce after heat treatment at 200 °C for 1 hour. Compared to the as-received material ( $M_w = 3064$  g/mol and  $M_n = 707$  g/mol), the heat-treated lignin has  $M_w$  and  $M_n$  values of 1957 g/mol and 539 g/mol, respectively. It is apparent that degradation reaction most likely occurred during the heating process and produced lower molecular weight lignin with more reactive sites. In-line with the FTIR results, ether bond cracking, which is the most dominant bond of the total linkages in lignin should be responsible for the depolymerization reaction.

Table 4.17: The average molecular weight and polydispersity index ( $M_w/M_n$ ) values of the as-received and thermally treated kraft lignin.

Lignin samples	$M_w$ (g/mol)	$M_n$ (g/mol)	PD ( $M_w/M_n$ )
As-received	3064	707	4.33
Thermally treated	1957	539	3.63

Furthermore, Figure 4.37 shows the overlaid molecular weight distributions of the as-received and thermally treated kraft lignin. The former sample has a broader weight distribution compared to the latter due to the degradation reaction. The as-received lignin PD value decreases from 4.33 to 3.63 after the heat treatment process (Table 4.17).

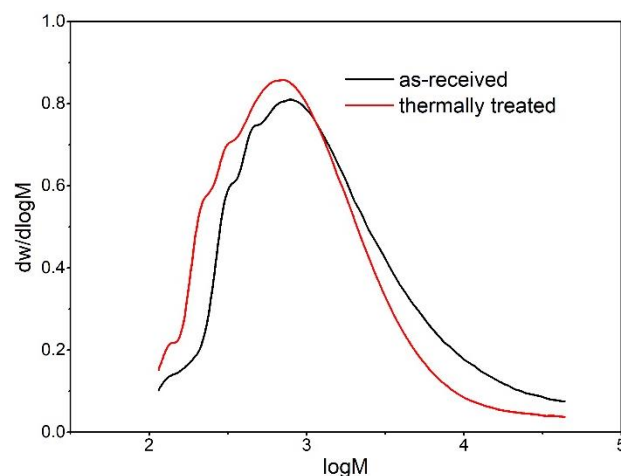


Figure 4.37: As-received and thermally treated kraft lignin overlaid molecular weight distributions from GPC measurements.

#### 4.3.4 FTIR-ATR analysis of the lignin-phenol-formaldehyde resins

Figure 4.38 shows the spectra profiles of the lignin-phenol-formaldehyde resins, the equivalent unmodified resole type (molar ratio = 1.5) and a commercial resole product. As expected, some slight peaks shift (with respect to highlighted peaks of 30LPF spectrum in Figure 4.38) was observed between each of the different resins. Regarding the conventional resole resins (commercial and laboratory synthesized ones), the absorption band across  $3375\text{ cm}^{-1}$  to  $3410\text{ cm}^{-1}$  range corresponds to OH stretch of the phenolic hydroxyl group. Some minor peaks were detected at  $\sim 2870\text{ cm}^{-1}$  and  $\sim 2940\text{ cm}^{-1}$  and were attributed to out of phase and in-phase stretching vibration of  $-\text{CH}_2$  group, respectively. The peaks at  $\sim 1455\text{ cm}^{-1}$  and  $\sim 1592\text{ cm}^{-1}$  correspond to  $\text{C}=\text{C}$  vibrations of the aromatic ring. The wavenumber at  $\sim 1374\text{ cm}^{-1}$  may be due to OH in-plane bend or  $\text{C}-\text{H}$  vibrations [140]. Also, the symmetric stretch of phenolic  $\text{C}-\text{C}-\text{OH}$  was

responsible for the one at  $1226\text{ cm}^{-1}$  [140]. The peaks at  $\sim 1020\text{ cm}^{-1}$  and  $\sim 1111\text{ cm}^{-1}$  were attributed to aliphatic hydroxyl group and the asymmetric stretching vibration of C–O–C aliphatic ether [206]. The region below  $\sim 900\text{ cm}^{-1}$  was characterized by CH deformation of aromatic rings. The peak at  $\sim 824\text{ cm}^{-1}$  and  $\sim 754\text{ cm}^{-1}$  correspond to out-of-plane, para-substituted and ortho-substituted CH positions, respectively [140]. The intensities of these two peaks suggested a high proportion of ortho-linkages (but lower compared to the LPF resins) in both the commercial and laboratory synthesized resole products. Furthermore, peaks were detected at  $\sim 692\text{ cm}^{-1}$ , which can be linked to C–H deformation outside the plane of phenol mono-substituted aromatic rings [206].

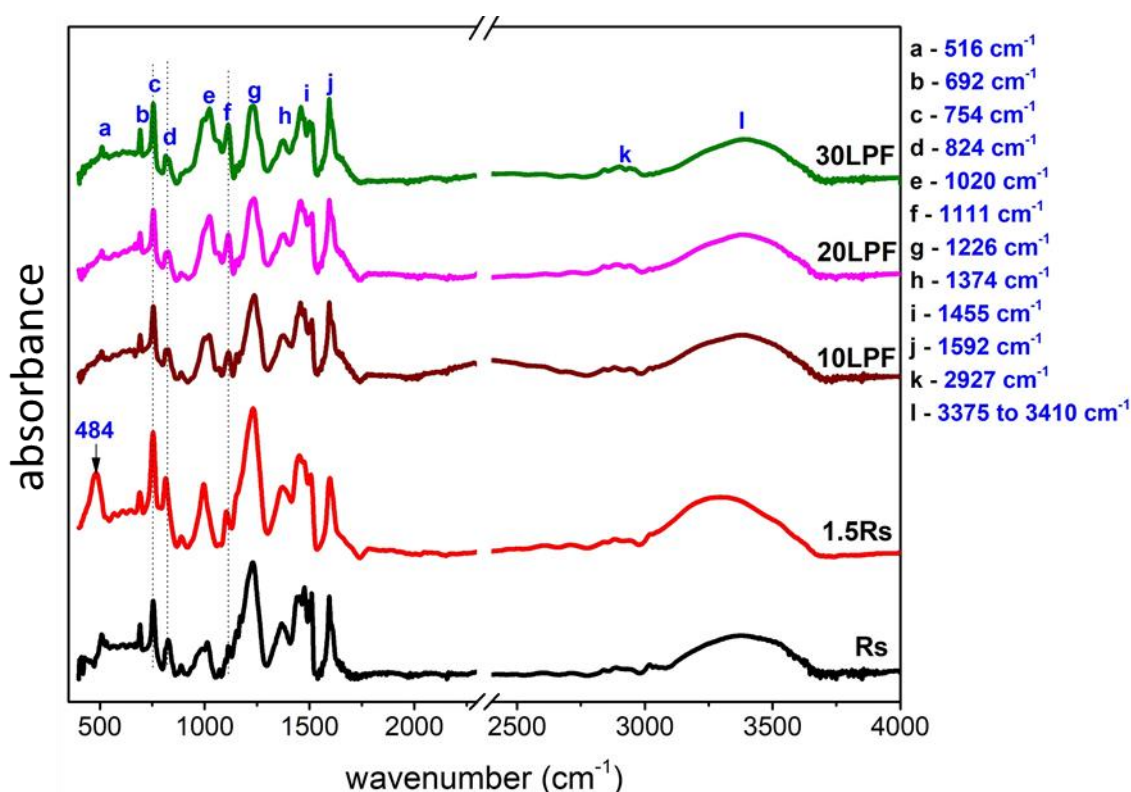


Figure 4.38: FTIR spectra of lignin-phenol-formaldehyde resins, equivalent unmodified resin and commercial resole product. Rs = commercial resole, 10LPF, 20LPF, 30LPF = 10-30 wt% lignin-modified phenolic resins, 1.5Rs = equivalent conventional resole based on formaldehyde to phenol ratio of 1.5.

The LPF resoles spectra look similar to the conventional ones. The spectra similarity suggests that lignin can be used as phenol substitute for the production

of resoles. Nevertheless, some of their peaks were assigned differently based on the primary reactants' monomer. The broad band at  $3410\text{ cm}^{-1}$  is due to OH stretching vibrations of the alcoholic and phenolic hydroxyl groups in hydrogen bonds [195]. The peaks at  $\sim 2927\text{ cm}^{-1}$  for the LPF resins are due to CH stretching vibration of the methoxyl group [195]. Phenolic hydroxyl group vibration of the guaiacyl unit corresponds to the one at  $\sim 1226\text{ cm}^{-1}$  [194, 195].

Moreover, the peak intensity corresponding to the asymmetric stretching of aliphatic ether increased directly with the weight percentage of lignin used for the synthesis. Similarly, the ortho-substituted links increased proportionally with the amount of lignin used (Table 4.18). 30LPF has the lowest para links among the lignin-modified phenolic resins. This suggested that the ease of graphitization of the resulting carbons may decrease with an increase in the amount of substituted phenol by lignin because of the higher cross-linking density. This observation agrees with the results obtained regarding the use of ferrocene as a graphitizing agent. However, this trend was not applicable to the boron compounds containing formulations. The observed difference may likely be due to the reactions that occur during the carbonization operation. Unlike ferrocene (which probably acted at high temperatures), boron compounds can participate in the resin cross-linking reactions [101, 178]. By implication, the resin primary structure should play a significant role in the catalytic graphitization of lignin modified phenolic resins by ferrocene, keeping other factors constant.

Table 4.18: Proportion of ortho and para-substituted linkages

Peaks position ( $\text{cm}^{-1}$ )	Rs	1.5Rs	10LPF	20LPF	30LPF
	Absorbance				
754	0.19011	0.28527	0.1685	0.14971	0.16616
826	0.09996	0.18064	0.07283	0.06273	0.05674
Para links proportion (%)	34	39	30.2	29.5	25.5



### 4.3.5 Structural organization of carbons derived from pristine lignin-phenol-formaldehyde

The XRD profiles of the plain LPF carbons are characterized with high-intensity peaks (compare to the conventional resole resin carbons) with a broad hump at  $\sim 24^\circ$  and  $\sim 43^\circ$  (Figure 4.39a). This observation suggests that the samples' atoms organization may be slightly better than the conventional one (Figure 4.39). Nevertheless, these profiles still present the features of non-graphitic carbons with a limited ordered atomic arrangement.

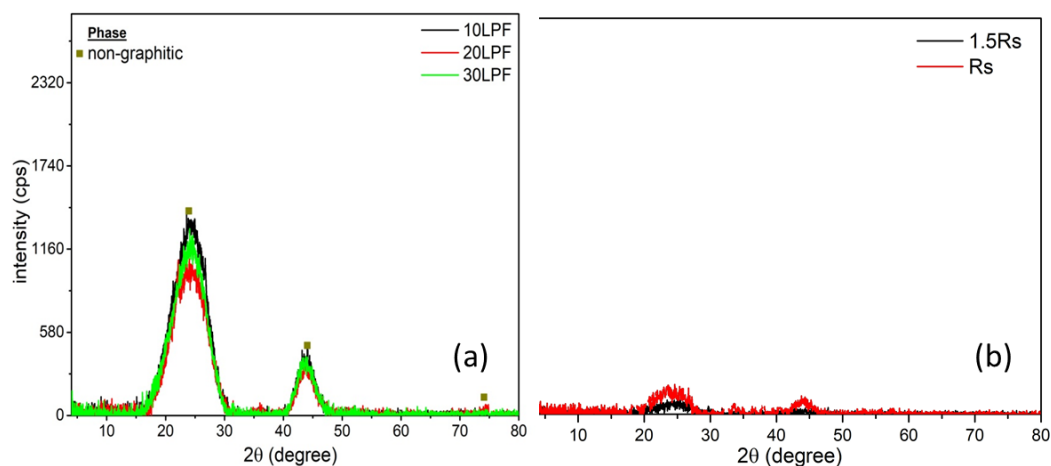


Figure 4.39: Diffractograms of lignin-phenol-formaldehyde resins carbons after pyrolysis at 1000 °C/5h. LPF = lignin-phenol-formaldehyde resin, 1.5Rs = laboratory synthesized resole based on 1.5 formaldehyde to phenol molar ratio, Rs = commercial resole resin.

The calculated interlayer spacing and crystallite height values (Table 4.19) are within the range obtained for amorphous carbons in previous studies [176]. Consequently, there is a need to induce graphitic carbon generation to enhance the thermomechanical performance of such resin-bonded CCR bricks.

Table 4.19: Interlayer spacing and crystallite height values of carbon derived from plain LPF resins after thermal treatment at 1000 °C for 5h under reducing environment.

Samples	$d_{002}$ (nm)	$L_c$ (002) (nm)	GL (%)
10LPF	0.3690	1.19	NS
20LPF	0.3700	1.17	NS
30LPF	0.3701	1.19	NS
*NS = not significant			

#### 4.3.6 Structural organization of carbons derived from lignin-phenol-formaldehyde formulations containing boron compound additives

Boron oxide (6 wt%) and boric acid (10 wt%) were used as agents to induce graphitic carbon generation during carbonization of lignin-phenol-formaldehyde resins (the amount of these additives was based on previous work [176]). Figure 4.40 shows the diffractograms of the carbons derived from the boron compound-modified resin formulations after subjecting them to a stepwise heat treatment procedure up to 1000 °C and 1500 °C. At 1000 °C, the obtained profiles depict a disordered atoms arrangement, characterized by a low-intensity hump across  $\sim 24^\circ$  (close to 002 plane of graphitic structure) and at  $\sim 43^\circ$  (100 in-plane symmetry), corresponding to turbostratic graphitic phase (Figure 4.40a and 4.40b). At that temperature, the available energy was not sufficient to induce graphite generation during the pyrolysis operation. Consequently, the samples were further heated at 1500 °C for 5 hours. At this stage, the XRD pattern clearly revealed the presence of graphitic carbons (Figure 4.40c and 4.40d). The asymmetric peak at  $26^\circ$  is due to graphene layer stacking corresponding to graphite presence. The results show that temperature is a critical factor in the catalytic graphitization of lignin-phenol-formaldehyde resins by boron-source additives. The higher temperature appears to provide sufficient energy to break an adequate number of bonds and cause atomic rotation that is required for crystallization. The highest amount of crystalline carbons was generated in the

resin formulation containing boric acid (up to 73 % for 20LPF-10H). Moreover, higher heating temperature did not lead to the production of crystalline carbon for the plain LPF resole (Figure 4.40e).

Atom ordering of carbon samples should occur during the thermal treatment when sufficient number of bonds are broken since the standard formation enthalpy of graphite is 0 kJ/mol [176]. However, the strong C–C cross-linking during carbonization of the pristine lignin modified phenolic resin prevents fusion or significant atoms movement that hinders the crystallization of the resulting carbon even at 1500 °C after 5 hours of dwell time (Figure 4.40e). The mechanism for phenolic resin carbon graphitization by boron compounds can be attributed to the presence of B–O–C bonds [176, 178]. This bond has a lower binding energy (~192.2 eV) than the plain C–C (~284.7 eV), which facilitated the needed rotation for graphitic carbon generation at 1500 °C.

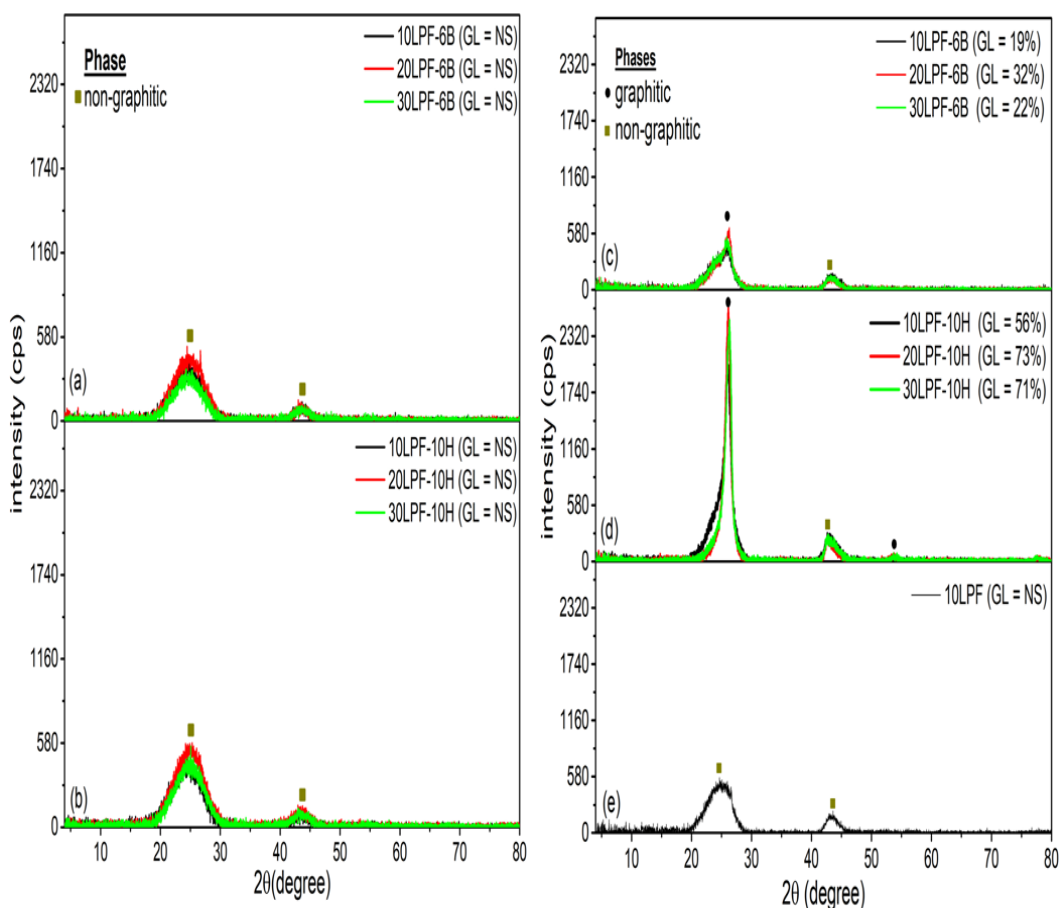


Figure 4.40: XRD profiles of carbons derived from lignin-phenol-formaldehyde resins containing boron compounds after pyrolysis at: (a-b) 1000 °C and (c-e) 1500 °C for 5hours. LPF = lignin-phenol-formaldehyde resin, 6B = 6 wt% boron oxide, 10H = 10 wt% boric acid, NS = not significant.

The interlayer spacing ( $d_{002}$ ) and crystallite height ( $L_c$ ) of the carbon samples from boron compounds modified LPF resins were calculated and the results are presented in Table 4.20. The  $d_{002}$  values of the sample fired at 1500 °C/5h were closer to that of graphite, which is 0.3354 nm. Boron incorporation via substitution can lead to increased orderliness by disrupting the carbon atom (intercalation) or creating a more attractive force between the  $\pi$ -electron cloud [176]. Consequently, the introduction of boron most likely made the graphene layers to come together, leading to reduced interlayer spacing. Similarly, the crystallite height of the samples carbonized up to 1500 °C increased significantly. At this instance, graphite growth was more pronounced in the c-direction.

Table 4.20: Interlayer spacing and crystallite height values of carbon derived from plain LPF resins containing boron compounds after firing at 1000 °C or 1500 °C/5h.

Samples	$d_{002}$ (nm)	$L_c$ (002) (nm)	GL
1000 °C			
10LPF-6B	0.3627	1.37	NS
20LPF-6B	0.3601	1.34	NS
30LPF-6B	0.3617	1.41	NS
10LPF-10H	0.3651	1.33	NS
20LPF-10H	0.3593	1.36	NS
30LPF-10H	0.3587	1.38	NS
1500 °C			
10LPF-6B	0.3413	5.94	19
20LPF-6B	0.3402	7.22	32
30LPF-6B	0.3417	5.82	22

10LPF-10H	0.3415	7.84	46
20LPF-10H	0.3393	9.10	74
30LPF-10H	0.3394	8.63	71
<i>*NS = not significant</i>			

The TEM image of 20LPF-10H carbon derived after carbonization at 1500 °C revealed partly rod-like and onion-like graphitic structure (Figure 4.41a) in the diameter range of 50 to 120 nm. This type of pattern has been observed in boron-containing graphitic carbons [208, 209] and is also peculiar to catalytically induced graphitization process [210]. The HRTEM image (Figure 4.41b) showed the presence of fringes and regions indicating a disordered atomic arrangement, which agrees with XRD results. The image also revealed lattice lines and amorphous regions, pointing out that 20LPF-10H sample was partly crystalline. The high-resolution image further confirmed the presence of onion-like structure in the carbon composition. The selected area electron diffraction (SAED) pattern relates with the HRTEM image and shows similar features of polycrystalline material with no preferred stacking orientations and short-range order. The crystal parameters estimated from the diffraction rings are 0.342 nm, 0.208 nm and 0.129 nm (Figure 4.41c). These values are close to the  $d_{002}$ ,  $d_{101}$  and  $d_{110}$  planes of graphite [211]. The appearance of the diffraction pattern belonging to 002, 101 and 110 planes is another confirmation of graphitic carbon generation from carbonized LPF resin due to the addition of boric acid.

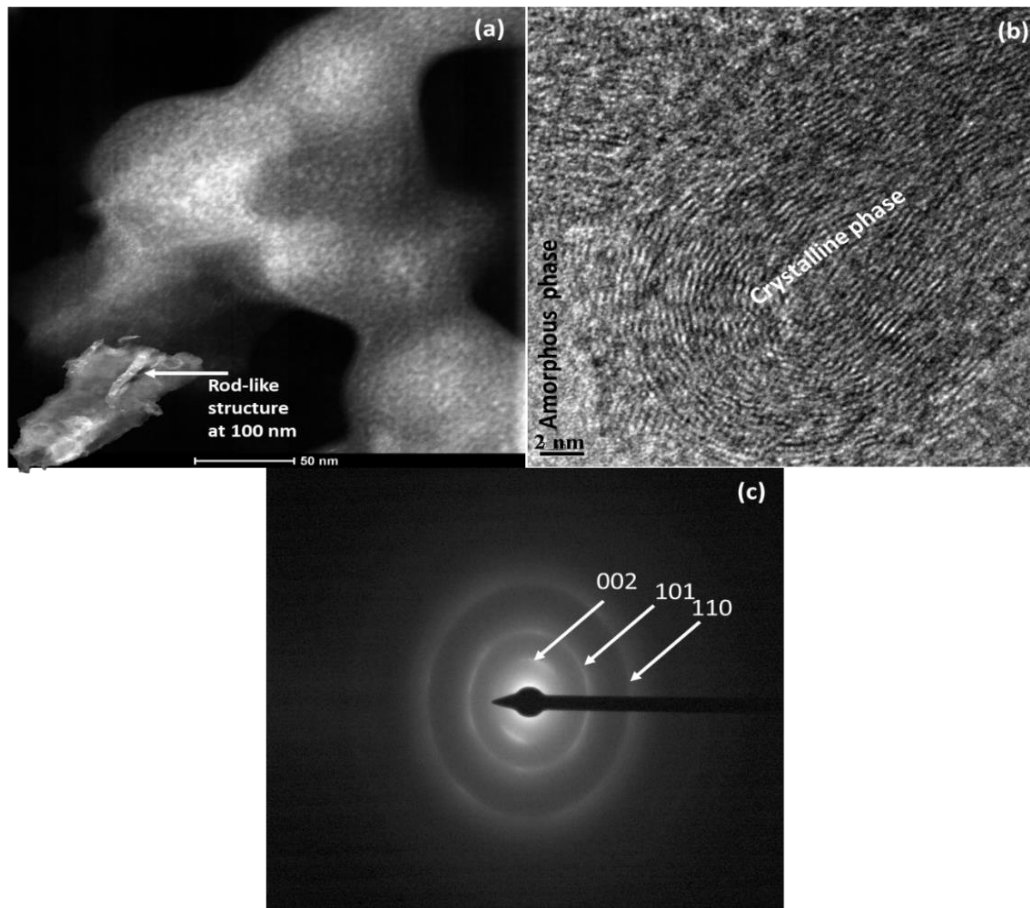


Figure 4.41: (a) TEM, (b) HRTEM and (c) SAED images of 20LPF-10H carbon sample prepared using sequential heat treatment process up to 1500 °C.

#### 4.3.7 Structural organization of carbons derived from lignin-phenol-formaldehyde formulations containing ferrocene

Ferrocene was used to induce graphitic carbon generation during the pyrolysis (stepwise heating procedure suitable for CCRs sintering) of LPF resins (10LPF, 20LPF and 30LPF). Some little amount of crystalline carbon phase was detected after carbonizing at 1000 °C for five hours. At that temperature, the samples diffractograms were characterized with peaks at 101 (44.8°), 102 (50.8°), and 004 (54°) reflections corresponding to graphite phase (Figure 4.42a-4.42c). Nevertheless, the graphene layer stacking at the 002 plane remained

broad near  $26^\circ$ . Another peak belonging to 102 plane of  $\text{Fe}_3\text{C}$  phase [212] (which may be due to ferrocene decomposition [131]) was also detected at  $43.7^\circ$ .

Based on the attained results, the formulations containing 5 wt% ferrocene were heated up to  $1500^\circ\text{C}$  for 5 hours. The resulting carbons' diffractograms (including that of the plain resin carbon) were presented in Figure 4.42d-4.42g. The amount of generated graphitic carbon in the ferrocene-containing samples significantly increased whereas the plain LPF resin carbon still retained its amorphous characteristic. Also, the peak attributed to the 102 plane of  $\text{Fe}_3\text{C}$  substantially diminished, whereas the one belonging to the 101-graphite plane ( $44.8^\circ$ ) increased at that higher temperature. Thus,  $\text{Fe}_3\text{C}$  may have acted as sites for crystalline carbon generation [213]. Consequently, the mechanism leading to the catalytic graphitization of LPF containing ferrocene composition should involve a dissolution-precipitation reaction in which graphitic carbon crystallizes from the iron carbide phase during thermal treatment. Similarly, the peak at  $26^\circ$ , which belongs to the 002 plane of graphite was detected after carbonizing at  $1500^\circ\text{C}$  for 5 hours. Consequently, increased heating temperature favoured the graphitization degree of LPF-Fc formulations.

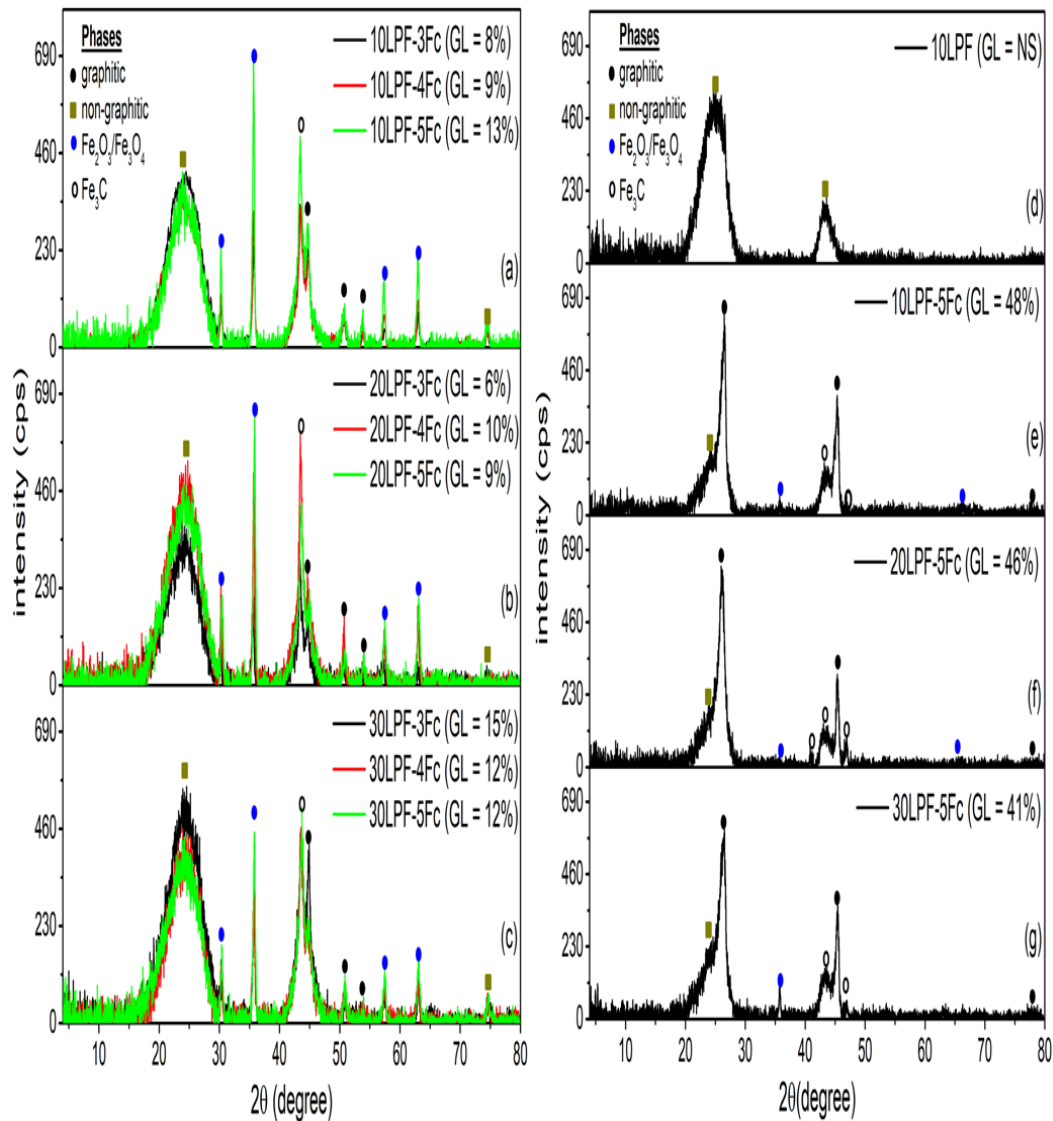


Figure 4.42: XRD profiles of carbons derived from lignin-phenol-formaldehyde resins containing ferrocene after pyrolysis at (a-c) 1000 °C, (d-g) 1500 °C for 5 hours. NS = not significant.

Moreover, the interlayer spacing ( $d_{002}$ ), crystallite height ( $L_c$ ) and crystallite size ( $L_a$ ) of the carbon samples were determined based on the 002 plane (interlayer spacing and crystallite height) and 101 one (crystallite size) using Scherer's and Bragg's equation [97, 133]. The results are presented in Table 4.21. As mentioned earlier, decrease in  $d_{002}$  value and increase in those of  $L_c$  and  $L_a$  are related to higher graphitization degree after pyrolysis at 1500 °C for 5 hours. Under these conditions, crystallization was also observed along the a-



direction (unlike with boron compound resin formulations) based on the XRD results.

Table 4.21: Interlayer spacing and crystallite height values of carbon derived from LPF resins containing ferrocene.

Samples	$d_{002}$ (nm)	$L_c(002)$ (nm)	$L_a(101)$ (nm)	GL
<b>1000 °C</b>				
10LPF	0.3690	1.19	-	-
20LPF	0.3700	1.17	-	-
30LPF	0.3701	1.19	-	-
10LPF-3Fc	0.3671	1.18	13.71	8
10LPF-4Fc	0.3711	1.20	13.76	9
10LPF-5Fc	0.3689	1.32	20.45	13
20LPF-3Fc	0.3733	1.27	15.77	6
20LPF-4Fc	0.3690	1.14	12.54	10
20LPF-5Fc	0.3686	1.20	12.54	9
30LPF-3Fc	0.3678	1.22	16.41	15
30LPF-4Fc	0.3657	1.20	13.49	12
30LPF-5Fc	0.3721	1.17	13.17	12
<b>1500 °C</b>				
10LPF	0.3605	2.13	-	-
10LPF-5Fc	0.3380	7.98	24.18	48
20LPF-5Fc	0.3398	7.28	31.02	44
30LPF-5Fc	0.3390	7.23	30.04	41
*NS = not significant				

Figure 4.43a shows the TEM image of 20LPF-5Fc carbon with a cage-like graphitic domain, which is peculiar to partially graphitized carbon that is mainly associated with the 002 plane [112]. Another phase corresponding to iron oxide (Fe = 88 wt%, O = 12 wt%) was detected in the carbon composition. The corresponding HRTEM image also revealed distinct fringes corresponding to 002

lattice plane with an average interlayer spacing value of 0.342 nm (Figure 4.43b). Regarding the SAED measurement (Figure 4.43c), the individual spots that represent the lattice plane distance corresponding to graphitic carbon  $d_{002}$  and Fe crystals were observed on the pattern. However, the diffraction rings were barely visible.

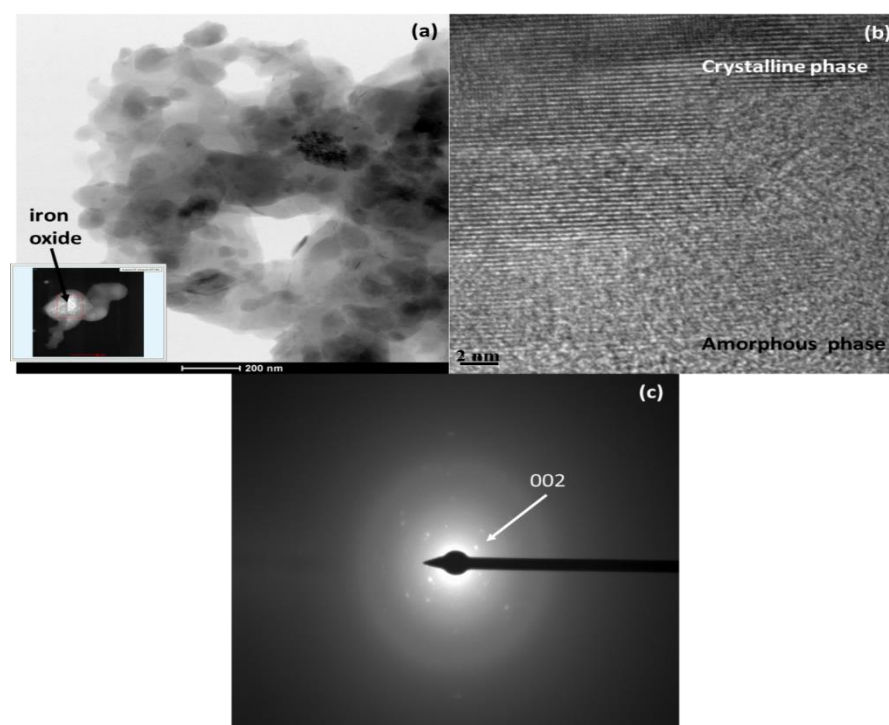


Figure 4.43: (a) TEM, (b) HRTEM and (c) SAED images of 20LPF-5Fc carbon sample prepared using sequential heat treatment process up to 1500 °C for 5 hours.

#### 4.3.8 Oxidation resistance of the carbon samples prepared from the resin formulations containing boric acid, boron oxide and ferrocene

The oxidation resistance of carbons derived from the LPF resins (10LPF, 20LPF, 30LPF) containing ferrocene, boron oxide or boric acid was determined. For the analysis, the samples were heated in an oxidizing environment up to 1000 °C and the resulting thermogravimetric profiles are shown in Figure 4.44a-4.44c.

The actual carbon loss values, which were calculated as described in Section 3.4.2.3, are presented in Table 4.22. Firstly, a direct correlation was not established between the samples' oxidation resistance and the attained graphitization. However, the carbons derived from the resin formulations containing boron-oxide presented the least carbon loss, irrespective of the resin type, i.e. 10LPF, 20LPF or 30LPF. Based on previous results, this observation was attributed to protective oxide formation due to the presence of boron oxide [178]. Nevertheless, 10LPF-5Fc and 20LPF-10H (with emphasis on the latter) may be the most suitable formulations for CCRs production due to the combined effect of their carbons' crystallinity ( $GL = 48\%$  and  $73\%$ , respectively) and thermal stability in air.

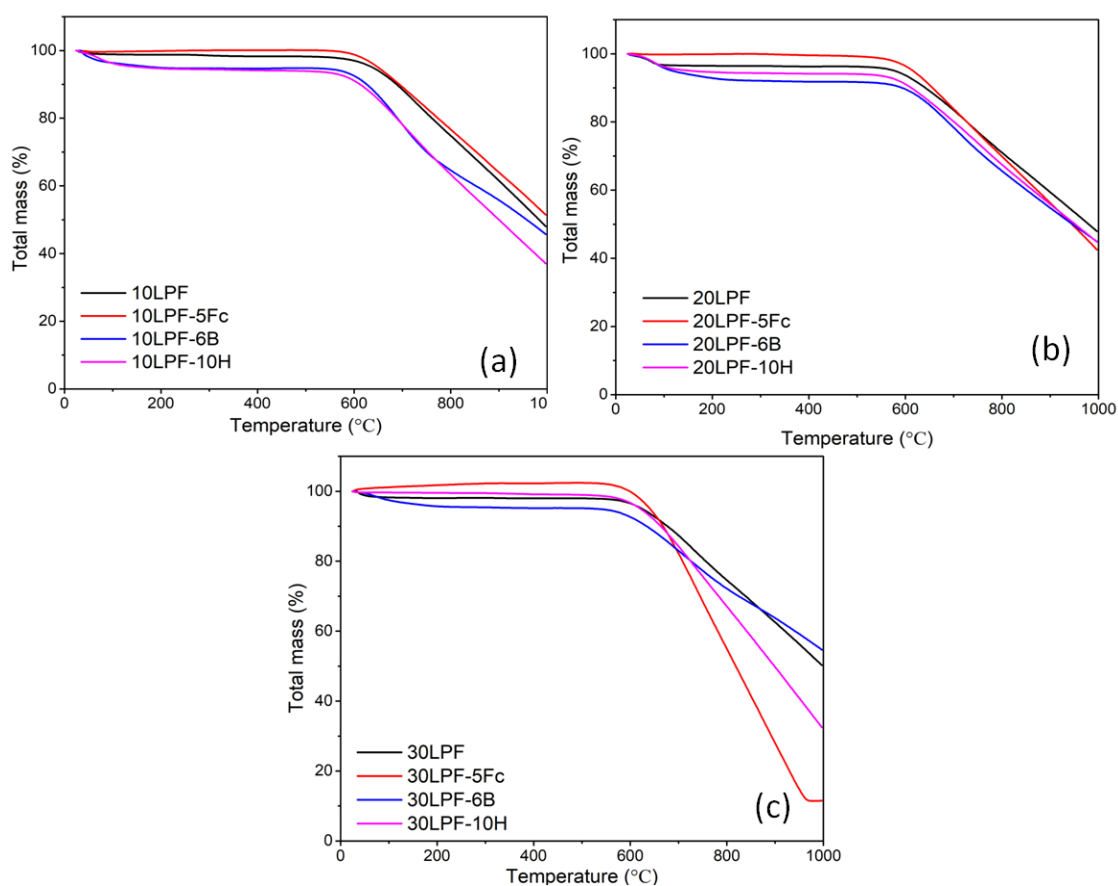


Figure 4.44: TG curves of carbon samples derived from plain LPF resin and the ones containing boron oxide, boric acid and ferrocene (a) 10LPF, (b) 20LPF and (c) 30LPF, synthesized with 10 wt%, 20 wt% and 30 wt% kraft lignin, respectively.

As observed in previous results, carbon oxidation resistance usually depends on a combination of factors such as chemical composition, atoms arrangement and bond strength. These parameters influence their high-temperature oxidizing behaviour. Consequently, it is difficult to isolate the effect of crystallization on reactivity during the thermogravimetric measurement of such samples. More so, unlike pure graphite in which oxidation occurs along a well-defined crystallographic path, the process is more dominant in the c-direction for pyrolytic carbons. Therefore, for amorphous carbon such as those obtained from LPF resins, the atoms cross-linking degree appears to play a significant role on thermal stability in an oxidizing environment due to strong covalent bond [130, 191]. This observation is evident in the higher oxidation initiation temperature ( $T_i$ ) values of 10LPF, 20LPF and 30LPF carbons (Table 4.22).

Table 4.22: Oxidation resistance of carbons derived the lignin-phenol-formaldehyde resins.

	<b>Reference</b>	<b>6 wt% B</b>	<b>10 wt% H</b>	<b>5 wt% Fc</b>	
Carbon loss (%)	10LPF	48	46.5	54.3	46.9
$T_i$ (°C)		632	606	600	612
Carbon loss (%)	20LPF	46.0	44.2	47.1	54.6
$T_i$ (°C)		610	606	593	594
Carbon loss (%)	30LPF	46.0	38.5	57.9	63.2
$T_i$ (°C)		619	595	603	617

In the last phase of this study, some effects of in-situ graphitization of carbon-containing refractory binder components were tested using commercial resole resin containing 5 wt% ferrocene. The commercial product was used due to the quantity of resin that was required for preparing the castables (the inability to synthesize such amount of resin). However, this was not a major challenge because the primary object was to evaluate some benefits of inducing graphitic carbon generation from the binder component of CCRs. Also, the refractory formulation used did not contain graphite to provide assurance that the measured properties were based on the contribution of the binder's carbon.

#### 4.4 Part 4: Physical and mechanical properties of resin-bonded castables developed based on in-situ graphitization of the binder component

This section described the physical and mechanical properties of resin-bonded  $\text{Al}_2\text{O}_3\text{-MgO}$  castables and the effect of in-situ generation of graphitic carbon from the binder component on the refractory performance. Resole resin (commercial product) and the formulation containing 5 wt% ferrocene (with respect to the resin weight) were selected as the binding material. The composition was selected based on results attained in this study. The quantity of required resin for the castable preparation was based on some series of experimental trials. Regarding the investigation, four different class of samples were prepared and designated as A, B, C, and D as described in Table 4.23. The classification was based on the composition and heating procedure employed during the curing stage. Sample A, B and C were prepared with the plain resin but subjected to different curing schedules, whereas sample D was prepared with the resin formulation containing 5 wt% ferrocene.

Table 4.23: Description of samples designation

<b>Samples designation</b>	<b>Description</b>
Sample A	Plain resin-bonded $\text{Al}_2\text{O}_3\text{-MgO}$ castables dried and fired at 50 °C (24 h) + 110 °C (24 h) + 500 °C (1 h) + 1500 °C (5 h)
Sample B	Plain resin-bonded $\text{Al}_2\text{O}_3\text{-MgO}$ castables dried and fired at 50 °C (24 h) + 110 °C (48 h) + 500 °C (1 h) + 1500 °C (5 h)
Sample C	Plain resin-bonded $\text{Al}_2\text{O}_3\text{-MgO}$ castables dried and fired at 50 °C (24 h) + 110 °C (72 h) + 500 °C (1h) + 1500 °C (5 h)
Sample D	Ferrocene modified resin-bonded $\text{Al}_2\text{O}_3\text{-MgO}$ castables dried and fired at 50 °C (24 h) + 110 °C (48 h) + 500 °C (1 h) + 1500 °C (5 h)

#### 4.4.1 Castables physical description during the preparation stages

$\text{Al}_2\text{O}_3$  aggregates and fine alumina and magnesia particles were properly wetted by the resin before and after casting (Figure 4.45a). The castables swelled at the open-end surface after curing at 110 °C for 24 hours as shown in Figure 4.45b. The observed expansion can be attributed to the chemical reaction during curing. From these samples, cylindrical specimens ( $d = 50 \text{ mm} \times h = 30 \text{ mm}$ ) were cut and fired initially at 500 °C for 1 hour and at 1500 °C for 5 hours. The dried and fired samples showed evidence of scattered-surface pores, which was more pronounced in the latter (Figure 4.45c and 4.45d). The resin appears to be the primary pore source due to escaped volatiles during the castables' thermal treatment.

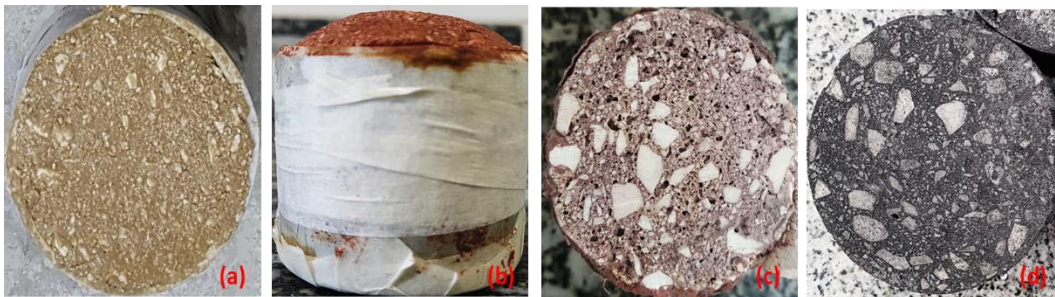


Figure 4.45:  $\text{Al}_2\text{O}_3$ -MgO resin-bonded castables (a) after casting, (b) after curing at temperature up to 110 °C for 24 hours, (c) sample cut from the dried castable and (d) sample fired at temperature up to 1500 °C for 5 hours.

#### 4.4.2 Apparent porosity and bulk density results

The apparent porosity (AP) and bulk density (BD) values of the resin-bonded castables are shown in Table 4.24. Firstly, it was observed that prolonged heat treatment at 50 °C reduced the green samples' open pores quantity. The apparent porosity of samples B ( $9.24 \pm 0.57 \%$ ) and C ( $7.38 \pm 0.89 \%$ ), which were dried at that temperature for 48 and 72 hours, respectively, significantly decreased when compared to sample A ( $20.61 \pm 0.18 \%$ , dried at 50 °C for 24

hours). These values point out that curing time (at 50 °C) has a major effect on the castables' green mechanical strength. Nevertheless, since it may not be practicable to cure such materials for 72 hours during industrial production, the 48 hours curing time was used during the preparation of Al<sub>2</sub>O<sub>3</sub>-MgO bonded with the resin containing 4 wt% ferrocene (relative to the refractory formulations). Moreover, compared to sample B, the apparent porosity of D composition before and after firing was slightly higher. This result might be due to the pocket of gas that was introduced during the initial mixing of the resin and ferrocene for the preparation of the refractory formulation containing the graphitizing additive. The attained results were compared with the experimental values reported for a conventional CCR castable (MgO-C) [214].

Table 4.24: Apparent porosity of green and fired resin-bonded castables prepared with the plain and modified resole resin. AP = apparent porosity and BD = bulk density.

	<b>Sample A</b>	<b>Sample B</b>	<b>Sample C</b>	<b>Sample D</b>	<b>MgO-C castable [214]</b>
AP (%) before firing	20.61±0.18	9.24±0.57	7.38±0.89	13.81±0.52	12.00
AP (%) after firing	-	29.29±0.47	23.17±0.72	32.44±0.51	20.00
BD (g/cm <sup>3</sup> ) before firing	2.77±0.04	2.67±0.25	2.06±0.10	2.76±0.03	2.65
BD (g/cm <sup>3</sup> ) after firing	-	2.43±0.37	2.93±0.05	2.42±0.26	2.54

#### 4.4.3 Cold crushing strength

Figure 4.46 shows the cold crushing strength (CCS) of the green samples after curing at temperatures up to 110 °C for 24 hours and the ones fired up to 1500 °C for 5 hours. The green and sintered castables (Sample C) prepared with the longest curing time (72 hours at 50 °C) has the highest CCS values of 56.9 MPa and 16.2 MPa, respectively. Moreover, no significant difference was observed between sample B and the one prepared based on in-situ graphitization of the binder component (D). This result suggests that crystallization of carbons derived from the resin material did not have any significant effect on CCS. The attained values are close to the ones obtained for a typical MgO-C castable (18 MPa) in a study by Aneziris and Dudczig [214].

The CCS of the cured samples was significantly higher than the fired ones because the bond strength generated by the cured resin was more than the one provided by carbon (from the resin) after pyrolysis, keeping other factors constant [214]. In other words, the stronger interlocking created during the resin polymerization broke after coking at elevated temperatures up to 1500 °C due to carbonization of the organic precursor and the escape of volatile materials.

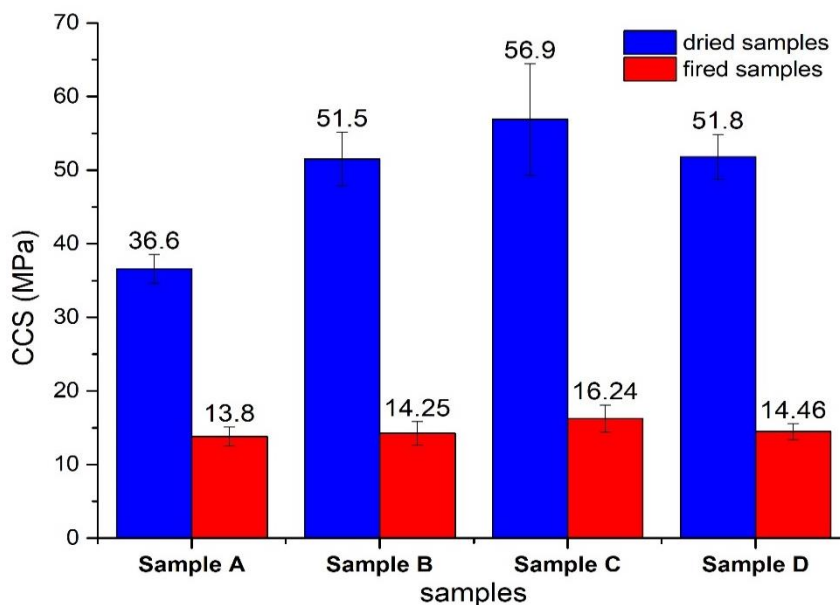


Figure 4.46: Cold crushing strength of green and fired resin bonded Al<sub>2</sub>O<sub>3</sub>-MgO castables.



#### 4.4.4 Oxidation resistance measurement

Two approaches were employed to measure the prepared castables oxidation resistance, namely, oxidation index determination and weight loss measurement. To a large extent, the carbon characteristics appear to influence the refractories' thermal stability in an oxidizing environment (Figure 4.47). Sample C with a lower open pores volume has a better oxidation resistance compared to sample B with the same carbon features. The benefit of in-situ graphitization of the binder component can be determined by comparing sample B and D. The latter composition, which contains some amount of graphitic carbon (based on in-situ graphitization of the resin) has the best resistance to carbon loss. Therefore, the in-situ graphitization of CCRs' binder component might improve the thermal stability of the refractory and by extension their service life. Of course, further and more extensive tests are still required, as not only oxidation but other factors should also play a role in the castables' service life during use.

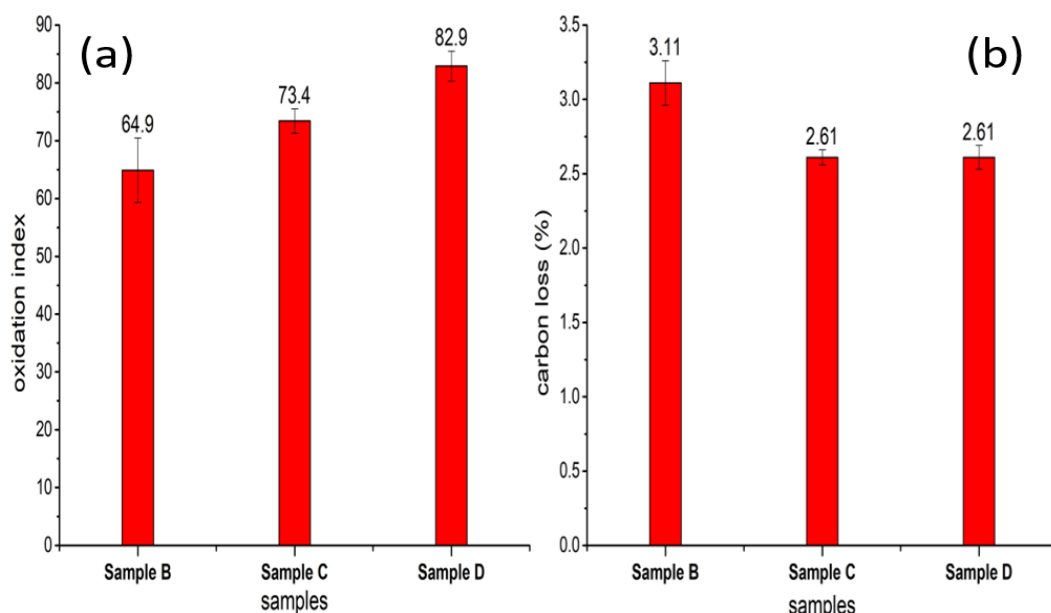


Figure 4.47: Oxidation resistance of the resin-bonded castables at temperatures up to 1000 °C. a = oxidation index measurement, b = weight loss measurement.

It is important to point out some key challenges, which were encountered during this experiment.

- i. Determining the adequate amount of resin needed to prepare the castables: The use of resins is more common in bricks and consolidated refractory pieces obtained via pressing procedure, which required lesser amounts of this binder for their preparation. In this study, the amount of resin in the refractory formulation affected the extent of swelling experienced by the castables after curing as well as their porosity and mechanical strength after pyrolysis. Higher quantities of resin correspond to increased swelling and a lower mechanical strength for the fired samples. Several formulations (based on different amounts of resin) were tried to achieve good wettability of the refractory composition by the resin (for casting purpose) while limiting the above-mentioned drawbacks. The adopted composition (with respect to resin quantity) presented the best results.
- ii. Demoulding the samples after curing: Due to the amount of resin used to prepare the castables, they somehow stuck to the mould after curing. To prevent this challenge, the aluminium mould interior was first covered with paper tape and vegetable oil (margarine) was later applied before casting.
- iii. Curing schedule: As highlighted earlier, the curing time affected the castables' mechanical strength and porosity level. This drawback was more pronounced due to the quantity of resin required for preparing the castables. The effect of curing time should be limited if bricks (prepared via pressing procedure) rather than castables were used for the evaluation.
- iv. Sample preparation for characterization: Due to swelling, samples with specific dimensions were cut from the cured materials before subsequent heat treatment of the green castables and for all the characterizations carried out.

Consequently, the above challenges could be mitigated if bricks and standard CCR formulations were used for the experiment. Thus, additional investigations are required to confirm the effects of in-situ graphitization on the performance of such refractories. Nevertheless, information from the literature

support the assertion that inducing graphitic carbon generation from CCRs' resin can lead to an improvement in their thermomechanical properties [3, 10]



## 5 CONCLUSIONS

Boron oxide and boric acid present ability to induce graphitic carbon generation during pyrolysis of novolac resin. Nv-6B-M and Nv-10H-M formulations (novolac resin containing 6 wt% boron oxide and 10 wt% boric acid, respectively), heat-treated using A3-procedure, showed the best graphitization level with an average of 47 %  $\pm$  10 and 49 %  $\pm$  12, respectively. The interlayer spacing and crystallite height of the carbons prepared in this way were also improved. For example, Nv-10H-M heat treated up to 1000 °C for 5 hours presented  $d_{002} = 0.3382 \pm 0.001$  nm and  $L_c = 10.66 \pm 2.09$  nm, whereas that of Nv (plain resin) was 0.3742 nm and 1.69 nm, respectively. There is a clear indication that the molecular structure's mobility plays a significant role on the catalytic graphitization of novolac resin by boron oxide and boric acid. Several factors such as ultrasonic mixing, vacuum degassing, heating rates promoted stronger cross-linking and limit bonds breakage, which is necessary for graphitic carbon generation (i.e. they have a negative impact on the graphitization process). Consequently, such processing parameters should be monitored during CCR development to prevent a higher degree of cross-linking for maximum formation of crystalline carbon from the modified resin binder. Regarding catalytic graphitization of the novolac resin by ferrocene, changes in heating sequence do not have any significant impact on the amount of generated graphitic carbon.

Ferrocene was found to be an excellent graphitizing agent for resole, irrespective of the difference in the chemistry and structure of the investigated resins. Nevertheless, the highest graphitization level of 71 % was attained with the addition of 5 wt% Fc to the laboratory synthesized product (i.e., 1.5Rs with formaldehyde to phenol ratio = 1.5) after a stepwise heating procedure at 3 °C/min heating rate. Compared to 2Rs (formaldehyde to phenol ratio = 2.0) and the commercial product (Rs), 1.5Rs resole formulations containing ferrocene were more susceptible to graphitization. The lower amount of methyl functional group and methylene bridges that resulted in a lesser cross-linking degree during the curing stage favour their crystallization. This observation shows that a high degree of bonding at the initial stage of pyrolysis will limit the amount of generated

graphitic carbon. The interlayer spacing of carbons derived from the resole formulations were close to those of graphite (0.3352 nm). For example, the  $d_{002}$  for carbons from 1.5Rs-5Fc composition was 0.3384 nm based on SAED measurement. Similarly, the crystallite heights of the graphitized carbons were higher than those derived from the plain ones. The microstructural information obtained from TEM and HRTEM images confirmed the crystallinity of these carbons. However, boron oxide and boric acid could not induce graphitic carbon generation from the resole-type phenolic resins after pyrolysis at temperature up to 1000 °C for 5 hours.

LPF resins were synthesized using thermally treated kraft lignin that is rich in OH group and characterized with syringyl and guaiacyl unit in its chemical structure. The heat treatment led to the cleavage of ether linkages, which induced better reactivity and easier synthesis. There was significant decrease in the molecular weight and polydispersity values of the as-received lignin after thermal treatment at 200 °C due to the depolymerization reaction caused by ether cleavage. However, no significant change in the glass transition temperature was observed. Furthermore, the amount of lignin used for the resin synthesis was found to influence the resulting product chemistry. The ortho-substituted links increased proportionally with the quantity of used lignin especially for 30LPF resin, which was developed with 30 wt% substituted phenol. After carbonization, the carbons derived from the LPF resins have an amorphous-like structure, which can limit the thermomechanical and chemical performance of CCRs. However, ferrocene, boron oxide and boric acid addition to the lignin-phenol-formaldehyde resins led to graphitic carbon generation during their thermal treatment. The highest graphitization level (73 %) was attained when 20LPF resin containing 10 wt% boric acid was pyrolyzed using sequential heating sequence up to 1500 °C for 5 hours. The microstructural images provided supporting information that attests to crystallization of the resulting carbons. More so, the less expensive boric acid acts as a better graphitizing agent compared to ferrocene.

Several factors including atoms arrangement, bond strength and composition were found to influence the oxidation resistance of carbons derived from phenolic resins. Due to the combination of those rate controlling-parameters,

the overall thermal stability of the graphitized samples in the oxidizing environment may be similar to the non-graphitic ones. For example, although significant amount of graphitic carbon was not generated during the pyrolysis of novolac resin containing the graphitizing additives and HMTA, carbons derived from these formulations have a good oxidation resistance. Factors that impede graphite generation during pyrolysis of such resins also promote improved oxidation stability. Hence, improved thermal stability in an oxidizing environment may be attained without necessarily achieving graphitization of carbons derived from these organic precursors. Nevertheless, the thermomechanical properties of CCRs depend on carbons with feature close to graphite. Hence, the importance of inducing graphite generation during pyrolysis of such refractory materials binder is not limited to improving the carbon component reactivity in air at high temperatures. Moreover, the refractory castables prepared in this study based on in-situ graphitization of the binder component exhibit better resistance to carbon loss.

Generally, graphitic carbons generation from the resin formulations containing the boron source additives was attributed to the formation and cleavage of B—O—C bond during heat treatments. The lower binding energy of this bond ( $\sim 190$  eV) compared to C—C one ( $\sim 284$  eV) promoted atoms rotation and rearrangement during the pyrolysis operation that favours crystallization of the resulting carbon. Ferrocene addition may have led to the formation of Fe and  $\text{Fe}_3\text{C}$ , which acts as active sites for the atoms reorganization that promoted crystallization of carbons derived from the investigated resins. Moreover, the investigation shows that the polymerization degree during the initial stages of carbonization affects the generation of crystalline carbon from  $\text{B}_2\text{O}_3$  or  $\text{H}_3\text{BO}_3$ -catalyzed novolac resin carbons.

Although some properties of the resin-bonded CCR castables were tested in this study, more work needs to be done to evaluate the other thermomechanical performances of such material. Nevertheless, in-situ crystallization of the binder's carbon led to an improvement in the oxidation resistance of the evaluated castables. However, at ambient temperature, there

was no noticeable difference in the mechanical properties of samples prepared using the binder with the graphitizing agent and the ones without it.



## 6 SUGGESTION FOR FUTURE STUDIES

The following suggestions have been made for future studies:

1. Further evaluations on the benefits of in-situ graphitization of carbon-containing refractories phenolic resins binder on thermomechanical properties should be carried out using bricks and castables.
2. Other types of lignin materials such as the organosolv ones and lignin decomposition products should be considered for the synthesis of lignin-modified phenolic resins.
3. Employing characterization tools such as Nuclear Magnetic Resonance (NMR) to analyze the resins and lignin will provide further information that can be related to graphitization.
4. Research design towards 100 % replacement of phenolic resins primary reactants (i.e., phenol and formaldehyde) with bio-based materials such as lignin and cellulose will be an impactful study.
5. The derived graphitic carbon from phenolic resin-ferrocene formulations can be considered as a supercapacitor material for energy storage application.
6. The synthesized resins can also be considered for other applications as adhesive and ablative materials.



## 7 REFERENCES

- [1] GARDZIELLA A., S. J., BELSUE M. Carbon from phenolic resins: carbon yield and volatile components. **Recent studies**, v. 41, Expert Fachmedien GmbH. 6, 1992.
- [2] RESENDE, W. S.; et al. Key features of alumina/magnesia/graphite refractories for steel ladle lining. **Journal of the European Ceramic Society**, v. 20, n. 9, p. 1419-1427, 2000.
- [3] JANSEN, H. Bonding of MgO-C bricks by catalytically activated resin. **Millennium Steel Int.**, p. 95-98, 2007.
- [4] EWAIS E. M. M. Carbon based refractories. **Journal of the Ceramic Society of Japan**, v. 112, p. 517-532, 2004.
- [5] GARDZIELLA, A.; PILATO L. A.; KNOP A. **Phenolic resins: chemistry, applications, standardization, safety and ecology**, second Ed. New York: Springer-Verlag Berlin Heidelberg, 2000.
- [6] LIAN, W., et al. The transformation of acetylene black into onion-like hollow carbon nanoparticles at 1000 °C using an iron catalyst. **Carbon**, v. 46, n. 3, p. 525-530, 2008.
- [7] PILATO, L. **Phenolic Resins: A Century of Progress**. Springer Berlin Heidelberg, 2010.
- [8] KRIVOKORYTOV, E. V.; GUR'EV A. G.; POLYAK, B. I. High-carbon binders in refractories and corrosion-resistant ceramics technology. **Glass and Ceramics**, v. 55, n. 5, p. 144-147, 1998.
- [9] RELICK, G. S. Carbon and graphite matrices in carbon-carbon composites: an overview of their formation, structure, and properties. **DTIC Document**, 1992.
- [10] BARTHA, P.; JANSEN H.; DALDRUP H.G. Carbonaceous refractory shaped body with improved oxidation behaviour and batch composition and method for producing the same. **Google Patents**, US6846766B1, 2005.
- [11] ZHU, B.; et al. Structure evolution and oxidation resistance of pyrolytic carbon derived from Fe doped phenol resin, in **Proceedings of the**

- Unified International Technical Conference on Refractories (UNITECR 2013)**. John Wiley & Sons, Inc. p. 1075-1080, 2014.
- [12] GROSSE, D. H.; Jansen H.; Bartha, P. Carbonaceous refractory shaped body with improved oxidation behaviour and batch composition and method for producing the same. **Google Patents**, CA2388675A1, 2001.
- [13] LEE, S. -H., et al. The effect of a magnetic field on the graphitization of carbon nanotubes and its application in field emission. **Diamond and Related Materials**, v. 25, p. 111-118, 2012.
- [14] XU, S., et al. The effect of magnetic field on the catalytic graphitization of phenolic resin in the presence of Fe–Ni. **Carbon**, v. 47, n. 14, p. 3233-3237, 2009.
- [15] LOH, G. C.; BAILLARGEAT, D. Graphitization of amorphous carbon and its transformation pathways. **Journal of Applied Physics**, v. 114, n. 3, p. 033534(1-7), 2013.
- [16] SAVAGE, G. **Carbon-Carbon Composites**. Chapman & Hall, 1993.
- [17] BITENCOURT, C. S.; et al. Role of catalytic agents and processing parameters in the graphitization process of a carbon-based refractory binder. **Ceramics International**, v. 41, n. 10, part A, p. 13320-13330, 2015.
- [18] OYA, A.; JIKIHARA, S.; OTANI, S. Catalytic graphitization of a phenolic resin carbon by nickel (~100 µm): Selective gasification of three resultant components as studied by SEM. **Fuel**, v. 62, n. 1, p. 50-55, 1983.
- [19] ŌYA, A.; ŌTANI, S. Catalytic graphitization of carbons by various metals. **Carbon**, v. 17, n. 2, p. 131-137, 1979.
- [20] ŌYA, A.; YAMASHITA, R.; ŌTANI, S. Catalytic graphitization of carbons by boron. **Fuel**, v. 58, n. 7, p. 495-500, 1979.
- [21] IMAMURA, R.; et al. A new role for phosphorus in graphitization of phenolic resin. **Carbon**, v. 37, n. 2, p. 261-267, 1999.
- [22] WEWERKA, E. M.; IMPRESCIA, R. J. The use of organometallic additives to promote graphitization of carbons derived from furfuryl alcohol resins. **Carbon**, v. 11, n. 4, p. 289-297, 1973.

- [23] ALONSO, M. V.; et al. Modification of ammonium liginosulfonate by phenolation for use in phenolic resins. **Bioresource Technology**, v. 96, n. 9, p. 1013-1018, 2005.
- [24] ALONSO, M. V., et al. Thermal degradation of lignin–phenol–formaldehyde and phenol–formaldehyde resol resins. **Journal of Thermal Analysis and Calorimetry**, v. 105, n. 1, p. 349-356, 2011.
- [25] SARKAR, S.; ADHIKARI, B. Lignin-modified phenolic resin: synthesis optimization, adhesive strength, and thermal stability. **Journal of Adhesion Science and Technology**, v. 14, n. 9, p. 1179-1193, 2000.
- [26] Schacht, C. **Refractories Handbook**. CRC Press, 2004.
- [27] BENAVIDEZ, E. R., et al. Thermal and mechanical properties of commercial MgO-C bricks. **Matéria**, v. 20, p. 571-579, 2015.
- [28] BAUDÍN, C.; ALVAREZ, C.; MOORE, R. E. Influence of chemical reactions in magnesia-graphite refractories: effects on texture and high-temperature mechanical properties. **Journal of the American Ceramic Society**, v. 82, n. 12, p. 3529-3538, 1999.
- [29] BARTHEL H. Carbon containing magnesia and magnesia-carbon bricks. 2 ed. **Pocket Manual Refractory Materials Basics – Structures – Properties**, ed. G. Routschka. Germany: Vulkan-Verlag GmbH, Essen, 2004.
- [30] SIDDIQI, N., et al. Slag–graphite wettability and reaction kinetics Part 2 Wettability influenced by reduction kinetics. **Ironmaking & Steelmaking**, v. 27, n. 6, p. 437-441, 2000.
- [31] LUZ, A. P., et al. Slag melting temperature and contact angle on high carbon containing refractory substrates. **Cerâmica**, v. 57: p. 140-149, 2011.
- [32] SAHAJWALLA, V.; KHANNA, R.; MEHTA, A. S. Influence of chemical compositions of slag and graphite on the phenomena occurring in the graphite/slag interfacial region. **Metallurgical and Materials Transactions B**, v. 35, n. 1, p. 75-83, 2004.

- [33] BAG, M.; ADAK, S.; SARKAR, R. Study on low carbon containing MgO-C refractory: Use of nano carbon. **Ceramics International**, v. 38, n. 3, p. 2339-2346, 2012.
- [34] Boquan, Z.; Wenjie Z. Research of low-carbon magnesia carbon bricks: present situation and development. **Refractories**, v. 40, n. 1, p. 90-95, 2008.
- [35] HALMANN, M.; FREI, A.; STEINFELD, A. Carbothermal reduction of alumina: Thermochemical equilibrium calculations and experimental investigation. **Energy**, v. 32, n. 12, p. 2420-2427, 2007.
- [36] Khanna, R.; et al. Chemical interactions of alumina-carbon refractories with molten steel at 1823K (1550 °C): implications for refractory degradation and steel quality. **Metallurgical and Materials Transactions B**, v. 42, n. 4, p. 677-684, 2011.
- [37] ZOGLMEYR, G. Technical and environment aspects of the use of phenolic resins in modern-day refractories. **Interceram**, v. 42, n. 3, p. 145-149, 1993.
- [38] ZHANG, S.; LEE, W. E. Carbon containing castables: current status and future prospects. **British Ceramic Transactions**, v. 101, n. 1, p. 1-8, 2002.
- [39] WATANABE, A.; TAKAHASHI, H.; NAKATANI, F. Mechanism of dense magnesia layer formation near the surface of magnesia-carbon brick. **Journal of the American Ceramic Society**, v. 69, n. 9, p. C-213-C-214, 1986.
- [40] ALI N. Z., HASHEMI B.; SADRNEZHAAD, S. K. Oxidation mechanisms in MgO-C refractories, in **Tehran International Conference on Refractories**, p. 134-140, 2004.
- [41] HALBIG, M. C. Oxidation kinetics and strength degradation of carbon fibers in a cracked ceramic matrix composite, in **28th International Conference on Advanced Ceramics and Composites B: Ceramic Engineering and Science Proceedings**, John Wiley & Sons, Inc. p. 137-146, 2008.

- [42] GHOSH, N. K.; GHOSH, D. N.; JAGANNATHAN, K. P. Oxidation mechanism of MgO–C in air at various temperatures. **British Ceramic Transactions**, v. 99, n. 3, p. 124-128, 2000.
- [43] HASHEMI, B.; MOGHIMI, Z.; NEMATI Z. A.; SADRNEZHAAD, S. K. Determination of kinetic parameters of MgO-C, **4th International Symposium on Advances in Refractories for the Metallurgical Industries**, Hamilton, Ontario, Canada, p. 581-591, 2004.
- [44] LIU, B.; et al. Effects of nanometer carbon black on performance of low-carbon MgO-C composites. **Journal of Iron and Steel Research, International**, v. 17, n. 10, p. 75-78, 2010.
- [45] BAG, M.; ADAK, S.; SARKAR, R. Nano carbon containing MgO-C refractory: Effect of graphite content. **Ceramics International**, v. 38, n. 6, p. 4909-4914, 2012.
- [46] ZHANG, S.; MARRIOTT, N.J.; LEE, W.E. Thermochemistry and microstructures of MgO–C refractories containing various antioxidants. **Journal of the European Ceramic Society**, v. 21, n. 8, p. 1037-1047, 2001.
- [47] BITENCOURT, C. S.; et al. Phase and microstructural evolution based on Al, Si and TiO<sub>2</sub> reactions with a MgO-C resin-bonded refractory. **Ceramics International**, v. 42, n. 15, p. 16480-16490, 2016.
- [48] FAN, H.; LI, Y.; SANG, S. Microstructures and mechanical properties of Al<sub>2</sub>O<sub>3</sub>–C refractories with silicon additive using different carbon sources. **Materials Science and Engineering: A**, v. 528, n. 7–8, p. 3177-3185, 2011.
- [49] Roger, E. W., Silver, S. M. Pitch-bonded refractory composition. **Google Patents**, USRE27111E, 1966.
- [50] ANEZIRIS, C.G., HUBÁLKOVÁ, J.; BARABÁS, R. Microstructure evaluation of MgO–C refractories with TiO<sub>2</sub>- and Al-additions. **Journal of the European Ceramic Society**, v. 27, n. 1, p. 73-78. 2007.
- [51] LEE, R. **Phenolic Resin chemistry and proposed mechanism for thermal decomposition**. NASA Marshall Space Flight Center, Washington, p. 7-13, 2007.

- [52] DANTE, R. C. **Binders and organic materials**, in Handbook of Friction Materials and their Applications. Woodhead Publishing, Boston. p. 135-153, 2016.
- [53] KAWAMOTO, A. M., PARDINI, L. C.; DINIZ, M. F.; LOURENÇO, V. L.; TAKAHASHI, M. F. K. Synthesis of a boron modified phenolic resin. **Journal Aerospace Technology Management**, v. 2, n. 2, p. 169-182, 2010.
- [54] IRIE, S.; RAPPOLT, J. **Phenolic resin for refractories, in phenolic resins: a century of progress**. Springer Berlin Heidelberg: Berlin, Heidelberg. p. 503-515, 2010.
- [55] FRANKLIN, R. E. Crystallite growth in graphitizing and non-graphitizing carbons. proceedings of the royal society of London. **Series A, Mathematical and Physical Sciences**, v. 209, n. 1097, p. 196-218, 1951.
- [56] WU, C.; SAHAJWALLA, V. Dissolution rates of coals and graphite in Fe-C-S melts in direct ironmaking: Influence of melt carbon and sulfur on carbon dissolution. **Metallurgical and Materials Transactions B**, v. 31, n. 2, p. 243-251, 2000.
- [57] WU, C.; SAHAJWALLA, V. Dissolution rates of coals and graphite in Fe-C-S melts in direct ironmaking: dependence of carbon dissolution rate on carbon structure. **Metallurgical and Materials Transactions B**, v. 31, n. 1, p. 215-216, 2000.
- [58] KHANNA, R.; et al. Dissolution of carbon from alumina-carbon mixtures into liquid iron: Influence of carbonaceous materials. **Metallurgical and Materials Transactions B**, v. 37, n. 4, p. 623-632, 2006.
- [59] NISHIMURA, D. Technical trends of phenolics for Japanese refractories. **Taikabutsu Overseas**, v. 15, n. 2, p. 10-14, 1995.
- [60] LIHONG, H.; HUI, P.; YONGHONG, Z.; MENG, Z. Method to improve lignin's reactivity as a phenol substitute and a replacement for other phenolic compounds: A brief review. **Bioresources**, v. 6, n. 3, p. 3515-3525, 2011.



- [61] GELLERSTEDT, G.; HENRIKSSON, G. **Lignins: major sources, structure and properties in monomers, polymers and composites from renewable resources**. Elsevier, Amsterdam, p. 201-224, 2008.
- [62] HATAKEYAMA, H.; HATAKEYAMA, T. **Lignin structure, properties, and applications in biopolymers: lignin, proteins, bioactive nanocomposites**. Springer Berlin Heidelberg, Berlin, Heidelberg, p. 1-63, 2010.
- [63] KLAPISZEWSKI, L.; et al. Activation of magnesium lignosulfonate and kraft lignin: influence on the properties of phenolic resin-based composites for potential applications, in abrasive materials. **International Journal of Molecular Sciences**, v. 18, n. 6, p. 1224, 2017.
- [64] SHEN, Q.; et al. Lignin-based activated carbon fibers and controllable pore size and properties. **Journal of Applied Polymer Science**, v. 121, n. 2, p. 989-994, 2011.
- [65] XU, C.; FERDOSIAN, F. **Lignin-Based Phenol-Formaldehyde (LPF) Resins/Adhesives, in Conversion of Lignin into Bio-Based Chemicals and Materials**. Springer Berlin Heidelberg, Berlin, Heidelberg, p. 91-109, 2017.
- [66] TEJADO, A.; et al. Isoconversional kinetic analysis of novolac-type lignophenolic resins cure. **Thermochimica Acta**, v. 471, n. 1, p. 80-85, 2008.
- [67] MATSUSHITA, Y.; et al. Surface characteristics of phenol-formaldehyde-lignin resin determined by contact angle measurement and inverse gas chromatography. **Industrial Crops and Products**, v. 23, n. 2, p. 115-121, 2006.
- [68] MA, Y.; et al. An approach to improve the application of acid-insoluble lignin from rice hull in phenol-formaldehyde resin. **Colloids and Surfaces A: Physicochemical and Engineering Aspects**, v. 377, n. 1, p. 284-289, 2011.
- [69] OLIVARES, M.; et al. Kraft lignin utilization in adhesives. **Wood Science and Technology**, v. 22, n. 2, p. 157-165, 1988.

- [70] CAVDAR, D. A.; KALAYCIOGLU, H.; HIZIROGLU, S. Some of the properties of oriented strandboard manufactured using kraft lignin phenolic resin. **Journal of Materials Processing Technology**, v. 202, n. 1, p. 559-563, 2008.
- [71] DANIELSON, B.; SIMONSON, R. Kraft lignin in phenol formaldehyde resin. Part 1. Partial replacement of phenol by kraft lignin in phenol formaldehyde adhesives for plywood. **Journal of Adhesion Science and Technology**, v. 12, n. 9, p. 923-939, 1998.
- [72] QIAO, W.; et al. Synthesis and characterization of phenol-formaldehyde resin using enzymatic hydrolysis lignin. **Journal of Industrial and Engineering Chemistry**, v. 21, p. 1417-1422, 2015.
- [73] JIN, Y.; CHENG, X.; ZHENG, Z. Preparation and characterization of phenol–formaldehyde adhesives modified with enzymatic hydrolysis lignin. **Bioresource Technology**, v. 101, n. 6, p. 2046-2048, 2010.
- [74] JING, Z.; et al. Preparation and characterization of novolac phenol–formaldehyde resins with enzymatic hydrolysis lignin. **Journal of the Taiwan Institute of Chemical Engineers**, v. 54, p. 178-182, 2015.
- [75] Nada, A. M. A.; Abou-Youssef, A.; El-Gohary, S. E. M. Phenol formaldehyde resin modification with lignin. **Polymer-Plastics Technology and Engineering**, v. 42, n. 4, p. 689-699, 2003.
- [76] ZHANG, W.; et al. Preparation and properties of lignin–phenol–formaldehyde resins based on different biorefinery residues of agricultural biomass. **Industrial Crops and Products**, v. 43, p. 326-333, 2013.
- [77] ZHANG, W.; et al. Lignocellulosic ethanol residue-based lignin–phenol–formaldehyde resin adhesive. **International Journal of Adhesion and Adhesives**, v. 40, p. 11-18, 2013.
- [78] KALAMI, S.; et al. Replacing 100 % of phenol in phenolic adhesive formulations with lignin. **Journal of Applied Polymer Science**, v. 134, v. 30, p. 45124(1-9), 2017.
- [79] HU, T. Q. **Chemical Modification, Properties, and Usage of Lignin**. Springer, US, 2002.

- [80] EL MANSOURI, N. E.; YUAN, Q.; HUANG, F. Synthesis and characterization of kraft lignin-based epoxy resins. **Bioresources**, v. 6, n. 3, p. 2492-2503, 2011.
- [81] ZHAO, M.; et al. Preparation and performance of lignin–phenol–formaldehyde adhesives. **International Journal of Adhesion and Adhesives**, v. 64, p. 163-167, 2016.
- [82] OHRA-AHO, T.; et al. S/G ratio and lignin structure among Eucalyptus hybrids determined by Py-GC/MS and nitrobenzene oxidation. **Journal of Analytical and Applied Pyrolysis**, v. 101, p. 166-171, 2013.
- [83] MIN, D.; et al. Improved protocol for alkaline nitrobenzene oxidation of woody and non-woody biomass. **Journal of Wood Chemistry and Technology**, v. 35, n. 1, p. 52-61, 2015.
- [84] QIN, Y.; YANG, D.; QIU, X. Hydroxypropyl sulfonated lignin as dye dispersant: effect of average molecular weight. **ACS Sustainable Chemistry & Engineering**, v. 3, n. 12, p. 3239-3244, 2015.
- [85] VÁZQUEZ, G.; et al. Effect of chemical modification of lignin on the gluebond performance of lignin-phenolic resins. **Bioresource Technology**, v. 60, n. 3, p. 191-198, 1997.
- [86] ALONSO, M. V.; et al. Determination of curing kinetic parameters of lignin–phenol–formaldehyde resol resins by several dynamic differential scanning calorimetry methods. **Thermochimica Acta**, v. 419, n. 1, p. 161-167, 2004.
- [87] VÁZQUEZ, G.; et al. Lignin-phenol-formaldehyde adhesives for exterior grade plywoods. **Bioresource Technology**, v. 51, n. 2, p. 187-192, 1995.
- [88] WANG, F.; et al. Preparation of organic/inorganic composite phenolic resin and application in Al<sub>2</sub>O<sub>3</sub>-C refractories. **International Journal of Applied Ceramic Technology**, v. 13, n. 1, p. 133-139, 2016.
- [89] ZHANG, S.; LEE, W. E. Influence of additives on corrosion resistance and corroded microstructures of MgO–C refractories. **Journal of the European Ceramic Society**, v. 21, n. 13, p. 2393-2405, 2001.

- [90] KO, T. -H.; KUO, W. -S.; CHANG, Y. -H. Microstructural changes of phenolic resin during pyrolysis. **Journal of Applied Polymer Science**, v. 81, n. 5, p. 1084-1089, 2001.
- [91] CONLEY, R. T.; QUINN, D.F. **Retardation of Combustion of Phenolic, Urea-Formaldehyde, Epoxy, and Related Resin Systems, in Flame-Retardant Polymeric Materials**. Springer US, Boston, MA. p. 337-369, 1975.
- [92] LYTLE, C. A.; BERTSCH, W.; MCKINLEY, M. Determination of novolac resin thermal decomposition products by pyrolysis-gas chromatography-mass spectrometry. **Journal of Analytical and Applied Pyrolysis**, v. 45, n. 2, p. 121-131, 1998.
- [93] DUNGAN, R. S.; REEVES, J. B. Pyrolysis of foundry sand resins: a determination of organic products by mass spectrometry. **Journal of Environmental Science and Health, Part A: Toxic/Hazardous Substances and Environmental Engineering**, v. 40, n. 8, p. 1557-1567, 2005.
- [94] KIPLING, J. J.; et al. Factors influencing the graphitization of polymer carbons. **Carbon**, v. 1, n. 3, p. 315-320, 1964.
- [95] BROOKS, J. D.; TAYLOR, G. H. The formation of graphitizing carbons from the liquid phase. **Carbon**, v. 3, n. 2, p. 185-193, 1965.
- [96] MARSH, H., MARTÍNEZ-ESCANDELL M.; RODRÍGUEZ-REINOSO, F. Semicokes from pitch pyrolysis: mechanisms and kinetics. **Carbon**, v. 37, n. 3, p. 363-390, 1999.
- [97] BEATTY, R. L. **Graphitization Kinetics of Fluidized-bed Pyrolytic Carbons**, University of Washington, 1974.
- [98] OBERLIN, A.; OBERLIN, M. Graphitizability of carbonaceous materials as studied by TEM and X-ray diffraction. **Journal of Microscopy**, v. 132, n. 3, p. 353-363, 1983.
- [99] OKAZAKI, S.; et al. Effect of gas atmosphere on graphitization of carbon powder. **Kagaku Kogaku Ronbunshu**, v. 40, n. 1, p. 12-17, 2014.

- [100] SAZANOV, Y. N.; GRIBANOV, A. V.; LYSENKO, V. A. The role of nitrogen atoms in forming the carbon structure in the carbonization of polymer composites. **Fibre Chemistry**, v. 40, n. 4, p. 355-364, 2008.
- [101] WANG, S.; et al. The thermal stability and pyrolysis mechanism of boron-containing phenolic resins: The effect of phenyl borates on the char formation. **Applied Surface Science**, v. 331, p. 519-529, 2015.
- [102] LEE, S. -H., et al. Magnetic field enhances the graphitized structure and field emission effect of carbon nanotubes. **Thin Solid Films**, v. 519, n. 13, p. 4166-4173, 2011.
- [103] ALEMANNI, E.; et al. Excimer laser-induced diamond graphitization for high-energy nuclear applications. **Applied Physics B**, v. 113, n. 3, p. 373-378, 2013.
- [104] KAMIYA, K.; SUZUKI, K. Preferential alignment of carbon layers around pores in hard carbon and multi-phase graphitization. **Carbon**, v. 13, n. 4, p. 317-320, 1975.
- [105] GHAZINEJAD, M.; et al. Graphitizing non-graphitizable carbons by stress-induced routes. **Scientific Reports**, v. 7, n. 1, p. 16551(1-10), 2017.
- [106] CANÇADO, L. G.; et al. General equation for the determination of the crystallite size  $L_a$  of nanographite by Raman spectroscopy. **Applied Physics Letters**, v. 88, n. 16, p. 163106(1-3), 2006.
- [107] WARREN, B. E. X-ray diffraction in random layer lattices. **Physical Review**, v. 59, n. 9, p. 693-698, 1941.
- [108] ZHAO, M.; SONG, H. Catalytic graphitization of phenolic resin. **Journal of Materials Science & Technology**, v. 27, n. 3, p. 266-270, 2011.
- [109] KUO, H. H.; LIN, J. H. C.; JU, C. P. Effect of carbonization rate on the properties of a PAN/phenolic-based carbon/carbon composite. **Carbon**, v. 43, n. 2, p. 229-239, 2005.
- [110] ŌYA, A.; ŌTANI, S. Effects of particle size of calcium and calcium compounds on catalytic graphitization of phenolic resin carbon. **Carbon**, v. 17, n. 2, p. 125-129, 1979.

- [111] SHEIKHALESLAMI, M. A. S.; GOLESTANIFARD, F.; SARPOOLAKY, H. Method of preparing phenolic resin/carbon nano materials (hybrid resin). **Google Patents**, 2009,
- [112] HARRIS, P. J. F. New perspectives on the structure of graphitic carbons. **Critical Reviews in Solid State and Materials Sciences**, v. 30, n. 4, p. 235-253, 2005.
- [113] GALLAGHER, K. G.; YUSHIN, G.; FULLER, T. F. The role of nanostructure in the electrochemical oxidation of model-carbon materials in acidic environments. **Journal of Electrochemical Society**, v. 157, n. 6, p. 820-830, 2010.
- [114] SMITH, W. R.; POLLEY, M. H. The oxidation of graphitized carbon black. **The Journal of Physical Chemistry**, v. 60, n. 5, p. 689-691, 1956.
- [115] STEIN, S. E.; BROWN, R. L. Chemical theory of graphite-like molecules. **Carbon**, v. 23, n. 1, p. 105-109, 1985.
- [116] DUBOIS, J.; AGACHE, C.; WHITE, J. L. The carbonaceous mesophase formed in the pyrolysis of graphitizable organic materials. **Materials Characterization**, v. 39, n. 2-5, p. 105-137, 1997.
- [117] BAMBUROV, V. G.; et al. Antioxidants in carbon-bearing refractories. **Refractories and Industrial Ceramics**, v. 41, n. 2, p. 33-36, 2000.
- [118] WANG, S.; et al. High char yield of aryl boron-containing phenolic resins: The effect of phenylboronic acid on the thermal stability and carbonization of phenolic resins. **Polymer Degradation and Stability**, v. 99, p. 1-11, 2014.
- [119] AL-FALAH, H. A. Catalytic graphitization of modified phenolic resin and its nanoparticles fillers behaviour towards high temperature. **Advanced Materials Research**, v. 925, p. 282-289, 2014.
- [120] BIAO LI, Y. Z.; ZHENG, Z.; ZHAO X. Characterization of boron modified phenolic resin and its curing behaviour. **Advanced Materials Research**, v. 233-235, p. 137-141, 2011.
- [121] XU, P.; JING, X. High carbon yield thermoset resin based on phenolic resin, hyperbranched polyborate, and paraformaldehyde. **Polymers for Advanced Technologies**, v. 22, n. 12, p. 2592-2595, 2011.

- [122] LIU, Y.; JING, X. Pyrolysis and structure of hyperbranched polyborate modified phenolic resins. **Carbon**, v. 45, n. 10, p. 1965-1971, 2007.
- [123] MARTÍN, C.; RONDA, J.C.; CÁDIZ, V. Boron-containing novolac resins as flame retardant materials. **Polymer Degradation and Stability**, v. 91, n. 4, p. 747-754, 2006.
- [124] WANG, J.; JIANG, N.; JIANG, H. Micro-structural evolution of phenol-formaldehyde resin modified by boron carbide at elevated temperatures. **Materials Chemistry and Physics**, v. 120, n. 1, p. 187-192, 2010.
- [125] WANG, S.; et al. Synthesis and characterization of novel phenolic resins containing aryl-boron backbone and their utilization in polymeric composites with improved thermal and mechanical properties. **Polymers for Advanced Technologies**, v. 25, n. 2, p. 152-159, 2014.
- [126] ABDALLA, M.O.; LUDWICK, A.; MITCHELL, T. Boron-modified phenolic resins for high performance applications. **Polymer**, v. 44, n. 24, p. 7353-7359, 2003.
- [127] YUN, J.; et al. The effect of introducing B and N on pyrolysis process of high ortho novolac resin. **Polymers**, v. 8, n. 3, p. 35(1-17), 2016.
- [128] SIMITZIS, J.; ZOUMPOULAKIS, L. Influence of FeCl<sub>3</sub> dopant on the electrical conductivity of pyrolyzed aromatic polymers. **Journal of Materials Science**, v. 31, n. 6, p. 1615-1620, 1996.
- [129] LIU, L.; YE, Z. Effects of modified multi-walled carbon nanotubes on the curing behavior and thermal stability of boron phenolic resin. **Polymer Degradation and Stability**, v. 94, n. 11, p. 1972-1978, 2009.
- [130] LUZ, A. P., et al. Graphitization of phenolic resins for carbon-based refractories. **Ceramics International**, v. 43, n. 11, p. 8171-8182, 2017.
- [131] STAMATIN, I.; et al. The synthesis of multi-walled carbon nanotubes (MWNTs) by catalytic pyrolysis of the phenol-formaldehyde resins. **Physica E: Low-dimensional Systems and Nanostructures**, v. 37, n. 1-2, p. 44-48, 2007.
- [132] ZHOU, Y. **Carbon: Proceedings of the Fourth Conference**. Elsevier Science, 2013.

- [133] VÁZQUEZ-SANTOS, M. B.; et al. Comparative XRD, Raman, and TEM study on graphitization of PBO-derived carbon fibers. **The Journal of Physical Chemistry C**, v. 116, n. 1, p. 257-268, 2012.
- [134] LYU, S. C.; et al. Synthesis of boron-doped double-walled carbon nanotubes by the catalytic decomposition of tetrahydrofuran and triisopropyl borate. **Carbon**, v. 49, n. 5, p. 1532-1541, 2011.
- [135] ROUZAUD, J. N.; OBERLIN, A.; BENY-BASSEZ, C. Carbon films: structure and microtexture (optical and electron microscopy, Raman spectroscopy). **Thin Solid Films**, v. 105, n. 1, p. 75-96, 1983.
- [136] WANG, Y.; ALSMEYER, D. C.; MCCREERY, R. L. Raman spectroscopy of carbon materials: structural basis of observed spectra. **Chemistry of Materials**, v. 2, n. 5, p. 557-563, 1990.
- [137] CUESTA, A.; et al. Comparative performance of X-ray diffraction and Raman microprobe techniques for the study of carbon materials. **Journal of Materials Chemistry**, v. 8, n. 12, p. 2875-2879, 1998.
- [138] WATSON, E. S.; O'NEILL M. J. Differential microcalorimeter. **Google Patents**, US3263484A, 1966.
- [139] LIU, Y., J. GAO, AND R. ZHANG, Thermal properties and stability of boron-containing phenol-formaldehyde resin formed from paraformaldehyde. **Polymer Degradation and Stability**, v. 77, n. 3, p. 495-501, 2002.
- [140] IDA P.; MATJAŽ K. Characterization of phenol-formaldehyde prepolymer resins by in line FT-IR spectroscopy. **Acta Chimica Slovenica**, v. 52, n. 3, p. 238-244, 2005.
- [141] THEODOROPOULOU, S.; et al. Structural and optical characterization of pyrolytic carbon derived from novolac resin. **Analytical and Bioanalytical Chemistry**, v. 379, n. 5, p. 788-791, 2004.
- [142] ERTUGRUL, A., MEHMET, H. A.; OKTAY, G.; ZEKI, C.; MURAT, E. FTIR Investigation of phenol formaldehyde resin modified with boric acid. in **Proceedings of the 55th International Convention of Society of Wood Science and Technology**, China, p. 480-487, 2012.



- [143] SARKAR, R., Particle Size Distribution for Refractory Castables: A Review. **Interceram - International Ceramic Review**, v. 65, n. 3, p. 82-86, 2016.
- [144] Standard Test Methods for Apparent Porosity, Liquid Absorption, Apparent Specific Gravity, and Bulk Density of Refractory Shapes by Vacuum Pressure, in **ASTM C830-00, ASTM International**: West Conshohocken, PA, 2016.
- [145] Standard Test Methods for Cold Crushing Strength and Modulus of Rupture of Refractories, in **ASTM C133-97, ASTM International**. West Conshohocken, PA, 2015.
- [146] HU, R.; CHUNG, T. C. Synthesis and characterization of novel B/C materials prepared by 9-chloroborabfluorene precursor. **Carbon**, v. 34, n. 10, p. 1181-1190, 1996.
- [147] JONES L. E., THROWERP A. Influence of boron on carbon fiber microstructure, physical properties, and oxidation behavior. **Carbon**, v. 29, n. 2, p. 251-269, 1991.
- [148] MARTIN, J. W. **Concise encyclopedia of the structure of materials**. Elsevier Science, 2006.
- [149] KIPLING, J. J.; SHOOTER, P. V.; YOUNG, R. N. The effect of sulphur on the graphitization of carbons derived from polyvinyl chloride-sulphur systems. **Carbon**, v. 4, n. 3, p. 333-341, 1966.
- [150] KIPLING, J. J.; SHOOTER, P.V. Factors affecting the graphitization of carbon: Evidence from polarized light microscopy. **Carbon**, v. 4, n. 1, p. 1-4, 1966.
- [151] ROWELL, V. M.; GUYER V. L. Liquid boric acid suspension, method and products. **Google Patents**, US3306860A, 1967.
- [152] BALZAR, D. X-Ray diffraction line broadening: modelling and applications to high-Tc superconductors. **Journal of Research of the National Institute of Standards and Technology**, v. 98, n. 3, p. 321-351.
- [153] FRANKLIN, R. E. Homogeneous and heterogeneous graphitization of carbon. **Nature**, v. 177, n. 4501, p. 239-239, 1956.

- [154] OKABE, K.; SHIRAIISHI, S.; OYA, A. Mechanism of heterogeneous graphitization observed in phenolic resin-derived thin carbon fibers heated at 3000 °C. **Carbon**, v. 42, n. 3, p. 667-669, 2004.
- [155] SEVILLA, M.; FUERTES, A. B. Catalytic graphitization of templated mesoporous carbons. **Carbon**, v. 44, n. 3, p. 468-474, 2006.
- [156] BURGESS, J. S.; et al. Boron-doped carbon powders formed at 1000 °C and one atmosphere. **Carbon**, v. 46, n. 13, p. 1711-1717, 2008.
- [157] ZHANG, X.; SOLOMON, D. H. Carbonization reactions in novolac resins, hexamethylenetetramine, and furfuryl alcohol mixtures. **Chemistry of Materials**, v. 11, n. 2, p. 384-391, 1999.
- [158] ENOKI, T.; SUZUKI, M.; ENDO, M. **Graphite intercalation compounds and applications**. Oxford University Press, 2003.
- [159] KÄÄRIK, M.; et al. The effect of graphitization catalyst on the structure and porosity of SiC derived carbons. **Carbon**, v. 46, n. 12, p. 1579-1587, 2008.
- [160] ZHAO, S. -G.; WANG, B. -C.; SUN, Q. Effect of physical disturbance on the structure of needle coke. **Chinese Physics B**, v. 19, n. 10, p. 108101, 2010.
- [161] SUSLICK, K. S.; NYBORG, W. L. Ultrasound: its chemical, physical and biological effects. **The Journal of the Acoustical Society of America**, v. 87, n. 2, p. 919-920, 1990.
- [162] PILKENTON, M.; LEWMAN, J.; CHARTOFF, R. Effect of oxygen on the cross-linking and mechanical properties of a thermoset formed by free-radical photocuring. **Journal of Applied Polymer Science**, v. 119, n. 4, p. 2359-2370, 2011.
- [163] EDWARDS, I. A. S.; MARSH, H. **Introduction to carbon science**. Butterworths, 1989.
- [164] BART, J. C. J. **Polymer Additive Analytics: Industrial Practice and Case Studies**. Firenze University Press, 2006.
- [165] ZHAO, C., ZHANG, G.; ZHAO, L. Effect of curing agent and temperature on the rheological behavior of epoxy resin systems. **Molecules**, v. 17, n. 7, p. 8587-8594, 2012.

- [166] KANDOLA, B.; EBDON, J.; CHOWDHURY, K. Flame retardance and physical properties of novel cured blends of unsaturated polyester and furan resins. **Polymers**, v. 7, n. 2, p. 298-315, 2015.
- [167] MANIKANDAN, G.; BOGESHWARAN, K. Effect of curing time on phenolic resins using latent acid catalyst. **International Journal of ChemTech Research**, v. 9, n. 1, p. 30-37, 2016.
- [168] PIMENTA, M. A.; et al. Studying disorder in graphite-based systems by Raman spectroscopy. **Physical Chemistry Chemical Physics**, v. 9, n. 11, p. 1276-1290, 2007.
- [169] DRESSELHAUS, M. S.; et al. Perspectives on carbon nanotubes and graphene Raman spectroscopy. **Nano Letters**, v. 10, n. 3, p. 751-758, 2010.
- [170] PARSONS, J. Vibrational spectra of orthorhombic metaboric acid. **The Journal of Chemical Physics**, v. 33, n. 6, p. 1860-1866, 1960.
- [171] ANDREWS, L.; BURKHOLDER, T. R. Infrared spectra of molecular B(OH)<sub>3</sub> and HOBO in solid argon. **The Journal of chemical physics**, v. 97, n. 10, p. 7203-7210, 1992.
- [172] MEDVEDEV, E. F.; KOMAREVSKAYA, A. S. IR spectroscopic study of the phase composition of boric acid as a component of glass batch. **Glass and Ceramics**, v. 64, n. 1, p. 42-46, 2007.
- [173] ERMOLAEVA, A. I.; KOSHELEV, N. I.; DVORNIKOV, S. A. Investigation of borophosphosilicate glasses synthesized by the sol-gel method. **Glass Physics and Chemistry**, v. 26, n. 3, p. 300-302, 2000.
- [174] MENACHEM L.; Atlas S. M.; PEARCE E. **Flame-retardant polymeric materials**. Springer Science & Business Media, 2012.
- [175] CONLEY, R. T.; BIERON, J. F. A study of the oxidative degradation of phenol-formaldehyde polycondensates using infrared spectroscopy. **Journal of Applied Polymer Science**, v. 7, n. 1, p. 103-117, 1963.
- [176] TALABI, S. I.; et al. Catalytic graphitization of novolac resin for refractory applications. **Ceramics International**, v. 44, n. 4, p. 3816-3824, 2018.

- [177] JIANG, D. -E.; et al. Simulating the initial stage of phenolic resin carbonization via the ReaxFF reactive force field. **The Journal of Physical Chemistry A**, v. 113, n. 25, p. 6891-6894, 2009.
- [178] TALABI, S.I.; et al. Structural evolution during the catalytic graphitization of a thermosetting refractory binder and oxidation resistance of the derived carbons. **Materials Chemistry and Physics**, v. 212, n. 15, p. 113-121, 2018.
- [179] YUSOF, N.; et al. Microstructure of polyacrylonitrile-based activated carbon fibers prepared from solvent-free coagulation process. **Journal of Applied Research and Technology**, v. 14, n. 1, p. 54-61, 2016.
- [180] ILA, D.; et al. A study of the thermally induced carbonization of phenolformaldehyde by combined ion beam and surface specific analyses. **Vacuum**, v. 45, n. 4, p. 451-454, 1994.
- [181] Šupová M.; et al. Relation between mechanical properties and pyrolysis temperature of phenol formaldehyde resin for gas separation membranes. **Ceramics-Silikáty**, v. 56, n. 1, p. 40-49, 2012.
- [182] SAVAGE, G. **Thermosetting resin matrix precursors, in carbon-carbon composites**. Springer Netherlands: Dordrecht. p. 117-156, 1993.
- [183] MANG, D.; et al. Inhibiting effect of incorporated nitrogen on the oxidation of microcrystalline carbons. **Carbon**, v. 30, n. 3, p. 391-398, 1992.
- [184] RUFF, O. Reactions of solid carbon with gases and liquids. **Transactions of the Faraday Society**, v. 34, p. 1022-1033, 1938.
- [185] BOBROWSKI, A.; GRABOWSKA, B. FTIR method in studies of the resol type phenol resin structure in the air atmosphere in some time intervals. **Metallurgy and Foundry Engineering**, v. 41, n. 3, p. 107-113.
- [186] LENGHAUS, K.; QIAO, G. G.; SOLOMON, D. H. The effect of formaldehyde to phenol ratio on the curing and carbonisation behaviour of resole resins. **Polymer**, v. 42, n. 8, p. 3355-3362, 2001.
- [187] BONNET, F.; et al. Study of the oxide/carbide transition on iron surfaces during catalytic coke formation. **Surface and Interface Analysis**, v. 34, n. 1, p. 418-422, 2002.

- [188] KUIVILA, C. S., Butt, J. B.; Stair, P. C. Characterization of surface species on iron synthesis catalysts by X-ray photoelectron spectroscopy. **Applied Surface Science**, v. 32, n. 1, p. 99-121, 1988.
- [189] Shabanova, I.N. and V.A. Trapeznikov, A study of the electronic structure of Fe<sub>3</sub>C, Fe<sub>3</sub>Al and Fe<sub>3</sub>Si by X-ray photoelectron spectroscopy. **Journal of Electron Spectroscopy and Related Phenomena**, v. 6, n. 4, p. 297-307, 1975.
- [190] RAND, B.; RAMOS, V. P. S.; AHMED, A. S. The role of carbon in refractories. **Iranian Journal of Materials Science & Engineering**, v. 1, n. 3, p. 9-15, 2004.
- [191] CHANG, H. W.; RHEE, S. K. Oxidation of carbon derived from phenolic resin. **Carbon**, v. 16, n. 1, p. 17-20, 1978.
- [192] PIZZI, A. Phenolic and tannin-based adhesive resins by reactions of coordinated metal ligands. II. Tannin adhesive preparation, characteristics, and application. **Journal of Applied Polymer Science**, v. 24, n. 5, p. 1257-1268, 1979.
- [193] LI, J.; et al. Preparation and characterization of lignin demethylated at atmospheric pressure and its application in fast curing biobased phenolic resins. **RSC Advances**, v. 6, n. 71, p. 67435-67443, 2016.
- [194] WATKINS, D.; et al. Extraction and characterization of lignin from different biomass resources. **Journal of Materials Research and Technology**, v. 4, n. 1, p. 26-32, 2015.
- [195] BOERIU, C. G.; et al. Characterisation of structure-dependent functional properties of lignin with infrared spectroscopy. **Industrial Crops and Products**, v. 20, n. 2, p. 205-218, 2004.
- [196] SANTOS, J.; et al. Evaluating lignin-rich residues from biochemical ethanol production of wheat straw and olive tree pruning by FTIR and 2D-NMR. **International Journal of Polymer Science**, v. 2015, p. 1-11, 2015.
- [197] KLINE, L. M.; et al. Simplified determination of lignin content in hard and soft woods via UV-spectrophotometric analysis of biomass dissolved in ionic liquids. **BioResources**, v. 5, n. 3, p. 1366-1383, 2010.

- [198] DURIE, R.; LYNCH, B.; STERNHELL, S. Comparative studies of brown coal and lignin. I. Infra-Red spectra. **Australian Journal of Chemistry**, v. 13, n. 1, p. 156-168, 1960.
- [199] BRIGGS, L. H.; et al. Infrared absorption spectra of methylenedioxy and aryl ether groups. **Analytical Chemistry**, v. 29, n. 6, p. 904-911, 1957.
- [200] HERGERT, H. L. Infrared spectra of lignin and related compounds. ii. conifer lignin and model compounds 1,2. **The Journal of Organic Chemistry**, v. 25, n. 3, p. 405-413, 1960.
- [201] LV, P.; ALMEIDA, G.; PERRÉ, P. TGA-FTIR analysis of torrefaction of lignocellulosic components (cellulose, xylan, lignin) in isothermal conditions over a wide range of time durations. **BioResources**, v. 10., n. 3, p. 4239-4251, 2015.
- [202] ZHANG, X.; et al. Carbon nanostructure of kraft lignin thermally treated at 500 to 1000 °C. **Materials**, v. 10, n. 8, p. 975(1-14), 2017.
- [203] KAWAMOTO, H. Lignin pyrolysis reactions. **Journal of Wood Science**, v. 63, n. 2, p. 117-132, 2017.
- [204] NAKAMURA, T.; KAWAMOTO, H.; SAKA, S. Pyrolysis behavior of Japanese cedar wood lignin studied with various model dimers. **Journal of Analytical and Applied Pyrolysis**, v. 81, n. 2, p. 173-182, 2008.
- [205] BYKOV, I. **Characterization of natural and technical lignins using FTIR spectroscopy**, in Department of Chemical Engineering and Geosciences. Lulea University of Technology. p. 43, 2008.
- [206] DOMÍNGUEZ, J. C.; et al. Structural, thermal and rheological behavior of a bio-based phenolic resin in relation to a commercial resol resin. **Industrial Crops and Products**, v. 42, p. 308-314, 2013.
- [207] TEJADO, A.; et al. Physico-chemical characterization of lignins from different sources for use in phenol–formaldehyde resin synthesis. **Bioresource Technology**, v. 98, n. 8, p. 1655-1663, 2007.
- [208] SATO, Y.; et al. Boron-assisted transformation to rod-like graphitic carbons from multi-walled carbon nanotubes in boron-mixed multi-walled carbon nanotube solids. **ACS Applied Materials & Interfaces**, v. 3, n. 7, p. 2431-2439, 2011.

- [209] KIM, J.S.; et al. Characterization of boron containing graphite using TEM and EELS. **Microscopy and Microanalysis**, v. 8, n. 2, p. 610-611, 2002.
- [210] CABIOC'H, T.; THUNE, E.; JAOUEN, M. Mechanisms involved in the formation of onionlike carbon nanostructures synthesized by ion implantation at high temperature. **Physical Review B**, v. 65, n. 13, p. 132103(1-4); 2002.
- [211] DUTTA, N. J., MOHANTY, S. R.; BUZARBARUAH, N. Modification on graphite due to helium ion irradiation. **Physics Letters A**, v. 380, n. 33, p. 2525-2530, 2016.
- [212] QIN, H., et al., Synthesis and properties of magnetic carbon nanocages particles for dye removal. **Journal of Nanomaterials**, v. 2015, p. 1-8, 2015.
- [213] TALABI, S.I.; et al. Synthesis and graphitization of resole resins by ferrocene. **Progress in Natural Science: Materials International**, v. 29, n. 1, p. 71-80, 2019.
- [214] ANEZIRIS, C. G.; DUDCZIG, S. Carbon containing castables and more. **Advances in Science and Technology**, v. 70, p. 72-81, 2011.